PATTERNS AND PROCESSES GOVERNING GREENHOUSE GAS EMISSIONS FROM TIDAL SALT MARSH SOILS

by

Margaret Capooci

A dissertation submitted to the Faculty of the University of Delaware in partial fulfillment of the requirements for the degree of Doctor of Philosophy in Water Science and Policy

Summer 2022

PATTERNS AND PROCESSES GOVERNING GREENHOUSE GAS EMISSIONS FROM TIDAL SALT MARSH SOILS

by

Margaret Capooci

Approved: _____

Erik H. Ervin, Ph.D.
Chair of the Department of Plant and Soil Sciences

Approved: _____

Calvin Keeler, Ph.D.
Dean of the College of Agriculture and Natural Resources

Approved: _____

Louis F. Rossi, Ph.D.
Vice Provost for Graduate and Professional Education and
Dean of the Graduate College

I certify that I have read this dissertation and that in my opinion it meets the academic and professional standard required by the University as a dissertation for the degree of Doctor of Philosophy.

Signed: _____

Rodrigo Vargas, Ph.D.
Professor in charge of dissertation

I certify that I have read this dissertation and that in my opinion it meets the academic and professional standard required by the University as a dissertation for the degree of Doctor of Philosophy.

Signed: _____

Yan Jin, Ph.D.
Member of dissertation committee

I certify that I have read this dissertation and that in my opinion it meets the academic and professional standard required by the University as a dissertation for the degree of Doctor of Philosophy.

Signed: _____

Angelia L. Seyfferth, Ph.D.
Member of dissertation committee

I certify that I have read this dissertation and that in my opinion it meets the academic and professional standard required by the University as a dissertation for the degree of Doctor of Philosophy.

Signed: _____

Craig R. Tobias, Ph.D.
Member of dissertation committee

ACKNOWLEDGMENTS

I would like to thank my advisor, Rodrigo Vargas, for his support, guidance, mentorship, and for taking a chance on me all those years ago. Thank you to my committee members, Dr. Angelia Seyfferth, Dr. Craig Tobias, and Dr. Yan Jin, for their guidance and their time.

Thank you to my lab mates, past and present, for innumerable lunches and endless support. A special thank you to Josep Barba, for teaching me all there is to know about measuring gases from soils, and to Alma Vázquez-Lule, Branko Trifunovic, and Andrew Hill, for memorable days in the field.

Thank you to Dr. Karis McFarlane and Dr. Niles Hasselquist for opening up their labs to me so I could learn more radio and stable isotopes. I would like to extend a special thank you to Dr. Kari St. Laurent and the staff at St. Jones Reserve for supporting this research at the marsh.

To my parents, Victor and Evelyn, I am eternally grateful for all your love, support, and visits throughout these years – this work would not have been possible without you. I appreciate it more than you could ever know. To my brother, Corey, my grandma, Sandra, the rest of my family, "The Council," and my Scranton family for all their moral support from afar. Finally, to all the wonderful people from UD that I get to call my friends, thank you for all of it.

I would like to dedicate this manuscript to those I lost during the last two years of my Ph.D., my grandma, Leona, my grandpa, Victor, and my nana, Irene. I am so lucky to have had you all in my life for as long as I did.

This research would not have been possible without support from the DENIN Fellowship, the NSF Graduate Research Fellowship (#1247394/#1940700), the NSF Graduate Research Opportunities Worldwide program, and the DOE Office of Science Graduate Student Research Program. Financial support was provided by the NSF (#1652594).

TABLE OF CONTENTS

LIST OF TABLES

LIST OF FIGURES

ABSTRACT

Coastal vegetated ecosystems, such as tidal salt marshes, mangrove forests, and seagrass beds, store large amounts of carbon and thereby have been referred to as "blue carbon" ecosystems. These ecosystems also release carbon in the form of carbon dioxide (CO_2) and methane (CH_4), as well as other climate-active trace gases such as nitrous oxide (N_2O), carbon disulfide (CS_2), and dimethylsulfide (DMS). There is high uncertainity about the production and emissions of these gases from salt marsh soils, as well as their spatiotemporal variability. Knowledge about soil trace gas fluxes is important for calculating budgets, calibrating models, and assessing the viability of marshes as natural climate solutions. This dissertation focuses on better understanding the patterns and processes that govern greenhouse (GHG; CO_2, CH_4, N_2O) and sulfur-based gas (CS_2, DMS) fluxes from soils in a Mid-Atlantic temperate tidal salt marsh. Fluxes were measured using a variety of chamber techniques, coupled with biophysical and biogeochemical measurements.

The first study presented in this dissertation investigates the effect of storm-surge salinity changes on GHG fluxes from tidal salt marsh soils, with the goal of understanding how fluxes respond to and recover from salinity changes. A flow-through mesocosm experiment was coupled with automated GHG flux and pore water chemistry measurements. Decreases in salinity contributed to an increase in GHG fluxes. Throughout the experiment, the role of different biogeochemical processes in producing GHG fluxes changed over time. This underscores the complex nature of the

production and emission of GHG, particularly during extreme events. Once salinity returned to the initial conditions, CH_4 and N_2O fluxes returned to baseline within 15 days, illustrating that tidal salt marshes are resilient ecosystems.

The second study sought to better quantify CO_2 fluxes, as well as identify its main biophysical drivers using long-term, continuous data collected in the field. Hourly averages of CO_2 flux were collected at two sites for ~20 months, as well as manual CO_2 flux data to assess spatial variability. This study comprises of the first long-term datasets of soil CO_2 flux measurements from a salt marsh. Although seasonal patterns of CO_2 fluxes were found, there were no consistent diel patterns. The main biophysical driver of CO_2 flux was air temperature, but other drivers such as water level, salinity, PAR, and NDVI played roles. Manual measurements collected every two weeks underestimated the annual flux, highlighting the need for high-frequency data to calculate annual budgets more accurately.

The third study built upon the questions about biophysical drivers and measurement techniques posed in the second chapter to include CH_4, N_2O, CS_2, and DMS. Continuous, automated chambers were deployed for ~72 hours throughout the year to obtain high-temporal frequency data to assess how gas fluxes changed throughout the day and over tidal cycles. No consistent diel patterns were found, but rather CH_4, N_2O, CS_2, and DMS fluxes were highly variable with frequent pulse emissions. Likewise, when continuous measurements were compared to discrete (during daytime, at low tide) measurements for these four gases, discrepancies arose due to high temporal variability. However, both continuous and discrete measurements of CO_2 provided similar information regarding the mean and distribution of CO_2 fluxes, providing support for the use of discrete measurements of CO_2 for budgets.

The fourth study sought to better understand CH_4 production and fate in tidal salt marsh soils. The continuous, automated measurements of CH_4 and CO_2 performed in the third study were coupled with measurements of soil CH_4 and CO_2 gas concentrations, stable and radioisotopes, pore water and organic carbon chemistry, and microbial community composition. CH_4 was found to be produced by two pathways: hydrogenotrophic and methylotrophic methanogenesis, the latter of which can produce CH_4 in the presence of sulfate reduction. Once produced, data showed that CH_4 can take a variety of pathways: diffusion into the atmosphere, CH_4 oxidation, and lateral transport to the tidal creek. The findings showed that CH_4 production and fate is biogeochemically heterogeneous and that each process involved varied in importance over the growing season.

Overall, this dissertation provided key insights into the spatiotemporal variability of greenhouse and sulfur-based fluxes from tidal salt marsh soils, as well as the processes that produce these gases. The findings from these studies will provide better insights for scientists and policymakers on the role salt marshes have in the carbon cycle as well as provide better GHG estimates for evaluating whether salt marshes are a net carbon sink.

Chapter 1

INTRODUCTION

1.1 Salt marshes and their importance

Tidal salt marshes lie at the intersection of the land and the coastal ocean and are characterized by tidal flooding, salt-tolerant vegetation, and soils with little to no oxygen availability. They cover between 0.07 to 0.22% of the Earth's surface (Duarte et al., 2013; NASEM, 2019; Spivak et al., 2019), but provide a disproportionate amount of ecosystem services relative to their size. Salt marshes provide protection to local communities from storm surges (Feagin et al., 2010), mitigate nutrient run-off (Brin et al., 2010), and offer a variety of recreational opportunities (Myers et al., 2010). Together, these ecosystem services, along with others such as nursery habitat for commercially important fish species, are valued at ~$10,000 per hectare (Barbier et al., 2011).

Salt marshes also store large amounts of carbon in their soil at rates forty times higher than tropical rainforests (Duarte et al., 2005; Rosentreter et al., 2018) due to their high primary productivity and slow decomposition rates. As a result, salt marshes, along with mangrove forests and seagrass beds, are referred to as "blue carbon" ecosystems (Nellemann et al., 2009). In recent years, the importance of blue carbon ecosystems in mitigating climate change has been recognized by the international community via the Paris Agreement (UNFCCC, 2015), as well as commercial marketplace via the Verified Carbon Standard, which developed a methodology to assess the carbon stored in tidal wetland restoration projects for

carbon market purposes (Emmer et al., 2021). While quantifying the carbon stocks of coastal wetlands is important, we also need to understand how much carbon is exported from these systems. For blue carbon ecosystems to be effective in mitigating climate change, more carbon needs to be stored than exported. There are knowledge gaps regarding the export of carbon from coastal wetlands, including how much carbon dioxide (CO_2) and methane (CH_4), as well as other climatically important gases, are released from the soils. These measurements are complicated by a variety of factors, including high spatial and temporal variability, as well as non-optimal conditions for analytical instruments, such as high humidity and salinity (Al-Haj and Fulweiler, 2020; Murray et al., 2015; Rosentreter et al., 2021).

1.2 Overview of trace gases from salt marsh soils

Salt marshes produce and emit a variety of gases, including the greenhouse gases (GHG), CO_2, CH_4, and nitrous oxide (N_2O), as well as sulfur-based gases such as carbon disulfide (CS_2) and dimethylsulfide (DMS). The processes that produce, consume, and release these gases from the soil to the atmosphere differs from gas to gas, but all are impacted by the unique characteristics of the salt marsh itself, such as tides, salinity, high sulfur concentrations, fluctuating oxygen levels, and specially adapted plant species.

Salt marshes emit between 120-240 g C m^{-2} yr^{-1} of carbon dioxide (Tobias and Neubauer, 2019 and references within). CO_2 can be produced via a variety of pathways, including autotrophic respiration and decomposition of organic matter via aerobic and anerobic microorganisms. However, within salt marshes, anaerobic respiration dominates due to flooded soils which contributes to the rapid use of oxygen near the soil surface and allows for other election acceptors (i.e., NO_3^-, Fe^{3+}, SO_4^{2-}) to

be used in microbial processes that produce CO_2 as a by-product (Ponnamperuma, 1972). The proportion of electron acceptors, particularly SO_4^{2-}, can change with salinity and thereby could affect CO_2 fluxes as salinity changes. In temperate terrestrial ecosystems, CO_2 fluxes from the soil (i.e., soil respiration) is strongly correlated with temperature (Bond-Lamberty and Thomson, 2010; Raich and Schlesinger, 1992). However, this relationship has only been tested in salt marshes via nighttime net ecosystem exchange data from eddy covariance (Guo et al., 2009; O'Connell et al., 2017), but not from long-term soil CO_2 flux data. There is a need to better understand the drivers of CO_2 flux from salt marsh soils, particularly in relation to temperature and salinity.

Globally, salt marshes release 0.005 to 0.006 Pg CH_4 yr^{-1} (Al-Haj and Fulweiler, 2020). Traditionally, methane fluxes were thought to be low in salt marshes due the two primary production pathways (acetoclastic and hydrogenotrophic methanogenesis) being out outcompeted by sulfate reducers. However, on a local scale, salt marshes range widely from net uptake of CH_4 (-93 μmol m^{-2} day^{-1}) to net emission (94,000 μmol m^{-2} day^{-1}; Al-Haj and Fulweiler, 2020 and references within), demonstrating that some marshes emit very high amounts of CH_4. Furthermore, CH_4 production can occur via the methylotrophic methanogenesis pathway within salt marshes and marine sediments (Seyfferth et al., 2020; Xiao et al., 2018; Zhuang et al., 2018). This pathway does not compete with sulfate reducers since the microbes use non-competitive substrates (i.e., methanol, methylsulfides) to produce CH_4. CH_4 can also be consumed via aerobic and anaerobic methanotrophs. However, very little research has been done on CH_4 oxidation in salt marsh soils. CH_4 can leave the soil via a variety of pathways, including diffusion, plant-mediated transport, and ebullition.

However, CH_4 fluxes from soils are highly variable and difficult to predict due to the many processes that produce, consume, and transport it. Since CH4 is a potent greenhouse gas, there is a need to better understand the patterns and processes that govern CH_4 fluxes within salt marshes.

Salt marshes also emit and uptake N_2O, though the magnitude of emissions or uptake depends on water residence time (Maavara et al., 2019), nitrate concentrations (Moseman-Valtierra et al., 2011), and plant competition for nitrogen (Moseman-Valtierra et al., 2011; Smith et al., 1983). N_2O can be produced by denitrification, nitrification, and nitrifier-denitrification, as well as consumed by denitrification, particularly when nitrate availability is low (Rosentreter et al., 2021). Globally, N_2O emissions from inland waters, estuaries, and coastal zones (which includes salt marshes) amount to 0.3 to 0.4 Tg N yr^{-1}, a small fraction of the overall N_2O budget (Tian et al., 2020). However, there is limited data on spatial and temporal N_2O dynamics in salt marshes to inform global estimates, as well as to assess the role marshes play as a source or a sink of N_2O (Rosentreter et al., 2021).

In addition to producing GHGs, salt marshes emit sulfur-based trace gases due to high sulfate inputs from the coastal ocean contributing to the prevalence of sulfur cycling within their soils. Sulfur-based trace gases were studied widely in the 1980s and early 1990s, but there has been very little research since. This contributes to large uncertainty in emissions (Andreae and Jaeschke, 1992; Carroll et al., 1986), despite coastal areas being a large source (Kellogg et al., 1972). Two dominant sulfur-based gases are CS_2 and DMS. CS_2 is a precursor to carbonyl sulfide (Whelan et al., 2013), which is the most abundant reduced sulfur compound in the atmosphere (Watts, 2000). While the pathways that produce CS_2 are not well understood, several have been

proposed, including organic matter degradation, photochemical production, and algal production (Xie and Morre 1999). DMS, another sulfur-based trace gas, is a by-product of dimethylsulfoniopropionate, a compound produced by salt marsh grasses *Spartina alterniflora*, *S. angelica*, and *S. foliosa* (Hines, 1996). DMS can also be produced by other pathways, such as methylation of sulfide (Carrión et al., 2019; Lomans et al., 2002; Sela-Adler et al., 2015). DMS plays an important role in the carbon-sulfur cycle, since it can act as a non-competitive substrate for methylotrophic methanogenesis (Kiene, 1988; Kiene and Visscher, 1987; Oremland et al., 1982). Due to the roles CS_2 and DMS play in global climate and salt marsh soil biogeochemistry, more studies are needed to quantify CS_2 and DMS emissions.

1.3 Measurement of trace gases in salt marshes

Traditionally, trace gases in salt marshes have been measured using manual survey chambers outfitted with a sampling port to extract headspace samples at periodic intervals (e.g., Cooper et al., 1987; De Mello et al., 1987). These samples were then run through a gas chromatograph (GC), from which a flux would be calculated. Nowadays, portable instrumentation, such as infrared gas analyzers (IRGA) and Fourier-transform infrared spectroscopy, can be used with chambers in the field, eliminating the need to take multiple headspace samples. Manual measurements, either through GC analyses or with a portable instrument, have several advantages. They can be used to sample large areas over a short period of time (Moseman-Valtierra et al., 2016; Simpson et al., 2019) and are less cost-intensive than continuous measurements. However, the measurements are labor-intensive and are temporally limited, typically measuring during daytime low tide (Koskinen et al., 2014; Savage et al., 2014; Vargas et al., 2011). In recent years, there have been

advancements in instrumentation that allows researchers to collect high-frequency measurements using continuous, automated systems. Such systems include Forced Diffusion CO_2 sensors and IRGAs coupled with automated chambers. These systems provide unprecedented temporal information and are less labor-intensive than manual measurements. However, their use in salt marshes has been limited by several factors, including high instrumentation costs, electricity requirements, and adverse environmental conditions such as high humidity and salinity that affect instrument performance. Both manual and continuous measurement techniques have advantages and disadvantages when used in salt marshes, but they both provide valuable data that can be used to inform our understanding of the patterns and processes that govern trace gas emissions from tidal salt marshes.

1.4 Importance of trace gas data

Trace gas data provide invaluable information to scientists, policymakers, and natural resource managers. Scientists can use the data to inform carbon, nitrogen, and sulfur budgets, as well as Earth system models, which combine physical, chemical, and biological processes with data that have been collected by researchers in field and laboratory settings (U.S. DOE, 2022). These models seek to better understand different Earth processes, such as carbon cycling. There is a need for more trace gas data from coastal ecosystems. In particular, how CO_2 and CH_4 fluxes vary over a range of spatiotemporal scales in coastal ecosystems (Bauer et al., 2013; Windham-Myers et al., 2018), as well as how coastal ecosystems respond to changes in water level and salinity from extreme events (Crooks et al., 2011; Mcleod et al., 2011). Trace gas data can also be important for policy makers and natural resource managers. Accurate data on carbon stocks and emissions, particularly CH_4, can provide

information on the utility of restoring marshes for carbon credit schemes (Al-Haj and Fulweiler, 2020; Murray et al., 2015; Rosentreter et al., 2021), as well as help inform natural resource managers on how to restore marshes while minimizing trace gas emissions.

1.5 Research questions

The overall objective of this research is to help address the knowledge gaps surrounding the patterns (i.e., annual, seasonal, diel) and processes (i.e., biophysical, biogeochemical) that govern greenhouse gas emissions from tidal salt marsh soils. This research has been divided into four chapters and includes lab experiments and field studies that center around the use of both manual and continuous trace gas measurements, supported by meteorological, water quality, and biogeochemical data. All studies were either conducted at St. Jones Reserve, a component of the Delaware National Estuarine Research Reserve, or were informed by events that occurred there.

Chapter 2 (published in *Science of the Total Environment*, 2019) addressed the role storm surges play in CO_2, CH_4, and N_2O emissions by experimentally replicating the salinity changes that occurred at St. Jones Reserve due to Hurricane Joaquin in 2015. This study involved flow-through mesocosms with soil from St. Jones. CO_2, CH_4, and N_2O fluxes were continuously measured from the mesocosms and coupled with pore water chemical analyses. Two hypotheses were addressed in this study: 1.) a decrease in salinity increases the emissions of all three GHGs due more favorable redox conditions for the biogeochemical processes that produce GHGs, and 2.) changes in salinity and subsequent biogeochemical processes affect the temporal pattern of GHG emissions.

Chapter 3 (published in *Science of the Total Environment*, 2022) described and quantified the temporal patterns and drivers of CO_2 efflux from two locations that were characterized by different vegetation and soil biogeochemistry. This study combined continuous, automated measurements (high temporal frequency) with manual measurements (broader spatial distribution). Four hypotheses are addressed in this study: 1.) there will be clear seasonal and diel patterns of CO_2 efflux, 2.) the two vegetation zones will have differences in soil CO_2 efflux magnitudes, 3.) CO_2 efflux will be primarily driven by temperature, but other biophysical factors (i.e., water quality, plant ecophysiology) will play a role, and 4.) the relationship between temperature and CO_2 efflux will be similar for continuous and manual measurements, but magnitudes, patterns, and annual soil CO_2 efflux estimates may differ between the two approaches. This study was the first use long-term soil CO_2 efflux data from a tidal salt marsh.

Chapter 4 (under review in *Biogeosciences*) sought to characterize the spatial and temporal variability of five trace gases (CO_2, CH_4, N_2O, CS_2, DMS) from tidal salt marsh soils. This study involved the deployment of continuous, automated chambers during short periods of time (~72 hours) throughout the growing season. Two questions were addressed: 1.) are there differences between measurements taken at daytime low tide and measurements taken hourly and 2.) do traditional measurement protocols based on manual measurements provide similar information as continuous measurement data, including the calculation of sustained global warming potential. This study was the first to capture high-temporal frequency data of CS_2 and DMS from tidal salt marsh soils.

Chapter 5 (in prep) investigated the processes and pathways of CH_4 production and fate in tidal salt marsh soils. This study combined measurements of soil CO_2 and CH_4 fluxes and gas concentrations, stable and radio isotopes, pore water and organic carbon chemistry, and microbial community composition, which were collected throughout the growing season. Two questions were addressed: 1.) are high CH_4 concentrations within the soil due to, in part, the presence of methylotrophic methanogens within the soil microbial community and 2.) what is the fate of CH_4 within the soil profile – does CH_4 persist in the soil, get vertically or laterally transported as CH_4, or get oxidized into CO_2 and lost vertically as CO_2 or moved laterally as dissolved inorganic carbon.

REFERENCES

Al-Haj, A.N., Fulweiler, R.W., 2020. A synthesis of methane emissions from shallow vegetated coastal ecosystems. Glob. Chang. Biol. 26, 2988–3005. https://doi.org/10.1111/gcb.15046

Andreae, M.O., Jaeschke, W.A., 1992. Exchange of sulfur between biosphere and atmosphere over temperate and tropical regions, in: Howarth, R.W., Stewart, J.W.B., Ivanov, M.V. (Eds.), Sulfur Cycling on the Continents. Wiley, New York.

Barbier, E.B., Hacker, S.D., Kennedy, C., Koch, E.W., Stier, A.C., Silliman, B.R., 2011. The value of estuarine and coastal ecosystem services. Ecol. Monogr. https://doi.org/10.1890/10-1510.1

Bauer, J.E., Cai, W.J., Raymond, P.A., Bianchi, T.S., Hopkinson, C.S., Regnier, P.A.G., 2013. The changing carbon cycle of the coastal ocean. Nature. https://doi.org/10.1038/nature12857

Bond-Lamberty, B., Thomson, A., 2010. A global database of soil respiration data. Biogeosciences 7, 1915–1926. https://doi.org/10.5194/bg-7-1915-2010

Brin, L.D., Valiela, I., Goehringer, D., Howes, B., 2010. Nitrogen interception and export by experimental salt marsh plots exposed to chronic nutrient addition. Mar. Ecol. Prog. Ser. 400, 3–17. https://doi.org/10.3354/meps08460

Carrión, O., Pratscher, J., Rciha, K., Rostant, W.G., Haque, M.F.U., Murell, J.C., Todd, J.D., 2019. Methanthoil and dimethylsulfide cycling in Stiffkey saltmarsh. Front. Mar. Sci. 10, 1-15. https://doi.org/10.3389/fmicb.2019.01040

Carroll, M.A., Heidt, L.E., Cicerone, R.J., Prinn, R.G., 1986. OCS, H_2S, and CS_2 fluxes from a salt water marsh. J. Atmos. Chem. 4, 375–395. https://doi.org/10.1007/BF00053811

Cooper, D.J., De Mello, W.Z., Cooper, W.J., Zika, R.G., Saltzman, E.S., Prospero, J.M., Savoie, D.L., 1987. Short-term variability in biogenic sulphur emissions from a Florida *Spartina alterniflora* marsh. Atmos. Environ. 21, 7–12.

Crooks, S., Herr, D., Tamelander, J., Laffoley, D., Vandever, J., 2011. Mitigating climate change through restoration and management of coastal wetlands and near-shore marine ecosystems: challenges and opportunities. Environment Department Paper. World Bank, Washington D.C.

De Mello, W.Z., Cooper, D.J., Cooper, W.J., Saltzman, E.S., Zika, R.G., Savoie, D.L., Prospero, J.M., 1987. Spatial and diel variability in the emissions of some biogenic sulfur compounds from a Florida *Spartina alterniflora* coastal zone. Atmos. Environ. 21, 987–990. https://doi.org/10.1016/0004-6981(87)90095-3

Duarte, C.M., Losada, I.J., Hendriks, I.E., Mazarrasa, I., Marbà, N., 2013. The role of coastal plant communities for climate change mitigation and adaptation. Nat. Clim. Chang. 3, 961–968. https://doi.org/10.1038/nclimate1970

Duarte, C.M., Middelburg, J.J., Caraco, N., 2005. Major role of marine vegetation on the oceanic carbon cycle. Biogeosciences 2, 1–8. https://doi.org/10.1111/j.2042-7158.1975.tb10261.x

Emmer, I., Needelman, B., Emmett-Mattox, S., Crooks, S., Beers, L., Megonigal, P., Myers, D., Oreska, M., McGlathery, K., Shoch, D., 2021. Methodology for Tidal Wetland and Seagrass Restoration. Verified Carbon Standard.

Feagin, R.A., Mukherjee, N., Shanker, K., Baird, A.H., Cinner, J., Kerr, A.M., Koedam, N., Sridhar, A., Arthur, R., Jayatissa, L.P., Lo Seen, D., Menon, M., Rodriguez, S., Shamsuddoha, M., Dahdouh-Guebas, F., 2010. Shelter from the storm? Use and misuse of coastal vegetation bioshields for managing natural disasters. Conserv. Lett. https://doi.org/10.1111/j.1755-263X.2009.00087.x

Guo, H., Noormets, A., Zhao, B., Chen, Jiquan, Sun, G., Gu, Y., Li, B., Chen, Jiakuan, 2009. Tidal effects on net ecosystem exchange of carbon in an estuarine wetland. Agric. For. Meteorol. 149, 1820–1828. https://doi.org/10.1016/j.agrformet.2009.06.010

Hines, M.E., 1996. Emissions of sulfur gases from wetlands. Mitt. lntemat. Verein. Limnol. 25, 153–161. https://doi.org/10.1080/05384680.1996.11904076

Kellogg, W.W., Cadle, R.D., Allen, E.R., Lazrus, A.L., Martell, E.A., 1972. The sulfur cycle. Science. 175, 587–596. https://doi.org/10.1016/S0074-6142(08)62696-0

Kiene, R.P., 1988. Dimethyl sulfide metabolism in salt marsh sediments. FEMS Microbiol. Lett. 53, 71–78. https://doi.org/10.1016/0378-1097(88)90014-6

Kiene, R.P., Visscher, P.T., 1987. Production and fate of methylated sulfur compounds from methionine and dimethylsulfoniopropionate in anoxic salt marsh sediments. Appl. Environ. Microbiol. 53, 2426–2434.

Koskinen, M., Minkkinen, K., Ojanen, P., Kämäräinen, M., Laurila, T., Lohila, A., 2014. Measurements of CO_2 exchange with an automated chamber system throughout the year: Challenges in measuring night-time respiration on porous peat soil. Biogeosciences 11, 347–363. https://doi.org/10.5194/bg-11-347-2014

Lomans, B.P., Van der Drift, C., Pol, A., Op den Camp, H.J.M., 2002. Microbial cycling of volatile organic sulfur compounds. Water Sci. Technol. 45, 55–60. https://doi.org/10.1007/s00018-002-8450-6

Maavara, T., Lauerwald, R., Laruelle, G.G., Akbarzadeh, Z., Bouskill, N.J., Van Cappellen, P., Regnier, P., 2019. Nitrous oxide emissions from inland waters: Are IPCC estimates too high? Glob. Chang. Biol. 25, 473–488. https://doi.org/10.1111/gcb.14504

Mcleod, E., Chmura, G.L., Bouillon, S., Salm, R., Björk, M., Duarte, C.M., Lovelock, C.E., Schlesinger, W.H., Silliman, B.R., 2011. A blueprint for blue carbon: Toward an improved understanding of the role of vegetated coastal habitats in sequestering CO_2. Front. Ecol. Environ. 9, 552–560. https://doi.org/10.1890/110004

Moseman-Valtierra, S., Abdul-Aziz, O.I., Tang, J., Ishtiaq, K.S., Morkeski, K., Mora, J., Quinn, R.K., Martin, R.M., Egan, K., Brannon, E.Q., Carey, J., Kroeger, K.D., 2016. Carbon dioxide fluxes reflect plant zonation and belowground biomass in a coastal marsh. Ecosphere 7. https://doi.org/10.1002/ecs2.1560

Moseman-Valtierra, S., Gonzalez, R., Kroeger, K.D., Tang, J., Chao, W.C., Crusius, J., Bratton, J., Green, A., Shelton, J., 2011. Short-term nitrogen additions can shift a coastal wetland from a sink to a source of N_2O. Atmos. Environ. 45, 4390–4397. https://doi.org/10.1016/j.atmosenv.2011.05.046

Murray, R.H., Erler, D. V., Eyre, B.D., 2015. Nitrous oxide fluxes in estuarine environments: Response to global change. Glob. Chang. Biol. 21, 3219–3245. https://doi.org/10.1111/gcb.12923

Myers, K.H., Parsons, G.R., Edwards, P.E.T., 2010. Measuring the recreational use value of migratory shorebirds on the Delaware Bay. Mar. Resour. Econ. 25, 247–264. https://doi.org/10.5950/0738-1360-25.3.247

NASEM, 2019. Negative emissions techologies and reliable sequestration: A research agenda. https://doi.org/https://doi.org/10.17226/25259

Nellemann, C., Corcoran, E., Duarte, C.M., Valdés, L., De Young, C., Fonseca, L., Grimsditch, G. (Eds), 2009. Blue carbon: A rapid response sssessment. United Nations Environment Programme, GRID-Arendal.

O'Connell, J.L., Mishra, D.R., Cotten, D.L., Wang, L., Alber, M., 2017. The tidal marsh inundation index (TMII): An inundation filter to flag flooded pixels and improve MODIS tidal marsh vegetation time-series analysis. Remote Sens. Environ. 201, 34–46. https://doi.org/10.1016/j.rse.2017.08.008

Oremland, R.S., Marsh, L.M., Polcin, S., 1982. Methane production and simultaneous sulphate reduction in anoxic, salt marsh sediments. Nature 296, 143–145.

Ponnamperuma, F.N., 1972. The chemistry of submerged soils. Adv. Agron. 24, 29–96.

Raich, J.W., Schlesinger, W.H., 1992. The global carbon dioxide flux in soil respiration and its relationship to vegetation and climate. Tellus, Ser. B 44 B, 81–99. https://doi.org/10.3402/tellusb.v44i2.15428

Rosentreter, J.A., Al-Haj, A.N., Fulweiler, R.W., Williamson, P., 2021. Methane and nitrous oxide emissions complicate coastal blue carbon assessments. Global Biogeochem. Cycles 35, e2020GB006858. https://doi.org/10.1029/2020GB006858

Rosentreter, J.A., Maher, D.T., Erler, D. V., Murray, R.H., Eyre, B.D., 2018. Methane emissions partially offset "blue carbon" burial in mangroves. Sci. Adv. 4, eaao4985. https://doi.org/10.1126/SCIADV.AAO4985

Savage, K., Phillips, R., Davidson, E., 2014. High temporal frequency measurements of greenhouse gas emissions from soils. Biogeosciences 11, 2709–2720. https://doi.org/10.5194/bg-11-2709-2014

Sela-Adler, M., Said-Ahmad, W., Sivan, O., Eckert, W., Kiene, R.P., Amrani, A., 2015. Isotopic evidence for the origin of dimethylsulfide and dimethylsulfoniopropionate-like compounds in a warm, monomictic freshwater lake. Environ. Chem. 13, 340–351. https://doi.org/https://doi.org/10.1071/EN15042

Seyfferth, A.L., Bothfeld, F., Vargas, R., Stuckey, J.W., Wang, J., Kearns, K., Michael, H.A., Guimond, J., Yu, X., Sparks, D.L., 2020. Spatial and temporal heterogeneity of geochemical controls on carbon cycling in a tidal salt marsh. Geochim. Cosmochim. Acta 282, 1–18. https://doi.org/10.1016/j.gca.2020.05.013

Simpson, L.T., Osborne, T.Z., Feller, I.C., 2019. Wetland soil CO_2 efflux along a latitudinal gradient of spatial and temporal complexity. Estuaries and Coasts 42, 45–54. https://doi.org/10.1007/s12237-018-0442-3

Smith, C.J.J., Delaune, R.D.D., Patrick, J.W.H., Patrick, W.H., 1983. Nitrous oxide emission from Gulf Coast wetlands. Geochim. Cosmochim. Acta 47, 1805–1814. https://doi.org/10.1016/0016-7037(83)90028-5

Spivak, A.C., Sanderman, J., Bowen, J.L., Canuel, E.A., Hopkinson, C.S., 2019. Global-change controls on soil-carbon accumulation and loss in coastal vegetated ecosystems. Nat. Geosci. 12, 685–692. https://doi.org/10.1038/s41561-019-0435-2

Tian, H., Xu, R., Canadell, J.G., Thompson, R.L., Winiwarter, W., Suntharalingam, P., Davidson, E.A., Ciais, P., Jackson, R.B., Janssens-Maenhout, G., Prather, M.J., Regnier, P., Pan, N., Pan, S., Peters, G.P., Shi, H., Tubiello, F.N., Zaehle, S., Zhou, F., Arneth, A., Battaglia, G., Berthet, S., Bopp, L., Bouwman, A.F., Buitenhuis, E.T., Chang, J., Chipperfield, M.P., Dangal, S.R.S., Dlugokencky, E., Elkins, J.W., Eyre, B.D., Fu, B., Hall, B., Ito, A., Joos, F., Krummel, P.B., Landolfi, A., Laruelle, G.G., Lauerwald, R., Li, W., Lienert, S., Maavara, T., MacLeod, M., Millet, D.B., Olin, S., Patra, P.K., Prinn, R.G., Raymond, P.A., Ruiz, D.J., van der Werf, G.R., Vuichard, N., Wang, J., Weiss, R.F., Wells, K.C., Wilson, C., Yang, J., Yao, Y., 2020. A comprehensive quantification of global nitrous oxide sources and sinks. Nature 586, 248–256. https://doi.org/10.1038/s41586-020-2780-0

Tobias, C., Neubauer, S.C., 2019. Salt marsh biogeochemistry – An overview, in: Perillo, G.M.E., Wolanski, E., Cahoon, D.R., Hopkinson, C.S. (Eds.), Coastal Wetlands: An Integrated Ecosystem Approach. Elsevier B.V., Amsterdam, pp. 539–596. https://doi.org/https://doi.org/10.1016/B978-0-444-63893-9.00016-2539

U.S. DOE, 2022. DOE Explains...Earth System and Climate Models [WWW Document]. URL https://www.energy.gov/science/doe-explainsearth-system-and-climate-models (accessed 4.6.22).

UNFCCC, 2015. Paris Agreement.

Vargas, R., Carbone, M.S., Reichstein, M., Baldocchi, D.D., 2011. Frontiers and challenges in soil respiration research: from measurements to model-data integration. Biogeochemistry 102, 1–13. https://doi.org/10.1007/s10533-010-9462-1

Watts, S.F., 2000. The mass budgets of carbonyl sulfide, dimethyl sulfide, carbon disulfide and hydrogen sulfide. Atmos. Environ. 34, 761–779. https://doi.org/10.1016/S1352-2310(99)00342-8

Whelan, M.E., Min, D.H., Rhew, R.C., 2013. Salt marsh vegetation as a carbonyl sulfide (COS) source to the atmosphere. Atmos. Environ. 73, 131–137. https://doi.org/10.1016/J.ATMOSENV.2013.02.048

Windham-Myers, L., Cai, W.-J., Alin, S., Andersson, A., Crosswell, J., Dunton, K.H., Hernandez-Ayon, J.M., Herrmann, M., Hinson, A.L., Hopkinson, C.S., Howard, J., Hu, X., Knox, S.H., Kroeger, K., Lagomasino, D., Megonigal, P., Najjar, R., Paulsen, M.-L., Peteet, D., Pidgeon, E., Schäfer, K., Tzortziou, M., Wang, Z.A., Watson, E.B., 2018. Chapter 15: Tidal Wetlands and Estuaries. Second State of the Carbon Cycle Report 596–648. https://doi.org/10.7930/SOCCR2.2018.Ch15

Xiao, K.Q., Beulig, F., Røy, H., Jørgensen, B.B., Risgaard-Petersen, N., 2018. Methylotrophic methanogenesis fuels cryptic methane cycling in marine surface sediment. Limnol. Oceanogr. 63, 1519–1527. https://doi.org/10.1002/lno.10788

Zhuang, G.-C., Heuer, V.B., Lazar, C.S., Goldhammer, T., Wendt, J., Samarkin, V.A., Elvert, M., Teske, A.P., Joye, S.B., Hinrichs, K.-U., 2018. Relative importance of methylotrophic methanogenesis in sediments of the Western Mediterranean Sea. Geochim. Cosmochim. Acta 224, 171–186. https://doi.org/10.1016/j.gca.2017.12.024

Chapter 2

EXPERIMENTAL INFLUENCE OF STORM-SURGE SALINITY ON GREENHOUSE GAS EMISSIONS FROM A TIDAL SALT MARSH

As published in *Science of the Total Environment*, 2019

DOI: 10.1016/j.scitotenv.2019.06.032

Margaret Capooci[1], Josep Barba[1], Angelia L. Seyfferth[1], Rodrigo Vargas[1]

[1] Department of Plant and Soil Sciences, University of Delaware, Newark, DE, USA

Abstract

Storm surges can substantially alter the water level and salinity in tidal salt marshes. Little is known about how changes experienced during storm surges affect greenhouse gas emissions (GHG; CO_2, CH_4, N_2O) from tidal salt marsh soils. Understanding how storm surges influence ecosystem processes is critical for evaluating the ecosystem's sensitivity to sea level rise. To explore how hurricane-induced changes in salinity affect GHG emissions, we exposed intact soil mesocosms (0–9 cm depth) from a Mid-Atlantic temperate salt marsh to pulse changes in salinity experienced at the site before, during, and after Hurricane Joaquin in 2015. Soil temperature, oxygen, and water level were kept constant to avoid confounding effects throughout the experiment. Automated measurements (hourly resolution) of soil GHG emissions were recorded in control (i.e., no salinity changes) and treatment

mesocosms, and combined with soil pore water chemistry (i.e., SO_4^{2-}, S^{2-}, Fe^{2+}, TN_b, redox potential, pH) to characterize the biogeochemical responses. Using mixed effects models, we found that the role of different biogeochemical processes, such as sulfur cycling, changed throughout the experiment, underscoring the complex nature of GHG emissions in tidal salt marsh soils. Overall, soils subjected to a salinity decrease had greater GHG emissions than control soils, which were maintained at 17 ppt. The treatment soils had a 24% and 23% increase in global warming potential (20- and 100-year scenarios, respectively) indicating that storm surges can produce pulses of GHG emissions. However, both CH_4 and N_2O emissions returned to baseline values (following hysteresis responses) when initial conditions were reestablished. The results support the fact that tidal salt marshes are resilient ecosystems, as soil GHG emissions recovered relatively quickly from the pulse event.

Highlights

- Studied the influence a pulse-change in salinity on salt marsh GHG biogeochemistry
- Coupled automated GHG measurements with pore water chemistry
- CO_2 decreased with decreased salinity; CH_4 and N_2O fluxes increased
- Salt marsh soils recovered from salinity changes relatively quickly

Keywords

Carbon cycle, biogeochemistry, extreme events, automated measurements

Graphical Abstract

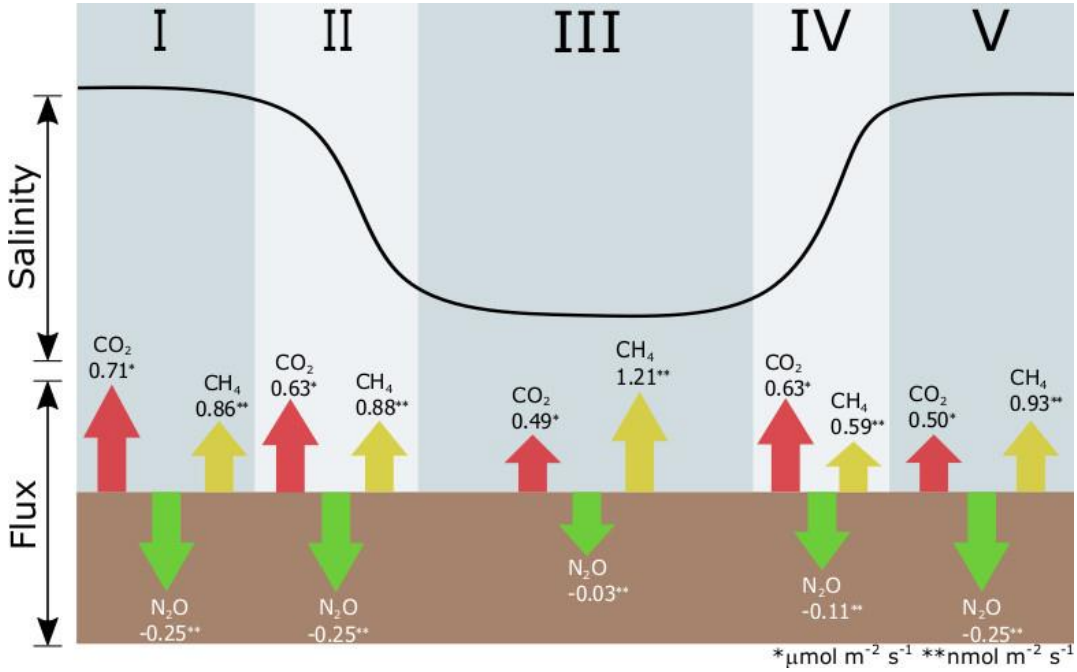

Figure 2.1: Graphical abstract showing how CO_2, CH_4, and N_2O fluxes changed throughout the different salinity stages (stages are denoted I, II, III, IV, V and salinity is represented by the black line). Numbers above/below each arrow denotes the mean flux for the respective gas during each phase. The asterisks (*, **) denote the flux units. Positive values indicate emission into the atmosphere, while negative values indicated uptake by the soil.

2.1 Introduction

Tidal salt marshes provide a wide variety of ecosystem services, including reactive nitrogen removal and carbon storage (Jordan et al., 2011; Valiela and Teal, 1979). Carbon stored in these ecosystems, along with mangrove forests and seagrass beds, is termed "blue carbon" and has become a topic of global interest. In the United States, wetlands cover 44.6 million hectares, with 2.6 million (5.8%) of the total comprised of salt marshes (Dahl, 2011; Dahl and Stedman, 2013). Despite their small area, salt marshes can sequester C at high rates with an average of 218 ± 24 g C m^{-2} yr^{-1} (McLeod et al., 2011). Blue carbon research typically focuses on quantifying C stocks and assessing how they will change under various climate change scenarios. However, there is also a need to quantify baselines for a wide range of greenhouse gas (GHG; CO_2, CH_4, N_2O) emissions and to ascertain how these fluxes are influenced by weather changes, particularly by pulse events (Crooks et al., 2011; McLeod et al., 2011).

According to the Intergovernmental Panel on Climate Change (IPCC), coastal systems will likely experience shifts in the frequency and/or intensity of storm events. For example, while hurricane frequency is not expected to change (Wong et al., 2014), storm intensity is likely to increase, with higher wind speeds and precipitation rates. Furthermore, the IPCC found that storm surges increased in the past 48 years, likely due to sea level rise (IPCC, 2014). Therefore, there is increased potential for storm surges and flooding from both terrestrial and oceanic storm events in coastal areas (IPCC, 2014). Thus, there is a critical need to assess how salt marsh GHG emissions respond to the salinity and tidal inundation shifts caused by hurricanes. These data may be useful for predicting how these ecosystems will respond to changing weather conditions and future climate scenarios.

In tidal salt marshes, CO_2 emissions from soils (i.e., soil CO_2 efflux) ranges from 240 to 720 g C m^{-2} y^{-1} and arises from a variety of processes, including autotrophic respiration and decomposition of organic matter via aerobic and anaerobic microorganisms (i.e. heterotrophic respiration) (Tobias and Neubauer, 2019). Due to the flooded soil conditions of tidal salt marshes, anaerobic respiration dominates. The most energetically-favorable electron acceptor, O_2, gets used rapidly near the soil surface. As a result, facultative anaerobic or strict anaerobic microorganisms use other electron acceptors, including NO_3^-, Fe^{3+}, SO_4^{2-}, and even CO_2, to produce GHGs (Ponnamperuma, 1972). Furthermore, as salinity changes, the proportion of various ions changes as well. Higher salinity water has higher levels of SO_4^{2-} due to greater ocean water inputs, which changes the proportions of available electron acceptors in anaerobic soils and the amount of CO_2 emitted. For example, if a storm event decreases the salinity of the marsh, there is the potential for a decrease in SO_4^{2-} availability, which may result in a decrease in CO_2 emissions (Chambers et al., 2013) and an increase in CH_4 emissions (Capone and Kiene, 1988). Therefore, there is a pressing need to provide information regarding how changes in salinity influence soil CO_2 and CH_4 efflux rates in salt marshes.

While wetlands do not contribute significantly to global CO_2 emissions, they are the largest natural source of CH_4 to the atmosphere (IPCC, 2000). CH_4 has a global warming potential 25 times that of CO_2 (Forster et al., 2007). In North America, freshwater wetlands emit CH_4 at a rate of 36.0 ± 5.0 g C m^{-2} yr^{-1}, while salt marshes emit CH_4 at a much lower rate of 3.6 ± 5.0 g C m^{-2} yr^{-1} (Bridgham et al., 2006). Salinity is a major control on CH_4 emissions in salt marshes, with higher salinity generally resulting in lower emissions (Poffenbarger et al., 2011). It is thought that the

limited amount of CH_4 released from salt marshes is due to methanogens being outcompeted for electron donors by SO_4^{2-} and Fe^{3+} reducers (Furukawa et al., 2004; King and Wiebe, 1978). Storm events can change the salinity of the water in tidal salt marshes on a short time-scale, causing an increase or decrease of CH_4 depending on proportion of freshwater to oceanic inputs during the flooding stage. Accordingly, these pulse events might result in changes in short-term emission of CH4 in tidal salt marshes.

In addition to CO_2 and CH_4, wetlands also emit small quantities of N_2O, which has a global warming potential 298 times that of CO_2 (Forster et al., 2007). However, wetlands can become small sinks of N_2O (Audet et al., 2014; Jørgensen and Elberling, 2012; Schaufler et al., 2010). The production and consumption of N_2O in wetlands appears to be strongly influenced by water level and its effect on O_2 availability in the soil (Davidson, 1991; Jørgensen and Elberling, 2012; Kliewer and Gilliam, 1995; Martikainen et al., 1993). N_2O production is more likely to occur during low levels of O_2 (Liikanen and Martikainen, 2003); however, depending on the conditions of the soil (i.e., gas transport properties, N_2O consumption rate, water level), the N_2O may be converted to N_2 or consumed before it gets emitted to the atmosphere (Chapuis-Lardy et al., 2007; Clough et al., 2005; Heincke and Kaupenjohann, 1999). Additionally, salinity has been shown to inhibit complete denitrification, potentially allowing for a build-up of N_2O (Inubushi et al., 1999; Menyailo et al., 1997). If a storm event lowers salinity levels, in addition to flooding the soils, there will likely be less build-up of N_2O in the soils due to less inhibition of complete denitrification. However, to the best of our knowledge, only one study has investigated the effects of storm events on N_2O production and consumption in tidal salt marshes (Diefenderfer et al., 2018).

For this study, we conducted a mesocosm experiment that simulated a decrease in salinity associated with a hurricane-induced storm surge event that was dominated by freshwater precipitation inputs. We used an automated system to continuously measure CO_2, CH_4, and N_2O emissions from soil mesocosms to obtain high temporal data resolution (hourly basis) and coupled these measurements with pore water chemical analyses. We hypothesized that: a) emissions of all three GHGs would increase with decreasing salinity due to less inhibition (i.e. more favorable redox conditions due to reduced SO_4^{2-} concentrations) on the biogeochemical processes that produce the GHGs; and b) the temporal pattern of GHG emissions would respond to the salinity regime and the subsequent shifts in potential biogeochemical pathways, such as sulfur and iron reduction.

2.2 Materials and methods

2.2.1 Study site and soil collection

Soil cores were collected from St. Jones Reserve, a subsection of the Delaware National Estuarine Research Reserve located near Dover, Delaware (39°05″ N, 75°26″ W). The site comprises mostly of a tidal salt marsh with salinities typically in the mesohaline range (5–18 ppt) (DNREC, 1999). The marsh is connected to the Atlantic Ocean via the St. Jones River and the Delaware Bay. Dominant plant species within the marsh include *Spartina alterniflora*, *Spartina patens*, and *Spartina cynosuroides*. The marsh soils are classified as a silty clay loam (10% sand, 61% silt, and 29% clay) as measured by the University of Delaware's Soil Testing Lab.

2.2.2 Mesocosms flow-through incubation

Six intact soil cores (i.e., mesocosms; 20 cm in diameter, 9 cm deep) were collected within a 1 x 1 m area near a tidal creek to ensure the mesocosms were as similar to each other as possible. Mesocosms were collected in January 2017 within a PVC collar, fixed to a polyethylene board, and sealed with duct tape to prevent soil and water loss during transport to the laboratory using previously reported methods (Northrup et al., 2018; Petrakis et al., 2017a). River water from the St. Jones River and Murderkill River (both <5 km from where the soils where collected), which differ in salinity (8.2 ± 1.8 ppt and 27.2 ± 1.1 ppt, respectively), was used to maintain continuously flooded conditions and to manipulate salinity levels during the experiment.

The experiment was designed to simulate salinity patterns observed during storm surges, such as the one produced by Hurricane Joaquin in 2015 at the site (Fig. 2.2a), when the water level in the tidal creek increased due to a combination of oceanic storm surge and freshwater rain inputs. As a result, the water (i.e., a mix of costal ocean and rain water sources) overtopped the creek banks and flooded the high marsh, which typically does not flood during high tides. The salinity in the tidal creek changed as well. The salinity decreased during the storm surge from 17 ppt to 12 ppt and remained stable for 12 days, before increasing again back to 17 ppt. The experiment was designed to replicate the salinity changes in the creek and was divided into five phases to capture GHG and pore water changes before, during, and shortly after the pulse event. The five phases were: I – 17 ppt, II – 17 to 12ppt, III – 12ppt, IV – 12 to 17ppt, and V– 17 ppt. Three mesocosms received the experimental treatment, while three replicate mesocosms served as controls, maintaining a salinity of 17 ppt,

the average high tide salinity in the St. Jones River in 2015 (NOAA National Estuarine Research Reserve System (NERRS), 2015).

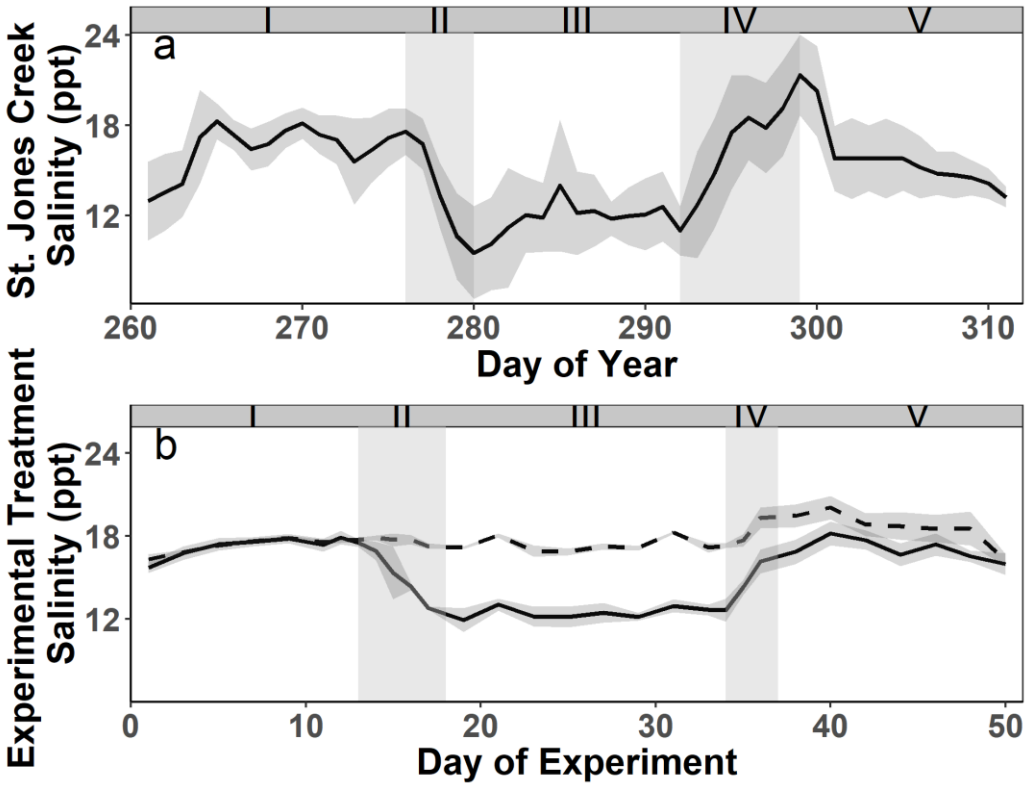

Figure 2.2: (a) Average daily salinity values before, during, and after Hurricane Joaquin's storm surge at St. Jones Reserve, Dover, DE in 2015 (NOAA National Estuarine Research Reserve System (NERRS), 2015). (b) Average daily experimental control (dashed line) and treatment (solid line) salinity data. In both graphs, shading denotes ± 1 SD. Salinity data at the study site was collected using a YSI 6600 (Yellow Springs, Ohio) probe.

For each mesocosm, we designed a flow-through system where water was pumped on top of the mesocosm (at a flow rate of 1.05 mL/min) and out the bottom of

the mesocosm (at a flow rate of 0.89 mL/min) using a peristaltic pump (Golander BT100s, Norcross, Georgia). The water table was maintained at 2 cm above the soil surface to replicate the flooded conditions during the storm surge. Salinity was changed by changing the proportions of the higher salinity Murderkill River water and the lower salinity St. Jones River water at predetermined points during the experiment. The outflow tubing was capped with a 100 μm nylon mesh to minimize soil loss. The flow-through system was designed to maintain hydrological connectivity and flooded conditions for the duration of the experiment. Soil temperature was maintained at a constant 22°C to avoid confounding effects.

Each soil mesocosm was instrumented with a soil moisture probe (Li-COR 8150–202, Lincoln, Nebraska) and a soil temperature sensor (Li-COR 8150–203, Lincoln, Nebraska). Oxygen sensors (Fibox 4, PreSens, Germany) were instrumented in three randomly selected mesocosms (1 control, 2 treatment mesocosms) to confirm that anoxic conditions were kept throughout the experiment. Additionally, a Rhizon sampler (Eikjelkamp, The Netherlands) was inserted into the soil of each mesocosm at a 45° angle for porewater collection using previously described methods (Seyfferth and Fendorf, 2012).

2.2.3 Greenhouse gas flux measurement and calculation

Greenhouse gas (GHG; CO_2, CH_4, N_2O) fluxes were measured in each soil mesocosm once per hour for the duration of the experiment using automated chambers (Li-COR 8100–104, Lincoln, Nebraska) coupled with both a closed-path infrared gas analyzer (LI-8100A, Li-COR, Lincoln, Nebraska) and a cavity ring-down spectrometer (Picarro G2508, Santa Clara, California) as described in previous studies (Petrakis et al., 2017a, 2017b). For each flux observation, gas concentrations were

measured every second for 3 min. Fluxes were calculated using Soil Flux Pro (v4.0: Li-COR, Lincoln, Nebraska) following the quality assurance and quality control protocol established in Petrakis et al. (2017b), with the following modification: if CO_2 fluxes had an $R^2 > 0.90$, we considered the micrometeorological conditions inside the chambers were stable enough for calculating the fluxes and the measurements for all three gases were kept. Measurements that did not meet this threshold were marked as not-a-number (NaN).

2.2.4 Soil pore water extraction and analysis

Soil pore water (~20 mL) was extracted every other day during Phase I, III, and V, and every day during Phase II and IV when salinity changes in treatment mesocosms were rapid. Pore water was collected into vials that were previously purged with N_2 and crimp sealed in an anaerobic glove bag (95% N_2/5% H_2). For all samples, salinity, pH, redox potential, sulfide, and ferrous iron were measured as described in Northrup et al. (2018). Sulfate was measured using a Dionex DX-500 (Sunnyvale, California). Additionally, TN_b was measured using an Elementar Vario-TOC Cube (Elementar Americas, Mount Laurel, New Jersey). TN_b measures a variety of dissolved nitrogen compounds, such as ammonia, nitrites, and nitrates.

2.2.5 Data analyses

Daily, hourly, and by phase flux averages were calculated for each gas for both the control and the treatment mesocosms. Averages are reported as mean ± SD. The Mann-Whitney *U* test was used to test for differences between the treatment and the control for each phase of the experiment.

Mixed effects models using daily data for each mesocosm were run on each experimental phase for each of the three gases to analyze the relationships between the gas fluxes and the pore water variables (salinity, pH, redox, sulfide, sulfate, ferrous iron, TN_b). Only variables and ecologically relevant first-order interactions were included in the saturated model to eliminate potential spurious correlations. Temperature, soil water content, and oxygen concentration were not included in the models because they were constant throughout the experiment. Prior to running the analyses, all variables were centered and scaled to improve the model's performance and to simplify the interpretation of the results (Gelman and Hill, 2007). The variance inflation factor (VIF) was tested for each model to ascertain if there were collinearity between variables and their interactions. If VIF > 3 for a variable and/or an interaction, we removed that variable from the model (Zuur et al., 2010). We included mesocosm identification in the random part of the model in order to account for temporal autocorrelation between measurements. For each gas and phase, we evaluated all possible models combining predictor variables and relevant first-order interactions in order to achieve the minimum adequate model in terms of the corrected Akaike Information Criterion (AIC_c). The AIC_c accounts for model overfitting. The best model was reported in the results.

The global warming potential (GWP), which converts the cumulative radiative forcing capacity of CH_4 and N_2O to CO_2 equivalents, was calculated by multiplying the cumulative daily sums (g m^2 day^{-1}) of the control and treatment emissions by their respective 20 and 100 year GWP scenarios (86 and 34 for CH_4, 268 and 298 for N_2O, respectively) to convert them into CO_2 equivalencies (CO_2-eq) (Myhre et al., 2013).

We report the 20 and 100 year GWP in CO_2-eq for each GHG flux as a practice to account for ranges in carbon-climate feedbacks (Petrakis et al., 2017b).

All analyses were carried out using R 3.4.3 (R Foundation for Statistical Computing, Vienna, Austria). Mixed effects models were performed using the R *nlme* package (Pinheiro et al., 2018) and model selection and comparison was done with the R *MuMIn* package (Barton, 2018).

2.3 Results

2.3.1 Experimental conditions

The salinity regime for the treatment mesocosms closely resembled the salinity changes that occurred during the Hurricane Joaquin storm surge (Fig. 2.2). Soils were constantly flooded, so soil oxygen levels were low, averaging 0.02 ± 0.16% throughout the experiment. The volumetric water content of the mesocosms was 0.42 ± 0.01 m^3/m^3. The soil temperature was 21.4 ± 0.5°C.

2.3.2 Soil greenhouse gas fluxes

CO_2 fluxes for the treatment and the control were similar throughout the first three phases of the experiment (Figs. 2.3a, 2.4a). By Phase IV, the CO_2 emissions from the treatment mesocosms were significantly higher than the control and remained so in Phase V ($p = 0.03$, p b 0.001, Fig. 2.4a). Fig. 2.3a shows a noticeable increase in treatment CO_2 emissions beginning at the end of Phase III and continuing midway through Phase V, which is reflected by the darker red colors in the heat maps (Fig. 2.3b, c).

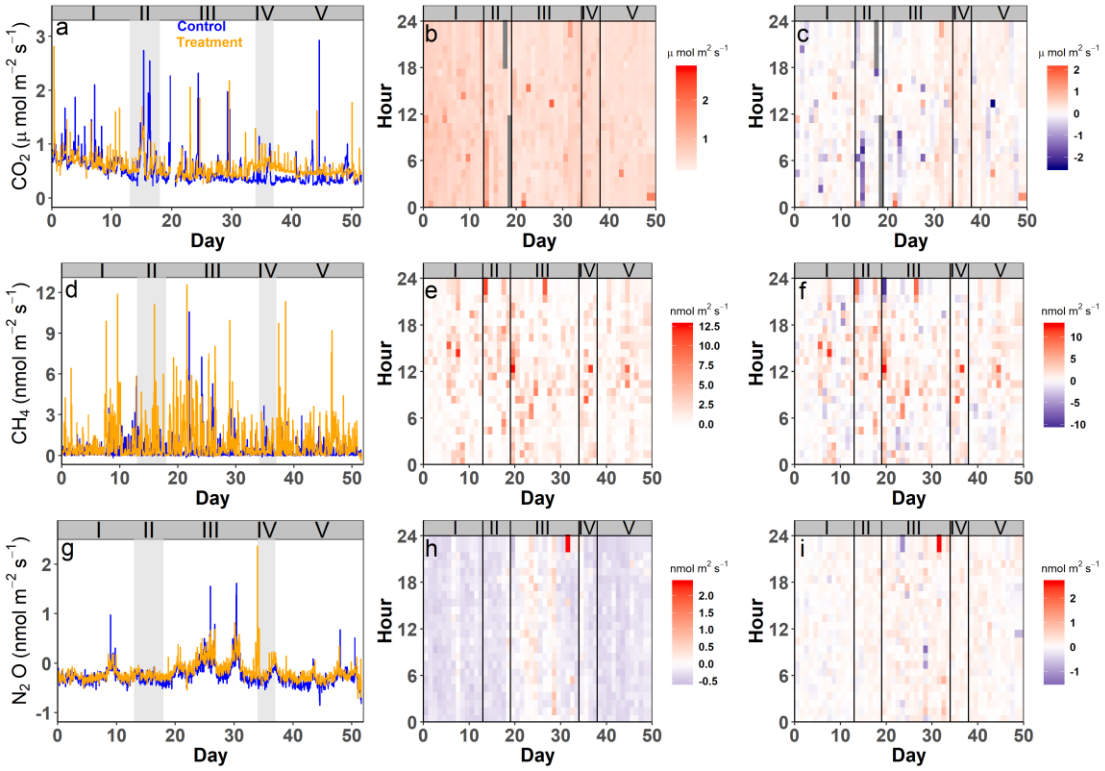

Figure 2.3: Averaged hourly time series of CO_2, CH_4, and N_2O, respectively (a, d, g). Heat maps of the hourly fluxes for each GHG gas in the treatment mesocosms (b, e, h). Heat maps of the difference between the treatment and control (c, f, i). For each heat map, each pixel represents the hourly average (b, e, h) or the difference between the hourly average of the treatment and the control for that day and time (c, f, i).

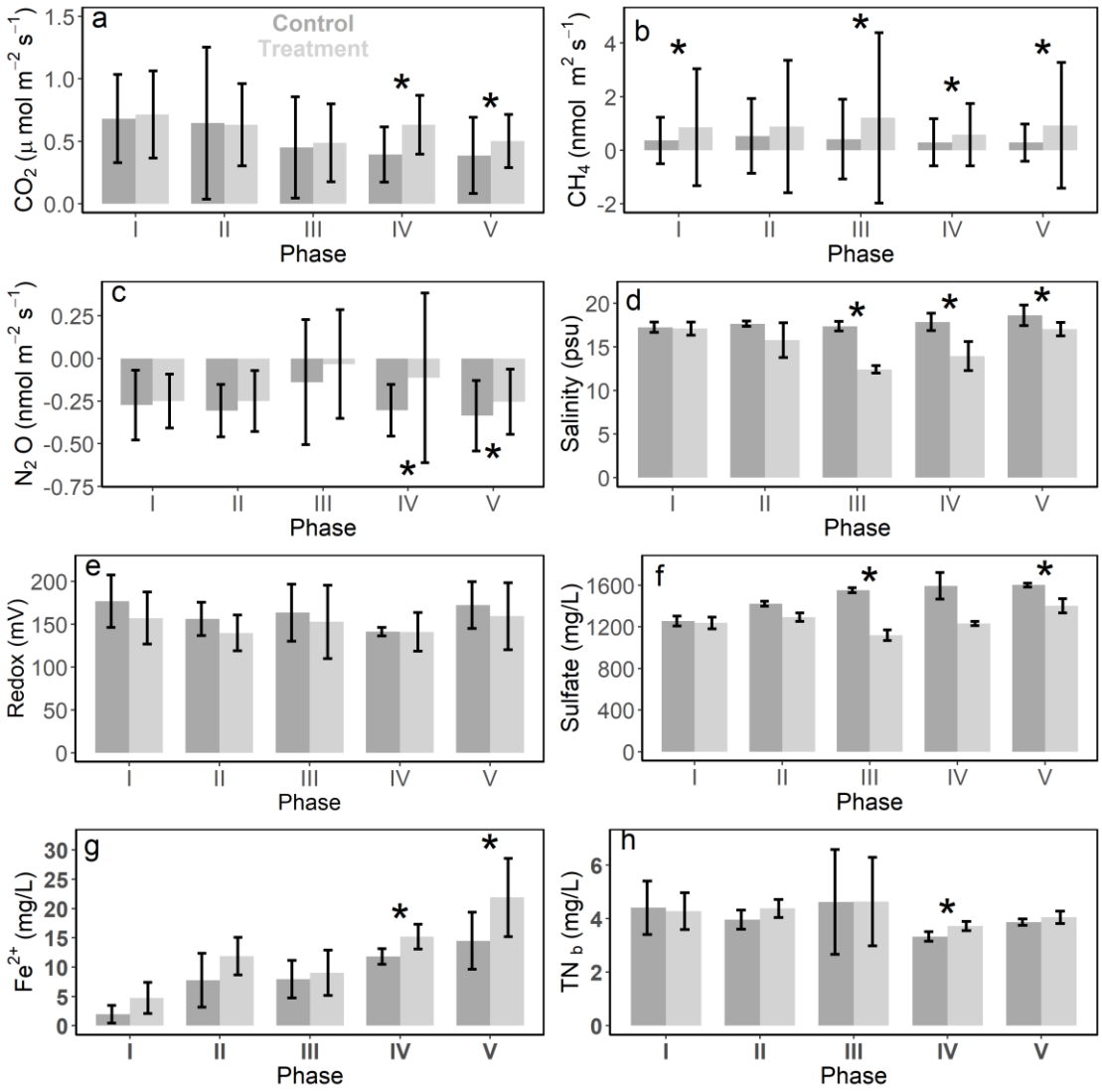

Figure 2.4: Bar graphs of the average by phase of the control and treatment of (a) CO_2, (b) CH_4, (c) N_2O, (d) salinity, (e) redox potential, (f) SO_4^{2-}, (g) Fe^{2+}, and (h) TN_b. Error bars represent ± 1 SD and asterisks indicate significant differences ($\alpha = 0.05$) between treatment and the control with the Mann-Whitney *U* test. Dark gray bars represent the control and light gray bars represent the treatment results.

CH_4 fluxes from the treatment mesocosms were more variable than the control mesocosms, particularly when the salinity decreased and remained low during Phases

II and III and right after the increase of salinity in Phase IV (Fig. 2.3d). In Phases I, III, IV, and V, the treatment mesocosms had significantly higher emissions than the control soils (p = 0.005, p b 0.001, p = 0.03, p b 0.001, Fig. 2.4b).

N_2O fluxes for both the control and the treatment mesocosms showed similar patterns and values throughout the experiment, with the treatment fluxes slightly increasing during Phases II, III, and IV, before declining back towards the control fluxes in Phase V (Fig. 2.3g, i). The treatment was significantly different from the control in Phases IV and V (p = 0.05, p = 0.04, Fig. 2.4c). For most of the experiment, the soils were sinks of N_2O, but in Phase III, both the control and the treatment mesocosms became sources of N_2O (Fig. 2.3g, h). Means by phase for each mesocosm are presented in Fig. A.1.

2.3.3 Soil pore water

Salinity was significantly different between the control and the treatment for Phases III (17.4 ± 0.5 ppt vs 12.4 ± 0.4 ppt, $p < 0.001$), IV (17.9 ± 1.0 ppt vs 14.0 ± 1.7 ppt, $p < 0.001$), and V (18.6 ± 1.2 ppt vs 17.0 ± 0.8 ppt, p = 0.03) (Fig. 2.4d). Redox (Fig. 2.4e), pH, and sulfide were not significantly different between control and treatment mesocosms for all phases of the experiment (Table A.1). While sulfide did not show significant differences between the treatment and the control, SO_4^{2-} was significantly higher in the control than the treatment in Phases III (306.9 ± 23.4 mg/L vs 206.9 ± 5.0 mg/L, $p < 0.001$) and V (316.6 ± 18.9 mg/L vs 260.0 ± 68.3 mg/L, p = 0.001) (Fig. 2.4f). For both the treatment and the control, Fe^{2+} concentrations increased as the experiment went on, with the treatment having significantly higher Fe^{2+} concentrations during Phases IV (11.8 ± 1.3 mg/L vs 15.3 ± 2.1 mg/L, p = 0.05) and V (14.5 ± 4.9 mg/L vs 21.9 ± 6.7 mg/L, p = 0.05) (Fig. 2.4g). The TN_b

concentrations were similar between control and treatment for most of the experiment, except in Phase IV, when the treatment had significantly higher concentrations than the control (3.33 ± 0.2 mg/L vs ± 3.72 ± 0.2, p = 0.03, Fig. 2.4h).

2.3.4 GHG flux hysteresis

We assessed whether the average GHG flux measured at the beginning of the experiment (Phase I) was recovered (or not) by Phase V. For CO_2, there was a clockwise hysteresis effect. The average flux in the beginning was higher than all subsequent phases (Fig. 2.5a). As the salinity decreased in Phase II and remained low in Phase III, the average CO_2 flux decreased along with it. When the salinity increased in Phase IV, the fluxes increased as well, and then decreased in Phase V. The average CO_2 fluxes at the beginning and the end of the experiment were significantly different (0.71 ± 0.35 μmol m^{-2} s^{-1} vs 0.50 ± 0.21 μmol m^{-2} s^{-1}).

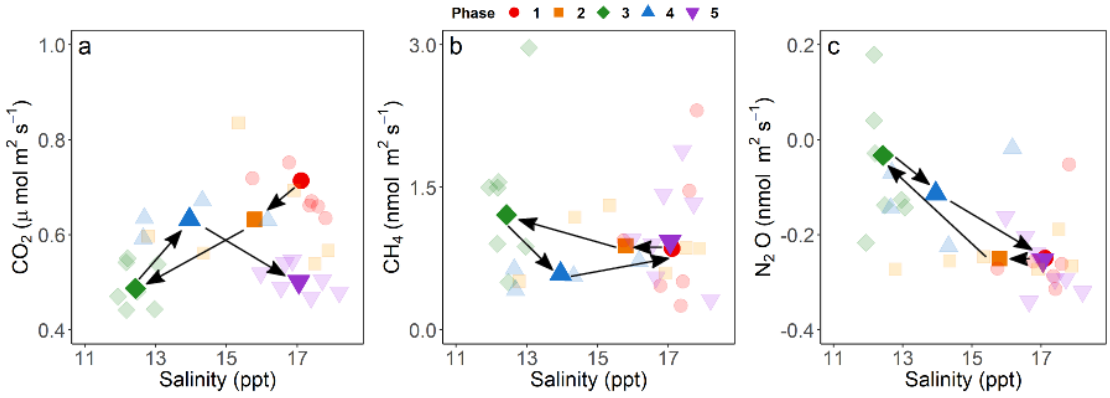

Figure 2.5: Hysteresis graphs of (a) CO_2, (b) CH_4, and (c) N_2O for the treatment mesocosms. Arrows indicate the direction of the hysteresis loop. Bolded shapes are the average flux and salinity values for each phase combining all treatment mesocosms. Faded shapes for the daily average flux and salinity values within each phase combining all treatment mesocosms.

CH_4 fluxes demonstrated a counter-clockwise hysteresis effect, increasing with decreasing salinity as seen by the increase in the average flux from Phase I to Phase III (Fig. 2.5b). When salinity increased in Phase IV, the average flux decreased, before increasing slightly in Phase V. The average CH_4 fluxes at the beginning and the end of the experiment were not significantly different (0.86 ± 2.18 nmol m^{-2} s^{-1} vs 0.93 ± 2.35 nmol m^{-2} s^{-1}).

Similar to CO_2, average fluxes of N_2O exhibited a slight clockwise hysteresis loop with N_2O fluxes increasing with decreasing salinity (Phases I - Phase III), before decreasing with an increase in salinity, as seen in the transition from Phase III to Phase V (Fig. 2.5c). The average N_2O fluxes in the beginning and the end of the experiment were not significantly different (-0.25 ± 0.16 nmol m^{-2} s^{-1} vs -0.25 ± 0.19 nmol m^{-2} s^{-1}).

2.3.5 Mixed effects models

For all gases, the variables that contributed to the changes in fluxes throughout the experiment differed among phases. Phase I represented conditions before the salinity treatment, no variables were significant because there was no difference between treatment and control collars, and fluxes were stable (i.e., null model was the best model in Phase I for the three gases; Table 2.1). The mixed effects model for CO_2 during Phase II was not significant, while the model for Phase III showed that variations in redox, along with pH, sulfide, and TN_b explained 49% of the variability in CO_2 fluxes, with pH having the strongest effect. Phase IV was not significant, while Phase V had 53% of its variability explained by changes in salinity and sulfate. For CH_4, only the model for Phase II was significant. All others (Phases I, III, IV, V) were not significant. For Phase II, pH and sulfide explained 49% of the

CH_4 variability. All of the N_2O models were significant (except for Phase I) and explained a large portion of N_2O variability. Sixty-two percent of the variability in N_2O fluxes during Phase II was explained by redox changes. Meanwhile, in Phase III, a variety of parameters contributed to explain 64% of the variation in N_2O flux, with the interaction between sulfate and sulfide having a strong positive effect. During Phase IV, the change in sulfide explained 72% of the flux. Sulfide had a negative relationship with N_2O during this phase. In the final phase of the experiment, redox and salinity contributed to 71% of the variation in N_2O fluxes.

2.3.6 Global warming potential

Over the duration of the experiment, the treatment mesocosms had higher emissions of CO_2 and CH_4 and were less of a N_2O sink than the control mesocosms (Table 2.2). The treatment mesocosms have a roughly 24% and 23% higher GWP than the control, for the 20- and 100-year scenarios, respectively.

Table 2.1: Summary of the results of the mixed effect model for each greenhouse gas (CO_2, CH_4, and N_2O) for each phase of the experiment. n.s. = not significant. Averages are reported as mean ± sd.

Model	Variable	Coefficient	SE	t-value	*p*-value
CO_2 – Phase I	n.s.				
CO_2 – Phase II	n.s.				
CO_2 – Phase III	Intercept	-0.38	0.18	-2.17	0.04
adj. R^2 = 0.49	pH	0.58	0.15	3.96	0.0004
P-value < 0.001	Redox	-0.17	0.09	-1.78	0.09
	Sulfide	0.51	0.20	2.56	0.02
	TN_b	-0.26	0.07	-3.79	0.0007
CO_2 – Phase IV	n.s.				
CO_2 – Phase V	Intercept	-0.26	0.15	-1.78	0.09
adj. R^2 = 0.53	Salinity	-0.37	0.17	-2.24	0.03
P-value = 0.008	Sulfide	-0.19	0.10	-1.86	0.07
CH_4 – Phase I	n.s.				
CH_4 – Phase II	Intercept	-0.04	0.21	-0.21	0.84
adj. R^2 = 0.49	pH	0.19	0.07	2.82	0.01
P-value = 0.009	Sulfide	0.09	0.06	1.55	0.13
CH_4 – Phase III	n.s.				
CH_4 – Phase IV	n.s.				
CH_4 – Phase V	n.s.				
N_2O – Phase I	n.s.				
N_2O – Phase II	Intercept	-0.37	0.21	-1.77	0.09
adj. R^2 = 0.62	Redox	-0.23	0.10	-2.36	0.03
P-value = 0.02					
N_2O – Phase III	Intercept	0.41	0.38	1.08	0.29
adj. R^2 = 0.64	Redox	0.37	0.12	2.93	0.01
P-value < 0.001	Sulfate	-0.19	0.21	-0.91	0.37
	Sulfide	0.61	0.25	2.40	0.02
	TN_b	-0.33	0.08	-3.97	0.001
	Salinity	-0.47	0.27	-1.71	0.10
	Sulfate*Sulfide	0.77	0.27	2.86	0.01
N_2O – Phase IV	Intercept	0.20	0.38	0.52	0.61
adj. R^2 = 0.72	Sulfide	-1.00	0.20	-5.07	0.0003
P-value < 0.001					
N_2O – Phase V	Intercept	-0.15	0.23	-0.64	0.53
adj. R^2 = 0.71	Redox	-0.21	0.06	-3.52	0.002
P-value < 0.001	Salinity	-0.51	0.17	-2.96	0.006

Table 2.2: The GWP of the control and the treatment cumulative GHG emissions over the entire experiment for the 20- and 100-year scenarios.

	CO_2 ($g\ m^{-2}$)	**CH_4** ($CO_{2\text{-eq}}$ ($g\ m^{-2}$))		**N_2O** ($CO_{2\text{-eq}}$ ($g\ m^{-2}$))		**Total** ($CO_{2\text{-eq}}$ ($g\ m^{-2}$))	
	Mean ± SD	20-year GWP scenario	100-year GWP scenario	20-year GWP scenario	100-year GWP scenario	20-year GWP scenario	100-year GWP scenario
Control	99.5 ± 57.1	2.3 ± 5.7	0.90 ± 0.3	-13.8 ± 9.7	-15.3 ± 10.8	88 ± 72.5	85.1 ± 68.2
Treatment	112.6 ± 48.3	5.9 ± 13.4	2.39 ± 5.3	-9.49 ± 11.2	-10.5 ± 12.5	109 ± 72.9	10.4 ± 66.1

2.4 Discussion

We sought to examine the changes in GHG emissions due to dynamic shifts in salinity before, during, and after a storm surge. High frequency measurements of GHG emissions coupled with pore water measurements were used to capture both immediate and temporal trends in GHG fluxes with changes in salinity. Thus, we were able to gain insights into the relative importance of various biogeochemical processes throughout the experiment.

As salinity decreased and remained low during Phases II and III, CO_2 emissions and porewater SO_4^{2-} decreased, while CH_4 emissions increased (Figs. 2.3a, d, 2.4a, b, f). A positive relationship between sulfide and CO_2 was found during Phase III. As the supply of SO_4^{2-} declined due to less oceanic water inputs, the amount of sulfide in the pore water increased due to sulfate reduction, releasing CO_2 in the process. At the same time, however, CH_4 emissions increased due to less competition from sulfate reducers (King and Wiebe, 1978), producing CH_4 from CO_2 during the process of methanogenesis and reducing the overall amount of CO_2 emitted from the mesocosms. Subsequently, when salinity increased during Phase IV and stabilized in

Phase V, CO_2 emissions increased and CH_4 decreased. As more saline water containing SO_4^{2-} entered the mesocosms, sulfate reduction became more energetically favorable than methanogenesis, resulting in increased CO_2 production and decreased CH_4 production (Capone and Kiene, 1988). During Phase V, there was a near significant negative relationship between CO_2 and SO_4^{2-}, as SO_4^{2-} was chemically reduced and more CO_2 was produced (Table 2.1, Chambers et al., 2013). These results underscore the dynamics between sulfur cycling and CO_2 and CH_4 emissions in tidal salt marsh soils.

Throughout the experiment, GHG emissions, particularly CH_4, were highly variable despite controlled temperature and soil moisture conditions (Fig. 2.3e). These spikes in CH_4 may be considered hot moments (i.e., short periods of disproportionately high fluxes relative to the time series as a whole (Leon et al., 2014; McClain et al., 2003)). Mechanistically, hot moments occur when all the reactants for a biogeochemical reaction are present at the same time (McClain et al., 2003). The spikes in CH_4 emissions may be due to an unmeasured response to changes in the reactants needed for methanogenesis. However, it is possible that the CH_4 spikes may be the result of ebullition, a known CH_4 transport process in tidal salt marshes and other types of wetlands (Baird et al., 2004; Chanton et al., 1989; Diefenderfer et al., 2018). Similar to Goodrich et al. (2011), we observed ebullition events when the chamber was closed, suggesting that some of the hot moments could be attributed to this process. While CO_2 and N_2O can also experience ebullition, we have not proposed it as a significant gas transport pathway for two reasons: (1) CO_2 and N_2O were not as variable as CH_4 throughout the experiment and (2) previous studies suggest that ebullition does not play a significant role in CO_2 and N_2O transport (Gao et al., 2013;

Komiya et al., 2015; Tuser et al., 2017). The variability present in CH_4 and to a lesser degree in CO_2 and N_2O, highlights the importance of high-frequency measurements in both field and lab settings in order to accurately capture the dynamics of GHG emissions.

For the majority of the experiment, the soils were sinks of N_2O (Fig. 2.3g, h). There have been reported instances of N_2O sinks in wetlands (Audet et al., 2014; Minami, 1997; Reddy and Delaune, 2008; Ryden, 1981; Slemr and Seiler, 1984). Diefenderfer et al. also found negative fluxes of N_2O in a *Sarcocornia* marsh during a storm surge (2018); however, the mechanisms behind N_2O consumption in salt marshes are not well-understood (Chapuis-Lardy et al., 2007). The soils in our experiments remained flooded, likely increasing N_2O consumption due to the lower diffusivity rate in water and the increased residence time of the gas (Arah et al., 1991). Generally, N_2O consumption occurs in soils with a high water-filled pore space and low NO_3^- availability (Clayton et al., 1997; Khalil et al., 2002; Ryden, 1983; Wagner-Riddle et al., 1997), which was the case during our experiment. Under these conditions, it is possible that some of the N_2O consumption could be attributed to N_2O serving as electron acceptor for denitrification (Butterbach-Bahl et al., 1998; Goossens et al., 2001; Rosenkranz et al., 2006). The persistence of the N_2O sink for all mesocosms raises questions about the potential of salt marsh soils to become sinks during storm surges or in sea level rise scenarios and how this capability could offset increased CO_2 and CH_4 emissions during periods of decreased salinity.

Redox and redox-sensitive ions and compounds likely affected N_2O fluxes. During Phase II, redox had a negative relationship with N_2O. Both the control and the treatment soils were lower than the N_2O reduction critical redox potential of 250 mV

(Letey et al., 1981; Smith et al., 1983; Yu and Patrick, 2003). However, as the salinity remained stable in Phase III, redox had a significant, positive relationship with N_2O. As treatment redox increased towards the N_2O reduction critical redox potential, the soils became less of a sink. Furthermore, the significant, negative relationship between TN_b and N_2O, suggests that nitrogen compounds were being consumed to produce N_2O. As the salinity increased, sulfide had a significant, negative relationship with N_2O. Though not much research has been done on the effect of sulfides on N_2O emission in wetlands, it may be that the presence of sulfides, a by-product of sulfate reduction, indicates that the system shifted from nitrate reduction to sulfate reduction.

Hysteresis graphs were used to assess the functional response of changes in salinity over the course of the experiment (Phillips et al., 2011; Riveros-Iregui et al., 2007; Vargas and Allen, 2008). All GHG showed hysteresis effects, though N_2O had only a slight hysteresis. CH_4 and N_2O had near-identical final and initial fluxes, which suggests that the potential processes that influence CH_4 and N_2O efflux had fully recovered within 15 days, illustrating the resiliency of tidal salt marsh soils to pulse events. A previous study done by Northrup et al. (2018) found that the in situ increase in As concentration during Hurricane Joaquin at our study site had returned to baseline concentrations within 1 week of the event, suggesting that the biogeochemical conditions (e.g. pH, redox) at the site had recovered quickly. The presence of hysteresis may be the result of differences in the rates of biogeochemical pathways due to changing quantities of reactants and inhibitors throughout the experiment. Hysteresis effects on GHG efflux due to salinity changes could be incorporated into modelling efforts since there is a non-linear response that increases or decreases the overall GHG efflux from the pulse event.

Overall, the simulated decrease in salinity caused by a hurricane-induced surge increased the 20- and 100-year GWP of the mesocosms. This increase in GWP from treatment mesocosms was mainly due to higher CH_4 fluxes, but these higher CH_4 fluxes were slightly offset by N_2O consumption. The strength of the N_2O sink was weaker in the treatment mesocosms compared to the control. These results prompt questions about processes that govern N_2O sinks (i.e., when do they occur and how do they change under different scenarios). Additionally, our results raise questions about the effect of sea level rise and its accompanying increase in salinity (mainly as sulfate) on GHG fluxes, as our data indicate that sea level rise could decrease CH_4 emissions from wetland soils. These processes should be explored in future research.

2.5 Conclusions

By combining high temporal frequency measurements of CO_2, CH_4, and N_2O with pore water chemistry, we were able to better understand how shifts in potential biogeochemical pathways, such as sulfate reduction, could impact GHG emissions. We found that efflux can be highly variable, especially for CH_4, despite controlling for confounding effects such as water level and temperature. This underscores the need to take continuous, high-frequency data in the field in order to capture the variability. Furthermore, we found that decreased salinity does increase GHG emissions under flooded conditions, and that the biogeochemical processes by which it does appears to continually evolve, with different electron acceptors playing roles at different times during the experiment. Overall, the lowered salinity in the treatment soils produced a 24% and 23% increase in GWP under 20- and 100-year scenarios, respectively, suggesting that pulse events can cause a burst of GHG emissions from tidal salt marsh soils. However, it is important to note that when initial conditions were restored, CH_4

and N_2O emissions returned to baseline within 15 days, likely by different pathways. Overall, the experimental results suggest that tidal salt marshes are resilient ecosystems that can recover from disturbances relatively quickly, but raises questions about the effects of increasing salinity (i.e., sea level rise) on GHG fluxes from tidal marshes.

Acknowledgements

MC acknowledges support from a DENIN Environmental Fellowship, as well as a National Science Foundation Graduate Research Fellowship (#1247394), RV acknowledges support from the National Science Foundation (#1652594), and ALS acknowledges support from the National Science Foundation (#175987). We thank the support from the staff at St. Jones Reserve, as well as the staff at the University of Delaware Soil Testing Lab.

Author contributions

MC, JB, ALS and RV designed the experiment. MC performed the experiment, analyzed data, and wrote the manuscript with input from all coauthors.

Supplementary data

Supplementary data to this article can be found online at https://doi.org/10.1016/j.scitotenv.2019.06.032 as well as Appendix A of this document.

REFERENCES

Arah, J.R.M., Smith, K.A., Crichton, I.J., Li, H.S., 1991. Nitrous oxide production and denitrification in Scottish arable soils. J. Soil Sci. 42, 351–367. https://doi.org/10.1111/ j.1365-2389.1991.tb00414.x.

Audet, J., Hoffmann, C.C., Andersen, P.M., Baattrup-Pedersen, A., Johansen, J.R., Larsen, S.E., Kjaergaard, C., Elsgaard, L., 2014. Nitrous oxide fluxes in undisturbed riparian wetlands located in agricultural catchments: Emission, uptake and controlling factors. Soil Biol. Biochem. 68, 291–299. https://doi.org/10.1016/j.soilbio.2013.10.011.

Baird, A.J., Beckwith, C.W., Waldron, S., Waddington, J.M., 2004. Ebullition of methane-containing gas bubbles from near-surface *Sphagnum* peat. Geophys. Res. Lett. 31, 2–5. https://doi.org/10.1029/2004GL021157.

Barton, K., 2018. MuMIn: Multi-Model Inference.

Bridgham, S.D., Megonigal, J.P., Keller, J.K., Bliss, N.B., Trettin, C., 2006. The carbon balance of North American wetlands. Wetlands 26, 889–916. https://doi.org/10.1672/0277- 5212(2006)26[889:tcbona]2.0.co;2.

Butterbach-Bahl, K., Gasche, R., Huber, C., Kreutzer, K., Papen, H., 1998. Impact of N-input by wet deposition on N-trace gas fluxes and CH_4-oxidation in spruce forest ecosystems of the temperate zone in Europe. Atmos. Environ. 32, 559–564. https://doi. org/10.1016/S1352-2310(97)00234-3.

Capone, D.G., Kiene, R.P., 1988. Comparison of microbial dynamics in marine and freshwater sediment. Limnol. Ocean. 33, 725–749.

Chambers, L.G., Osborne, T.Z., Reddy, K.R., 2013. Effect of salinity-altering pulsing events on soil organic carbon loss along an intertidal wetland gradient: A laboratory experiment. Biogeochemistry 115, 363–383. https://doi.org/10.1007/s10533-013-9841-5.

Chanton, J.P., Martens, C.S., Kelley, C.A., 1989. Gas transport from methane-saturated, tidal freshwater and wetland sediments. Limnol. Oceanogr. 34, 807–819. https://doi.org/ 10.4319/lo.1989.34.5.0807.

Chapuis-Lardy, L., Wrage, N., Metay, A., Chotte, J.-L., Bernoux, M., 2007. Soils, a sink for N_2O? A review. Glob. Biogeochem. Cycles 13, 1–17. https://doi.org/10.1111/j.1365- 2486.2006.01280.x.

Clayton, H., McTaggart, I.P., Parker, J., Swan, L., Smith, K.A., 1997. Nitrous oxide emissions from fertilised grassland: A 2-year study of the effects of N fertiliser form and environmental conditions. Biol. Fertil. Soils 25, 252–260.

Clough, T.J., Sherlock, R.R., Rolston, D.E., 2005. A review of the movement and fate of N_2O in the subsoil. Nutr. Cycl. Agroecosystems 72, 3–11. https://doi.org/10.1007/s10705- 004-7349-z.

Crooks, S., Herr, D., Tamelander, J., Laffoley, D., Vandever, J., 2011. Mitigating climate change through restoration and management of coastal wetlands and near-shore marine ecosystems: Challenges and opportunities. Environment Department Paper. World Bank, Washington D.C.

Dahl, T.E., 2011. Status and trends of wetlands in the conterminous United States 2004 to 2009. U.S. Dep. Inter. Fish Wildl. Serv, p. 108.

Dahl, T.E., Stedman, S.M., 2013. Status and trends of wetlands in the coastal watersheds of the conterminous United States 2004 to 2009. U.S. Dep. Inter. Fish Wildl. Serv. NOAA Nat. Mar. Fish Serv, p. 146.

Davidson, E.A., 1991. Fluxes of nitrous oxide and nitric oxide from terrestrial ecosystems. In: Rogers, J.E., Whitman, W.B. (Eds.), Microbial Production and Consumption of Greenhouse Gases: Methane, Nitrogen Oxides, and Halomethanes. American Society of Microbiology, Washington D.C., pp. 219–235.

Diefenderfer, H.L., Cullinan, V.I., Borde, A.B., Gunn, C.M., Thom, R.M., 2018. High-frequency greenhouse gas flux measurement system detects winter storm surge effects on salt marsh. Glob. Chang. Biol. 24, 5961–5971. https://doi.org/ 10.1111/gcb.14430.

DNREC, 1999. Delaware National Estuarine Research Reserve Estuarine Profile

Forster, P., Ramaswany, V., Artaxo, P., Berntsen, T., Betts, R., Fahey, D.W., Haywood, J., Lean, J., Lowe, D.C., Myhre, G., Nganga, J., Prinn, R., Raga, G., Schulz, M., Van Dorland, R., 2007. Changes in atmospheric constituents and in radiative forcing. In: Solomon, S., Qin, D., Manning, M., Chen, Z., Marquis, M., Averyt, K.B., Tignor, M., Miller, H.L. (Eds.), Climate Change 2007: The Physical Science Basis. Contribution of Working Group I to the Fourth Assessment Report of the Intergovernmental Panel on Climate Change. Cambridge, UK, pp. 129–234 https://doi.org/10.1103/PhysRevB.77.220407.

Furukawa, Y., Smith, A.C., Kostka, J.E., Watkins, J., Alexander, C.R., Dava Dalton, A., Vaughan, C., Dollhopf, S., Dollhopf, M., Skelton, H., Petrie, L., Adams, H., 2004. Quantification of macrobenthic effects on diagenesis using a multicomponent inverse model in salt marsh sediments. Limnol. Ocean. 49, 2058–2072.

Gao, Y., Liu, X., Yi, N., Wang, Y., Guo, J., Zhang, Z., Yan, S., 2013. Estimation of N_2 and N_2O ebullition from eutrophic water using an improved bubble trap device. Ecol. Eng. 57, 403–412. https://doi.org/10.1016/J.ECOLENG.2013.04.020.

Gelman, A., Hill, J., 2007. Data Analysis Using Regression and Multilevel/Hierarchical Models. 1st ed. Cambridge University Press, Cambridge, UK.

Goodrich, J.P., Varner, R.K., Frolking, S., Duncan, B.N., Crill, P.M., 2011. High-frequency measurements of methane ebullition over a growing season at a temperate peatland site. Geophys. Res. Lett. 38. https://doi.org/10.1029/2011GL046915 n/a-n/a.

Goossens, A., De Visscher, A., Boeckx, P., Cleemput, O. Van, 2001. Two-year field study on the emission of N_2O from coarse and middle-textured Belgian soils with different land use. Nutr. Cycl. Agroecosyst. 60 (1-3), 23–34.

Heincke, M., Kaupenjohann, M., 1999. Effects of soil solution on the dynamics of N_2O emissions: a review. Nutr. Cycl. Agroecosystems 55, 133–157.

Inubushi, K., Barahona, M.A., Yamakawa, K., 1999. Effects of salts and moisture content on N_2O emission and nitrogen dynamics in yellow soil and andosol in model experiments. Biol. Fertil. Soils 29, 401–407.

IPCC, 2000. Land Use, Land-Use Change, and Forestry: Summary for Policymakers. IPCC, 2014. Climate Change 2014: Synthesis Report. Contribution of Working Groups I, II and III to the Fifth Assessment Report of the Intergovernmental Panel on Climate Change. Geneva, Switzerland. https://doi.org/10.1017/CBO9781107415324.004.

Jordan, S.J., Stoffer, J., Nestlerode, J.A., 2011.Wetlands as sinks for reactive nitrogen at continental and global scales: A meta-analysis. Ecosystems 14, 144–155.

Jørgensen, C.J., Elberling, B., 2012. Effects of flooding-induced N_2O production, consumption and emission dynamics on the annual N_2O emission budget in wetland soil. Soil Biol. Biochem. 53, 9–17. https://doi.org/10.1016/j.soilbio.2012.05.005.

Khalil, M.I., Rosenani, A.B., Van Cleemput, O., Fauziah, C.I., Shamshuddin, J., 2002. Nitrous oxide emissions from an Ultisol of the humid tropics under maize–groundnut rotation. J. Environ. Qual. 31, 1071. https://doi.org/10.2134/jeq2002.1071.

King, G.M., Wiebe, W.J., 1978. Methane release from soils of a Georgia salt marsh. Geochim. Cosmochim. Acta. 42 (343–10).

Kliewer, B.A., Gilliam, J.W., 1995. Water table management effects on denitrification and nitrous oxide evolution. Soil Sci. Soc. Am. J. 59, 1694. https://doi.org/10.2136/ sssaj1995.03615995005900060027x.

Komiya, S., Noborio, K., Katano, K., Pakoktom, T., Siangliw, M., Toojinda, T., 2015. Contribution of ebullition to methane and carbon dioxide emission from water between plant rows in a tropical rice paddy field. Int. Sch. Res. Not. 2015, 1–8. https://doi.org/ 10.1155/2015/623901.

Leon, E., Vargas, R., Bullock, S., Lopez, E., Panosso, A.R., La Scala, N., 2014. Hot spots, hot moments, and spatio-temporal controls on soil CO_2 efflux in a water-limited ecosystem. Soil Biol. Biochem. 77, 12–21. https://doi.org/10.1016/J.SOILBIO.2014.05.029.

Letey, J., Valoras, N., Focht, D.D., Ryden, J.C., 1981. Nitrous oxide production and reduction during denitrification as affected by redox potential. Soil Sci. Soc. Am. J. 45, 727–730. https://doi.org/10.2136/sssaj1981.03615995004500040010x.

Liikanen, A., Martikainen, P.J., 2003. Effect of ammonium and oxygen on methane and nitrous oxide fluxes across sediment-water interface in a eutrophic lake. Chemosphere 52, 1287–1293. https://doi.org/10.1016/S0045-6535(03)00224-8.

Martikainen, P.J., Nykanen, H., Crill, P., Silvola, J., 1993. Effects of a lowered water table on nitrous oxide fluxes from northern peatlands. Nature 366.

McClain, M.E., Boyer, E.W., Dent, C.L., Gergel, S.E., Grimm, N.B., Groffman, P.M., Hart, S.C., Harvey, J.W., Johnston, C.A., Mayorga, E., Mcdowell, W.H., Pinay, G., 2003. Biogeochemical hot spots and hot moments at the interface of terrestrial and aquatic ecosystems. Ecosystems 6, 301–312. https://doi.org/10.1007/s10021-003-0161-9.

McLeod, E., Chmura, G.L., Bouillon, S., Salm, R., Björk, M., Duarte, C.M., Lovelock, C.E., Schlesinger, W.H., Silliman, B.R., 2011. A blueprint for blue carbon: Toward an improved understanding of the role of vegetated coastal habitats in sequestering CO_2. Front. Ecol. Environ. 9, 552–560. https://doi.org/10.1890/110004.

Menyailo, O., Stepanov, A., Umarov, M.M., 1997. The transformation of nitrous oxide by denitrifying bacteria in Solonchaks. Eurasian Soil Sci 30, 178–180.

Minami, K., 1997. Atmospheric methane and nitrous oxide: Sources, sinks and strategies for reducing agricultural emissions. Nutr. Cycl. Agroecosystems 49, 203–211.

Myhre, G., Shindell, D., Bréon, F.-M., Collins, W., Fuglestvedt, J., Huang, J., Koch, D., Lamarque, J.-F., Lee, D., Mendoza, B., Nakajima, T., Robock, A., Stephens, G., Takemura, T., Zhang, H., Qin, D., Plattner, G., Tignor, M., Allen, S., Boschung, J., Nauels, A., Xia, Y., Bex, V., Midgley, P., 2013. Anthropogenic and natural radiative forcing. Climate Change 2013: The Physical Science Basis. Contribution of Working Group I.

NOAA National Estuarine Research Reserve System (NERRS), 2015. System-Wide Monitoring Program. WWW Document. NOAA NERRS Cent. Data Manag. Off.

Northrup, K., Capooci, M., Seyfferth, A.L., 2018. Effects of extreme events on arsenic cycling in salt marshes. J. Geophys. Res. Biogeosci. 123, 1086–1100. https://doi.org/ 10.1002/2017JG004259.

Petrakis, S., Barba, J., Bond-Lamberty, B., Vargas, R., 2017a. Using greenhouse gas fluxes to define soil functional types. Plant Soil https://doi.org/10.1007/s11104-017-3506-4.

Petrakis, S., Seyfferth, A., Kan, J., Inamdar, S., Vargas, R., 2017b. Influence of experimental extreme water pulses on greenhouse gas emissions from soils. Biogeochemistry 133, 147–164. https://doi.org/10.1007/s10533-017-0320-2.

Phillips, C.L., Nickerson, N., Risk, D., Bond, B.J., 2011. Interpreting diel hysteresis between soil respiration and temperature. Glob. Chang. Biol. 17, 515–527. https://doi.org/ 10.1111/j.1365-2486.2010.02250.x.

Pinheiro, J., Bates, D., DebRoy, S., Sarkar, D., R Core Team, 2018. Nlme: Linear and Nonlinear Mixed Effects Models.

Poffenbarger, H.J., Needelman, A., Megonigal, J.P., 2011. Salinity influence on methane emissions from tidal marshes. Wetlands https://doi.org/10.1007/s13157-011-0197-0.

Ponnamperuma, F.N., 1972. The chemistry of submerged soils. Adv. Agron. 24, 29–96. Reddy, K.R., Delaune, R.D., 2008. Biogeochemistry of Wetlands: Science and Applications. CRC Press, Boca Ration, FL.

Riveros-Iregui, D.A., Emanuel, R.E., Muth, D.J., McGlynn, B.L., Epstein, H.E., Welsch, D.L., Pacific, V.J., Wraith, J.M., 2007. Diurnal hysteresis between soil CO_2 and soil temperature is controlled by soil water content. Geophys. Res. Lett. 34, 1–5. https://doi.org/ 10.1029/2007GL030938.

Rosenkranz, P., Brüggemann, N., Brüggemann, B., Papen, H., Xu, Z., Seufert, G., Butterbach-Bahl, K., 2006. N_2O, NO and CH_4 exchange, and microbial N turnover over a Mediterranean pine forest soil. Biogeosciences 3, 121–133.

Ryden, J.C., 1981. N_2O exchange between a grassland soil and the atmosphere. Nature 292, 235–237. https://doi.org/10.1038/292235a0.

Ryden, J.C., 1983. Denitrification loss from a grassland soil in the field receiving different rates of nitrogen as ammonium nitrate. J. Soil Sci. 34, 355–365. https://doi.org/ 10.1111/j.1365-2389.1983.tb01041.x.

Schaufler, G., Kitzler, B., Schindlbacher, A., Skiba, U., Sutton, M.A., Zechmeister-Boltenstern, S., 2010. Greenhouse gas emissions from European soils under different land use: Effects of soil moisture and temperature. Eur. J. Soil Sci. 61, 683–696. https://doi.org/10.1111/j.1365-2389.2010.01277.x.

Seyfferth, A.L., Fendorf, S., 2012. Silicate mineral impacts on the uptake and storage of arsenic and plant nutrients in rice (*Oryza sativa* L.). https://doi.org/10.1021/es3025337.

Slemr, F., Seiler, W., 1984. Field measurements of NO and NO_2 emissions from fertilized and unfertilized soils. J. Atmos. Chem. 2, 1–24. https://doi.org/10.1007/BF00127260.

Smith, C.J., DeLaune, R.D., Patrick, J.W.H., 1983. Nitrous oxide emission from Gulf Coast wetlands. Geochim. Cosmochim. Acta 47, 1805–1814. https://doi.org/10.1016/0016- 7037(83)90028-5.

Tobias, C., Neubauer, S.C., 2019. Salt marsh biogeochemistry – An overview. Coastal Wetlands: An Integrated Ecosystem Approach, pp. 445–492.

Tuser, M., Picek, T., Sajdlov, Z., Jůza, T., Muska, M., Frouzov, J., 2017. Seasonal and spatial dynamics of gas ebullition in a temperate water-storage reservoir. Water Resour. Res. 53, 8266–8276. https://doi.org/10.1002/2017WR020694.

Valiela, I., Teal, J.M., 1979. The nitrogen budget of a salt marsh ecosystem. Nature 280, 652–656. https://doi.org/10.1038/280652a0.

Vargas, R., Allen, M.F., 2008. Diel patterns of soil respiration in a tropical forest after hurricaneWilma. J. Geophys.Res. Biogeosci. 113, 1–10. https://doi.org/10.1029/ 2007JG000620.

Wagner-Riddle, C., Thurtell, G.W., Kidd, G.K., Beauchamp, E.G., Sweetman, R., 1997. Estimates of nitrous oxide emissions from agricultural fields over 28 months. Can. J. Soil Sci. 77, 135–144.

Wong, P.P., Losanda, I.J., Gattuso, J.-P., Hinkel, J., Khattabi, A., McInnes, K.L., Saito, Y., Sallenger, A., 2014. Coastal systems and low-lying areas. In: Field, C.B., Barros, V.R., Dokken, D.J., Mach, K.J., Mastrandrea, M.D., Bilir, T.E., Chatterjee, M., Ebi, K.L., Estrada, Y.O., Genova, R.C., Girma, B., Kissel, E.S., Levy, A.N., MacCracken, S., Mastrandrea, P.R., White, L.L. (Eds.), Climate Change 2014: Impacts, Adaptation, and Vulnerability. Part a: Global and Sectoral Aspects. Contribution of Working Group II to the Fifth Assessment Report of the Intergovernmental Panel on Climate Change. Cambridge University Press, Cambridge, UK, pp. 361–409.

Yu, K., Patrick, W.H., 2003. Redox range with minimum nitrous oxide and methane production in a rice soil under different pH. Soil Sci. Soc. Am. J. 67, 1952. https://doi. org/10.2136/sssaj2003.1952.

Zuur, A.F., Ieno, E.N., Elphick, C.S., 2010. A protocol for data exploration to avoid common statistical problems. Methods Ecol. Evol. 1, 3–14. https://doi.org/10.1111/j.2041- 210X.2009.00001.x

Chapter 3

DIEL AND SEASONAL PATTERNS OF SOIL CO_2 EFFLUX IN A TEMPERATE TIDAL MARSH

As published in *Science of the Total Environment*, 2022

DOI: 10.1016/j.scitotenv.2021.149715

Margaret Capooci[1], Rodrigo Vargas[1]

[1] Department of Plant and Soil Sciences, University of Delaware, Newark, DE, USA

Abstract

Tidal marshes store large amounts of carbon; however, little is known about the patterns, magnitudes, and bio-physical drivers that regulate CO_2 efflux from these ecosystems. Due to harsh environmental conditions (e.g., flooding), it is difficult to measure continuous soil CO_2 efflux in tidal marshes. These data are necessary to inform empirical and process-based models and to better quantify carbon budgets. We performed automated (30 min) and manual (bi-monthly) soil CO_2 efflux measurements, for ~20 months, at two sites in a temperate tidal marsh: tall *Spartina* (TS; dominated by *S. cynosuroides*) and short *Spartina* (SS; dominated by *S. alterniflora*). These measurements were coupled with water quality, canopy spectral reflectance, and meteorological measurements. There were no consistent diel patterns of soil CO_2 efflux, suggesting a decoupling of soil CO_2 efflux with diel variations in

temperature and tides (i.e., water level) showing a hysteresis effect. Mean soil CO_2 efflux was significantly higher at SS (2.15 ± 1.60 μmol CO_2 m^{-2} s^{-1}) than at TS (0.55 ± 0.80 μmol CO_2 m^{-2} s^{-1}), highlighting distinct biogeochemical spatial variability. At the annual scale, air temperature explained >50% of the variability in soil CO_2 efflux at both sites; and water level and salinity were secondary drivers of soil CO_2 efflux at SS and TS, respectively. Annual soil CO_2 efflux varied from 287-876 to 153-211 g C m^{-2} y^{-1} at SS and TS, respectively, but manual measurements underestimated the annual flux by <67% at SS and <23% at TS. These results suggest that measuring and modeling diel soil CO_2 efflux variability in tidal marshes may be more challenging than previously expected and highlight large discrepancies between manual and automated soil CO_2 efflux measurements. New technical approaches are needed to implement long-term automated measurements of soil CO_2 efflux across wetlands to properly estimate the carbon balance of these ecosystems.

Highlights

- Measured ~20 months of continuous soil CO_2 efflux in a tidal salt marsh
- No consistent diel patterns, suggesting a decoupling from tides and temperature
- Air temperature explained >50% of variability at the annual scale
- Soil CO_2 efflux showed diel hysteresis pattern with temperature
- Manual measurements underestimate annual soil CO_2 efflux by up to 60%

Keywords

Wetland; carbon dioxide; soil respiration; aquatic-terrestrial interface; blue carbon; hysteresis

Graphical Abstract

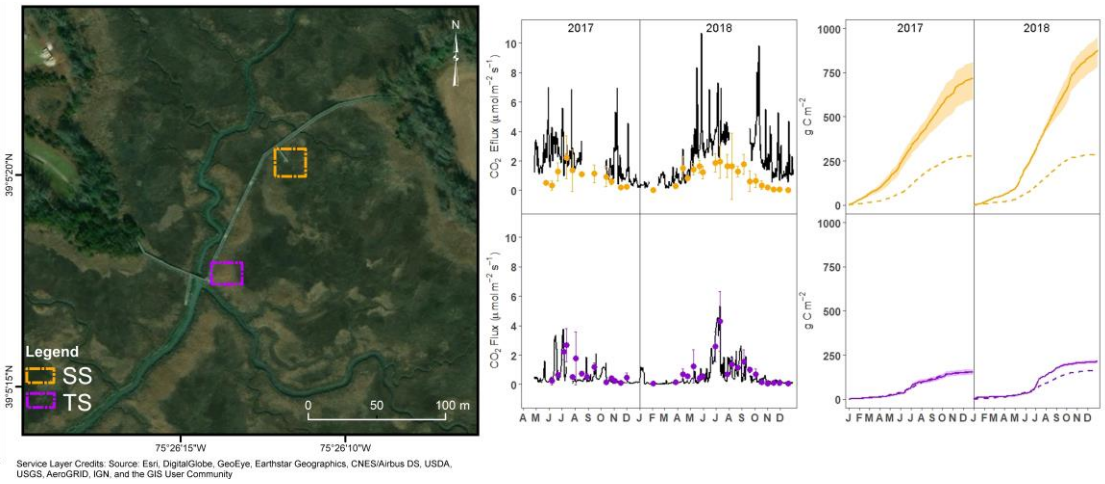

Figure 3.1: Graphical abstract showing an aerial view of the study site (left panel) with the two subsites, short *Spartina* (SS) and tall *Spartina* (TS), outlined in orange and purple, respectively. The middle panel shows the time series of the daily mean CO_2 efflux from the SS and TS sites. Dots with error bars represent the daily average ± SD of the manual measurements taken throughout the study period. The right panel shows the cumulative daily CO_2 efflux annual sum for the SS and TS sites. Solid line denotes the cumulative daily CO_2 efflux annual sum for the continuous measurements. Dashed line represents the cumulative sums of the manual measurements. Shaded area represents the 95% confidence interval.

3.1 Introduction

Blue carbon ecosystems, such as tidal salt marshes, seagrass beds, and mangrove forests, are capable of sequestering large amounts of carbon. Despite covering only 0.07-0.22% of the Earth's surface, blue carbon ecosystems bury between 0.08 and 0.22 Pg C yr^{-1}, amounting to roughly 10% of the net residual land sink (i.e., the difference between C emissions and the net terrestrial C sink) (Duarte et al., 2013; NASAM, 2019; Spivak et al., 2019). These ecosystems can lose carbon to the atmosphere via respiration processes that result in CO_2 and CH_4 emissions, or lateral exchanges of organic (i.e., POC, DOC) and inorganic (i.e., CO_2/CH_4 emissions, DIC) compounds with rivers and the coastal ocean (Battin et al., 2009; Tobias and Neubauer, 2019). Consequently, to better understand the carbon balance in these ecosystems, as well as to better quantify regional-to-global carbon budgets, scientists need a better understanding of multiple carbon fluxes across these ecosystems (Hayes et al., 2018). In particular, there is a knowledge gap in assessing the magnitudes and patterns of greenhouse gas (GHG; CO_2, CH_4, N_2O) fluxes between blue carbon ecosystems and the atmosphere, as well as how different environmental drivers influence them (Capooci et al., 2019; Macreadie et al., 2019). Blue carbon ecosystems are unique because they are influenced by key environmental drivers such as tides and biochemical gradients that contribute to high spatial and temporal variability in carbon dynamics (Seyfferth et al., 2020; Simpson et al., 2019). However, there is a pressing need to advance our understanding of carbon dynamics to inform Earth Systems Models, particularly for terrestrial-aquatic interface components, and to calculate ecosystem carbon budgets and blue carbon offsets (Macreadie et al., 2019; Sapkota and White, 2020; Ward et al., 2020).

Tidal salt marsh soils play a large role in the global carbon cycle despite their small footprint (Duarte et al., 2013; NASAM, 2019); consequently, it is important to close the knowledge gap about patterns and magnitudes of soil-atmosphere CO_2 dynamics. Soil CO_2 efflux (also referred as soil respiration; R_s) represents the contribution of both autotrophic and heterotrophic respiration from the soil to the atmosphere. It is difficult to obtain CO_2 efflux measurements in tidal marshes due to constant or intermittent waterlogged/flooded soils and high salinity which jeopardizes instrument performance and hinders long-term deployments. Traditionally, most CO_2 efflux measurements in wetland soils have been done manually with static chambers (Chimner, 2004; Han et al., 2014) since they are an excellent approach to better understand the spatial variability of soil CO_2 efflux across an ecosystem. Furthermore, several studies (e.g., Moseman-Valtierra et al., 2016; Simpson et al., 2019) have targeted multiple coastal wetlands over a large geographical area, a task that manual measurements are uniquely suited to.

While manual measurements can obtain high spatial resolution by targeting different areas of an ecosystem and can be used under a variety of environmental conditions, they usually have low temporal resolution (e.g., weekly, bi-monthly, monthly) and are labor-intensive (Koskinen et al., 2014; Savage et al., 2014). Thus, manual soil respiration measurements typically do not capture diel cycles and could be biased due to collection time (Cueva et al., 2017). In contrast, researchers have used high-temporal frequency measurements (e.g., hourly) with opaque chambers to capture diel patterns in soil CO_2 efflux in temperate forest, grass, and shrub ecosystems (Carbone et al., 2008; Jia et al., 2013; Liu et al., 2006; Phillips et al., 2010). High-temporal frequency measurements also enable scientists to capture

synoptic events, calculate more accurate annual sums, and determine nonlinear relationships between R_s and various drivers (Vargas et al., 2011b). Despite the need for high-frequency CO_2 efflux data from tidal salt marsh soils, harsh environmental conditions (e.g., waterlogged soils, tides, high salinity, and relative humidity), and high instrumentation costs have hindered efforts. In recent years, researchers have built/modified automated, continuous measurement systems and/or have developed/ utilized new technologies capable of obtaining high-frequency soil CO_2 efflux measurements in wetland ecosystems (Capooci et al., 2019; Diefenderfer et al., 2018; Järveoja et al., 2018; Lavoie et al., 2012; Petrakis et al., 2017; Trifunovic et al., 2020). These new systems have the potential to generate high-frequency, long-term data sets, giving scientists a better understanding of the patterns and magnitudes of CO_2 efflux over a variety of time scales (Petrakis et al., 2017).

Traditionally, soil CO_2 efflux has been modelled based on an exponential temperature relationship developed in terrestrial ecosystems (Lloyd and Taylor, 1994). That said, several studies have found positive relationships between temperature and CO_2 efflux using manual chamber measurements in temperate coastal wetlands with relatively large gradients in seasonal temperature. However, tidal salt marshes have other environmental drivers that can potentially influence soil CO_2 efflux patterns (e.g., tides, salinity, phenology) and alter the expected relationship with temperature. In particular, tides can be asynchronous with temperature's diel cycle, alter canopy photosynthesis due to flooding, and affect nighttime net ecosystem exchange (NEE) differently during spring and neap tides (Guo et al., 2009; O'Connell et al., 2017). While several studies found that ecosystem-scale nighttime CO_2 emissions were lower during higher tides, studies that parse out both the individual and combined effects of

tides and temperature over multiple time scales are limited (Forbrich and Giblin, 2015; Guo et al., 2009; Knox et al., 2018; Vázquez-Lule and Vargas, 2021).

Furthermore, tides, in combination with plant communities, create different zones within a marsh that are characterized by soil biogeochemical conditions that subsequently can affect carbon dynamics (Seyfferth et al., 2020). Some studies have attributed differences in soil CO_2 emissions to plant-based properties, such as primary productivity and plant turnover (Moseman-Valtierra et al., 2016; Simpson et al., 2019), while other studies have proposed that microbial substrate availability, such as % soil C, DOC concentrations, or plant decomposition rates, were contributing factors (Nyman and Delaune, 1991; Seyfferth et al., 2020). The drivers behind spatial variability in salt marsh soil CO_2 efflux are likely to be a combination of microbial processes, driven by substrate availability and redox conditions, and plant species and productivity, which can contribute to the amount and availability of carbon to microbial populations. As a result, it is important to measure soil CO_2 efflux across different areas in tidal marshes to help better understand the drivers behind spatial variability.

While automated measurements provide more temporal information (i.e., data points in a time series) than manual measurements, there is a need to test whether richer temporal information results in similar deductions (e.g., relationships between soil CO_2 efflux and covariates, annual sums) than using data derived from manual measurements. Savage and Davidson (2003) compared manual (weekly, 12 locations) to automated (hourly, 3 locations) soil CO_2 efflux measurements in a temperate forest to examine the trade-offs between the two. They found that seasonal flux estimates from both systems were nearly identical, but the automated measurements showed the

effects of wetting events on soil CO_2 efflux, as well as contributed to better empirical modeling of the effects of soil temperature and moisture. However, no such comparisons have been done in tidal wetlands where soil CO_2 efflux is potentially influenced (and confounded) by more environmental drivers (e.g., tides, salinity gradients, temperature, precipitation, redox conditions) than in terrestrial ecosystems.

Our main objective is to describe and quantify the temporal patterns and drivers of CO_2 efflux from two distinctive vegetation types in a temperate tidal salt marsh. To address this objective, we used a combination of continuous, automated measurements combined with spatially distributed manual CO_2 efflux measurements. We postulate four interrelated hypotheses.

First (H1), CO_2 efflux will demonstrate clear seasonal and diel patterns, as expected in temperate terrestrial ecosystems where temperature fluctuations mainly determine the temporal trends (Vargas et al., 2011a). Alternatively, diel patterns could be dampened due to physical effects of the tidal cycle by regulating soil CO_2 diffusion rates and minimizing temperature fluctuations in the soil. Consequently, during spring tides, it is possible to have lower soil CO_2 efflux due to increased flooding compared to neap tides (Guo et al., 2009).

Second (H2), the two vegetation zones will have differences in soil CO_2 efflux due to different plant community composition and topographic location (Moseman-Valtierra et al., 2016; Stribling et al., 2006). We expect that areas where soils are saturated and there are low water level fluctuations will have lower soil CO_2 efflux rates, while larger water level fluctuations could increase oxygen and soil CO_2 diffusion resulting in higher soil CO_2 efflux rates.

Third (H3), temperature will be the main driver of CO_2 efflux at both sites (Abdul-Aziz et al., 2018), but other biophysical factors such as water quality (i.e., water level, salinity), and plant ecophysiology (using PAR and NDVI as proxies), as postulated in H2, will play a role in regulating soil CO_2 efflux.

Fourth (H4), manual and continuous measurements will show comparable temperature ~ soil CO_2 efflux dependence (i.e., similar functional relationships). However, differences in magnitudes, patterns, and annual soil CO_2 efflux estimates may emerge due to the continuous measurements capturing the short-term variability in soil CO_2 efflux.

3.2 Materials and methods

3.2.1 Study site

St. Jones Reserve (SJR), a subsection of the Delaware National Estuarine Research Reserve, is a mesohaline tidal salt marsh (DNREC, 1999) located near Dover, Delaware, USA. SJR falls within the Delaware Estuary and is tidally connected to the Delaware Bay via the St. Jones River. The tides range from −0.98 m to 1.43 m (referenced to NAVD88). The ecosystem is characterized by high primary productivity and medium seasonality, with a peak of phenology during summer (Villarreal et al., 2018). Dominant plant species consist of *Spartina alterniflora*, *S. patens*, and *S. cynosuroides*, but note that the genus *Spartina* has been reclassified as *Sporobolus* (Peterson et al., 2014). Soils are silty clay loam (10% sand, 61% silt, and 29% loam, Capooci et al., 2019). We selected two sites with distinct biogeochemical conditions (Seyfferth et al., 2020) located approximately 90 m apart that fall within the footprint of an eddy covariance tower located on the site (AmeriFlux site ID: US-StJ;

Hill et al., 2021; Vázquez-Lule and Vargas, 2021). The tall *Spartina* (TS) site is mainly dominated by *S. cynosuroides* with soils characterized by iron reduction. The short *Spartina* (SS) site is mainly dominated by *S. alterniflora* and is relatively lower in elevation with soils characterized by sulfur reduction (Seyfferth et al., 2020).

3.2.2 Continuous CO_2 efflux measurements

A forced diffusion soil CO_2 sensor (eosense eosFD, Dartmouth, Nova Scotia, Canada) was placed at each location (i.e., TS, SS) in April 2017. The TS eosFD is ~16 m from the main tidal channel and ~10 m from a secondary tidal channel, while the SS eosFD is located ~53 m from the main channel. Data was collected every 5 min for the duration of the study period but aggregated as half hourly measurements (April 26, 2017 - December 31, 2018). Flux data calculated by the eosFD underwent a QA/QC protocol to remove a) data flagged by the eosFD software, b) data collected during times when the eosFD pump malfunctioned, and c.) negative values. Negative values comprised of ~3.7% of the SS dataset, with ~3.2% of those values associated with pump malfunctions, while the TS dataset consisted of ~2.9% negative values, the majority of which were near zero ($\leq$0.1 μmol m^{-2} s^{-1}). Negative values were considered measurement errors since a previous study found a large pool of CO_2 within the subsurface (i.e., >10%) that should contribute to a net CO_2 efflux from the soil to the atmosphere (Seyfferth et al., 2020) Overall, missing data represent 7.5% of the dataset at TS and 20.8% at SS.

3.2.3 Manual CO_2 efflux measurements

Manual CO_2 efflux measurements were taken approximately every two weeks during the growing season (March - October) and monthly throughout the winter

(November - February). Four replicate 15-cm diameter PVC collars were installed at each site to assess spatial variability of soil CO_2 efflux. Plant biomass was removed from the collars ~1 month before the first set of measurements. Before subsequent measurements, any new vegetation was carefully removed. Measurements were taken for four minutes using an Ultraportable Greenhouse Gas Analyzer (Los Gatos Research, Mountain View, CA, USA) and an opaque 15-cm diameter soil chamber that fit snugly over the soil collars. Measurements were taken between 8:00 and 12:00, regardless of the tidal cycle, but measurements were never performed if the collars were completely submerged. Soil CO_2 efflux was calculated using a published protocol (Pearson et al., 2016; Warner et al., 2017). We used air temperature from the nearby meteorological station instead of soil temperature to calculate CO_2 efflux to avoid disturbing the soil near the collars. A total of 275 manual measurements were taken during the study period (for TS, n= 144; for SS, n= 131). We used an QA/QC protocol where measurements with an $R^2 \geq 0.90$ were used for the study as they represented measurements that met micrometeorological requirements. Fluxes between 0 and 0.2 μmol m^{-2} s^{-1} were also kept to account for the low soil CO_2 efflux during the winter. After this selection process, a total of 235 manual measurements were used for analyses (TS, n = 120; SS, n = 115), demonstrating that ~85% of our measurements met the QA/ QC conditions.

3.2.4 Ancillary measurements

Meteorological and water quality data were obtained from the site. Meteorological data was collected using a CR1000 Meteorological Monitoring Station (Campbell Scientific, Logan, UT, USA), while water quality data were measured using a YSI 6600 sonde (YSI Inc., OH, USA). The collection of the meteorological

and water quality data follows the National Estuarine Research Reserve's Centralized Data Management Protocol (NOAA National Estuarine Research Reserve System (NERRS), 2015). Meteorological data can be accessed via the National Estuarine Research Reserve System's Centralized Data Management Office (NERR CDMO; station: delsjmet-p). The data underwent a QA/QC protocol and was gap-filled using data from nearby NERR CDMO stations (stations: delslwq (water quality), cbmjbmet (meteorological)). Spring and neap tidal days were obtained from NOAA for the nearest station to St. Jones Reserve (StationId: 8555388; Murderkill River Entrance, DE).

Normalized Difference Vegetation Index (NDVI) was collected every five minutes using a multiband radiometer (spectral reflectance sensor, METER Group, Washington, USA). One upward and one downward facing sensor was installed over the canopy at each site. NDVI is the ratio between red and near-infrared wavelengths and is related to the vegetation's greenness. Different phenophases were identified for the study periods as described previously (Hill et al., 2021; Trifunovic et al., 2020). Phenophases included (a) Dormant for the period of plant inactivity, (b) Greenup for the period of initial growth after the Dormant phenophase, (c) Maturity for the period of peak plant greenness, and (d) Senescence for the period when plants lose their greenness before entering the Dormant phenophase.

3.2.5 Data analysis

The average and standard deviation was calculated at daily and hourly intervals for the continuous soil CO_2 efflux measurements at each site, while the manual measurements were calculated at daily intervals for each site. The average and standard deviation was calculated at daily and hourly intervals for the ancillary

measurements, except for NDVI where the daily average and standard deviation was calculated from measurements collected between 11:00 and 13:00 local time. t-tests were used to determine if means were significantly different between locations (TS and SS).

Linear models were used to assess the relationship between daily air temperature and daily log-transformed CO_2 efflux for both the continuous and manual measurements at each site. Daily CO_2 efflux was log-transformed to improve linearity. The residuals from the models were then plotted against daily water level, salinity, NDVI, and PAR. The goodness of fit with linear relationships was assessed and reported for both manual and continuous measurements at both sites. Both the daily continuous and manual soil CO_2 efflux time series were gap-filled using the empirical soil CO_2 efflux ~ air temperature equation derived from the models described above to calculate annual sums. All analyses were carried out using R 3.6.1 (R Foundation for Statistical Computing, Vienna, Austria).

3.3 Results

3.3.1 Meteorological and water quality

Air temperature, PAR, and NDVI exhibited strong seasonal patterns, with the highest values during the summer and the lowest during the winter (Fig. 3.2). Daily air temperature ranged from −12.7°C to 29.3°C with an average of 15.0 ± 9.4°C, while daily PAR ranged from 21.0 mmol m^{-2} to 693.1 mmol m^{-2} with an average of 307.7 mmol m^{-2} ± 169.8 mmol m^{-2}. While daily NDVI showed similar patterns at both sites throughout the study period, the SS NDVI daily mean was significantly lower than the TS NDVI daily mean (t-test, $p < 0.001$). SS NDVI averaged 0.35 ± 0.23 with a range

of 0.0002 to 0.72, while TS NDVI averaged 0.51 ± 0.24 with a range of 0.12 to 0.91. Daily water level varied throughout the year from -0.37 m (as referenced to NAVD88) to 1.03 m, with an average level of 0.29 ± 0.17 m. Daily salinity also varied throughout the study period from 1.5 ppt to 18.7 ppt, with an average of 8.4 ± 3.9 ppt.

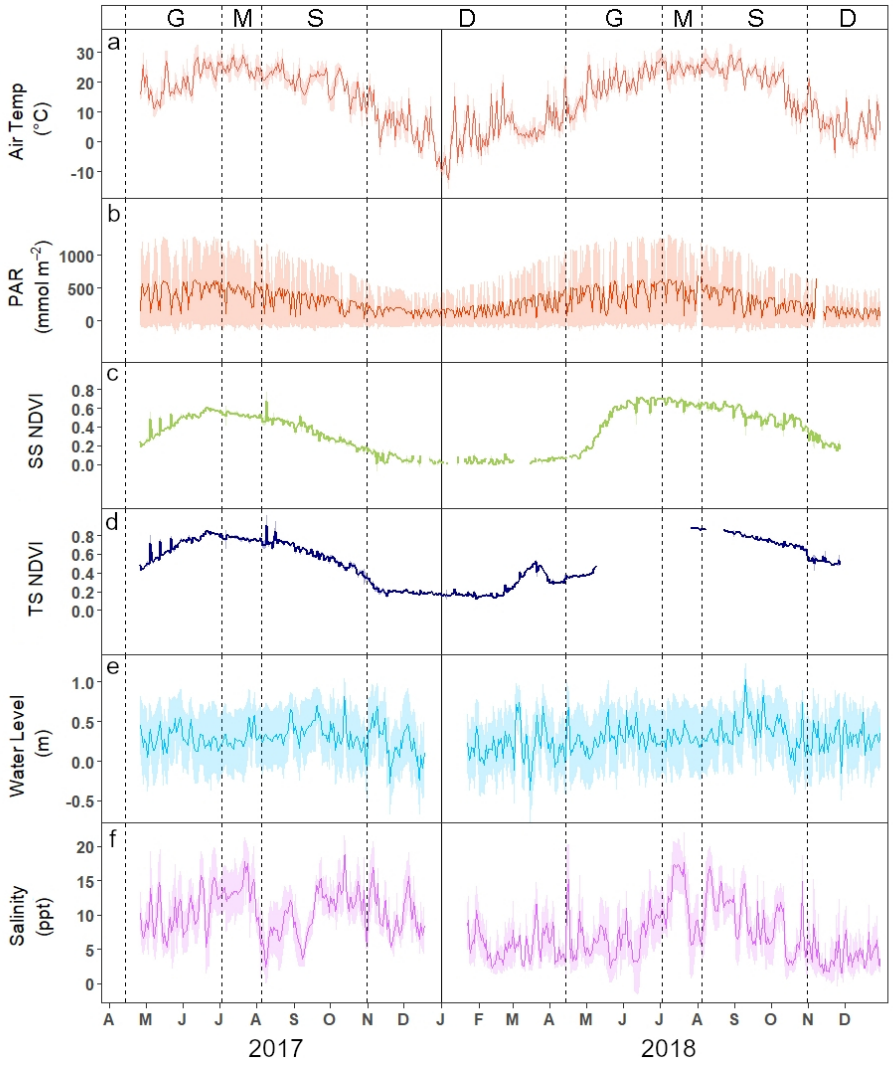

Figure 3.2: Time series of daily mean ± SD (shaded region around the daily mean) of (a) air temperature, (b) PAR, (c) SS NDVI, (d) TS NDVI, (e) water level, and (f) salinity from April 26, 2017 to December 31, 2018. G = greenup, M = maturity, S = senescence, D= dormant.

3.3.2 Soil CO_2 efflux

The mean CO_2 efflux was significantly higher at the SS site than the TS site (Fig. 3.3; t-test, $p < 0.001$), with average of 2.15 ± 1.60 μmol CO_2 m^{-2} s^{-1} and 0.55 ± 0.80 μmol CO_2 m^{-2} s^{-1}, respectively, throughout the study period. The mean from manual measurements of CO_2 efflux were not significantly different from continuous measurements for the TS site (Fig. 3.3b) but were significantly different at the SS site (Fig. 3.3a, $p < 0.001$). Consequently, average CO_2 efflux derived from manual measurements were not significantly different (SS: 0.94 ± 0.70 μmol CO_2 m^{-2} s^{-1}, TS: 0.87 ± 0.93 CO_2 m^{-2} s^{-1}). SS showed a stronger seasonal pattern than the TS fluxes, but overall, both had higher fluxes during the summer (SS: 3.05 ± 1.18 μmol CO_2 m^{-2} s^{-1}, TS: 1.22 ± 0.70 μmol CO_2 m^{-2} s^{-1}) than in the winter (SS: 0.91 ± 0.78 μmol CO_2 m^{-2} s^{-1}, TS: 0.16 ± 0.25 μmol CO_2 m^{-2} s^{-1}). For both sites, the Dormant phenophase (SS: 1.14 ± 1.06 μmol CO_2 m^{-2} s^{-1}, TS: 0.15 ± 0.19 μmol CO_2 m^{-2} s^{-1}) had significantly lower fluxes than the other three phases (t-test, $p < 0.001$). The Greenup (2.83 ± 1.43 μmol CO_2 m^{-2} s^{-1}), Maturity (3.12 ± 1.43 μmol CO_2 m^{-2} s^{-1}), and Senescence (2.74 ± 1.78 μmol CO_2 m^{-2} s^{-1}) phenophases at the SS site were not significantly different from each other. Meanwhile at the TS site, the Greenup (0.75 ± 0.92 μmol CO_2 m^{-2} s^{-1})/Maturity (1.49 ± 1.51 μmol CO_2 m^{-2} s^{-1}) and Maturity/Senescence (0.60 ± 0.55 μmol CO_2 m^{-2} s^{-1}) phenophases were significantly different ($p = 0.002$; $p < 0.001$, respectively). The difference between Greenup/Senescence was marginally significant ($p = 0.08$).

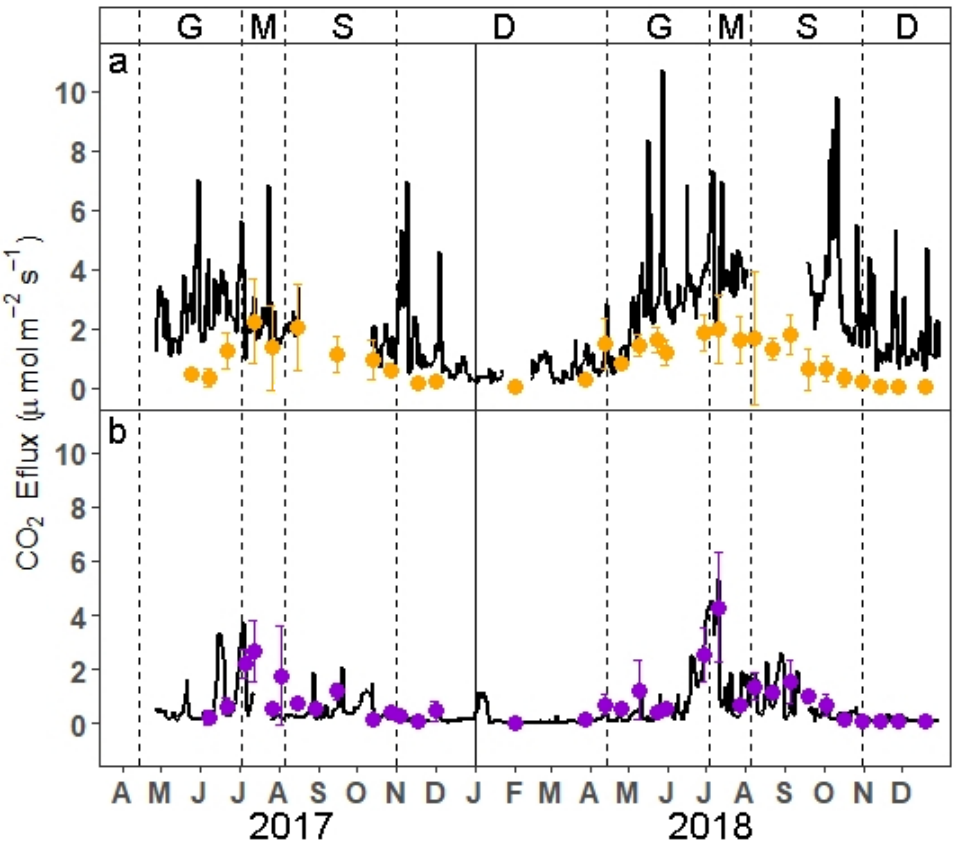

Figure 3.3: Time series of the daily mean CO_2 efflux from the (a) SS and (b) TS sites from April 26, 2017 to December 31, 2018. Dots with error bars represent the daily average ± SD of manual measurements taken throughout the study period. G = greenup, M = maturity, S = senescence, D = dormant.

Diel patterns of CO_2 efflux and water level during representative spring tide days do not show similar efflux patterns both between and within sites. Fig. 3.4c, g, and h showed a pattern similar to the rise and fall of the tides, while Fig. 3.4a, b, e, and f show higher efflux at low tide and vice versa. Similar variations in efflux patterns are also found during representative neap tide days (Fig. 3.5). We found no significant difference between the daily mean values at spring tide vs neap tide.

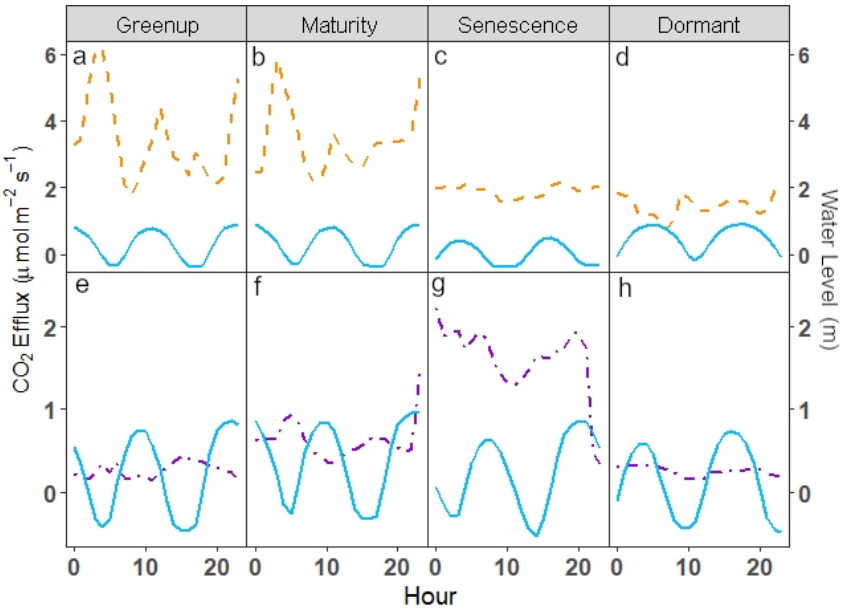

Figure 3.4: Diel patterns of hourly CO_2 efflux (dashed lines) and water level (solid blue line) on a selected spring tide day during each phenophase at (a–d) SS and (e-h) TS.

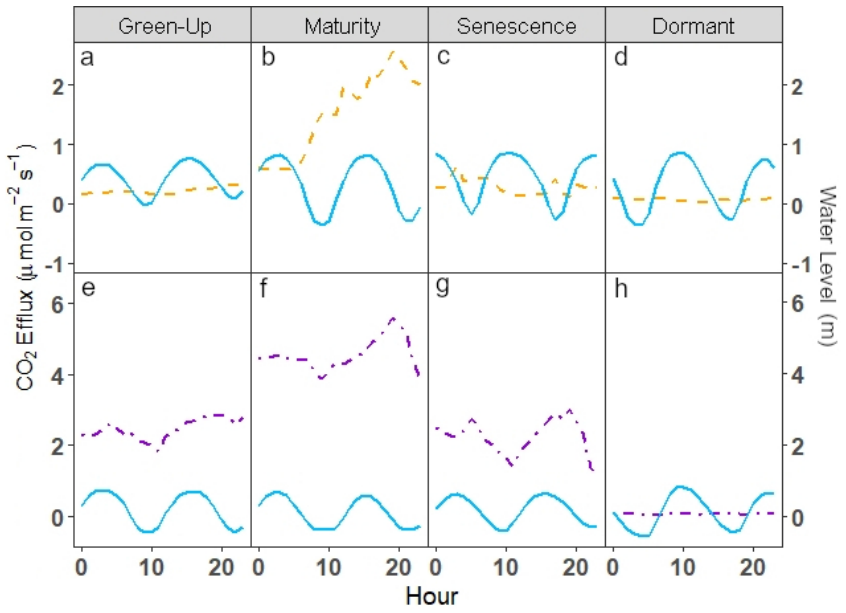

Figure 3.5: Diel patterns of hourly CO_2 efflux (dashed lines) and water level (solid blue line) on a selected neap tide day during each phenophase at (a–d) SS and (e–h) TS.

Furthermore, we found different types of hysteresis loops between CO_2 efflux and air temperature. The patterns of these loops change from day to day, but we highlight three general patterns: counterclockwise (Fig. 3.6a, b), double peaks (Fig. 3.6c), and figure-8 (Fig. 3.6d).

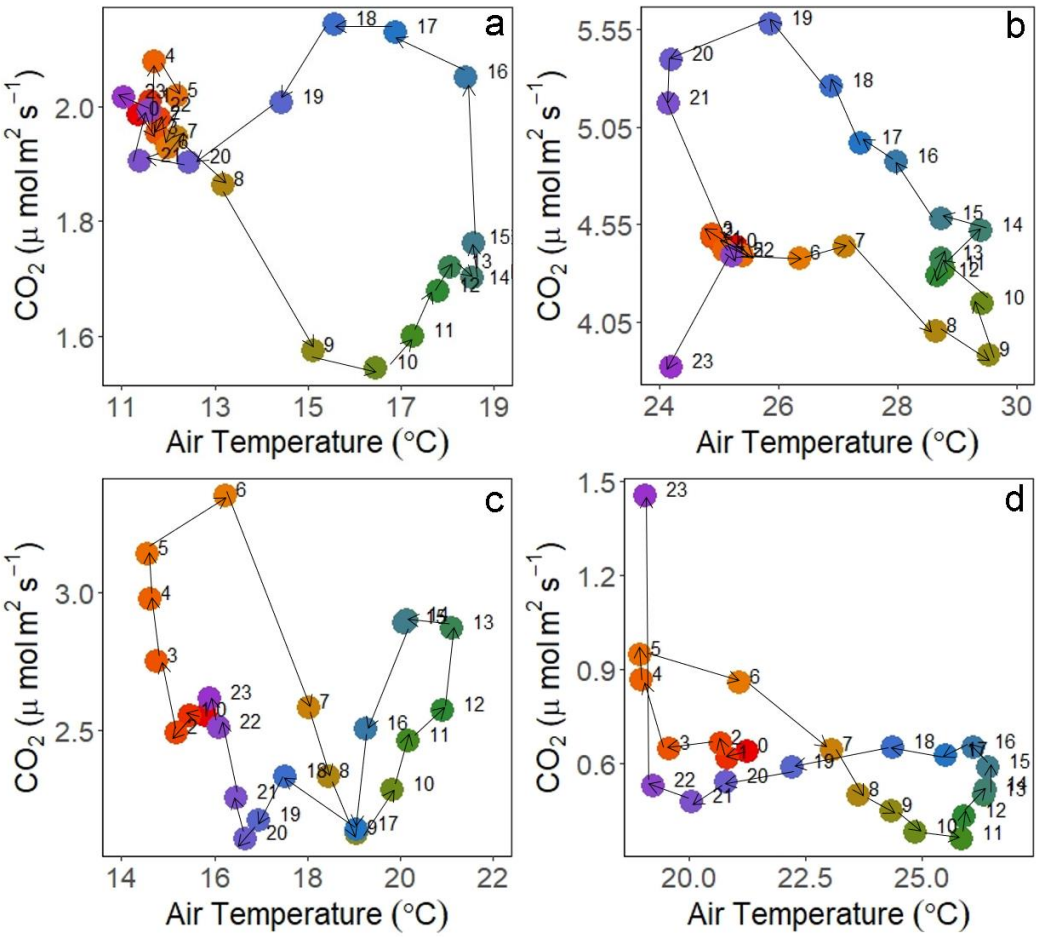

Figure 3.6: Examples of hysteresis loops between soil CO_2 efflux and air temperature from SS (a, c) and TS (b, d). Note: scales of both x- and y-axes differ between graphs to better show hysteresis loops.

3.3.3 Relationship between CO_2 efflux and biophysical drivers

Fig. 3.7 shows the relationship between both continuous and manual CO_2 efflux and air temperature at each site. Using log transformed CO_2 efflux data derived from automated measurements, we found that roughly half of the variability at the SS and TS sites was explained by air temperature. Air temperature also explains a substantial portion of the variability in the manual measurements, with an R^2 of 0.73 and 0.65 for the SS and TS sites, respectively (Figs. 3.7c, d). All models were significant (Table B.1).

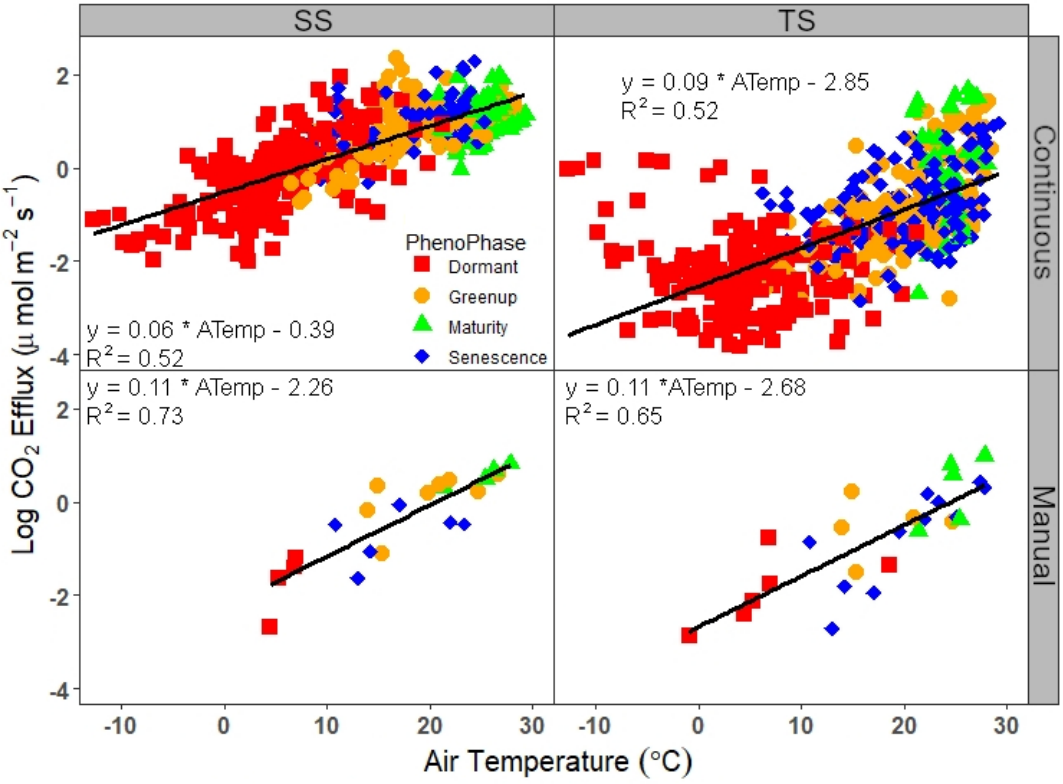

Figure 3.7: Relationship between daily (a) automated SS, (b) automated TS, (c) manual SS, and (d) manual TS CO_2 efflux and daily air temperature throughout the study period. Colored shapes indicate different phenophases.

Manual measurements overestimate the strength of the temperature dependence of soil CO_2 efflux. Using the 95% confidence interval of each model's slopes, we found that the slopes for the continuous SS ($0.058 < m < 0.070$) and the continuous TS models were significantly different ($0.086 < m < 0.103$), as well as the continuous SS and the manual SS ($0.78 < m < 0.141$). The 95% confidence intervals for the slopes of the manual TS and continuous TS models overlapped and therefore are not significantly different (Table B.1).

The residuals from the CO_2 efflux ~ air temperature models for the SS show that water level had the strongest correlation with model residuals, explaining 24% of the residual variability (Fig. 3.8). NDVI, PAR, and salinity had significant relationships with the model residuals, but the correlations are weak. At the TS site, salinity had the strongest correlation with model residuals, explaining 12% of the variability. NDVI and water level also had significant, but weak relationships with the model residuals. Residuals from the linear models using manual measurements did not have any significant relationships with NDVI, water level, salinity, or PAR for both sites.

In both 2017 and 2018, the SS site had a higher cumulative annual CO_2 efflux than the TS site (Fig. 3.9). The cumulative annual fluxes in the SS were 716 g C m^{-2} and 876 g C m^{-2}, with a 95% CI from 597 to 808 g C m^{-2} and from 783 to 950 g C m^{-2}, for 2017 and 2018 respectively. The TS site had cumulative annual efflux of 153 g C m^{-2} and 211 g C m^{-2}, with 95% CI from 138 to 170 g C m^{-2} and from 202 to 221 g C m^{-2}, respectively. The cumulative annual efflux for manual measurements at the SS site were significantly lower than the annual efflux calculated for the continuous measurements, but were similar for both years (278 vs 287 g C m^{-2}). Likewise, the

cumulative annual efflux for the manual measurements at the TS site were similar for both years (155 vs 162 g C m^{-2}). However, during 2017, the annual cumulative flux calculated for both the manual and continuous measurements at the TS site were similar, while in 2018 the manual annual cumulative flux was lower than the continuous measurements.

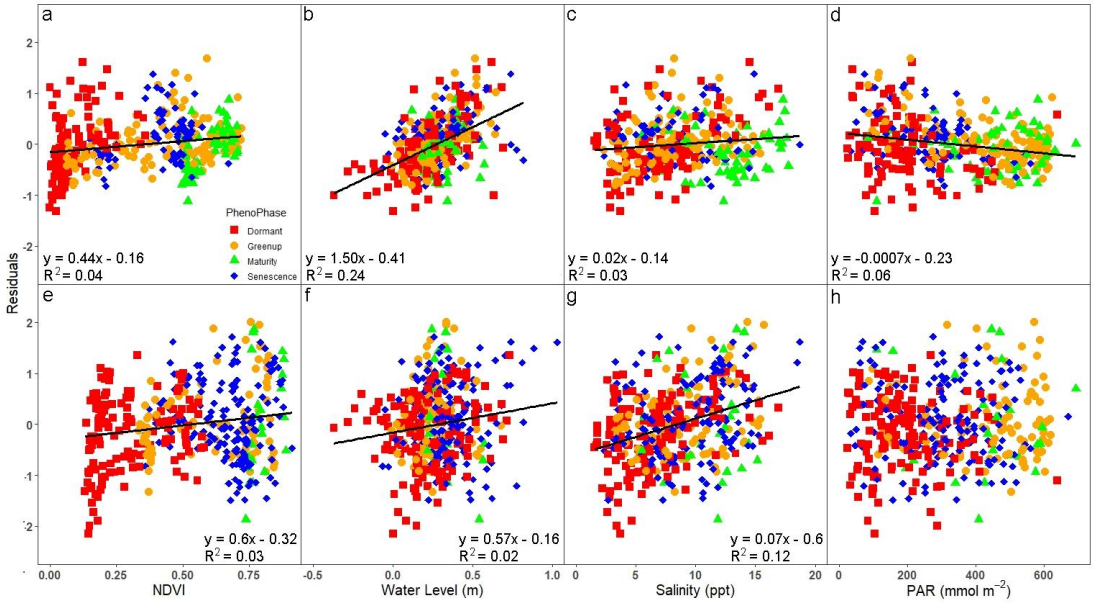

Figure 3.8: Relationships between CO_2 efflux ~ air temperature model residuals and biophysical variables for (a-d) SS and (e-h) TS. Colored shapes indicate different phenophases. All models except panel h are significant ($p < 0.05$).

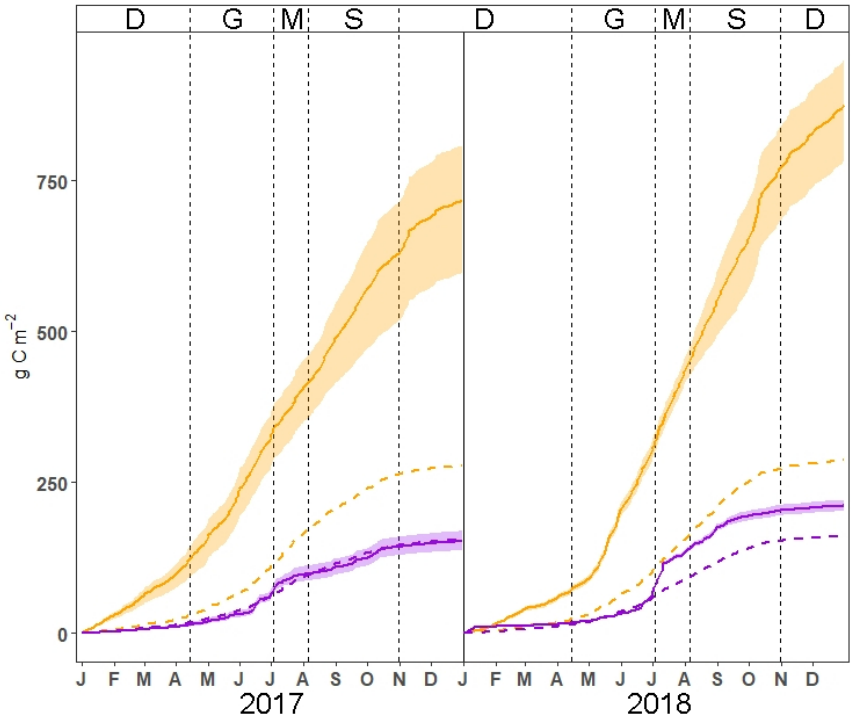

Figure 3.9: Cumulative daily CO_2 efflux annual sum for SS (orange) and TS (purple) (± 95% confidence intervals are shown by the shaded areas). Solid line denotes the cumulative daily CO_2 efflux annual sum for the continuous measurements. Dashed line represents the cumulative sums of the manual measurements. Phenophases are as follows: D = dormant, G = greenup, M = maturity, and S = senescence.

3.4 Discussion

Our study used a combination of manual and continuous, automated measurements to investigate the patterns and drivers of CO_2 efflux in tidal salt marsh soils. To the best of our knowledge, this is the first long-term (i.e., >20 months), hourly dataset of soil CO_2 efflux in a tidal temperate salt marsh. Our data set showed unprecedented and unexpected temporal dynamics, particularly the lack of diel patterns, which complicates efforts to model soil CO_2 efflux on sub-daily and diel scales. However, a strong relationship between soil CO_2 efflux and temperature

emerged on the seasonal scale, despite other potentially confounding factors (i.e., tides, salinity), which provides support for using models based on temperature dependence functions. We also found both similarities and discrepancies between manual and automated measurements, which underscores the need to assess spatial and temporal variability to gain a better understanding of the heterogeneity of salt marsh soil CO_2 efflux.

Our first hypothesis stated that CO_2 efflux will follow clear seasonal and diel patterns (as expected for terrestrial ecosystems; (Hibbard et al., 2005)), but diel patterns might be dampened due to tidal cycles, which can regulate soil CO_2 diffusion rates and soil temperature fluctuations. As expected for temperate ecosystems, both the SS and TS sites demonstrated a clear seasonal pattern following temperature trends during both study years, with higher fluxes in the summer (Fig. 3.3). Seasonal patterns in CO_2 efflux have been found in other marshes, likely due to increased heterotrophic respiration and substrate availability (Simpson et al., 2019). The seasonal pattern was weaker at the TS site, likely a result of its proximity to the tidal creek and its tidal patterns. The larger changes in water level at TS compared to SS may have reduced the influence of seasonal changes in temperature and plant productivity due to shifts in redox (Seyfferth et al., 2020). Furthermore, the TS site's hydraulic connectivity to the tidal creek may contribute to the loss of CO_2 via lateral exchange (Trifunovic et al., 2020). Higher fluxes during the summer compared to the winter has also been observed at other temperate wetland sites (Bridgham and Richardson, 1992; Seyfferth et al., 2020; Simpson et al., 2019; Yu et al., 2019). Additionally, the daily mean CO_2 efflux values measured at both the SS and TS sites fall within the range of values reported in other temperate coastal wetlands (Duarte et al., 2013; Seyfferth et al.,

2020), but are higher than in a sub-tropical marsh (Simpson et al., 2019). Our values were also higher than nighttime R_s values reported in temperate salt marshes on Cape Cod (Abdul-Aziz et al., 2018). Our findings show the presence of seasonal patterns and support the use of seasonal relationships to model soil CO_2 efflux in temperate tidal salt marshes.

In contrast with terrestrial ecosystems, we did not find consistent diel patterns in soil CO_2 efflux at either site. One previous study using limited information (only 35 days) from automated measurements in wetland soils also showed highly variable CO_2 efflux throughout the day (Diefenderfer et al., 2018). At our study site, some days had higher fluxes during low tide (i.e., Figs. 3.4e–f, 3.5c), while other days had higher fluxes during high tide (i.e., Figs. 3.4c, 3.5e–g). We highlight that soil CO_2 efflux did not peak around midday or shortly after, when air temperature peaks, suggesting that air temperature is not the dominant driver of soil CO_2 efflux at the diel scale. This finding differs from what researchers have observed in temperate forests, where diel relationships between CO_2 efflux and temperature occur frequently (Jia et al., 2013; Liu et al., 2006; Phillips et al., 2010). Furthermore, neither site consistently had lower soil CO_2 efflux at higher creek water levels, suggesting that creek water level is not the sole driver of soil CO_2 efflux at diel scales either. It is likely that diel patterns in CO_2 efflux are driven by a combination of temperature and tide that changes from day to day within a spring-neap tidal cycle.

There were no significant differences in soil CO_2 efflux between days with spring or neap tides. These results appear to contrast with past research that has shown lower nighttime NEE during spring tides that inundate the marsh (Forbrich and Giblin, 2015; Guo et al., 2009; Knox et al., 2018). We clarify that nighttime NEE, which

measures respiration processes that occur at night, could be used as a proxy for soil CO_2 efflux in eddy covariance studies (Mahecha et al., 2010). That said, it is important to note that nighttime NEE, which includes both plant and soil respiration, cannot be assumed to fully represent soil CO_2 efflux (Barba et al., 2018) and this may be especially relevant for tidal wetlands (Trifunovic et al., 2020). Our study sites rarely flood during spring tides unless it coincides with a rain event and the vegetation is rarely submerged (only after hurricane events). Therefore, we postulate that proximity to the tidal creek and marsh elevation are important factors in whether soil CO_2 efflux is influenced by spring tides since locations closer to the creek and/or lower in elevation would be more hydraulically connected and therefore experience more frequent flooding events. The SS site, despite being lower in elevation than the TS site, may be too far from the main tidal channel to be heavily influenced by tides. While it appears that soil CO_2 efflux at TS is not tidally controlled at diel scale despite its proximity to the main tidal channel, CO_2 produced there may be laterally transported into the creek. A previous study conducted at the site found high concentrations of pCO_2 in the creek water (upwards of 10,000 μmol/mol) as well as higher CO_2 efflux from the water surface compared to the soil (Trifunovic et al., 2020). These findings suggest lateral movement into and export of CO_2 from the tidal creek, potentially affecting the soil CO_2 concentrations and efflux at sites near the creek. Our findings suggest that the role of tides in soil CO_2 efflux is complex and may require detailed hydrological information of how tides affect localized water levels at specific soil CO_2 efflux measurement sites in coastal wetlands.

We found diel hysteresis loops between soil CO_2 efflux and air temperature or water level. Furthermore, the direction of these loops (i.e., clockwise and

counterclockwise) change throughout our measurements demonstrating that although temperature and water level are important controls for diel patterns, they represent non-linear influences on soil CO_2 efflux that will be difficult to model at the diel scale. That said, the hysteresis loops with temperature generally moved in a counterclockwise direction, indicating that the highest fluxes occurred after the highest temperatures (Fig. 3.6a, b). This pattern is not uncommon in terrestrial ecosystems, as several studies have shown that peak soil respiration rates may lag several hours behind peak daily temperatures (Barron-Gafford et al., 2011; Phillips et al., 2011; Vargas and Allen, 2008). The saturated soils in tidal wetlands reduce CO_2 diffusivity from where it is produced within the soil to the atmosphere, slowing diffusion by roughly 10,000 times compared to diffusion through air (Suarez and Simunek, 1993). Low gas diffusivity results in an increase in the time CO_2 remains in the soil and delays the soil CO_2 efflux response to temperature. Another explanation for counterclockwise hysteresis loops is that photosynthesis lags due to photosynthate travel times, which can take hours to weeks depending on the plant size (Kuzyakov and Cheng, 2001; Vargas et al., 2011a; Zhang et al., 2018). Recently fixed carbon in *S. alterniflora* plants have been found in soil bacteria within 24 h (Spivak and Reeve, 2015). While most of the soil CO_2 efflux ~ air temperature hysteresis loops are counter-clockwise, there are loops with two peaks (Fig. 3.6c, B.1a, B.3b) and figure-8 loops (Fig. 3.6b). Hysteresis loops with double peaks may be the result of asynchronous peaks in substrate supply and soil temperature (Phillips et al., 2011). Meanwhile, Zhang et al. (2015) suggests figure-8 loops result from the transition between counterclockwise and clockwise loops (or vice versa) due to changes in the photosynthesis lag time. We postulate that in tidal salt marshes, this asynchrony may

be influenced by the interaction between tides and substrate. Tides bring in nutrients and substrates that may be used in microbial processes, in addition to altering soil redox and CO_2 diffusivity. More research is needed to better understand how different environmental factors, particularly tides, interact to influence CO_2 efflux at the diel scale.

Our second hypothesis (H2) was rejected due to the SS site having significantly higher soil CO_2 efflux (2.15 ± 1.60 μmol CO_2 m^{-2} s^{-1}) than the TS site (0.55 ± 0.80 μmol CO2 m^{-2} s^{-1}), highlighting distinct biogeochemical spatial variability. The SS site's disproportionately higher soil CO_2 efflux suggests that the location may be a hot spot within the landscape (Leon et al., 2014; McClain et al., 2003), especially when compared to the manual measurements conducted nearby during this study and by Seyfferth et al. (2020), which generally ranged from 0 to 5 μmol CO_2 m^{-2} s^{-1}. Seyfferth et al. (2020) showed that the SS site had lower concentrations of DOC in the porewater, lower %C in the soil, and higher water table elevation than the TS site, which would suggest that the SS site would have lower overall CO_2 efflux. However, it is possible that the location of our automated measurements within the SS site had a lower water table, higher elevation, higher DOC, and/or higher % soil C content than the surrounding area due to slight changes in microtopography, resulting in higher soil CO_2 efflux rates. Short *S. alterniflora* covers 66% (Vázquez-Lule and Vargas, 2021) of the marsh and can potentially have multiple hot spots located in areas where local biogeochemical conditions support high fluxes. Even with the exclusion of the SS hot spot, there were no significant differences between the manual measurements conducted at both sites, as well as between the continuous TS and manual SS measurements. Our finding highlights the

importance of assessing spatial variability within tidal salt marshes. Studies have shown that soil biogeochemistry differs within a tidal salt marsh. For example, areas nearby tidal creeks tend to have higher concentrations of ferrous iron, whereas locations further from or less influenced by the tidal creeks tend to have large amounts of sulfide (Seyfferth et al., 2020; Taillefert et al., 2007). Furthermore, changes in microtopography can affect sediment biogeochemistry (Stribling et al., 2006) and can likely have an impact on soil CO_2 efflux by creating multiple hot spots within the marsh where the soil is not as saturated. By combining high-frequency measurements with spatially diverse point measurements, scientists will be better able to locate and confirm hot spots within a marsh, as well as assess spatial heterogeneity.

Using linear models, we found that air temperature was the strongest overall driver of soil CO_2 efflux at both of our sites and for both manual and automated measurements, confirming one component of our third hypothesis. Our results are consistent with previous research that show the importance of temperature on soil CO_2 efflux, particularly at longer time scales. For example, Simpson et al. (2019) found that soil temperature explained 42% of the variability in soil CO_2 efflux measured at Florida mangrove and salt marsh sites. Another study, which used ecosystem respiration (R_{eco}) derived from nighttime EC measurements, found that on a semiannual scale, temperature explained between 9 and 93.1% of the nighttime fluxes, but the proportion of R_{eco} explained by temperature varied widely over shorter time scales (i.e., monthly, seasonally) as the importance of tides increased (Xie et al., 2014).

While temperature explains a similar proportion of variation in soil CO_2 efflux at both continuous measurement locations, the slopes are significantly different,

underscoring that different locations within the marsh have different temperature sensitivities. The TS site has a higher slope (m = 0.09) than the SS site (m = 0.06) suggesting higher temperature sensitivity at that site. However, the manual measurements at both sites had near identical slopes (m = ~0.11). The manual and continuous measurements at the TS site had similar slopes as well. These results highlight the complexity of determining the temperature sensitivity of soil CO_2 efflux within a salt marsh, which may be highly variable across the landscape depending on local conditions that affect soil CO_2 efflux (i.e., water level, microbial community, substrate availability). We highlight that emergent machine learning methods may be able to predict non-linear patterns of soil CO_2 efflux in these and other ecosystems (Vargas et al., 2018).

The second component of our third hypothesis, that water quality and plant biology play a role in soil CO_2 efflux, was confirmed. With the effect of temperature removed from the time series, we found that all four biophysical variables (NDVI, water level, salinity, and PAR) were significant for SS and three (NDVI, water level, salinity) were significant for TS for continuous measurements. Salinity and water level are the most important drivers at the TS and SS sites, respectively. At the TS site, salinity appears to play a role, with higher CO_2 efflux at higher salinities. Due to its proximity to the tidal creek, salinity levels at TS likely experience a large enough variation to affect soil CO_2 efflux. Previous research has shown a positive relationship between salinity and CO_2 fluxes since salt water introduces more SO_4^{2-} into the soil pore water, causing a shift from methanogenesis to sulfate reduction, which is more energetically favorable (Capone and Kiene, 1988; Capooci et al., 2019; Chambers et al., 2013). We expected that creek water level would play a bigger role at the TS site

rather than the SS site, due to its proximity to the tidal creek contributing to large changes in water level. Our finding that creek water level plays a more significant role at the SS site, which is less influenced by tidal creek water levels due to the formation of natural levee at the creek bank, as well the positive relationship between soil CO_2 efflux and creek water level runs counter to our hypothesis. Since the location of the SS measurement site is further from the tidal creek, it is possible that there is a lag between the high-water level in the creek and the high-water level at the SS site. Localized measurements of soil water level would be better suited to understanding the effect of water level on soil CO_2 efflux, particularly in a heterogeneous landscape.

While air temperature explained 73% and 65% of the variability in the manual measurements at the SS and TS sites, respectively, the other four biophysical variables did not significantly explain the remaining variability. These linear model results suggest that measuring and modeling diel soil CO_2 efflux variability in salt marshes may be more challenging than previously expected due to large discrepancies between manual and automated soil CO_2 efflux measurements, supporting our fourth hypothesis. It is difficult to model certain patterns when measurements are collected every two weeks. It is likely that the high-frequency data from the continuous measurements was able to capture the constant changes in water level and salinity and the slight deviations in NDVI and PAR from its seasonal pattern, whereas the manual measurements could only give a biweekly snapshot. While the manual measurement frequency (every two weeks) was sufficient to capture similar soil CO_2 efflux ~ air temperature relationships as the continuous measurements, it was not able to account for the remaining soil CO_2 efflux variability with the other biophysical variables. In tidal salt marshes, researchers should select the measurement frequency that best

answers their question: manual measurements to capture spatial variability, continuous measurements for better understanding the role other biophysical factors play in soil CO_2 efflux, particularly if the biophysical variables, such as tides and salinity, are constantly changing on sub-daily timescales.

Furthermore, we found that manual measurements underestimated the annual flux by <67% at SS and <23% at TS. This discrepancy highlights the inability of manual measurements to capture short-term variability in soil CO_2 efflux, as well as hot spots as seen at the SS site. While the continuous SS annual soil CO_2 efflux is significantly higher than the annual soil CO_2 efflux calculated for the manual SS, as well both manual and continuous TS, it falls within the mid-range of global annual R_s values reported in Jian et al. (2020) and within the range of 576.08 ± 393.82 g C m^{-2} yr^{-1} reported by Warner et al. (2019) for permanent wetlands. However, the annual soil CO_2 efflux from the TS site are lower than values reported from a New England salt marsh (Howes et al., 1985) and from *S. alterniflora* in a South Carolina salt marsh (Morris and Whiting, 1986). Both studies measured CO_2 fluxes monthly at low tide, which may result in an overestimation of the annual cumulative flux since CO_2 fluxes generally seem higher at low tide.

The discrepancies between manual and continuous measurements underscore the importance of obtaining data at daily time scales. In particular, modeling efforts such as the Community Earth System Model (Lu et al., 2018; Randerson et al., 2015) would benefit from long term, continuous data that helps elucidate how various environmental factors within a tidal salt marsh affect soil CO_2 efflux. Furthermore, high-frequency soil respiration data can be beneficial in partitioning NEE, as measured by eddy covariance towers, into gross ecosystem carbon uptake and R_{eco}. It

is important to verify R_{eco} produced via partitioning of eddy covariance data with automated measurements since there can be discrepancies between the two (Barba et al., 2018). This may be especially important in tidal salt marshes, where the short-term relationship between temperature and nighttime R_{eco} is confounded by tidal fluctuations and cannot be as easily extrapolated to daytime R_{eco}.

3.5 Conclusion

High-frequency, long-term measurements of soil CO_2 efflux at a tidal salt marsh showed the importance of continuous measurements in capturing temporal variability, particularly at the diel scale, where we found that soil CO_2 efflux did not appear to follow temperature or tidal variation over the course of the day, nor did it follow spring-neap tidal cycles. The lack of diel patterns underscores the complex interactions between the biophysical variables that influence soil CO_2 efflux in these ecosystems. In contrast, on the annual scale we found strong relationships between temperature and soil CO_2 efflux, reinforcing the importance of temperature on soil respiration. These results highlight the need for more research on the biophysical controls, particularly temperature and tides, of soil CO_2 efflux on the diel scale and underscores the difficultly of modeling daily soil CO_2 efflux in tidal salt marshes.

Furthermore, by incorporating periodic manual measurements throughout the automated measurement period, we were able to better assess the spatial variability of soil CO_2 efflux in two distinct zones in a tidal salt marsh. The differences in soil CO_2 efflux derived from manual and continuous measurements in the SS zone underscored the spatial heterogeneity that exists within a salt marsh. This result highlights the need to better understand how local plant communities and biogeochemical conditions affect soil CO_2 efflux in tidal salt marshes to better assess how soil CO_2 efflux changes

across the landscape. The combination of spatial and high-frequency temporal measurements can provide better estimates of salt marsh soil CO_2 efflux to be used in models, ecosystem carbon budgets, and blue carbon offset calculations.

Acknowledgements

This research was supported by the National Science Foundation (#1652594). MC acknowledges support from the Delaware Environmental Fellowship and an NSF Graduate Research Fellowship (#1247394). We thank the onsite support from Kari St. Laurent and the Delaware National Estuarine Research Reserve (DNERR), Josep Barba for field support in collecting manual measurements, and Alma Vázquez-Lule for assistance with the NDVI data and the graphical abstract. The authors acknowledge the land on which they conducted this study is the traditional home of the Lenni-Lenape tribal nation (Delaware nation).

CRediT authorship contribution statement

Margaret Capooci: Conceptualization, Methodology, Formal analysis, Investigation, Writing – original draft, Writing – review & editing.

Rodrigo Vargas: Conceptualization, Methodology, Resources, Writing – review & editing, Supervision, Funding acquisition.

Supplementary data

Supplementary data to this article can be found online at https://doi.org/10.1016/j.scitotenv.2021.149715, as well as Appendix B of this document. The appendix contains a table of linear model results, as well as hysteresis

graphs of CO_2 flux vs. air temperature and CO_2 flux vs. water level during several spring and neap tide days throughout the study period.

REFERENCES

Abdul-Aziz, O.I., Ishtiaq, K.S., Tang, J., Moseman-Valtierra, S., Kroeger, K.D., Gonneea, M.E., Mora, J., Morkeski, K., 2018. Environmental controls, emergent scaling, and predictions of greenhouse gas (GHG) fluxes in coastal salt marshes. J. Geophys. Res. Biogeosci. 123, 2234–2256. https://doi.org/10.1029/2018JG004556.

Barba, J., Cueva, A., Bahn, M., Barron-Gafford, G.A., Bond-Lamberty, B., Hanson, P.J., Jaimes, A., Kulmala, L., Pumpanen, J., Scott, R.L., Wohlfahrt, G., Vargas, R., 2018. Comparing ecosystem and soil respiration: Review and key challenges of tower-based and soil measurements. Agric. For. Meteorol. 249, 434–443. https://doi.org/10.1016/j. agrformet.2017.10.028.

Barron-Gafford, G.A., Scott, R.L., Jenerette, G.D., Huxman, T.E., 2011. The relative controls of temperature, soil moisture, and plant functional group on soil CO_2 efflux at diel, seasonal, and annual scales. J. Geophys. Res. Biogeosci. 116, 1–16. https://doi.org/ 10.1029/2010JG001442.

Battin, T.J., Luyssaert, S., Kaplan, L.A., Aufdenkampe, A.K., Richter, A., Tranvik, L.J., 2009. The boundless carbon cycle. Nat. Geosci. 2, 598–600. https://doi.org/10.1038/ngeo618.

Bridgham, S.D., Richardson, C.J., 1992. Mechanisms controlling soil respiration (CO_2 and CH_4) in southern peatlands. Soil Biol. Biochem. 24 (11), 1089–1099.

Capone, D.G., Kiene, R.P., 1988. Comparison of microbial dynamics in marine and freshwater sediment. Limnol. Ocean. 33, 725–749.

Capooci, M., Barba, J., Seyfferth, A.L., Vargas, R., 2019. Experimental influence of storm- surge salinity on soil greenhouse gas emissions from a tidal salt marsh. Sci. Total Environ. 686, 1164–1172. https://doi.org/10.1016/j.scitotenv.2019.06.032.

Carbone, M.S., Winston, G.C., Trumbore, S.E., 2008. Soil respiration in perennial grass and shrub ecosystems: Linking environmental controls with plant and microbial sources on seasonal and diel timescales. J. Geophys. Res. Biogeosci. 113. https://doi.org/10. 1029/2007JG000611.

Chambers, L.G., Osborne, T.Z., Reddy, K.R., 2013. Effect of salinity-altering pulsing events on soil organic carbon loss along an intertidal wetland gradient: A laboratory experiment. Biogeochemistry 115, 363–383. https://doi.org/10.1007/s10533-013-9841-5.

Chimner, R.A., 2004. Soil respiration rates of tropical peatlands in Micronesia and Hawaii. Wetlands 24, 51–56. https://doi.org/10.1672/0277-5212(2004)024[0051:SRROTP]2. 0.CO;2.

Cueva, A., Bullock, S.H., López-Reyes, E., Vargas, R., 2017. Potential bias of daily soil CO_2 efflux estimates due to sampling time. Sci. Rep. 7, 1–8. https://doi.org/10.1038/ s41598-017-11849-y.

Diefenderfer, H.L., Cullinan, V.I., Borde, A.B., Gunn, C.M., Thom, R.M., 2018. High-frequency greenhouse gas flux measurement system detects winter storm surge effects on salt marsh. Glob. Chang. Biol. 24, 5961–5971. https://doi.org/10.1111/gcb.14430.

DNREC, 1999. Delaware National Estuarine Research Reserve Estuarine Profile.

Duarte, C.M., Losada, I.J., Hendriks, I.E., Mazarrasa, I., Marbà, N., 2013. The role of coastal plant communities for climate change mitigation and adaptation. Nat. Clim. Chang. 3, 961–968. https://doi.org/10.1038/nclimate1970.

Forbrich, I., Giblin, A.E., 2015. Marsh-atmosphere CO_2 exchange in a New England salt marsh. J. Geophys. Res. Biogeosci. 120, 1825–1838. https://doi.org/10. 1002/2015JG003044.

Guo, H., Noormets, A., Zhao, B., Chen, Jiquan, Sun, G., Gu, Y., Li, B., Chen, Jiakuan, 2009. Tidal effects on net ecosystem exchange of carbon in an estuarine wetland. Agric. For. Meteorol. 149, 1820–1828. https://doi.org/10.1016/j.agrformet.2009.06.010.

Han, G., Xing, Q., Luo, Y., Rafique, R., Yu, J., Mikle, N., 2014. Vegetation types alter soil respiration and its temperature sensitivity at the field scale in an estuary wetland. PLoS One 9. https://doi.org/10.1371/journal.pone.0091182.

Hayes, D.J., Vargas, R., Alin, S.R., Conant, R.T., Hutyra, L.R., Jacobson, A.R., Kurz, W.A., Lui, S., McGuire, A.D., Poulter, B., Woodall, C.W., 2018. Chapter 2: the North American carbon budget. In: Cavallaro, N., Shrestha, G., Birdsey, E., Mayes, M.A., Najjar, R.G., Reed, S.C., Romero-Lankao, P., Zhu, Z. (Eds.), Second State of the Carbon Cycle Report (SOCCR2): A Sustained Assessment Report. U.S. Global Change Research Program, Washington D.C, pp. 71–108 https://doi.org/10.7930/SOCCR2.2018.Ch2.

Hibbard, K.A., Law, B.E., Reichstein, M., Sulzman, J., 2005. An analysis of soil respiration across northern hemisphere temperate ecosystems. Biogeochemistry 73, 29–70. https://doi.org/10.1007/s10533-004-2946-0.

Hill, A, Vázquez-Lule, A, Vargas, R, 2021. Linking vegetation spectral reflectance with ecosystem carbon phenology in a temperate salt marsh. Agricultural and Forest Meteorology 307, 108481. https://doi.org/10.1016/j.agrformet.2021.108481.

Howes, B.L., Dacey, J.W.H., Teal, J.M., 1985. Annual carbon mineralization and belowground production of *Spartina alterniflora* in a New England salt marsh. Ecology 66, 595–605.

Järveoja, J., Nilsson, M.B., Gažovic, M., Crill, P.M., Peichl, M., 2018. Partitioning of the net CO_2 exchange using an automated chamber system reveals plant phenology as key control of production and respiration fluxes in a boreal peatland. Glob. Chang. Biol. 24, 3436–3451. https://doi.org/10.1111/gcb.14292.

Jia, X., Zha, T., Wu, B., Zhang, Y., Chen, W., Wang, X., Yu, H., He, G., 2013. Temperature response of soil respiration in a Chinese pine plantation: Hysteresis and seasonal vs. diel Q_{10}. PLoS One 8. https://doi.org/10.1371/journal.pone.0057858.

Jian, J., Vargas, R., Anderson-Teixeira, K., Stell, E., Herrmann, V., Horn, M., Kholod, N., Manzon, J., Marchesi, R., Paredes, D., Bond-Lamberty, B., 2020. A restructured and updated global soil respiration database (SRDB-V5). Earth System Science Data Discussions. Earth Syst. Sci. Data https://doi.org/10.5281/zenodo.3876443.

Knox, S.H., Windham-Myers, L., Anderson, F., Sturtevant, C., Bergamaschi, B., 2018. Direct and indirect effects of tides on ecosystem-scale CO_2 exchange in a brackish tidal marsh in northern California. J. Geophys. Res. Biogeosci. 123, 787–806. https://doi. org/10.1002/2017JG004048.

Koskinen, M., Minkkinen, K., Ojanen, P., Kämäräinen, M., Laurila, T., Lohila, A., 2014. Measurements of CO_2 exchange with an automated chamber system throughout the year: Challenges in measuring night-time respiration on porous peat soil. Biogeosciences 11, 347–363. https://doi.org/10.5194/bg-11-347-2014.

Kuzyakov, Y., Cheng, W., 2001. Photosynthesis controls of rhizosphere respiration and organic matter decomposition. Soil Biol. Biochem. 33, 1915–1925.

Lavoie, M., Owens, J., Risk, D., 2012. A new method for real-time monitoring of soil CO_2 efflux. Methods Ecol. Evol. 3, 889–897. https://doi.org/10.1111/j.2041-210X.2012. 00214.x.

Leon, E., Vargas, R., Bullock, S., Lopez, E., Panosso, A.R., La Scala, N., 2014. Hot spots, hot moments, and spatio-temporal controls on soil CO_2 efflux in a water-limited ecosystem. Soil Biol. Biochem. 77, 12–21. https://doi.org/10.1016/J.SOILBIO.2014.05.029.

Liu, Q., Edwards, N.T., Post, W.M., Gu, L., Ledford, J., Lenhart, S., 2006. Temperature-independent diel variation in soil respiration observed from a temperate deciduous forest. Glob. Chang. Biol. 12, 2136–2145. https://doi.org/10.1111/j.1365-2486.2006. 01245.x.

Lloyd, J., Taylor, J.A., 1994. On the temperature dependence of soil respiration. Funct. Ecol. 8, 315–323.

Lu, X., Zhou, Y., Zhuang, Q., Prigent, C., Liu, Y., Teuling, A., 2018. Increasing methane emissions from natural land ecosystems due to sea-level rise. J. Geophys. Res. Biogeosci. 123, 1756–1768. https://doi.org/10.1029/2017JG004273.

Macreadie, P.I., Anton, A., Raven, J.A., Beaumont, N., Connolly, R.M., Friess, D.A., Kelleway, J.J., Kennedy, H., Kuwae, T., Lavery, P.S., Lovelock, C.E., Smale, D.A., Apostolaki, E.T., Atwood, T.B., Baldock, J., Bianchi, T.S., Chmura, G.L., Eyre, B.D., Fourqurean, J.W., Hall-Spencer, J.M., Huxham, M., Hendriks, I.E., Krause-Jensen, D., Laffoley, D., Luisetti, T., Marbà, N., Masque, P., McGlathery, K.J., Megonigal, J.P., Murdiyarso, D., Russell, B.D., Santos, R., Serrano, O., Silliman, B.R., Watanabe, K., Duarte, C.M., 2019. The future of blue carbon science. Nat. Commun. 10. https://doi.org/10.1038/ s41467-019-11693-w.

Mahecha, M.D., Reichstein, M., Carvalhais, N., Lasslop, G., Lange, H., Seneviratne, S.I., Vargas, R., Ammann, C., Altaf Arain, M., Cescatti, A., Janssens, I.A., Migliavacca, M., Montagnani, L., Richardson, A.D., 2010. Global convergence in the temperature sensitivity of respiration at ecosystem level. Science 329, 838–840. https://doi.org/10.1126/science.1184984.

McClain, M.E., Boyer, E.W., Dent, C.L., Gergel, S.E., Grimm, N.B., Groffman, P.M., Hart, S.C., Harvey, J.W., Johnston, C.A., Mayorga, E., Mcdowell, W.H., Pinay, G., 2003. Biogeochemical hot spots and hot moments at the interface of terrestrial and aquatic ecosystems. Ecosystems 6, 301–312. https://doi.org/10.1007/s10021-003-0161-9.

Morris, J.T., Whiting, G.J., 1986. Emission of gaseous carbon dioxide from salt-marsh sediments and its relation to other carbon losses. Estuaries 9, 9–19.

Moseman-Valtierra, S., Abdul-Aziz, O.I., Tang, J., Ishtiaq, K.S., Morkeski, K., Mora, J., Quinn, R.K., Martin, R.M., Egan, K., Brannon, E.Q., Carey, J., Kroeger, K.D., 2016. Carbon dioxide fluxes reflect plant zonation and belowground biomass in a coastal marsh. Ecosphere 7. https://doi.org/10.1002/ecs2.1560.

NASAM, 2019. Negative emissions technologies and reliable sequestration: A research agenda. doi:10.17226/25259.

NOAA National Estuarine Research Reserve System (NERRS), 2015. System-wide Monitoring Program [WWW Document]. NOAA NERRS Cent. Data Manag. Off.

Nyman, J.A., Delaune, R.D., 1991. CO_2 emission and soil Eh responses to different hydrological conditions in fresh, brackish, and saline marsh soils. Limnol. Oceanogr. 36, 1406–1414.

O'Connell, J.L., Mishra, D.R., Cotten, D.L., Wang, L., Alber, M., 2017. The tidal marsh inundation index (TMII): An inundation filter to flag flooded pixels and improve MODIS tidal marsh vegetation time-series analysis. Remote Sens. Environ. 201, 34–46. https://doi. org/10.1016/j.rse.2017.08.008.

Pearson, A.J., Pizzuto, J.E., Vargas, R., 2016. Influence of run of river dams on floodplain sediments and carbon dynamics. Geoderma 272, 51–63. https://doi.org/10.1016/j. geoderma.2016.02.029.

Peterson, P.M., Romaschenko, K., Arrieta, Y.H., Saarela, J.M., 2014. A molecular phylogeny and new subgeneric classification of *Sporobolus* (Poaceae: Chloridoideae: Sporobolinae). Taxon. https://doi.org/10.12705/636.19.

Petrakis, S., Seyfferth, A., Kan, J., Inamdar, S., Vargas, R., 2017. Influence of experimental extreme water pulses on greenhouse gas emissions from soils. Biogeochemistry 133, 147–164. https://doi.org/10.1007/s10533-017-0320-2.

Phillips, S.C., Varner, R.K., Frokling, S., Munger,W., Bubier, J.L., Wofsy, S.C., Crill, P.M., 2010. Interannual, seasonal, and diel variation in soil respiration relative to ecosystem respiration at a wetland to upland slope at Harvard Forest. J. Geophys. Res. 115. https:// doi.org/10.1029/2008JG000858.

Phillips, C.L., Nickerson, N., Risk, D., Bond, B.J., 2011. Interpreting diel hysteresis between soil respiration and temperature. Glob. Chang. Biol. 17, 515–527. https://doi.org/10. 1111/j.1365-2486.2010.02250.x.

Randerson, J.T., Lindsay, K., Munoz, E., Fu, W., Moore, J.K., Hoffman, F.M., Mahowald, N.M., Doney, S.C., 2015. Multicentury changes in ocean and land contributions to the climate-carbon feedback. Glob. Biogeochem. Cycles 29, 744–759. https://doi.org/10.1111/1462-2920.13280.

Sapkota, Y., White, J.R., 2020. Carbon offset market methodologies applicable for coastal wetland restoration and conservation in the United States: A review. Sci. Total Environ. https://doi.org/10.1016/j.scitotenv.2019.134497.

Savage, K.E., Davidson, E.A., 2003. A comparison of manual and automated systems for soil CO_2 flux measurements: Trade-offs between spatial and temporal resolution. J. Exp. Bot. 54, 891–899. https://doi.org/10.1093/jxb/erg121.

Savage, K., Phillips, R., Davidson, E., 2014. High temporal frequency measurements of greenhouse gas emissions from soils. Biogeosciences 11, 2709–2720. https://doi. org/10.5194/bg-11-2709-2014.

Seyfferth, A.L., Bothfeld, F., Vargas, R., Stuckey, J.W., Wang, J., Kearns, K., Michael, H.A., Guimond, J., Yu, X., Sparks, D.L., 2020. Spatial and temporal heterogeneity of geochemical controls on carbon cycling in a tidal salt marsh. Geochim. Cosmochim. Acta 282, 1–18. https://doi.org/10.1016/j.gca.2020.05.013.

Simpson, L.T., Osborne, T.Z., Feller, I.C., 2019. Wetland soil CO_2 efflux along a latitudinal gradient of spatial and temporal complexity. Estuar. Coasts 42, 45–54. https://doi. org/10.1007/s12237-018-0442-3.

Spivak, A.C., Reeve, J., 2015. Rapid cycling of recently fixed carbon in a *Spartina alterniflora* system: A stable isotope tracer experiment. Biogeochemistry 125, 97–114. https://doi.org/10.1007/s10533-015-0115-2.

Spivak, A.C., Sanderman, J., Bowen, J.L., Canuel, E.A., Hopkinson, C.S., 2019. Global-change controls on soil-carbon accumulation and loss in coastal vegetated ecosystems. Nat. Geosci. 12, 685–692. https://doi.org/10.1038/s41561-019-0435-2.

Stribling, J.M., Glahn, O.A., Chen, X.M., Cornwell, J.C., 2006. Microtopographic variability in plant distribution and biogeochemistry in a brackish-marsh system. Mar. Ecol. Prog. Ser. 320, 121–129. https://doi.org/10.3354/meps320121.

Suarez, D.L., Simunek, J., 1993. Modeling of carbon dioxide transport and production in soil 2. Parameter selection, sensitivity analysis, and comparison of model predictions to field data. Water Resour. Res. 29, 499–513.

Taillefert, M., Neuhuber, S., Bristow, G., 2007. The effect of tidal forcing on biogeochemical processes in intertidal salt marsh sediments. Geochem. Trans. 8. https://doi.org/10. 1186/1467-4866-8-6.

Tobias, C., Neubauer, S.C., 2019. Salt marsh biogeochemistry – an overview. In: Perillo, G.M.E., Wolanski, E., Cahoon, D.R., Hopkinson, C.S. (Eds.), Coastal Wetlands: An Integrated Ecosystem Approach. Elsevier B.V., Amsterdam, pp. 539–596 https://doi.org/ 10.1016/B978-0-444-63893-9.00016-2 539.

Trifunovic, B., Vázquez-Lule, A., Capooci, M., Seyfferth, A.L., Moffat, C., Vargas, R., 2020. Carbon dioxide and methane emissions from temperate salt marsh tidal creek. J. Geophys. Res. Biogeosci. 125. https://doi.org/10.1029/2019JG005558.

Vargas, R., Allen, M., 2008. Diel patterns of soil respiration in a tropical forest after Hurricane Wilma. J. Geophys. Res. Biogeosci. 113, 1–10. https://doi.org/10.1029/ 2007JG000620.

Vargas, R., Baldocchi, D.D., Bahn, M., Hanson, P.J., Hosman, K.P., Kulmala, L., 2011a. On the multi-temporal correlation between photosynthesis and soil CO_2 efflux: reconciling lags and observations. New Phytol. 191, 1006–1017.

Vargas, R., Carbone, M.S., Reichstein, M., Baldocchi, D.D., 2011b. Frontiers and challenges in soil respiration research: From measurements to model-data integration. Biogeochemistry 102, 1–13. https://doi.org/10.1007/s10533-010-9462-1.

Vargas, R., Sánchez-Cañete, P.E., Serrano-Ortiz, P., Curiel Yuste, J., Domingo, F., López- Ballesteros, A., Oyonarte, C., 2018. Hot-moments of soil CO_2 efflux in a water-limited grassland. Soil Syst. 2, 47. https://doi.org/10.3390/soilsystems2030047.

Vázquez-Lule, A., Vargas, R., 2021. Biophysical drivers of net ecosystem and methane exchange across phenological phases in a tidal salt marsh. Agric. For. Meteorol. 300. https://doi.org/10.1016/j.agrformet.2020.108309.

Villarreal, S., Guevara, M., Alcaraz-Segura, D., Brunsell, N.A., Hayes, D., Loescher, H.W., Vargas, R., 2018. Ecosystem functional diversity and the representativeness of environmental networks across the conterminous United States. Agric. For. Meteorol. 262, 423–433. https://doi.org/10.1016/j.agrformet.2018.07.016.

Ward, N., Megongial, J.P., Bond-Lamberty, B., Bailey, V.L., Butman, D., Canuel, E.A., Diefenderfer, H., Gnaju, N.K., Goñi, M.A., Graham, E.B., Hopkinson, C.S., Khangaonkar, T., Langley, J.A., McDowell, N.G., Myers-Pigg, A.N., Neumann, R.B., Osburn, C.L., Price, R.M., Rowland, J., Sengupta, A., Simard, M., Thornton, P.E., Tzortziou, M., Vargas, R., Weisenhorn, P.B., Windham-Myers, L., 2020. Representing the function and sensitivity of coastal interfaces in Earth system models. Nat. Commun. 11, 1–14. https://doi.org/10.1038/s41467-020-16236-2.

Warner, D.L., Villarreal, S., McWilliams, K., Inamdar, S., Vargas, R., 2017. Carbon dioxide and methane fluxes from tree stems, coarse woody debris, and soils in an upland temperate forest. Ecosystems 20, 1205–1216. https://doi.org/10.1007/s10021-016- 0106-8.

Warner, D.L., Bond-Lamberty, B., Jian, J., Stell, E., Vargas, R., 2019. Spatial predictions and associated uncertainty of annual soil respiration at the global scale. Glob. Biogeochem. Cycles 0–2. https://doi.org/10.1029/2019GB006264.

Xie, X., Zhang, M.-Q., Zhao, B., Guo, H.-Q., 2014. Dependence of coastal wetland ecosystem respiration on temperature and tides: A temporal perspective. Biogeosciences 11, 539–545. https://doi.org/10.5194/bg-11-539-2014.

Yu, X., Ye, S., Olsson, L., Wei, M., Krauss, K.W., Brix, H., 2019. A 3-year in-situ measurement of CO_2 efflux in coastal wetlands: Understanding carbon loss through ecosystem respiration and its partitioning. Wetlands https://doi.org/10.1007/s13157-019-01197-0.

Zhang, Q., Katul, G.G., Oren, R., Daly, E., Manzoni, S., Yang, D., 2015. The hysteresis response of soil CO_2 concentration and soil respiration to soil temperature. J. Geophys. Res. 120, 1605–1618. https://doi.org/10.1002/2015JG003047.

Zhang, Q., Phillips, R.P., Manzoni, S., Scott, R.L., Oishi, A.C., Finzi, A., Daly, E., Vargas, R., Novick, K.A., 2018. Changes in photosynthesis and soil moisture drive the seasonal soil respiration-temperature hysteresis relationship. Agric. For. Meteorol. 259, 184–195. https://doi.org/10.1016/j.agrformet.2018.05.005

Chapter 4

TRACE GAS FLUXES FROM TIDAL SALT MARSH SOILS: IMPLICATIONS FOR CARBON-SULFUR BIOGEOCHEMISTRY

Preprint under review in *Biogeosciences*

DOI: https://doi.org/10.5194/bg-2022-101

Margaret Capooci[1], Rodrigo Vargas[1]

[1] Department of Plant and Soil Sciences, University of Delaware, Newark, DE, USA

Abstract

Tidal salt marsh soils can be a dynamic source of greenhouse gases such as carbon dioxide (CO_2), methane (CH_4), and nitrous oxide (N_2O), as well as sulfur-based trace gases such as carbon disulfide (CS_2) and dimethylsulfide (DMS) which play roles in global climate and carbon-sulfur biogeochemistry. Due to the difficulty in measuring trace gases in coastal ecosystems (e.g., flooding, salinity), our current understanding is based on snap-shot instantaneous measurements (e.g., performed during daytime low tide) which complicates our ability to assess the role of these ecosystems for natural climate solutions. We performed continuous, automated measurements of soil trace gas fluxes throughout the growing season to obtain high-temporal frequency data and to provide insights into magnitudes and temporal variability across rapidly changing conditions such as tidal cycles. We found that soil CO_2 fluxes did not show a consistent diel pattern, CH_4, N_2O, and CS_2 fluxes were

highly variable with frequent pulse emissions (>2,500%, >10,000%, and >4,500% change, respectively), and DMS fluxes only occurred mid-day with changes >185,000%. When we compared continuous measurements with discrete temporal measurements (during daytime, at low tide), discrete measurements of soil CO_2 fluxes were comparable with those from continuous measurements, but misrepresent the temporal variability and magnitudes of CH_4, N_2O, DMS, and CS_2. Discrepancies between the continuous and discrete measurement data result in differences for calculating the sustained global warming potential (SGWP), mainly by an overestimation of CH_4 fluxes when using discrete measurements. The high temporal variability of trace gas fluxes complicates the accurate calculation of budgets for use in blue carbon accounting and earth system models. Continuous measurements should be considered alongside discrete measurements to better capture the complex temporal and spatial variability of carbon-sulfur dynamics in tidal salt marshes.

4.1 Introduction

Coastal vegetated ecosystems such as tidal salt marshes, mangrove forests, and seagrass beds provide a wide range of ecosystem services, such as mitigating storm surge and providing nursery areas for fish species (Barbier et al., 2011; Möller et al., 2014). They also store large amounts of carbon at rates forty times higher than tropical rainforests (Duarte et al., 2005; Rosentreter et al., 2018) and are referred to as "blue carbon" ecosystems. The importance of coastal vegetated ecosystems in climate change policies has been recognized by the Paris Agreement (UNFCCC, 2015). Prior to the Paris Agreement, there has been increased interest in better quantifying the net balance between carbon storage and carbon release in coastal vegetated ecosystems for both scientific and carbon market purposes. For example, the Verified Carbon Standard developed a methodology to assess and verify the amount of carbon removed from the atmosphere in tidal wetland and seagrass restoration projects for carbon market purposes (Emmer et al., 2021). However, there are major knowledge gaps in assessing blue carbon in coastal vegetated ecosystems. Specifically, the high spatial and temporal variability of greenhouse gas (GHG) emissions, particularly for CH_4 and N_2O, in coastal vegetated ecosystems complicates blue carbon offset calculations (Al-Haj and Fulweiler, 2020; Capooci et al., 2019; Murray et al., 2015; Rosentreter et al., 2021). Thus, there is a need for developing measurement protocols to fully quantify the contribution of multiple GHGs in blue carbon ecosystems.

To improve our understanding of blue carbon ecosystems in global biogeochemical cycles we need to think beyond traditional GHG trace gases (i.e., CO_2, CH_4, N_2O). Tidal salt marshes produce sulfur-based trace gases due to the prevalence of sulfur cycling within their soils, which has implications for carbon-sulfur biogeochemistry and the global climate. While coastal areas are major sources

of sulfur gases (Kellogg et al., 1972), there is large uncertainty in emission rates (Andreae and Jaeschke, 1992; Carroll et al., 1986). Dimethyl sulfide (DMS) is one of the dominant sulfur-based gases emitted from salt marshes (Hines, 1996), and dimethylsulfoniopropionate (DMSP), a DMS precursor, can be produced by salt marsh plant species *Spartina alterniflora, S. anglica,* and *S. foliosa* (Hines, 1996). DMS plays an important role in linking together carbon and sulfur biogeochemistry in salt marsh soils. It can be decomposed by not only sulfate-reducing bacteria, but can also act as a non-competitive substrate for methylotrophic methanogenesis (Kiene, 1988; Kiene and Visscher, 1987; Oremland et al., 1982) which allows methane production to occur in soils dominated by sulfate reduction (Seyfferth et al., 2020). Another sulfur-based trace gas released from tidal salt marshes is carbon disulfide (CS_2). CS_2 can be produced by biological processes (Brimblecombe, 2014) and is a precursor to carbonyl sulfide (COS; Whelan et al., 2013). COS is the most abundant reduced sulfur compound in the atmosphere and can form sulfate aerosols that affect the Earth's radiative properties by reflecting sunlight, thereby having a cooling effect on the climate (Taubman and Kasting, 1995; Watts, 2000). Despite sulfur-based trace gases playing a role in wetland soil biogeochemistry and in global climate, there is a need to quantify coastal wetland sulfur emissions and to connect those emissions to both the salt marsh sulfur cycle and to global budgets (DeLaune et al., 2002; Whelan et al., 2013).

Historically, both soil GHGs and S-based fluxes are measured using manual survey chambers, particularly during daytime low tide (e.g., De Mello et al., 1987) when soils are less likely to be submerged and are accessible to researchers. Manual measurements have a number of advantages, including the ability to sample over large

areas over short periods of time (Moseman-Valtierra et al., 2016; Simpson et al., 2019), but these measurements are labor-intensive and provide limited information regarding temporal variability (Koskinen et al., 2014; Savage et al., 2014; Vargas et al., 2011). On the other hand, recent advances in high temporal-frequency soil efflux measurements (Capooci and Vargas, 2022; Diefenderfer et al., 2018; Järveoja et al., 2018) have provided researchers with unprecedented temporal information to better understand diel and tidal patterns, as well as the influence of pulse events on trace gas emissions within salt marshes. While the use of automated systems is becoming more common in measuring salt marsh fluxes, their use is limited by high instrumentation costs, electricity requirements, and logistical challenges associated with installing these instruments in an environment prone to flooding and with high humidity. As automated systems become more prevalent, it provides researchers with the opportunity to evaluate data collected from manual measurements, such as daily means, that have been used to inform models and budgets, particularly for understudied trace gases such as N_2O, CS_2, and DMS.

The objective of this study is to characterize the spatial and temporal variability of trace gases from soils in a tidal salt marsh. Specifically, we focus on CO_2, CH_4, N_2O, CS_2, and DMS to assess the differences between measurements taken at a particular time of day (i.e., daytime low tide) and measurements with high-temporal frequency (i.e., continuous measurements). Few studies have measured GHG fluxes from tidal salt marshes using continuous, automated measurements (Capooci and Vargas, 2022; Diefenderfer et al., 2018), and this is a pioneering study that provides unprecedented information about the magnitudes and patterns of CS_2 and DMS fluxes via continuous measurements. Furthermore, this study tests whether

traditional measurement protocols based on discrete temporal measurements provide similar information as data derived from continuous measurements, including the calculation of the sustained global warming potential (SGWP). Development of new technologies and incorporation of this information has important implications for calculating greenhouse and trace gas budgets, as well as the role salt marshes play in global biogeochemical cycles.

4.2 Materials and methods

4.2.1 Study site

The study was conducted at St. Jones Reserve, the brackish estuarine component of the Delaware National Estuarine Research Reserve. The site is part of the Delaware Estuary and is tidally connected to the Delaware Bay via the St. Jones River. St. Jones is classified as a mesohaline tidal salt marsh (DNREC, 1999) and has silty clay loam soils (10% sand, 61% silt, 29% loam, Capooci et al 2019). The study was conducted in a section of the marsh dominated by *Spartina alterniflora* (= *Sporobolus alterniflorus* (Loisel.); Peterson et al., 2014) and will be referred to as SS as established in previous studies (Capooci and Vargas, 2022; Seyfferth et al., 2020). This area is lower in elevation relative to the rest of the marsh, is characterized by sulfur reduction (Seyfferth et al., 2020), and covers ~66% of the salt marsh landscape (Vázquez-Lule and Vargas, 2021).

4.2.2 Experimental set-up

The experiment was performed over the course of 6 campaigns to cover a full growing season: greenup (G), maturity (M), senescence (S), and dormancy (D) as described by the canopy phenology of the study site (Hill et al., 2021). The campaigns

began during the latter half of the 2020 growing season and continued into the beginning of the 2021 growing season (M1 – 29 June to 2 July, M2 – 31 July to 3 Aug, S1 – 31 Aug to 3 Sept, S2 – 28 Sept to 1 Oct, D1 – 13 Apr to 16 Apr, and G1 – 31 May to 3 June) due to delays related to the COVID-19 pandemic. We installed six PVC collars (diameter: 20 cm), placed ~1.2 meters apart, four months prior to the beginning of the experiment in the year 2020. Any vegetation that grew inside these collars in between campaigns was carefully removed prior to the start of the measurements. These collars were used to set down six automated chambers (LICOR 8100-104, Lincoln, Nebraska) to measure trace gas fluxes as described below.

4.2.3 Trace gas flux measurements and QA/QC

The autochambers were coupled with a closed-path infrared gas analyzer (LI-8100A, LICOR, Lincoln, Nebraska) and a Fourier transform infrared spectrometer (DX4040, Gasmet Technologies Oy, Vantaa, Finland). The LI-8100A and the DX4040 were connected in parallel since the DX4040 has its own internal pump and flow rates. Trace gas fluxes were measured once per hour per chamber (i.e., all six chambers were measured within an hour). Measurements were 5 minutes long and each chamber was flushed for 5 minutes total (pre-purge and post-purge were both 2.5 minutes long) to help reduce the impacts of humidity on the instruments. Each campaign lasted approximately 72 hours where approximately 416 measurements were recorded.

At the beginning of each campaign and every 24 hours after, we performed a zero calibration on the DX4040 using ultra-pure 99.999% N_2 gas. It is recommended that zero calibrations are performed every 24 hours and when the ambient temperature changes by 10°C, so the experiment was paused for ~30 minutes during the zero

calibrations each day. Gas fluxes were calculated using Soil Flux Pro (v4.2.1, LICOR, Lincoln, Nebraska) and underwent standardized quality assurance and quality control protocol as established in previous publications (Capooci et al., 2019; Petrakis et al., 2017). Briefly, QAQC included removing all values due to instrumental errors, comparing exponential and linear fits to select for the measurement with the higher R^2, removing all measurements during times where the R^2 for $CO_2 < 0.90$, and removing all negative CO_2 fluxes.

4.2.4 Ancillary measurements

Meteorological (station: delsjmet-p) and water quality (station: Aspen Landing) data were obtained from the National Estuarine Research Reserve's Centralized Data Management Office (CDMO) and collected according to their protocol (NOAA National Estuarine Research Reserve System (NERRS), 2015). Meteorological data was collected using a CR1000 Meteorological Monitoring Station (Campbell Scientific, Logan, UT, USA). Water quality data were measured using a YSI 6600 sonde (YSI Inc., OH, USA). Both data sets were cleaned and gap-filled following the protocol established in Capooci et. al. (2022).

Phenological data were obtained from the PhenoCam network (site: stjones, Seyednasrollah et al., 2019) as described previously (Hill et al., 2021; Trifunovic et al., 2020). Briefly, a single mid-day photo (12:00:00 h) was selected for each of the days in the study period and was visually inspected to remove images with obvious distortions. Since the images included a variety of vegetation types, the region of interest delineated to only the area containing *S. alterniflora*, the main species at the study site. Then the phenopix R package (Filippa et al., 2020) was used to extract and

calculate the greenness index, as well as delineate the phenophases for the study period (Hill et al., 2021).

4.2.5 Data analyses

Daily averages and associated standard deviations were calculated for meteorological and water quality data, except for the greenness index. Soil trace flux data were averaged into hourly and daily means and standard deviations. For heat maps, average hourly and campaign-length coefficients of variation were calculated.

We extracted measurements from the time series of the automated measurements to represent information collected from discrete temporal measurements conducted during daytime low tide. This approach aimed to represent a measurement protocol derived from manual (i.e., survey) measurements where most measurements are performed at daytime and low tide for logistical reasons. To identify and extract these measurements, we identified when low tide occurred during each day (between 9:00:00 and 17:00:00 h) of the campaigns from water level data obtained from the tidal creek. All automated measurements that fell between 1 hour before and 1 hour after low tide were extracted, averaged into a daily value, and classified as "discrete" measurements. For example, if low tide fell at 13:00:00 h, all continuous measurements that fell between 12:00:00 and 14:00:00 h were then extracted and averaged to obtain a daily mean. Daily means were also calculated for all automated measurements collected during the day and will be referred to as the "continuous" daily mean. Differences in the means and distributions of the continuous and discrete fluxes were assessed using a t-test and a Kolmogorov-Smirnov test, respectively.

Sustained global warming potential (SGWP) was calculated for both the campaign-long and daytime low tide fluxes for CO_2, CH_4, and N_2O. SGWP accounts

for sustained gas emissions over time compared to the global warming potential which accounts for a pulse emission over time (Neubauer and Megonigal, 2019). To calculate the SGWP, data from Day 2 and 3 of each campaign was used since measurements on Day 1 and 4 did not always occur during daytime low tide. Fluxes were converted into g m^{-2} and multiplied by the 20 and 100-year SGWP (Neubauer and Megonigal, 2019). SGWP were compared to see whether extrapolating SGWP from daily-averaged manual measurements done at low tide yielded similar values as hourly-averaged from high temporal frequency measurements.

4.3 Results

4.3.1 Meteorological and water quality

Air temperature and greenness index show traditional seasonal patterns of temperate salt marshes (Fig. 4.1). Daily mean air temperature ranged from -3.5℃ to 29.9℃, with an average daily temperature of 13.8 ± 9.1℃, while greenness index ranged from 0.30 to 0.42 with an average of 0.34 ± 0.04. Relative humidity, barometric pressure, water level, and salinity varied throughout the year. Relative humidity ranged from 32.6% to 100% with an average of 79.1% ± 16.7%. Barometric pressure was between 999.7 and 1036 mb with an average value of 1018.3 ± 6.8 mb. Daily water level ranged from -0.30 m to 0.76 m with an average height of 0.25 ± 0.2 m, while salinity ranged from 1.1 ppt to 20.4 ppt with an average of 8.0 ± 4.45 ppt.

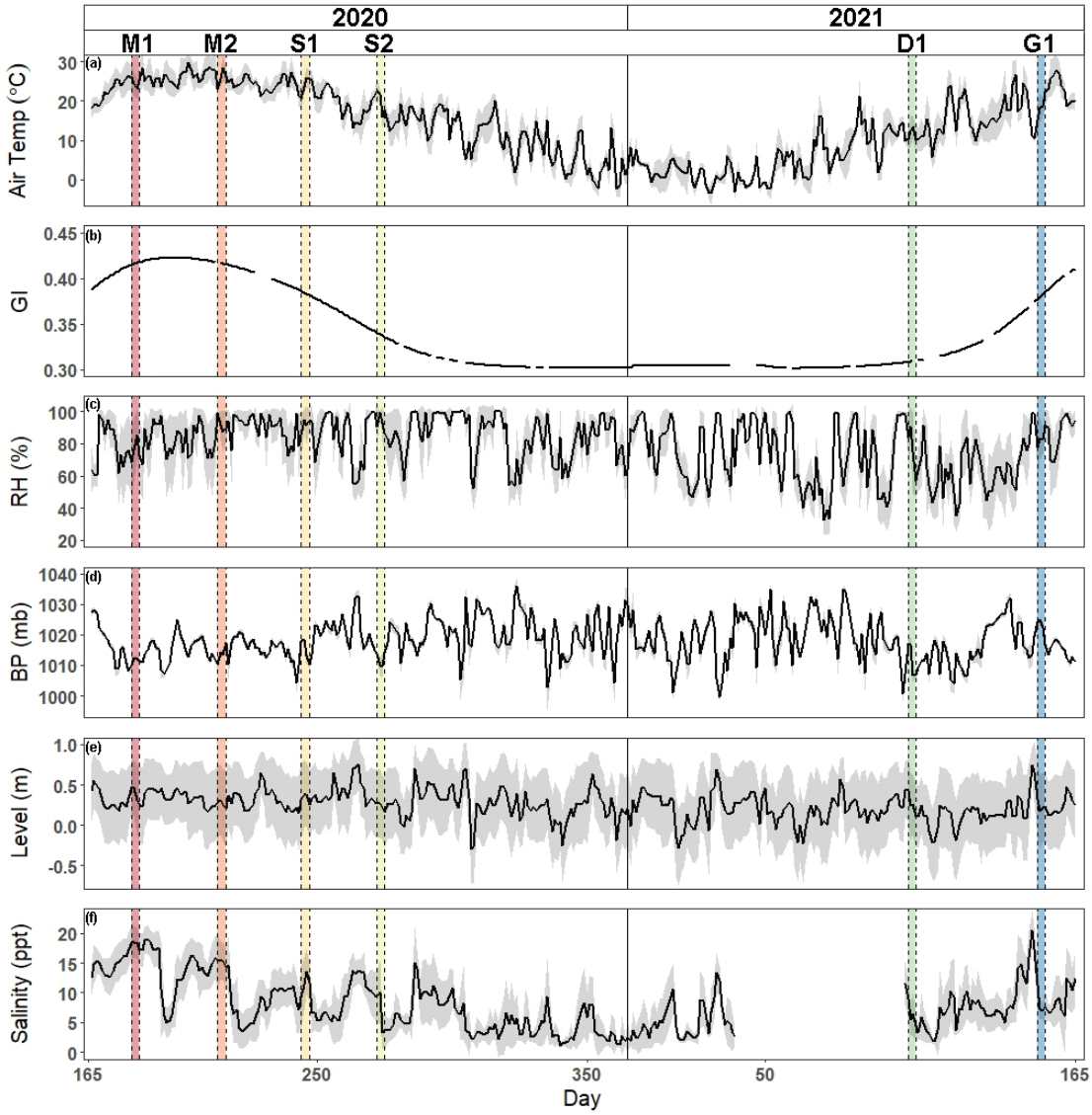

Figure 4.1: Time series of hourly mean ± SD (gray shaded region) of (a) air temperature, (b) greenness index, (c) relative humidity, (d) barometric pressure, (e) water level, and (f) salinity from June 14, 2020 to June 14, 2021. Vertical shaded areas correspond to each of the campaigns (M = maturity, S = senescence, D = dormancy, and G = greenup)

4.3.2 Greenhouse gas and sulfur-based trace gas patterns and variability

Average CO_2 fluxes were significantly different in each campaign, with the highest average fluxes occurring during the G1 campaign and the lowest during the D1 campaign (Fig. 4.2a). During some campaigns, such as S1, CO_2 fluxes did not show similar temporal patterns between chambers, whereas during other campaigns, such as M2 and G1, all six chambers had similar patterns. While there is a seasonal pattern in CO_2 fluxes, with higher fluxes occurring during warmer months, diel patterns were not consistent between campaigns. One notable exception is the G1 campaign, during which a clear diel pattern was observed. CO_2 fluxes had consistent variability from one hour to the next during each of the 6 campaigns (Fig. 4.3a), with overall average variability ranging from 28.9% during M2 to 49.6% during Dl.

CH_4 fluxes were low most of the time, particularly during the G1 campaign (Fig. 4.2b). However, CH_4 pulses occurred during 5 out of the 6 campaigns, with S1and S2 having the most frequent pulse emissions. S2 had the largest CH_4 pulse,13,488 nmol m^{-2} s^{-1}, which was 2,599% higher than the average flux. The highest average CH_4 fluxes also occurred during S1 and S2, while the highest hourly variability occurred in both S1 and S2, as well as in M2 (Fig. 4.3b). Mean CH_4 variability ranged from -108% in M1 to 91.0% in S1.

Most N_2O fluxes were near-zero, with periodic pulses of emissions or uptake that ranged from -33.8 to 19.0 nmol m^{-2} s^{-1} (Fig. 4.2c), with a maximum percent change from the mean of 10,231%. Four out of the six campaigns (M1, S2, D1, and G1) had net N_2O uptake, while two campaigns (M2, S1) had net N_2O fluxes. There were no significant differences between campaigns except for M1 and S1. Meanwhile, N_2O fluxes had very high hourly variability ranging from -106,964% to 26,208% (Fig.

4.3c). Consequently, average variability during each campaign was highly variable from -1,032% to 129%.

Figure 4.2: Time series of fluxes from each chamber during each campaign for (a) CO_2, (b) CH_4, (c) N_2O, (d) CS_2, and (e) DMS. Each color designates a different chamber. The campaign means [LCI, UCI] are listed on each panel. The y-axis for CH_4 fluxes was shortened to show the variability. Full range of CH_4 fluxes during S2 can be seen in Appendix C (Fig. C.1).

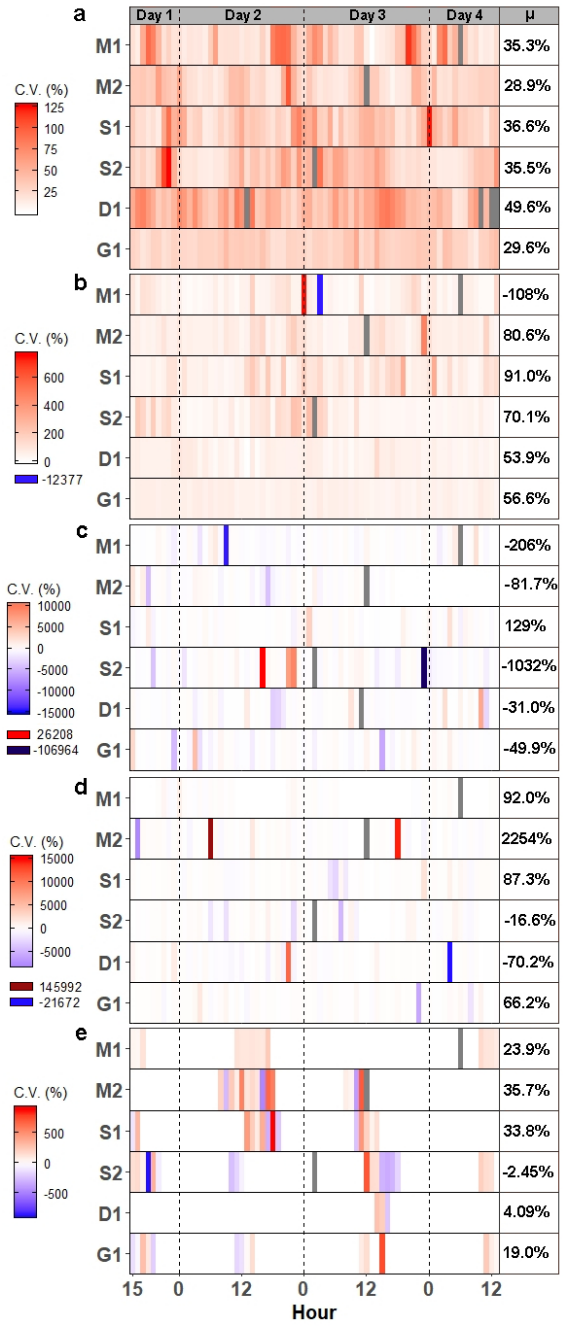

Figure 4.3: Heat maps of hourly coefficient of variance (CV) for (a) CO_2, (b) CH_4, (c) N_2O, (d) CS_2, and (e) DMS during each campaign. Each pixel represents the average CV for that hour. Mean CV for each campaign is listed in the μ column. Grayed out pixels represent NA. Note: legend scale is different for each gas and campaigns start at 15:00:00 h on Day 1 and end at 13:00:00 h on Day 4.

Similarly to CH_4 and N_2O, CS_2 fluxes were low the majority of the time, with occasional pulses of emissions or uptake (Fig. 4.2d). CS_2 fluxes ranged from -386.9 to 306.2 nmol m^{-2} s^{-1}, with a maximum percent change from the mean of 4,785%. All campaigns had net emissions despite periodic pulses of CS_2 uptake. CS_2 fluxes also had high hourly variability, with overall means for each campaign ranging from -70.2% during D1 to 2254% during M2 (Fig. 4.3d).

DMS emissions were zero for most of the campaigns (Fig. 4.2e). Pulses of emissions and uptake tended to occur during mid-day. DMS fluxes ranged from -158.5 to 230 nmol m^{-2} s^{-1}, with a maximum percent change from the mean of 185,987%. D1 and G1 had net uptake, while the other four campaigns had net emissions of DMS. During periods of emissions and uptake, hourly variability ranged from -870.5% to 888.7% (Fig. 4.3e). The extended periods of no DMS fluxes contributed to low overall mean variability during each campaign, ranging from -2.45% in S2 to 35.7% in M2.

4.3.3 Comparisons between continuous and discrete measurement scenarios

A subset of the continuous measurements that fall during daytime low tide was selected to represent data collected using traditional discrete, manual measurements which are commonly reported for tidal salt marshes. Information from continuous and discrete datasets are compared to elevate whether they provide similar distributions, daily means, flux-temperature relationships, and SGWP.

Continuous and discrete flux distributions can be seen via density plots (Fig. 4.4). While the distributions for continuous and discrete fluxes overlap for each of the five gases, four of the five gases have significantly different distributions of fluxes when comparing the continuous and the discrete datasets (Table 4.1). The only gas that had similar distributions between the two sampling intervals was CO_2 (Table 4.1).

For all gases, the continuous distribution had higher kurtosis values and higher C.V. than the discrete fluxes (Table 4.1). Of the five gases, CS_2 was the only one with a more skewed discrete data distribution and significantly different means between continuous and discrete measurement scenarios (Fig. 4.4b, Table 4.1).

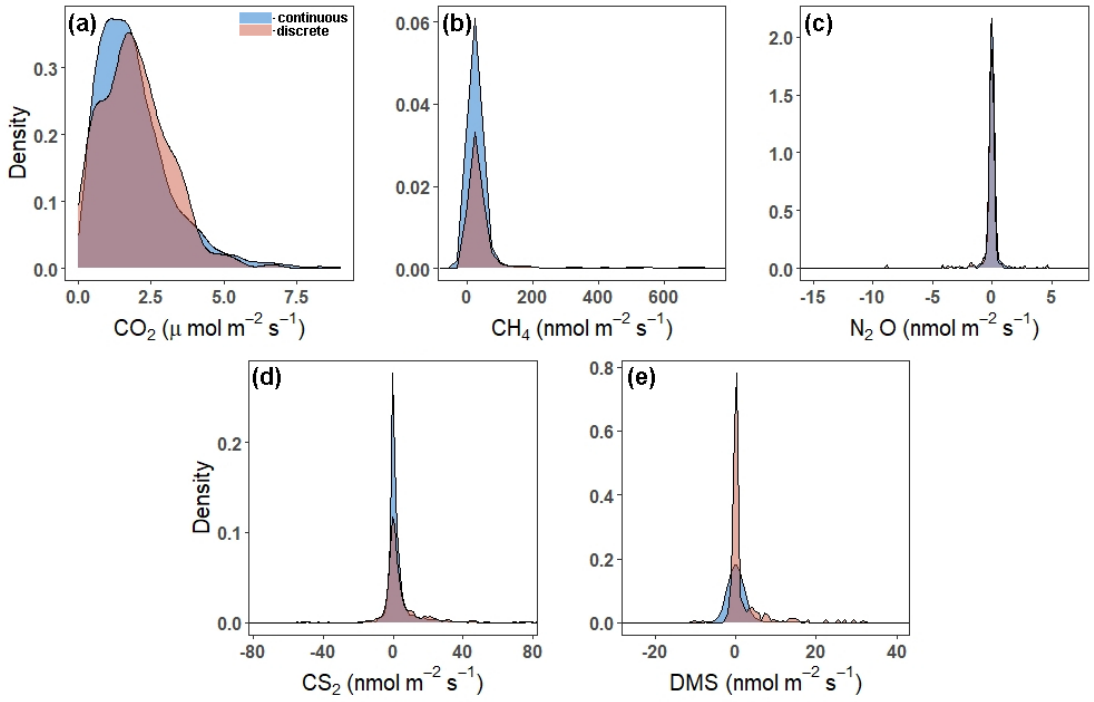

Figure 4.4: Density plots comparing the distribution of fluxes throughout all campaigns (continuous) to those measured during daytime low tide (discrete) for (a) CO_2, (b) CH_4, (c) N_2O, (d) CS_2, and (e) DMS. Note: the scales on the x- and y-axis are different. The tails have been cut off to better seek the peaks for (b), (c), (d), and (e). To see plots with full distributions, see Fig. C.2.

Table 4.1: Summary of continuous and discrete measurement data and distributions for each gas. An alpha of < 0.05 was used to determine significant differences between the means and the distributions. Note: means for CO_2 are in μmol m^{-2} s^{-1}.

Gas	Sampling Frequency	Mean	95% CI	C.V.	Skewness	Kurtosis	Means Different?	Distributions Different?
CO_2	Continuous	1.92	1.86–1.97	67.2%	1.53	6.51	No	No
	Discrete	1.90	1.74–2.07	62.3%	0.67	3.65		
CH_4	Continuous	41.2	29.5–52.9	708%	41.6	1903	No	Yes
	Discrete	57.6	39.2–76.0	234%	5.21	34		p = 0.02
N_2O	Continuous	-0.06	-0.13–0.009	2686%	-4.67	133	No	Yes
	Discrete	-0.16	-0.29 – -0.04	556%	-4.39	47.8		p < 0.01
CS_2	Continuous	3.39	2.45–4.33	673%	1.51	116	Yes	Yes
	Discrete	6.44	3.70–9.18	312%	3.93	22.9	p = 0.04	p = 0.05
DMS	Continuous	1.11	0.70–1.51	907%	8.74	223	No	Yes
	Discrete	1.77	1.06–2.48	295%	3.40	16.6		p < 0.001

For CS_2 and DMS, discrete measurements had higher overall daily mean fluxes (Fig. 4.5d, e), while the opposite occurred for CH_4 and N_2O (Fig. 4.5b, c). CO_2 fluxes from continuous and discrete measurements had nearly a 1:1 relationship (Fig. 4.5a). Both CO_2 and DMS had strong relationships between continuous and discrete daily means, with r-squares higher than 0.7, while N_2O and CS_2 had moderate relationships. CH_4 had a poor fit between continuous and discrete measurements.

Next, relationships between trace gas flux and air temperature were evaluated for each gas under continuous and discrete measurement scenarios. CO_2 and CH_4 fluxes had statistically significant relationships for both discrete and continuous measurements versus air temperature (Fig. 4.6a-d). Air temperature explained 38% and 21% of the variability for discrete and continuous measurements for CO_2, respectively (Fig. 4.6a, b), while air temperature explained 32% and 7% of the variability for discrete and continuous measurement for CH_4 (Fig. 4.6c, d). The slopes

for both discrete and continuous CO_2 fluxes were not significantly different (95% CI; 0.029 - 0.12, 0.037 - 0.054, respectively), as well as for CH_4 (95% CI; 2.14 - 12.7, 1.31 - 2.71, respectively). For N_2O, CS_2, and DMS, there were no significant relationships between discrete daily mean fluxes and air temperature, but there were significant relationships between continuous hourly mean fluxes and air temperature (Fig. 4.6e-j). Air temperature explained very little variability for N_2O, CS_2, and DMS.

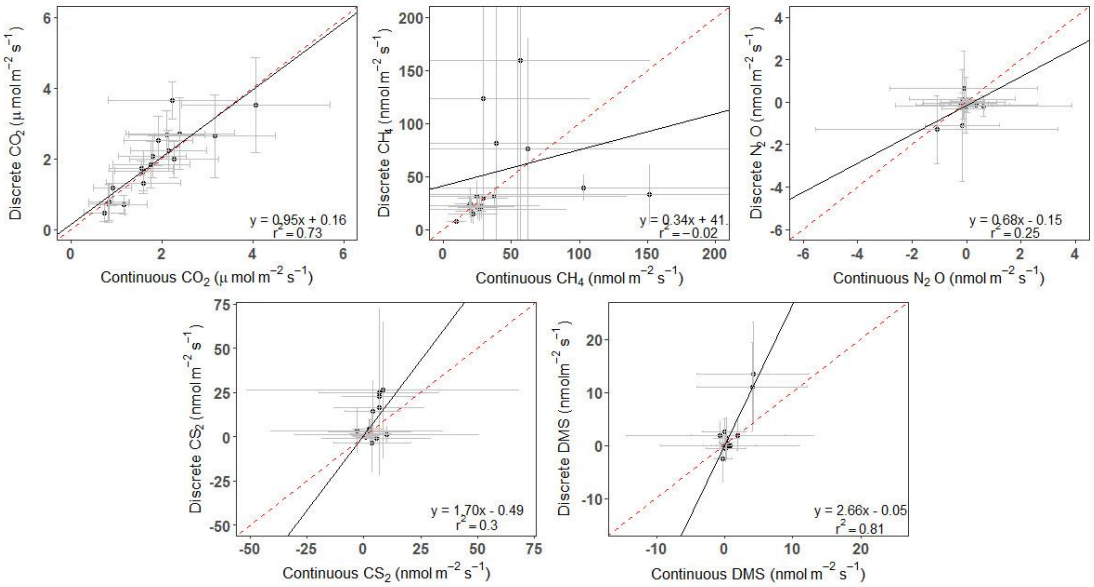

Figure 4.5: Plots comparing the daily average of continuous to discrete measurements for (a) CO_2, (b) CH_4, (c) N_2O, (d) CS_2, and (e) DMS. Error bars represent the SD and have been cut off in panel (b) to show data better. See Fig. C.3 for full error bars for panel b. Red dashed line is the 1:1 line, while the black solid line is the trend line.

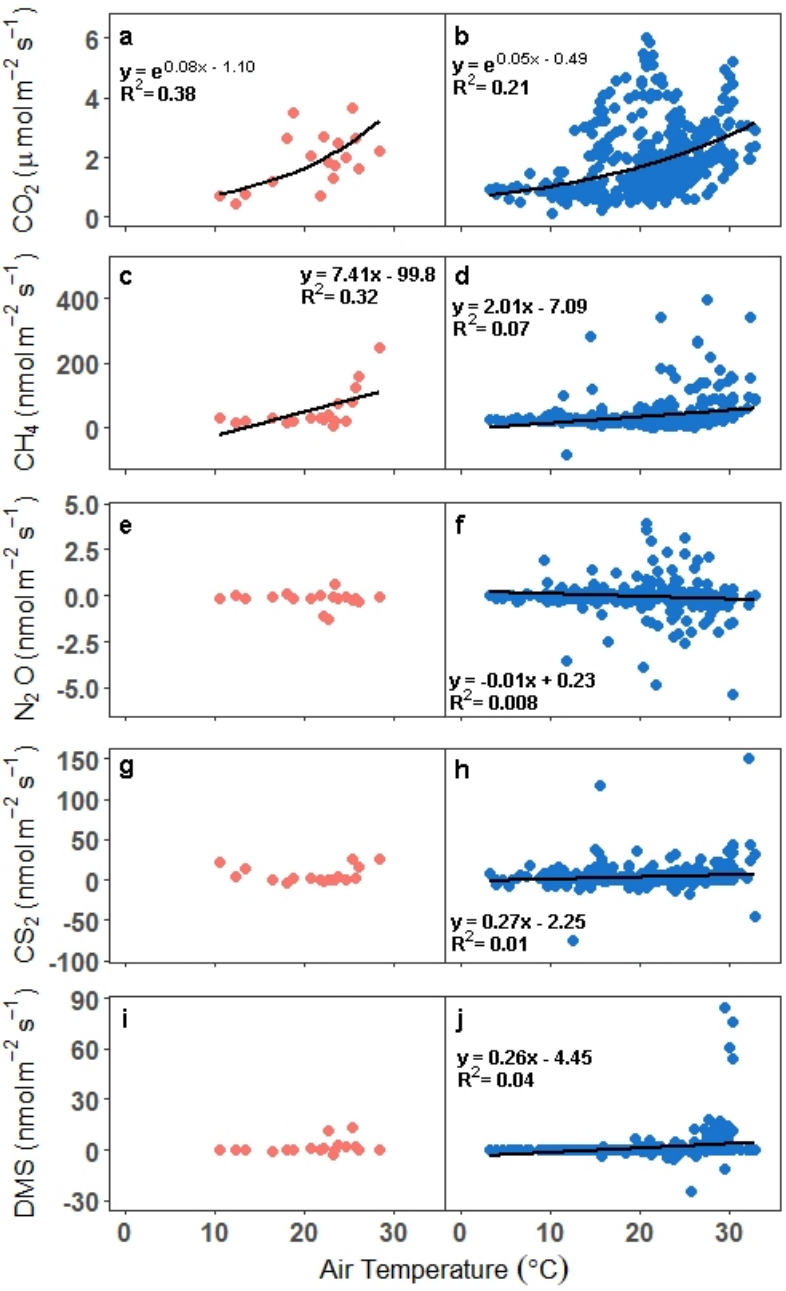

Figure 4.6: Comparison of fluxes versus air temperature for all campaigns. In panels a, c, e, g, and i, the hourly continuous mean is compared to the hourly air temperature, while in panels b, d, f, h, and k, the discrete daily mean is compared to the daily air temperature. The trend lines for significant relationships at alpha < 0.05 are plotted. Note: in panel d, the outlier hourly mean of 2,275 nmol m^{-2} s^{-1} is not included in the trend line or the graph.

Discrete measurements had a higher SGWP potential than the continuous measurements (Table 4.2). While the discrete measurements had a slightly lower SGWP for CO_2 and a slightly higher SWGP for N_2O, the difference between continuous and discrete SGWP was driven by CH_4. The 20-yr and 100-yr SGWP for discrete measurements of CH_4 were up to ~38% higher than the respective continuous measurements, contributing to an overall increase of ~18% and ~11% for the discrete measurement's 20- and 100-year SGWP.

Table 4.2: Sustained global warming potential (SGWP) derived from continuous and discrete temporal (during daytime low tide) measurements in a tidal salt marsh.

Frequency	CO_2 ($g\ m^{-2}$)	CH_4 ($CO_{2\text{-eq}}$ ($g\ m^{-2}$))		N_2O ($CO_{2\text{-eq}}$ ($g\ m^{-2}$))		Total ($CO_{2\text{-eq}}$ ($g\ m^{-2}$))	
		20-yr SGWP	100-yr SGWP	20-yr SGWP	100-yr SGWP	20-yr SGWP	100-yr SGWP
Continuous	84.9	70.4	33.0	0.27	0.30	155.57	118.2
Discrete	82.7	103.2	48.4	0.40	0.44	186.3	131.54

4.4 Discussion

4.4.1 Measuring all the time: seasonal and diel patterns and hot moments of soil trace gases

Spatial variability between the individual chambers at SS were low, but CO_2 fluxes showed temporal variability that corresponded to changes in temperature. The relatively low spatial variability within our experimental setting contrasts with previously reported high spatial variability of CO_2 fluxes attributed to the presence of a hot spot (Capooci and Vargas, 2022). However, previous CO_2 fluxes measured at the

SS site ranged from 0-10 μmol m^{-2} s^{-1}, with the bulk of the measurements between 0-4 μmol m^{-2} s^{-1}, with higher fluxes associated with hot spots or warmer temperatures (Capooci and Vargas, 2022; Seyfferth et al., 2020). Therefore, location of measurements within a landscape could be influenced by hot spots, which complicates ecosystem scale calculations of soil CO_2 fluxes (Barba et al., 2018). In addition, there was a seasonal pattern evident in the CO_2 fluxes, with higher emissions during the growing season, as typical in temperate ecosystems, as well in the significant relationship between CO_2 and air temperature. Other studies at temperate wetland sites have found higher fluxes during the summer (Bridgham and Richardson, 1992; Simpson et al., 2019; Yu et al., 2019), as well as relationships between CO_2 fluxes and temperature (Capooci and Vargas, 2022; Simpson et al., 2019; Xie et al., 2014) highlighting that CO_2 fluxes in temperate salt marshes exhibit a temperature dependency over seasonal scales, even in the presence of tides.

While CO_2 fluxes show seasonal patterns, there are no diel patterns that persist throughout the year. During G1, the peak of high tide coincided with peak daily temperature. This scenario also occurred during D1, but fluxes were too low to discern patterns. During all other campaigns, low tide and peak temperatures coincided. These results suggest that diel patterns may occur periodically under certain conditions. For example, at the SS site, it may be that diel patterns occur during high tide at the temperature peak. While we expected the highest fluxes during low tides due to increased oxygen exposure, there may be a lag between low tide in the creek and low water levels at the SS site, resulting in higher fluxes during high tide in the creek. However, these results can vary from site to site and with proximity to the tidal creek. More research using high temporal frequency measurements are needed to parse out

the role of temperature and tides on CO_2 fluxes across salt marshes to properly represent the pattern in earth system models (Ward et al., 2020)

Similarly to CO_2, CH_4 has a significant relationship with air temperature, however it explains less variability in the fluxes. Several studies have found positive correlations between soil CH_4 fluxes and temperature (Bartlett et al., 1985; Emery and Fulweiler, 2014; Wang and Wang, 2017) in temperate salt marshes, while others have not (Wilson et al., 2015). It is important to note that while, in general, salt marsh CH_4 fluxes are positively related to temperature (Al-Haj and Fulweiler, 2020), the ability of temperature to explain CH_4 flux variability is low, compounded by many, often site-specific, factors that affect methane production and consumption, such as organic matter supply, microbial communities, and diffusion rates (Al-Haj and Fulweiler, 2020; Bartlett et al., 1985).

At our study site, CH_4 fluxes were highest and pulses were most frequent during senescence, agreeing with findings from ecosystem-scale measurements derived using the eddy covariance technique (Vázquez-Lule and Vargas, 2021). In most wetland ecosystems, the highest fluxes have been reported during the summer (Kim et al., 1998; Livesley and Andrusiak, 2012; Rinne et al., 2007; Van Der Nat and Middelburg, 2000), but we highlight that there is a lack of measurements during the winter (Al-Haj and Fulweiler, 2020). In *S. alterniflora* marshes, highest mean CH_4 fluxes have been found in both the summer and the fall (Bartlett et al., 1985; Emery and Fulweiler, 2014). At a site dominated by *S. alterniflora*, both high fluxes and porewater CH_4 concentrations were found in September, indicating either a continual build-up of CH_4 in the pore water over the growing season and/or increased CH_4 production in the fall (Zhang and Ding, 2011). For our site, it is likely higher CH_4

emissions during senescence were due to an input of labile organic matter from plant die-off (Seyfferth et al., 2020). Furthermore, a recent study has shown that porewater DMS, a non-competitive substrate for methylotrophic methanogenesis that is produced from the breakdown of DMSP, a metabolite produced by *S. alterniflora* (Dacey et al., 1987), peaks during the fall (Tong et al., 2018). Therefore, we postulate that an influx of DMS may also contribute to higher CH_4 fluxes during senescence in marshes dominated by *S. alterniflora*. This finding highlights the importance of carbon-sulfur biogeochemistry and measuring fluxes during non-summer months; particularly in marshes that have plant communities that provide substrates used in methylotrophic methanogenesis (Seyfferth et al., 2020).

On a diel timescale, pulse emissions of CH_4 from the soil tend to occur during the warmest time of the day, as well as during low and rising tides. There are very few studies that report high-temporal frequency data of CH_4 emissions, most of which include plants within their scope (via transparent chambers or eddy covariance) or focus on tidal creeks, making it difficult to ascertain whether the diel patterns seen in this study are typical of tidal salt marsh soils. Considering the broader range of studies about CH_4 fluxes in coastal vegetated ecosystems, CH_4 emissions have been found to peak at various points in the day, from during the day (Tong et al., 2013; Yang et al., 2017, 2018), at night (Diefenderfer et al., 2018), or highly variable (Jha et al., 2014; Xu et al., 2017). At our site, CH_4 fluxes tended to peak at the confluence of peak daily temperature and low to rising tides, indicating that physical forcing may contribute to CH_4 pulses (Bahlmann et al., 2015; Middelburg et al., 1996). However, pulses did occur during other times throughout the day and within the tidal cycle. While some of the pulse emissions may be a result of ebullition, the majority are associated with high

R^2's, indicating that they are sustained over the measurement period. Our results demonstrate the importance of conducting high-temporal frequency CH_4 measurements in tidal salt marsh soils for several reasons, including the need for more data to better understand the drivers of CH_4 fluxes at diel scales and how that affects model predictions.

N_2O emissions and uptake loosely followed a seasonal pattern, likely driven by the canopy phenological stages. During the growing season, it has been shown that highly productive plants can compete with soil microbes for NO_3^- and NH_4^- (Cheng et al., 2007; Granville et al., 2021; Xu et al., 2017; Yu et al., 2012; Zhang et al., 2013), shifting denitrifiers into consuming N_2O and resulting in a net uptake during G1 and M1. As the plants reach peak maturity, the system shifts into net emission of N_2O during M2 and S1. One study found that nitrogen additions resulted in a pulse of N_2O in July when most of the plant growth had occurred, but no response in April, suggesting that the competition for NO_3^- and NH_3^+ decreases when plant growth has slowed down (Moseman-Valtierra et al., 2011). Increased substrate availability combined with warm temperatures likely contributed to the marsh being a net source of N_2O during the later stages of the growing season. As temperatures drop, the system shifts back into net uptake, as seen during S2 and D1. Similar seasonal patterns have been seen in other studies, albeit shifted by a month or two depending on the local climate and phenophases (Emery and Fulweiler, 2014; Granville et al., 2021). These findings highlight balance between processes that produce N_2O (e.g., nitrification, denitrification, and nitrifier-denitrification) and consume N_2O (e.g., denitrification), as well as substrate availability and plant phenology in determining whether a marsh is a source or sink of N_2O at any given point.

As with seasonality, diel patterns of N_2O showed both emissions and uptake. Several studies have also reported both emissions and uptake during a 24-hour period (Tong et al., 2013; Yang et al., 2017). We found that pulses of uptake and emissions occurred both during the day and at night, as well as during different phases of the tidal cycle. Studies have found higher fluxes during the day (Tong et al., 2013; Yang et al., 2017) and at night (Bauza et al., 2002; Laursen and Seitzinger, 2002; Yang et al., 2017). Generally, fluxes were slightly higher at night throughout the campaigns, perhaps as a result of increased availability of NH_4^+ at night due decreased competition from photosynthesizers (Bauza et al., 2002). Overall, N_2O fluxes were near-zero with a < 0.50 nmol m^{-2} s^{-1} difference between daytime and nighttime mean fluxes, suggesting that N_2O fluxes do not play a major role in GHG emissions at this salt marsh.

Our automated measurements of sulfur-based trace gases show high variability in CS_2, with low fluxes punctuated by occasional pulse emissions. There are no previous studies with automated measurements to compare our findings, but previous studies have noted that CS_2 fluxes are highly variable (Hines, 1996; Steudler and Peterson, 1985), with periods of emission and uptake. However, fluxes at SS were, on average, an order of magnitude higher than values reported in the literature (Supplementary Table C.1). There could be several reasons for the difference in magnitudes: 1) improvement in instrumentation to detect CS_2, 2.) sampling technique differences, and 3.) site-specific characteristics. Since the influx of sulfur-based trace gas measurements in the 1980s, instrumentation has advanced from using molecular sieves and cryotraps to store samples before measuring them on a gas chromatograph (e.g., Carroll et al., 1986; Cooper et al., 1987; Steudler and Peterson, 1984) to using

portable Fourier transform infrared (FTIR) spectrometers that measure trace gas concentrations in near real-time. These instrumentation advances subsequently led to changes in sampling techniques. Traditionally, it was common to keep the chamber closed for upwards of 24-hours, with samples being collected over hourly intervals throughout the day (Carroll et al., 1986; Goldan et al., 1987). Sweep air free of sulfur trace gases was also commonly used to avoid the need to take samples at both the inlet and outlets of the chambers (Goldan et al., 1987). However, others used ambient air because it more closely resembled *in situ* conditions (Steudler and Peterson, 1985). With recent advances, sampling techniques have changed to eliminate the need for very long closure times and reduce the effects the chambers have on micrometeorological conditions. Now, high-temporal frequency, long-term data can be obtained, thereby capturing pulse emissions that otherwise may be missed. The third reason for difference in magnitude could be due to site-specific differences in CS_2 fluxes. While the mechanisms by which CS_2 is produced are poorly understood, there are several potential production pathways: OM degradation, photochemical production, and algal production (Xie and Moore, 1999). The most likely pathway for our site is the microbially-mediated reaction between H_2S and organic matter due to high sulfur concentrations, anaerobic conditions, and a large pool of decaying organic matter. Finally, CS_2 is a short-lived sulfur gas but the major product of CS_2 oxidation is COS; consequently, understanding CS_2 production and oxidation is important for recognizing the role of salt marshes in COS dynamics (Whelan et al., 2013).

The mean of measured DMS fluxes generally fall within those reported in the literature, but with pulses higher than previously reported and different temporal patterns. We found that DMS fluxes only occurred during the middle of the day, near

when air temperatures peaked. This is contrary to several studies that have found DMS fluxes during other times of the day (DeLaune et al., 2002; Morrison and Hines, 1990; Steudler and Peterson, 1985). Some studies have found diel patterns related to temperature (W. J. Cooper et al., 1987; De Mello et al., 1987) and incoming tides (Dacey et al., 1987; Goldan et al., 1987; Morrison and Hines, 1990). Our results indicate that DMS fluxes from the SS site are associated with temperature and light-related processes, whether these variables influence microbial activity, plant physiology, or a combination of both. A study found that DMS fluxes peaked after a full daylight period in a Danish estuary (Jørgensen and Okholm-Hansen, 1985). However, there is no information on the diel patterns of DMS in the sediment pore water or its release from *S. alterniflora* plants. DMS is also produced by other pathways that occur under anoxic conditions, such as methylation of sulfide and methanethiol (Carrión et al., 2019; Lomans et al., 2002; Sela-Adler et al., 2015), microbial reduction of dimethylsulfoxide (Capone and Kiene, 1988), and/or the incorporation of inorganic substrates (i.e., CO_2) and organic methylated compounds (Finster et al., 1990; Lin et al., 2010; Moran et al., 2008). To better understand DMS fluxes, more research into the dynamics between *S. alterniflora*, pore water DMS, and DMS fluxes is needed, as it plays an important role in carbon-sulfur biogeochemistry, particularly as a non-competitive substrate for methylotrophic methanogenesis (Seyfferth et al., 2020).

4.4.2 Continuous versus discrete measurements: do we get the same information?

Our results show that discrete temporal measurements of CO_2 during daytime low tide throughout the year (including dormancy) may be sufficient to obtain a

representative mean of the temporal variability of soil CO_2 flux. This has implications for calculating carbon budgets. Furthermore, the distribution of continuous and discrete CO_2 fluxes is similar, indicating that discrete measurements are capturing similar variability as continuous measurements. This observation is reinforced by the CO_2 ~ air temperature relationships, which do not have significantly different slopes (discrete: 0.03 - 0.12, continuous: 0.04 - 0.05), providing further support for the utility of daytime low tide discrete measurements in evaluating potential drivers of CO_2 variability.

In contrast, high variability in CH_4 fluxes resulted in the means for discrete and continuous measurements to be similar, but with significantly different distributions. In salt marshes, CH_4 fluxes are characterized by high variability (Rosentreter et al., 2021), making it difficult to assess the processes that control CH_4 fluxes (Vázquez-Lule and Vargas, 2021). While the means were not significantly different despite ~33% higher mean flux using discrete measurements, it is important to note that the 95% confidence interval and the coefficient of variation are broad and very high, resulting in potential error cancellation for the calculation of the mean. We postulate that the discrete measurement approach can be used to calculate budgets with the caveat of large uncertainties and that they likely overestimate the mean CH_4 flux. Discrete measurements do not capture similar variability as the continuous measurements and have a stronger air temperature ~ CH_4 flux relationship than continuous measurements, despite the overlap between their confidence intervals (2.14 - 12.7 and 1.31 - 2.71, respectively). However, continuous measurements provide a more accurate depiction of the patterns and magnitudes of CH_4 and can provide stronger insights into the interrelated drivers of CH_4 fluxes.

Regardless of the sampling interval, N_2O fluxes had means that are near-zero. Due to fluxes consistently being near zero, the discrete and continuous measurements will likely get similar overall results due to error cancellation even if the distributions were significantly different. The continuous measurements capture a wider range of fluxes than the discrete measurements, as seen with its very high coefficient of variance and a different distribution. However, the skewness between the two approaches is very similar, due to the bulk of the measurements falling around the same values. It is important to note that this site is nitrogen-limited, which constrains N_2O production. In marshes that are not nitrogen-limited, sampling intervals will likely play a more important role since fluxes will be higher.

For CS_2, discrete and continuous measurements did not have similar means or distributions, likely due to the high variability found in these measurements. Previous studies using discrete measurements of CS_2 have noted its high variability (e.g., De Mello et al., 1987), with one highlighting the need for frequent measurements of sulfur-based trace gases during the day in order to obtain an accurate mean daily flux value (Steudler and Peterson, 1985). We found that discrete measurements taken during daytime low tide result in a daily mean that is nearly twice that of the daily mean from the continuous measurements. The average CS_2 fluxes measured during our field campaigns were up to an order of magnitude higher than previously reported. We advocate for more measurements of CS_2 fluxes beyond focusing on low tide windows and during different canopy phenological phases across salt marshes to better understand the dynamics of this trace gas.

When measuring DMS fluxes during daytime low tide, the mean is similar to the continuous measurement mean, but the distributions are significantly different.

However, caution should be taken in using discrete measurements of DMS to calculate daily means, particularly if those measurements fall during the warmest part of the day when DMS fluxes are the most active. This could result in overestimating the daily mean since extended periods of no fluxes are not accounted for. One approach to measuring DMS fluxes would be to use the strong relationship between discrete and continuous measurements to correct for the overestimation of discrete fluxes. However, this approach would still require the use of a continuous, automated system at different points throughout the year to establish a site-specific correction of discrete mean DMS fluxes, particularly if DMS fluxes are used to calculate DMS budgets.

4.5 Conclusion – what are we missing: potential caveats?

Discrete measurements have the clear advantage of capturing the spatial variability of soil trace gas fluxes across an ecosystem, but this approach is also used to describe the temporal variability. Here we discuss the advantages and differences from discrete and continuous measurements derived from this study. Discrete measurement campaigns are suitable for calculating budgets, particularly for CO_2 and N_2O since they capture very similar means. While we found that CH_4 and DMS means were not significantly different between the two approaches, there are caveats that must be considered when using discrete measurements. The high variability inherent in CH_4 fluxes can contribute to the lack of significant differences between the two approaches and result in discrete measurements overestimating the overall CH_4 fluxes from a tidal salt marsh. This has implications when calculating SGWP where differences in CH_4 means largely contribute to the differences in SGWP between the two approaches and can affect how scientists and policymakers view tidal salt marshes and blue carbon as a natural climate solution (Macreadie et al., 2021). For DMS, it is

important to assess diel patterns to ensure that fluxes are representative, particularly at sites that have patterns similar to what is seen at our study site. When evaluating variability or trying to parse out the processes that drive GHG and trace gas emissions from tidal salt marshes, using continuous, automated measurements would be the best approach. This is particularly important for CH_4, where pulse emissions are frequent during the growing season and can be very high. Using continuous measurements is also important in scenarios where discrete measurements do not capture a similar mean or distribution, as with CS_2 fluxes. However, discrete measurements are more capable of representing spatial variability, and until we have a better understanding of which source of variability is higher, temporal, or spatial, both techniques should be considered for ecosystem assessments.

Acknowledgements

This research was supported by the National Science Foundation (#1652594). MC acknowledges support from an NSF Graduate Research Fellowship (#1247394). We thank the onsite support from Kari St. Laurent and the Delaware National Estuarine Research Reserve (DNERR), as well as from Victor and Evelyn Capooci for field assistance during the first campaign. We thank George Luther for inspiring discussions about carbon-sulfur biogeochemistry in salt marshes. The authors acknowledge the land on which they conducted this study is the traditional home of the Lenni-Lenape tribal nation (Delaware nation).

Author contributions

MC and RV conceptualized the study, designed the methodology, and conducted project administration. MC conducted the formal analysis, investigation, and visualization, as well as wrote the original draft. RV provide funding, resources, supervision, as well as reviewed and edited the manuscript.

Data availability and supplementary materials

Meteorological (station: delsjmet-p) and water quality (station: Aspen Landing) data are available from the National Estuarine Research Reserve's Centralized Data Management Office (CDMO) at https://cdmo.baruch.sc.edu/. Phenological data are available from the PhenoCam network (site: stjones) at https://phenocam.sr.unh.edu/webcam/sites/stjones/. Data from trace gas fluxes will be publicly available in a FAIR data repository (e.g., Figshare) before publication of this research.

Supplementary data can be found at https://doi.org/10.5194/bg-2022-101 as well as in Appendix C of this document.

REFERENCES

Al-Haj, A.N., Fulweiler, R.W., 2020. A synthesis of methane emissions from shallow vegetated coastal ecosystems. Glob. Chang. Biol. 26, 2988–3005. https://doi.org/10.1111/gcb.15046

Andreae, M.O., Jaeschke, W.A., 1992. Exchange of sulfur between biosphere and atmosphere over temperate and tropical regions, in: Howarth, R.W., Stewart, J.W.B., Ivanov, M.V. (Eds.), Sulfur Cycling on the Continents. Wiley, New York.

Bahlmann, E., Weinberg, I., Lavrič, J. V, Eckhardt, T., Michaelis, W., Santos, R., Seifert, R., 2015. Tidal controls on trace gas dynamics in a seagrass meadow of the Ria Formosa lagoon (southern Portugal). Biogeosciences 12, 1683–1696. https://doi.org/10.5194/bg-12-1683-2015

Barba, J., Cueva, A., Bahn, M., Barron-Gafford, G.A., Bond-Lamberty, B., Hanson, P.J., Jaimes, A., Kulmala, L., Pumpanen, J., Scott, R.L., Wohlfahrt, G., Vargas, R., 2018. Comparing ecosystem and soil respiration: Review and key challenges of tower-based and soil measurements. Agric. For. Meteorol. 249, 434–443. https://doi.org/10.1016/j.agrformet.2017.10.028

Barbier, E., Hacker, S., Kennedy, C., Stier, A., Silliman, B., 2011. The value of estuarine and coastal ecosystem services. Ecol. Monogr. 81, 169–193.

Bartlett, K.B., Harriss, R.C., Sebacher, D.I., 1985. Methane flux from coastal salt marshes. J. Geophys. Res. 90, 5710–5720.

Bauza, J.F., Morell, J.M., Corredor, J.E., 2002. Biogeochemistry of nitrous oxide production in the red mangrove (*Rhizophora mangle*) forest sediments. Estuar. Coast. Shelf Sci. 55, 697–704. https://doi.org/10.1006/ecss.2001.0913

Bridgham, S.D., Richardson, C.J., 1992. Mechanisms controlling soil respiration (CO_2 and CH_4) in southern peatlands. Soil Biol. Biochem. 24, 1089–1099. https://doi.org/10.1016/0038-0717(92)90058-6

Brimblecombe, P., 2014. The Global Sulfur Cycle, in: Holland, H.D., Turekian, K.K. (Eds.), Treatise on Geochemistry. Elsevier Science, pp. 559–591. https://doi.org/10.1016/B978-0-08-095975-7.00814-7

Capone, D.G., Kiene, R.P., 1988. Comparison of microbial dynamics in marine and freshwater sediment. Limnol. Ocean. 33, 725–749.

Capooci, M., Barba, J., Seyfferth, A.L., Vargas, R., 2019. Experimental influence of storm-surge salinity on soil greenhouse gas emissions from a tidal salt marsh. Sci. Total Environ. 686, 1164–1172. https://doi.org/10.1016/j.scitotenv.2019.06.032

Capooci, M., Vargas, R., 2022. Diel and seasonal patterns of soil CO_2 efflux in a temperate tidal marsh. Sci. Total Environ. 802. https://doi.org/10.1016/j.scitotenv.2021.149715

Carrión, O., Pratscher, J., Rciha, K., Rostant, W.G., Haque, M.F.U., Murell, J.C., Todd, J.D., 2019. Methanthoil and dimethylsulfide cycling in Stiffkey saltmarsh. Front. Mar. Sci. 10, 1-15. https://doi.org/10.3389/fmicb.2019.01040

Carroll, M.A., Heidt, L.E., Cicerone, R.J., Prinn, R.G., 1986. OCS, H_2S, and CS_2 fluxes from a salt water marsh. J. Atmos. Chem. 4, 375–395. https://doi.org/10.1007/BF00053811

Cheng, X., Peng, R., Chen, Jiquan, Luo, Y., Zhang, Q., An, S., Chen, Jiakuan, Li, B., 2007. CH_4 and N_2O emissions from *Spartina alterniflora* and *Phragmites australis* in experimental mesocosms. Chemosphere 68, 420–427. https://doi.org/10.1016/J.CHEMOSPHERE.2007.01.004

Cooper, D.J., De Mello, W.Z., Cooper, W.J., Zika, R.G., Saltzman, E.S., Prospero, J.M., Savoie, D.L., 1987. Short-term variability in biogenic sulphur emissions from a Florida *Spartina alterniflora* marsh. Atmos. Environ. 21, 7–12.

Cooper, W.J., Cooper, D.J., Saltzman, E.S., Mello, W.Z. d., Savoie, D.L., Zika, R.G., Prospero, J.M., 1987. Emissions of biogenic sulphur compounds from several wetland soils in Florida. Atmos. Environ. 21, 1491–1495. https://doi.org/10.1016/0004-6981(87)90311-8

Dacey, J.W.H., King, G.M., Wakeham, S.G., 1987. Factors controlling emission of dimethylsulphide from salt marshes. Nature 330, 643–645. https://doi.org/10.1038/330643a0

De Mello, W.Z., Cooper, D.J., Cooper, W.J., Saltzman, E.S., Zika, R.G., Savoie, D.L., Prospero, J.M., 1987. Spatial and diel variability in the emissions of some biogenic sulfur compounds from a Florida *Spartina alterniflora* coastal zone. Atmos. Environ. 21, 987–990. https://doi.org/10.1016/0004-6981(87)90095-3

DeLaune, R.D., Devai, I., Lindau, C.W., 2002. Flux of reduced sulfur gases along a salinity gradient in Louisiana coastal marshes. Estuar. Coast. Shelf Sci. 54, 1003–1011. https://doi.org/10.1006/ecss.2001.0871

Diefenderfer, H.L., Cullinan, V.I., Borde, A.B., Gunn, C.M., Thom, R.M., 2018. High-frequency greenhouse gas flux measurement system detects winter storm surge effects on salt marsh. Glob. Chang. Biol. 24, 5961–5971. https://doi.org/10.1111/gcb.14430

DNREC, 1999. Delaware National Esturaine Research Reserve Estuarine Profile.

Duarte, C.M., Middelburg, J.J., Caraco, N., 2005. Major role of marine vegetation on the oceanic carbon cycle. Biogeosciences 2, 1–8. https://doi.org/10.1111/j.2042-7158.1975.tb10261.x

Emery, H.E., Fulweiler, R.W., 2014. *Spartina alterniflora* and invasive *Phragmites australis* stands have similar greenhouse gas emissions in a New England marsh. Aquat. Bot. 116, 83–92. https://doi.org/10.1016/j.aquabot.2014.01.010

Emmer, I., Needelman, B., Emmett-Mattox, S., Crooks, S., Beers, L., Megonigal, P., Myers, D., Oreska, M., McGlathery, K., Shoch, D., 2021. Methodology for Tidal Wetland and Seagrass Restoration.

Filippa, G., Cremonese, E., Migliavacca, M., Galvagno, M., Folker, M., Richardson, A.D., Tomelleri, E., 2020. phenopix: Process Digital Images of a Vegetation Cover. R Packag. version 2.4.2.

Finster, Kai, King, G.M., Bak, F., Finster, K, 1990. Formation of methylmercaptan and dimethylsulfide from methoxylated aromatic compounds in anoxic marine and fresh water sediments. FEMS Microbiol. Ecol. 74, 295–302. https://doi.org/10.1111/j.1574-6968.1990.tb04076.x

Goldan, P.D., Kuster, W.C., Albritton, D.L., Fehsenfeld, F.C., 1987. The measurement of natural sulfur emissions from soils and vegetation: Three sites in the Eastern United States revisited. J. Atmos. Chem. 5, 439–467. https://doi.org/10.1007/BF00113905

Granville, K.E., Ooi, S.K., Koenig, L.E., Lawrence, B.A., Elphick, C.S., Helton, A.M., 2021. Seasonal patterns of denitrification and N_2O production in a southern New England salt marsh. Wetlands 41, 1–13. https://doi.org/10.1007/s13157-021-01393-x

Hill, A.C., Vázquez-Lule, A., Vargas, R., 2021. Linking vegetation spectral reflectance with ecosystem carbon phenology in a temperate salt marsh. Agric. For. Meteorol. 307, 108481. https://doi.org/10.1016/j.agrformet.2021.108481

Hines, M.E., 1996. Emissions of sulfur gases from wetlands. Mitt. lntemat. Verein. Limnol. 25, 153–161. https://doi.org/10.1080/05384680.1996.11904076

Järveoja, J., Nilsson, M.B., Gažovič, M., Crill, P.M., Peichl, M., 2018. Partitioning of the net CO_2 exchange using an automated chamber system reveals plant phenology as key control of production and respiration fluxes in a boreal peatland. Glob. Chang. Biol. 24, 3436–3451. https://doi.org/10.1111/gcb.14292

Jha, C.S., Rodda, S.R., Thumaty, K.C., Raha, A.K., Dadhwal, V.K., 2014. Eddy covariance based methane flux in Sundarbans mangroves, India. J. Earth Syst. Sci. 123, 1089–1096. https://doi.org/10.1007/s12040-014-0451-y

Jørgensen, B.B., Okholm-Hansen, B., 1985. Emissions of biogenic sulfur gases from a Danish estuary. Atmos. Environ. 19, 1737–1749. https://doi.org/10.1016/0004-6981(85)90001-0

Kellogg, W.W., Cadle, R.D., Allen, E.R., Lazrus, A.L., Martell, E.A., 1972. The sulfur cycle. Science. 175, 587–596. https://doi.org/10.1016/S0074-6142(08)62696-0

Kiene, R.P., 1988. Dimethyl sulfide metabolism in salt marsh sediments. FEMS Microbiol. Lett. 53, 71–78. https://doi.org/10.1016/0378-1097(88)90014-6

Kiene, R.P., Visscher, P.T., 1987. Production and fate of methylated sulfur compounds from methionine and dimethylsulfoniopropionate in anoxic salt marsh sediments. Appl. Environ. Microbiol. 53, 2426–2434.

Kim, J., Verma, S.B., Billesbach, D.P., Clement, R.J., 1998. Diel variation in methane emission from a midlatitude prairie wetland: Significance of convective throughflow in *Phragmites australis*. J. Geophys. Res. Atmos. 103, 28029–28039. https://doi.org/10.1029/98JD02441

Koskinen, M., Minkkinen, K., Ojanen, P., Kämäräinen, M., Laurila, T., Lohila, A., 2014. Measurements of CO_2 exchange with an automated chamber system throughout the year: Challenges in measuring night-time respiration on porous peat soil. Biogeosciences 11, 347–363. https://doi.org/10.5194/bg-11-347-2014

Laursen, A.E., Seitzinger, S.P., 2002. Measurement of denitrification in rivers: An integrated, whole reach approach. Hydrobiologia 485, 67–81.

Lin, Y.S., Heuer, V.B., Ferdelman, T.G., Hinrichs, K.-U., 2010. Microbial conversion of inorganic carbon to dimethyl sulfide in anoxic lake sediment (Plußsee, Germany). Biogeosciences 7, 2433–2444. https://doi.org/10.5194/bg-7-2433-2010

Livesley, S.J., Andrusiak, S.M., 2012. Temperate mangrove and salt marsh sediments are a small methane and nitrous oxide source but important carbon store. Estuar. Coast. Shelf Sci. 97, 19–27. https://doi.org/10.1016/j.ecss.2011.11.002

Lomans, B.P., Van der Drift, C., Pol, A., Op den Camp, H.J.M., 2002. Microbial cycling of volatile organic sulfur compounds. Water Sci. Technol. 45, 55–60. https://doi.org/10.1007/s00018-002-8450-6

Macreadie, P.I., Costa, M.D.P., Atwood, T.B., Friess, D.A., Kelleway, J.J., Kennedy, H., Lovelock, C.E., Serrano, O., Duarte, C.M., 2021. Blue carbon as a natural climate solution. Nat. Rev. Earth Environ. 2, 826–839. https://doi.org/https://doi.org/10.1038/s43017-021-00224-1

Middelburg, J.J., Klaver, G., Nieuwenhuize, J., Wielemaker, A., de Hass, W., Vlug, T., van der Nat, J.F.W.A. 1996. Organic matter mineral sediments along an estuarine gradient. Mar. Ecol. Prog. Ser. 132, 157–168.

Möller, I., Kudella, M., Rupprecht, F., Spencer, T., Paul, M., Van Wesenbeeck, B.K., Wolters, G., Jensen, K., Bouma, T.J., Miranda-Lange, M., Schimmels, S., 2014. Wave attenuation over coastal salt marshes under storm surge conditions. Nat. Geosci. 7, 727–731. https://doi.org/10.1038/NGEO2251

Moran, J.J., House, C.H., Vrentas, J.M., Freeman, K.H., 2008. Methyl sulfide production by a novel carbon monoxide metabolism in *Methanosarcina acetivorans*. Appl. Environ. Microbiol. 74, 540–542. https://doi.org/10.1128/AEM.01750-07

Morrison, M.C., Hines, M.E., 1990. The variability of biogenic sulfur flux from a temperate salt marsh on short time and space scales. Atmos. Environ. Part A. Gen. Top. 24A, 1771–1779. https://doi.org/10.1016/0960-1686(90)90509-L

Moseman-Valtierra, S., Abdul-Aziz, O.I., Tang, J., Ishtiaq, K.S., Morkeski, K., Mora, J., Quinn, R.K., Martin, R.M., Egan, K., Brannon, E.Q., Carey, J., Kroeger, K.D., 2016. Carbon dioxide fluxes reflect plant zonation and belowground biomass in a coastal marsh. Ecosphere 7, e01560.

Moseman-Valtierra, S., Gonzalez, R., Kroeger, K.D., Tang, J., Chao, W.C., Crusius, J., Bratton, J., Green, A., Shelton, J., 2011. Short-term nitrogen additions can shift a coastal wetland from a sink to a source of N_2O. Atmos. Environ. 45, 4390–4397. https://doi.org/10.1016/j.atmosenv.2011.05.046

Murray, R.H., Erler, D. V., Eyre, B.D., 2015. Nitrous oxide fluxes in estuarine environments: Response to global change. Glob. Chang. Biol. 21, 3219–3245. https://doi.org/10.1111/gcb.12923

Neubauer, S.C., Megonigal, J.P., 2019. Correction to: Moving beyond global warming potentials to quantify the climatic role of ecosystems. Ecosyst. 2019 228 22, 1931–1932. https://doi.org/10.1007/S10021-019-00422-5

NOAA National Estuarine Research Reserve System (NERRS), 2015. System-wide Monitoring Program [WWW Document]. NOAA NERRS Cent. Data Manag. Off.

Oremland, R.S., Marsh, L.M., Polcin, S., 1982. Methane production and simultaneous sulphate reduction in anoxic, salt marsh sediments. Nature 296, 143–145.

Peterson, P.M., Romaschenko, K., Arrieta, Y.H., Saarela, J.M., 2014. A molecular phylogeny and new subgeneric classification of *Sporobolus* (Poaceae: Chloridoideae: Sporobolinae). Taxon 63, 1212–1243. https://doi.org/10.12705/636.19

Petrakis, S., Seyfferth, A., Kan, J., Inamdar, S., Vargas, R., 2017. Influence of experimental extreme water pulses on greenhouse gas emissions from soils. Biogeochemistry 133, 147–164. https://doi.org/10.1007/s10533-017-0320-2

Rinne, J., Riutta, T., Pihlatie, M., Aurela, M., Haapanala, S., Tuovinen, J.P., Tuittila, E.S., Vesala, T., 2007. Annual cycle of methane emission from a boreal fen measured by the eddy covariance technique. Tellus, Ser. B Chem. Phys. Meteorol. 59, 449–457. https://doi.org/10.1111/j.1600-0889.2007.00261.x

Rosentreter, J.A., Al-Haj, A.N., Fulweiler, R.W., Williamson, P., 2021. Methane and nitrous oxide emissions complicate coastal blue carbon assessments. Global Biogeochem. Cycles 35, e2020GB006858. https://doi.org/10.1029/2020GB006858

Rosentreter, J.A., Maher, D.T., Erler, D. V., Murray, R.H., Eyre, B.D., 2018. Methane emissions partially offset “blue carbon” burial in mangroves. Sci. Adv. 4, eaao4985. https://doi.org/10.1126/SCIADV.AAO4985

Savage, K., Phillips, R., Davidson, E., 2014. High temporal frequency measurements of greenhouse gas emissions from soils. Biogeosciences 11, 2709–2720. https://doi.org/10.5194/bg-11-2709-2014

Sela-Adler, M., Said-Ahmad, W., Sivan, O., Eckert, W., Kiene, R.P., Amrani, A., 2015. Isotopic evidence for the origin of dimethylsulfide and dimethylsulfoniopropionate-like compounds in a warm, monomictic freshwater lake. Environ. Chem. 13, 340–351. https://doi.org/https://doi.org/10.1071/EN15042

Seyednasrollah, B., Young, A.M., Hufkens, K., Milliman, T., Friedl, M.A., Frolking, S., Richardson, A.D., Abraha, M., Allen, D.W., Apple, M., Arain, M.A., Baker, J., Baker, J.M., Baldocchi, D., Bernacchi, C.J., Bhattacharjee, J., Blanken, P., Bosch, D.D., Boughton, R., Boughton, E.H., Zona, D., 2019. PhenoCam dataset v2.0: Vegetation phenology from digital camera imagery. Oak Ridge, Tennessee. https://doi.org/https://doi.org/10.3334/ORNLDAAC/1674

Seyfferth, A.L., Bothfeld, F., Vargas, R., Stuckey, J.W., Wang, J., Kearns, K., Michael, H.A., Guimond, J., Yu, X., Sparks, D.L., 2020. Spatial and temporal heterogeneity of geochemical controls on carbon cycling in a tidal salt marsh. Geochim. Cosmochim. Acta 282, 1–18. https://doi.org/10.1016/j.gca.2020.05.013

Simpson, L.T., Osborne, T.Z., Feller, I.C., 2019. Wetland soil CO_2 efflux along a latitudinal gradient of spatial and temporal complexity. Estuaries and Coasts 42, 45–54. https://doi.org/10.1007/s12237-018-0442-3

Steudler, P.A., Peterson, B.J., 1985. Annual cycle of gaseous sulfur emissions from a New England *Spartina alterniflora* marsh. Atmos. Environ. 19, 1411–1416. https://doi.org/10.1016/0004-6981(85)90278-1

Steudler, P.A., Peterson, B.J., 1984. Contribution of gaseous sulphur from salt marshes to the global sulphur cycle. Nature 311, 455–457. https://doi.org/10.1038/311455a0

Taubman, S.J., Kasting, J.F., 1995. Carbonyl sulfide: No remedy for global warming. Geophys. Res. Lett. 22, 803–805. https://doi.org/10.1029/95GL00636

Tong, C., Huang, J.F., Hu, Z.Q., Jin, Y.F., 2013. Diurnal variations of carbon dioxide, methane, and nitrous oxide vertical fluxes in a subtropical estuarine marsh on neap and spring tide days. Estuaries and Coasts 36, 633–642. https://doi.org/10.1007/s12237-013-9596-1

Tong, C., Morris, J.T., Huang, J., Xu, H., Wan, S., 2018. Changes in pore-water chemistry and methane emission following the invasion of *Spartina alterniflora* into an oliogohaline marsh. Limnol. Oceanogr. 63, 384–396. https://doi.org/10.1002/lno.10637

Trifunovic, B., Vázquez-Lule, A., Capooci, M., Seyfferth, A.L., Moffat, C., Vargas, R., 2020. Carbon dioxide and methane emissions from temperate salt marsh tidal creek. J. Geophys. Res. Biogeosciences 125. https://doi.org/10.1029/2019JG005558

UNFCCC, 2015. Paris Agreement.

van der Nat, F., Middelburg, J.J., 2000. Methane emission from tidal freshwater marshes. Biogeochemistry 49, 103–121.

Vargas, R., Carbone, M.S., Reichstein, M., Baldocchi, D.D., 2011. Frontiers and challenges in soil respiration research: From measurements to model-data integration. Biogeochemistry 102, 1–13. https://doi.org/10.1007/s10533-010-9462-1

Vázquez-Lule, A., Vargas, R., 2021. Biophysical drivers of net ecosystem and methane exchange across phenological phases in a tidal salt marsh. Agric. For. Meteorol. 300. https://doi.org/10.1016/j.agrformet.2020.108309

Wang, Jinxin, Wang, Jinshu, 2017. *Spartina alterniflora* alters ecosystem DMS and CH_4 emissions and their relationship along interacting tidal and vegetation gradients within a coastal salt marsh in eastern China. Atmos. Environ. 167, 346–359. https://doi.org/10.1016/J.ATMOSENV.2017.08.041

Ward, N., Megonigal, P.J., Bond-Lamberty, B., Bailey, V., Butman, D., Canuel, E., Diefenderfer, H., Ganju, N.K., Goñi, M.A., Graham, E.B., Hopkinson, C.S., Khangaonkar, T., Langley, J.A., McDowell, N.G., Myers-Pigg, A.N., Neumann, R.B., Osburn, C.L., Price, R.M., Rowland, J., Sengupta, A., Simard, M., Thornton, P.E., Tzortziou, M., Vargas, R., Weisenhorn, P.B., Windham-Myers, L., 2020. Representing the function and sensitivity of coastal interfaces in Earth system models. Nat. Commun. 11, 1–14. https://doi.org/10.1038/s41467-020-16236-2

Watts, S.F., 2000. The mass budgets of carbonyl sulfide, dimethyl sulfide, carbon disulfide and hydrogen sulfide. Atmos. Environ. 34, 761–779. https://doi.org/10.1016/S1352-2310(99)00342-8

Whelan, M.E., Min, D.H., Rhew, R.C., 2013. Salt marsh vegetation as a carbonyl sulfide (COS) source to the atmosphere. Atmos. Environ. 73, 131–137. https://doi.org/10.1016/J.ATMOSENV.2013.02.048

Wilson, B.J., Mortazavi, B., Kiene, R.P., 2015. Spatial and temporal variability in carbon dioxide and methane exchange at three coastal marshes along a salinity gradient in a northern Gulf of Mexico estuary. Biogeochemistry 123, 329–347. https://doi.org/10.1007/s10533-015-0085-4

Xie, H., Moore, R.M., 1999. Carbon disulfide in the North Atlantic and Pacific Oceans. J. Geophys. Res. Ocean. 104, 5393–5402. https://doi.org/10.1029/1998jc900074

Xie, X., Zhang, M.-Q., Zhao, B., Guo, H.-Q., 2014. Dependence of coastal wetland ecosystem respiration on temperature and tides: A temporal perspective. Biogeosciences 11, 539–545. https://doi.org/10.5194/bg-11-539-2014

Xu, X., Fu, G., Zou, X., Ge, C., Zhao, Y., 2017. Diurnal variations of carbon dioxide, methane, and nitrous oxide fluxes from invasive *Spartina alterniflora* dominated coastal wetland in northern Jiangsu Province. Acta Oceanol. Sin. 36, 105–113. https://doi.org/10.1007/s13131-017-1015-1

Yang, W.-B. Bin, Yuan, C.-S.S., Tong, C., Yang, P., Yang, L., Huang, B.-Q.Q., 2017. Diurnal variation of CO_2, CH_4, and N_2O emission fluxes continuously monitored in-situ in three environmental habitats in a subtropical estuarine wetland. Mar. Pollut. Bull. 119, 289–298. https://doi.org/10.1016/j.marpolbul.2017.04.005

Yang, W.-B., Yuan, C.-S., Huang, B.-Q., Tong, C., Yang, L., 2018. Emission characteristics of greenhouse gases and their correlation with water quality at an estuarine mangrove ecosystem – the application of an in-situ on-site NDIR monitoring mechnique. Wetl. 2018 384 38, 723–738. https://doi.org/10.1007/S13157-018-1015-8

Yu, X., Ye, S., Olsson, L., Wei, M., Krauss, K.W., Brix, H., 2019. A 3-year in-situ measurement of CO_2 efflux in coastal wetlands: Understanding carbon loss through ecosystem respiration and its partitioning. Wetlands. https://doi.org/10.1007/s13157-019-01197-0

Yu, Z., Li, Y., Deng, H., Wang, D., Chen, Z., Xu, S., 2012. Effect of *Scirpus mariqueter* on nitrous oxide emissions from a subtropical monsoon estuarine wetland. J. Geophys. Res. Biogeosciences 117, 2017. https://doi.org/10.1029/2011JG001850

Zhang, Y., Ding., W., 2011. Diel methane emissions in stands of *Spartina alterniflora* and *Suaeda salsa* from a coastal salt marsh. Aquat. Bot., 95, 262-267. https://doi.org/10.1016/j.aquabot.2011.08.005

Zhang, Y., Wang, L., Xie, X., Huang, L., Wu, Y., 2013. Effects of invasion of *Spartina alterniflora* and exogenous N deposition on N_2O emissions in a coastal salt marsh. Ecol. Eng. 58, 77–83. https://doi.org/10.1016/j.ecoleng.2013.06.011

Chapter 5

METHANE DYNAMICS IN TIDAL SALT MARSH SOILS: A MULTI-DISCIPLINARY APPROACH TO UNDERSTANDING PRODUCTION AND FATE

In preparation

Margaret Capooci[1], Jennifer F. Biddle[2], Malique Bowen[2], Alexandra Hedgpeth[3], Karis J. McFarlane[4], Angelia L. Seyfferth[1], Craig R. Tobias[5], Andrew S. Wozniak[2], Rodrigo Vargas[1]

[1] Department of Plant and Soil Sciences, University of Delaware, Newark, DE, USA

[2] School of Marine Science and Policy, University of Delaware, Lewes, DE, USA

[3] Department of Geography, University of California - Los Angeles, Los Angeles, CA, USA

[4] Center for Accelerator Mass Spectrometry, Lawrence Livermore National Laboratory, Livermore, CA, USA

[5] Department of Marine Sciences, University of Connecticut, Groton, CT, USA

Abstract

Tidal salt marshes emit CH_4, but there remains large uncertainities regarding the spatiotemporal variability of emissions, as well as the processes that dictate it. Recent evidence has shown CH_4 can be produced within marshes via methylotrophic methanogenesis, a process that can occur alongside sulfate reduction, necessitating a

revaluation of the role of salt marshes in CH_4 cycling. Thus, we performed continuous, automated measurements of soil CO_2 and CH_4 fluxes coupled with soil CH_4 and CO_2 gas concentrations, stable and radioisotopes, pore water chemistry, and microbial community composition to assess the production and fate of CH_4 within a tidal salt marsh. Measurement campaigns were conducted throughout the growing season to evaluate CH_4 temporal variability. We found that CH_4 within the soils is produced by methylotrophic and hydrogenotrophic methanogensis, which varies seasonally with higher CH_4 production during plant senescence. CH_4 and CO_2 within the soil profile were produced from young carbon, with mostly $\Delta^{14}C\text{-}CH_4$ and $\Delta^{14}C\text{-}CO_2$ values of modern or >modern, indicating higher turnover of CH_4 and CO_2 within the soil. Data showed evidence of several pathways CH_4 can take once produced: diffusion into the atmosphere, CH_4 oxidation, and lateral export to the tidal creek. However, more research is needed to better quantify the roles each play in CH_4 fate. Our findings demonstrate that CH_4 production and fate is biogeochemically heterogeneous, with multiple processes and pathways that can occur simultaneously and vary in importance over the growing season. Future research is needed to better quantify the role each of these processes have in CH_4 dynamics in a tidal salt marsh, so that we can better represent CH_4 dynamics in carbon cycle models, CH_4 budgets, and blue carbon assessments.

5.1 Introduction

Methane (CH_4) production in tidal salt marshes has long been thought to be little to non-existent despite anaerobic soil conditions. Studies have shown that salinity is negatively correlated with CH_4 in marshes, with higher emissions at lower salinities (Al-Haj and Fulweiler, 2020; Poffenbarger et al., 2011). In addition to salinity, high sulfate concentrations in salt marsh soils are thought to contribute to low CH_4 emissions because sulfate reducing bacteria outcompete the two dominant forms of methanogenesis (hydrogenotrophic and acetoclastic; Mer and Roger, 2001) for substrates such as H_2, CO_2, and acetate (Ponnamperuma, 1972), thereby suppressing methanogenesis until sulfate levels have been depleted (King and Wiebe, 1980). Therefore, there has been little interest in better quantifying and understanding CH_4 dynamics in tidal salt marsh soils, despite CH_4's high global warming potential.

Recently, there has been increased interest in better quantifying and understanding the processes behind CH_4 production in tidal wetlands. While the coastal and open ocean, which includes salt marshes, releases an estimated 4 to 10 Tg CH_4 yr^{-1} (Saunois et al., 2020), there are large uncertainties in this calculation, due to the need to better quantify CH_4 emissions from the ecosystem types that fall within this category. This issue also arises in representing coastal areas in Earth system models, where there is insufficient data regarding methanogenesis substrate limitations, spatiotemporal variability in CH_4 fluxes, and the processes that dictate CH_4 production and emission (Ward et al., 2020). Concurrently, there has been increased interest in tidal salt marshes, along with mangrove forests and seagrass beds (i.e., "blue carbon" ecosystems), for their ability to store large amounts of carbon (Nellemann et al., 2009). However, there is still uncertainty about whether greenhouse gas emissions from these ecosystems offsets their carbon storage capacity. For

example, one study found that salt marshes and mangroves emit enough CH_4 to offset >100% of their carbon sequestration (Al-Haj and Fulweiler, 2020), while other studies have demonstrated that blue carbon ecosystems store more carbon than they release (Oreska et al., 2020; Rosentreter et al., 2018; Taillardat et al., 2020). Until there is a better understanding of CH_4 dynamics in coastal wetlands, it will be difficult to assess the role they play in mitigating climate change.

Along with increased interest in CH_4 fluxes, there have been recent developments regarding the current paradigm surrounding CH_4 production in coastal ecosystems. Two pieces of information have recently challenged this paradigm. One, a recent synthesis study found that CH_4 fluxes from coastal ecosystems, which include salt marshes, can range widely from net uptake (-93 μmol m^{-2} day^{-1}) to net emission (94,000 μmol m^{-2} day^{-1}; Al-Haj and Fulweiler, 2020 and references within). The median CH_4 fluxes from salt marshes are low (224.44 μmol m^{-2} day^{-1}, Al-Haj and Fulweiler, 2020), but the wide range of fluxes measured necessitates a closer look at the processes that control methanogenesis in marshes. Two, a third methanogenesis pathway, methylotrophic methanogenesis, may occur in salt marshes and marine sediments (Seyfferth et al., 2020; Xiao et al., 2018; Zhuang et al., 2018). Methylotrophic methanogenesis uses non-competitive substrates such as methanol, methylsulfides, and methylamines, thereby enabling CH_4 to be produced even in the presence of sulfate reduction (Oremland et al., 1982; Xiao et al., 2018). Notably, *Spartina alterniflora*, a common salt marsh plant species, releases trimethylamine (TMA), which is a substrate for methylotrophic methanogenesis (Wang and Lee, 1995, 1994). Since CH_4 in tidal salt marsh soils have long been thought to be produced via hydrogenotrophic and acetoclastic methanogenesis, there is a need to

further explore the role methylotrophic methanogenesis may play in CH_4 fluxes from tidal salt marsh soils, and how that affects CH_4 budgets, carbon cycle models, and blue carbon assessments.

Thus, this study's objective is to investigate the patterns and processes that govern CH_4 production, oxidation, and movement from soils in a temperate tidal salt marsh. This study is conducted in a marsh where high concentrations of CH_4 have been reported within the soil (Seyfferth et al., 2020). We ask two questions:

1. Are high CH_4 concentrations within the soil due to, in part, the presence of methylotrophic methanogens within the soil microbial community?
2. What is the fate of the CH_4 within the soil profile? Does CH_4 persist in the soil, get vertically or laterally transported as CH_4, or get oxidized into CO_2 and lost vertically as CO_2 or moved laterally as DIC?

5.2 Materials and methods

5.2.1 Study site

The study was conducted in a short *S. alterniflora* (= *Sporobolus alterniflorus* (Loisel.); Peterson et al., 2014) dominated area of St. Jones Reserve, the brackish estuarine component of the Delaware National Estuarine Research Reserve. The site is a mesohaline tidal salt marsh (DNREC, 1999) with silty clay loam soils (10% sand, 61% silt, 29% clay; (Capooci et al., 2019). The marsh is located within the Delaware Estuary and is tidally connected to the Delaware Bay via the St. Jones River. The study site is lower in elevation than the rest of the marsh, is characterized by evidence of simultaneous sulfate reduction and CH_4 production (Seyfferth et al., 2020), and will

be referred to as SS as established in previous studies (Capooci and Vargas, 2022a, 2022b; Seyfferth et al., 2020).

The SS site is located within a spring-neap hydrological zone, meaning that the area floods during very high tides, such as spring high tide or during storm events, due to the presence of a levee near the tidal creek (Guimond et al., 2020; Seyfferth et al., 2020). As a result, the pore waters are stagnant and redox potentials can reach -200 mV, particularly in depths below 12 cm (Seyfferth et al., 2020). Above 12 cm, particularly from 0 to 7 cm, there is diurnal tidal influence on water levels and redox values are higher, upwards of 200 mV (Guimond et al., 2020; Seyfferth et al., 2020). Therefore, the site experiences strong redox gradients with variations in redox, ranging from oxic to anoxic, in the near surface due to diurnal tidal influence to being strongly reducing at 12 cm and below due to mixing occurring on spring-neap tidal cycles.

5.2.2 Experimental set-up

The experimental set-up was divided into two components, continuous, automated measurements and manual sampling, that were performed over the course of six campaigns throughout the growing season. The campaigns began during maturity (M) in the latter half of 2020 (M1 - June 29 to July 2; M2 - July 31 - Aug. 3) followed by senescence (S1 - Aug. 31 to Sept. 31, S2 - Sept. 28 to Oct. 1). During 2021, two more campaigns occurred, in dormancy (D1 - Mar. 22 to 26 & Apr. 13-16) and in greenup (G1 - May 31 to June 3).

Along one side of the boardwalk, six PVC collars (diameter: 20 cm) were placed ~1.2 meters apart, four months prior to the M1 campaign (Fig. D.1). On the other side of the boardwalk, four additional PVC collars (diameter: 15 cm) were installed in 2017 for a previous study. The six 20 cm collars were used to set down

automated chambers (LICOR 8100-104, Lincoln, Nebraska), while the four 15 cm collars were used for manual sampling described below. Prior to each campaign, any aboveground vegetation that grew inside the collars was carefully clipped.

In addition to soil gas flux measurements, soil, water, and gas samples were collected for a suite of analyses. Soil samples were collected for 16s rRNA gene sequencing and radiocarbon measurements. Water samples from both pore water and surface water were collected to measure salinity, sulfide, DOC, DIC, $SUVA_{254}$, and fluorescence index. Gas samples from the soil surface, as well as from within the soil profile were collected for stable and radiocarbon analyses, as well as concentration measurements.

5.2.3 Belowground and surface CH_4 and CO_2 measurements

Depth profiles of CH_4 and CO_2 concentrations within the sediments were measured using a passive gas sampler. The passive gas sampler was built as described in Seyfferth et al., (2020), with gas-permeable silicone tube (Jacinthe and Groffman, 2001), located at -15.5, -40, -56, and -70 cm below the soil surface. Depths were selected based on the soil horizonation at SS (Seyfferth et al., 2020). The sampler was installed in summer 2018. Gas concentrations were measured using a non-dispersive infrared (NDIR) sensor that measures both CH_4 and CO_2 concentrations (MH-Z92 Dual Gas CO_2/CH_4, CO_2 Meter, Ormond Beach, Florida). Prior research at the site found that CH_4 concentrations exceeded the range of the Ultraportable Greenhouse Gas Analyzer (UGGA; Los Gatos Research, San Jose, CA), requiring the use of a different sensor. The NDIR sensor was chosen due to its high detection range (0-100% vol CH_4, 0-50% vol CO_2). At the start of each campaign (day 1), each silicone tube was flushed with N_2 using a gas bladder bag attached to one of the two-way valves.

The other two-way valve was open to ensure that the air inside of the tube was flushed out. After flushing, both valves were closed to allow the silicone tubes to equilibrate to the gas concentrations at the respective depths. On day 5, gas concentrations were measured. Data from Jacinthe and Groffman (2001) demonstrated that equilibrium between the silicone tubing and the surrounding soil was achieved in <12 h and sampling was done every 3 to 4 days. The sensor was connected to a diaphragm pump and an in-line sampling port, along with a water trap and particulate filter to protect both the sensor and the pump, and a sampling port to collect samples. Tubing connected each end of the sampling set-up to the passive sampler, such that when the two-way valves were opened, subsurface gas circulated through the set-up in a closed loop. Gas concentrations were measured in ppmv and subsequently converted into mM for ease of comparison with pore water data (Appendix D.1).

Surface CH_4 and CO_2 fluxes were measured as described previously (Capooci and Vargas, 2022b). Briefly, autochambers were placed on 20 cm diameter collars and coupled with a closed-path infrared gas analyzer (LI-8100A, LICOR, Lincoln, Nebraska) in parallel with a Fourier transform infrared spectrometer (DX4040, Gasmet Technologies Oy, Vantaa, Finland). Measurements were 5 minutes long and each campaign lasted approximately 72 hours. Gas fluxes were calculated in SoilFluxPro (v4.2.1, LICOR, Lincoln, Nebraska) and underwent previously established QAQC protocols (Capooci et al., 2019; Capooci and Vargas, 2022b; Petrakis et al., 2017b, 2017a).

5.2.4 Gas, water, and soil sample collection

Both belowground CH_4 and CO_2, as well as surface CO_2 gas flux were collected for stable ($\delta^{13}C$) and radiocarbon ($\Delta^{14}C$) isotope measurements during low

tide. After belowground concentrations were measured on day 5, an air-tight syringe was used to extract gas from each depth using the in-line sampling port. Samples designated for $\Delta^{14}C$ analyses were injected into a pre-evacuated serum vial capped with a septa, while samples for $\delta^{13}C$ were injected into N_2-filled exetainers.

To collect gas emitted from the soil surface for $\delta^{13}C$, a chamber outfitted with a fan and an in-line sampling port in the tubing was connected to the UGGA. The chamber was placed on a 15 cm collar and samples were taken from the in-line port using a gas-tight syringe at 0, 5, 10, and 15 minutes after chamber closure. Gas samples were injected into N_2-filled exetainers and the process was repeated for the remaining three collars.

To collect gas emitted from the soil surface for $\Delta^{14}C$, first a chamber outfitted with a fan, a soda lime trap, and two ball valves was connected to the UGGA to purge the headspace of CO_2. Then the ball valves were closed and the UGGA was disconnected to allow for CO_2 to accumulate in the headspace. Once enough CO_2 accumulated, the headspace was extracted via a flow controller and a water trap into a 1 L stainless steel flask. This process was repeated for two additional collars.

Pore water samples were collected using a PushPoint (M.H.E Products) connected to a peristaltic pump via tubing with a needle at the outlet. Samples were pumped from -15.5, -40, -56, and -70 cm below the soil surface during low tide and collected in N_2-filled 60 mL glass serum vials capped with a septa. Surface water samples were collected from the tidal creek at low and high tide, as well as from the nearby St. Jones River and were stored in 60 mL glass serum vials. All water samples were stored on ice in the field until they could be transported to the lab to be aliquoted into transport tubes (salinity, sulfide) or filtered through a 0.2 µm syringe filter into

PETG vials (DOC, DIC, EEMS, UV-VIS) in an anaerobic chamber. Sulfide and conductivity were done immediately, while DOC, DIC, EEMS, and UV-VIS samples were stored in the freezer (DOC, DIC) or in the refrigerator (EEMS, UV-VIS).

A soil core was collected with a gouge auger during the S2 campaign and was sectioned into 5 cm increments from 0 – 70 cm. Subsamples from each increment were wrapped in aluminum foil for ^{14}C analyses and placed in sterile vials for 16s rRNA sequencing. Vials were placed on ice to be transported to the lab so they could be stored in a -80 °C freezer until sequencing. Subsamples for ^{14}C were air-dried on aluminum foil in the lab and intact organic material was removed prior to processing and analyses.

5.2.5 Radiocarbon and stable isotope measurements

CH_4 and CO_2 from flasks and serum vials were processed at the Center for Accelerator Mass Spectrometry (CAMS) at Lawrence Livermore National Laboratory. CH_4 samples were extracted from serum vials and injected into a 5 L gasbag filled with zero air before being introduced to a cryogenic extraction line based on Kittler et al., (2017) and Petrenko et al. (2008) and described by McNicol et al., (2020). Briefly, gas samples were introduced to the vacuum line at ambient pressure, cryogenically purified to remove water and CO_2, combusted into CO_2 via a furnace set to 790°C, and further cryogenically purified before being recovered in a glass tube. For CO_2 samples, a series of cryogenic traps was used to purify and isolate the CO_2 before being recovered. A *S. alterniflora* sample, used to approximate local atmospheric $\Delta^{14}C$, was processed with an acid-base-acid pretreatment prior to combustion. Soil samples were combusted in a sealed-tube in the presence of CuO and Ag. Prior to graphitization, both plant and soil sample-derived CO_2 was split to measure $\delta^{13}C$ of

the bulk soil and the plant sample. All purified samples were then reduced to graphite onto Fe powder in the presence of H_2 (Vogel et al., 1984).

Graphite derived from gas samples was measured on the Van de Graaff FN accelerator mass spectrometer (AMS), while graphite derived from soil and plant samples was measured on the NEC 1.0 MV Model 3SDH-1 Tandem Accelerator at CAMS. Radiocarbon data is reported in $\Delta^{14}C$ notation and has been corrected for $\Delta^{14}C$ decay since 1950 (Stuiver and Polach, 1977), as well as mass-dependent fractionation with measured $\delta^{13}C$ values. Error across all samples for both instruments was 3.2 ± 0.8 ‰.

All stable isotope analyses ($\delta^{13}C$-CO_2, $\delta^{13}C$-CH_4) for gas samples were performed at the University of California-Davis Stable Isotope Facility using a ThermoScientific Delta V Plus isotope ratio mass spectrometer (IRMS). Splits from combustion of bulk soil and plant samples were sent to the Stable Isotope Geosciences Facility at Texas A&M and were measured on a ThermoScientific MAT 253 Dual Inlet IRMS.

5.2.6 Pore and surface water chemistry analyses

Pore and surface water samples were measured for salinity and sulfide as described by Northrup et al., (2018). DOC concentrations were determined by high temperature catalytic oxidation using a Shimadzu TOC-VCPH Total Organic Analyzer (Sharp, 2002). DIC concentrations were calculated by subtracting DOC concentration from the TOC concentration, whereby TOC was measured on filtered, un-acidified samples with the Shimadzu TOC-VCPH Total Organic Analyzer.

Absorption and 3-D excitation-emission matrix (EEM) scans were measured on filtered samples using a Horiba Aqualog, which characterizes both colored and

fluorescent dissolved organic matter using absorption and fluorescence spectroscopy. Specific ultraviolet absorbance (SUVA) was calculated by dividing the UV absorbance of a sample at 254 nm by the DOC concentration (Chin et al., 1994; Weishaar et al., 2003). For EEMs, wavelengths were scanned from 230 to 700 nm in 2 nm increments. Data were corrected from inter-filter effects and normalized using the ramen area method. Fluorescence index (FI) was calculated by taking the ratio of λ_{em} 470 to 520 nm at λ_{ex} of 370 nm (Cory and McKnight, 2005; McKnight et al., 2001).

5.2.7 Microbial community analyses

Sediment samples were homogenized with 100 mL of 1X PBS to create a slurry to ensure microbial presence was even across the individual samples. DNA was extracted from all samples using the Qiagen DNeasy Power Soil Pro kit. The extracted DNA was sent to UCONN Core Sequencing facility for amplicon sequencing of the 16S rRNA gene in regions V3-V4. After receiving forward and reverse sequences from UCONN, they were quality checked and only the forward sequence reads were further processed. The forward sequence reads were processed using a MOTHUR pipeline (Schloss et al., 2009). Forward sequences were trimmed to 130-200 bp range, ambiguous nucleotides were removed, and then OTUs with a 3% dissimilarity were created. OTUs were then aligned and classified using the Silva138 database (Quast et al., 2013).

5.2.8 Ancillary measurements

Phenological data was used to determine which phenophase each campaign occurred and was obtained from the PhenoCam network (site: stjones, Seyednasrollah et al., 2019) as described previously (Hill et al., 2021; Trifunovic et al., 2020). For

each day, an image from 12:00 h was selected and visually inspected for quality. Then a region of interest was delineated to include only *S. alterniflora*. The greenness index and phenophases were calculated using the phenopix R package (Filippa et al., 2020).

5.2.9 Data analyses

CH_4 and CO_2 concentrations are reported as the median value within a 1-minute timeframe when concentrations were steady. The mean and standard deviation of the CH_4 and CO_2 fluxes, as well as DOC and DIC concentrations were calculated. Keeling plots were fitted with model II regression using the R package 'lmodel2' (Legendre, 2018) in order to calculate the $\delta^{13}C$-CH_4 and $\delta^{13}C$-CO_2 of soil efflux (Pataki et al., 2003). The 95% confidence intervals associated with the regression were reported in Fig. D.2 and were calculated using a bootstrapping method. Selected microbial taxa associated with aerobic methanotrophy, anaerobic methanotrophy, hydrogenotrophic methanogenesis, methylotrophic methanogenesis, and sulfate reduction were identified within the database and summed up for each category.

5.3 Results

5.3.1 Pore water characteristics and CH_4 and CO_2 gas measurements

CH_4 concentrations in the soil ranged from 0 mM to 6.0 mM, while CO_2 concentrations ranged from 0 mM to 20.8 mM (Fig. 5.1a-b). CH_4 concentrations generally peaked at 56 cm and declined closer to the soil surface. CO_2 concentrations did not appear to have a consistent pattern with depth. Overall, soil gas concentrations were generally higher during the maturity and senescence stages of plant growth than in greenup and dormancy.

Pore water salinity ranged from 6.6 ppt to 14.5 ppt (Fig. 5.1c). Generally, pore water salinity increased closer to the soil surface. The pore water typically had higher salinity than the river and the tidal creek at high tide, but was similar to the salinity of the tidal creek at low tide. S^{2-} was present in the soil pore water in concentrations ranging from 0 mM to 1.2 mM (Fig. 5.1d). S^{2-} was generally higher later in the growing season and was positively correlated with CH_4 concentration, illustrating that CH_4 concentrations increase even in the presence of sulfate reduction (Fig. D.3).

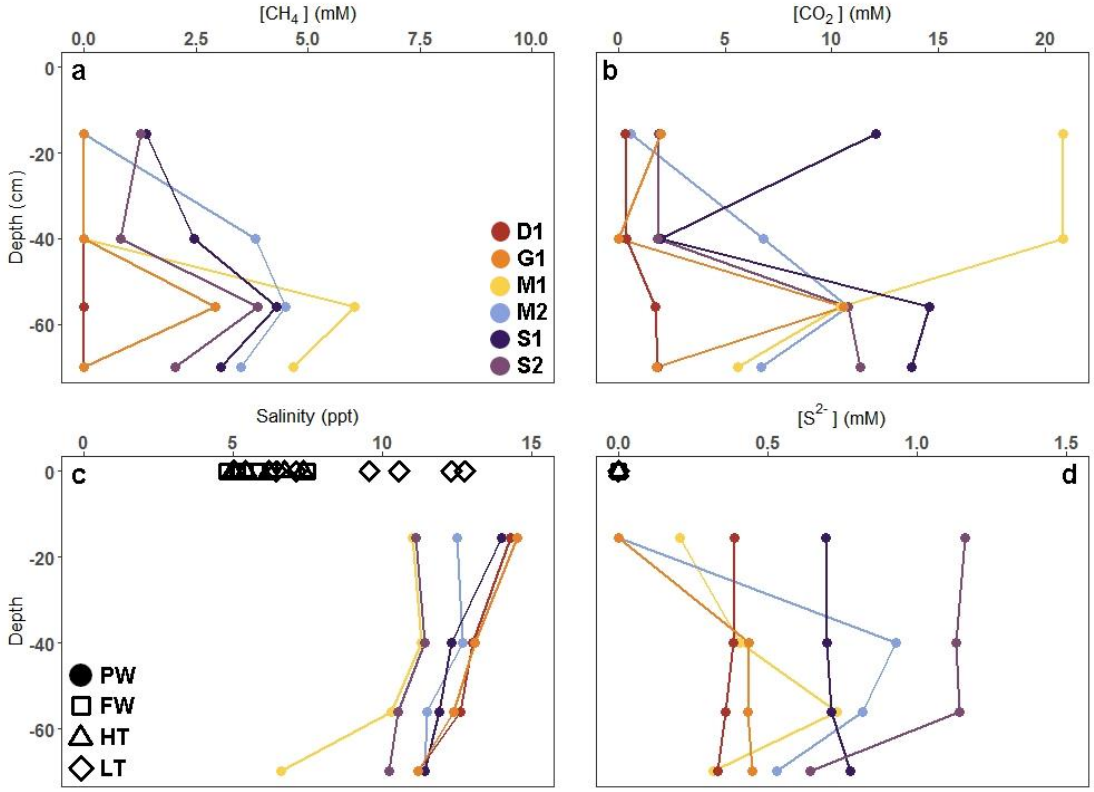

Figure 5.1: Depth profiles of (a) CH_4 and (b) CO_2 concentrations, as well as pore water and surface water (c) salinity and (d) S^{2-} during each of the six campaigns. PW = pore water, FW = surface water at St. Jones River, HT = tidal creek at high tide, LT = tidal creek at low tide, D= dormancy, G = greenup, M = maturity, S = senescence.

Mean CH_4 fluxes ranged from 0.02 nmol m^{-2} s^{-1} during G1 to 0.08 nmol m^{-2} s^{-1} during S2 (Fig. 5.2a). CH_4 fluxes showed a seasonal pattern with higher fluxes during S1 and S2 and lower fluxes during D1 and G1. Mean CO_2 fluxes ranged from 0.81 μmol m^{2-} s^{-1} during D1 to 3.33 μmol m^{2-} s^{-1} during G1 (Fig. 5.2c). CO_2 fluxes also had a seasonal pattern, however CO_2 fluxes peaked earlier in the growing season (G1) compared to CH_4 fluxes. When comparing the gas concentration near the surface (at -15.5 cm) to the flux from the soil surface, we found that there was a significant relationship for CH_4 ($p = 0.03$) with higher gas concentrations near the soil surface corresponding to higher CH_4 fluxes from the surface (Fig. 5.2b). We did not find a similar relationship for CO_2, suggesting that the surface fluxes may be decoupled from the soil CO_2 pool at -15.5 cm (Fig. 5.2d).

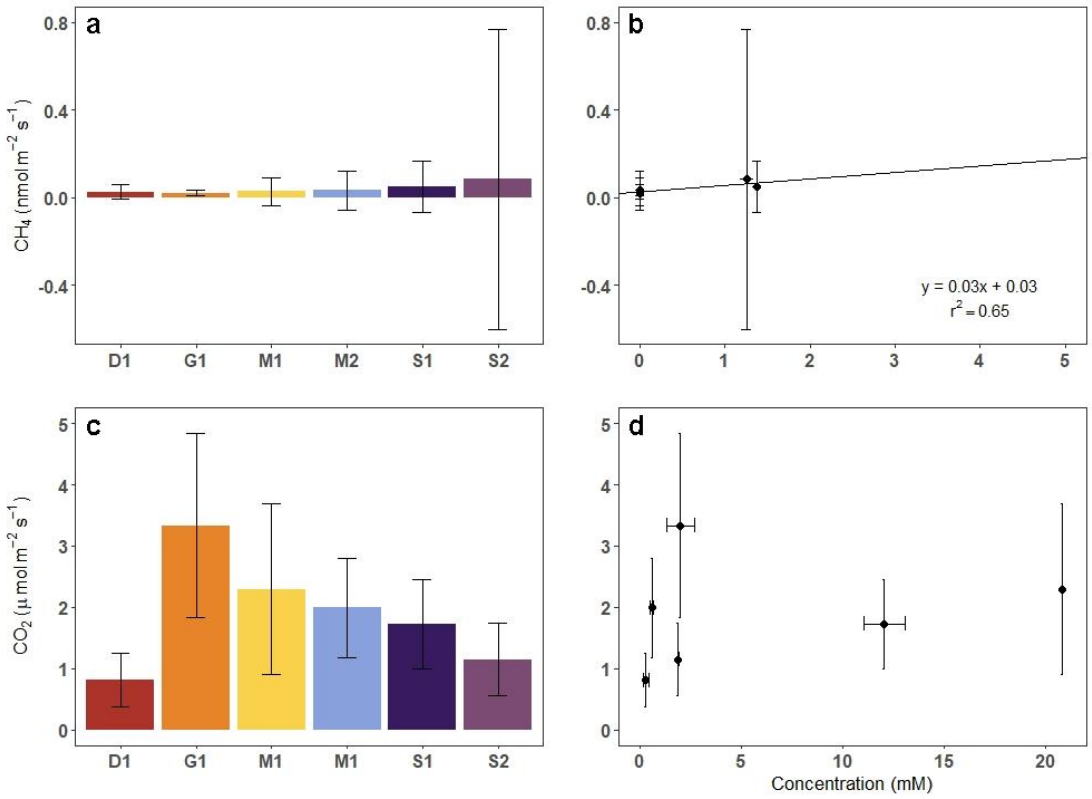

Figure 5.2: Mean ± SD of (a) CH_4 and (c) CO_2 fluxes during each campaign. Panels (b) and (d) show the relationship between the median concentration of CH_4 and CO_2 at -15.5 cm compared to the corresponding mean flux for each campaign.

5.3.2 Stable and radioisotopes

The δ^{13}C-CH_4 within the soil ranged from -68.8‰ to -46.4‰ with similar trends with depth across the campaigns (Fig. 5.3a). Generally, the most enriched δ^{13}C-CH_4 for each campaign was at -40 cm. The δ^{13}C-CH_4 from soil surface fluxes had a broader range of values from -80.1‰ to -17.7‰, but were generally between -60‰ to -40‰ (Fig. 5.3a). The δ^{13}C-CO_2 for both the depth profiles and the soil surface fluxes were generally more enriched than the corresponding δ^{13}C-CH_4 values. Depth profiles of δ^{13}C-CO_2 had little variation and ranged from -19.6‰ to -12.2‰ (Fig. 5.3b). The

δ^{13}C-CO_2 from the soil surface flux had a broader range of values from -31.0‰ to -2.4‰. We found no relationship between δ^{13}C-CH_4 and δ^{13}C-CO_2 (Fig. 5.3c).

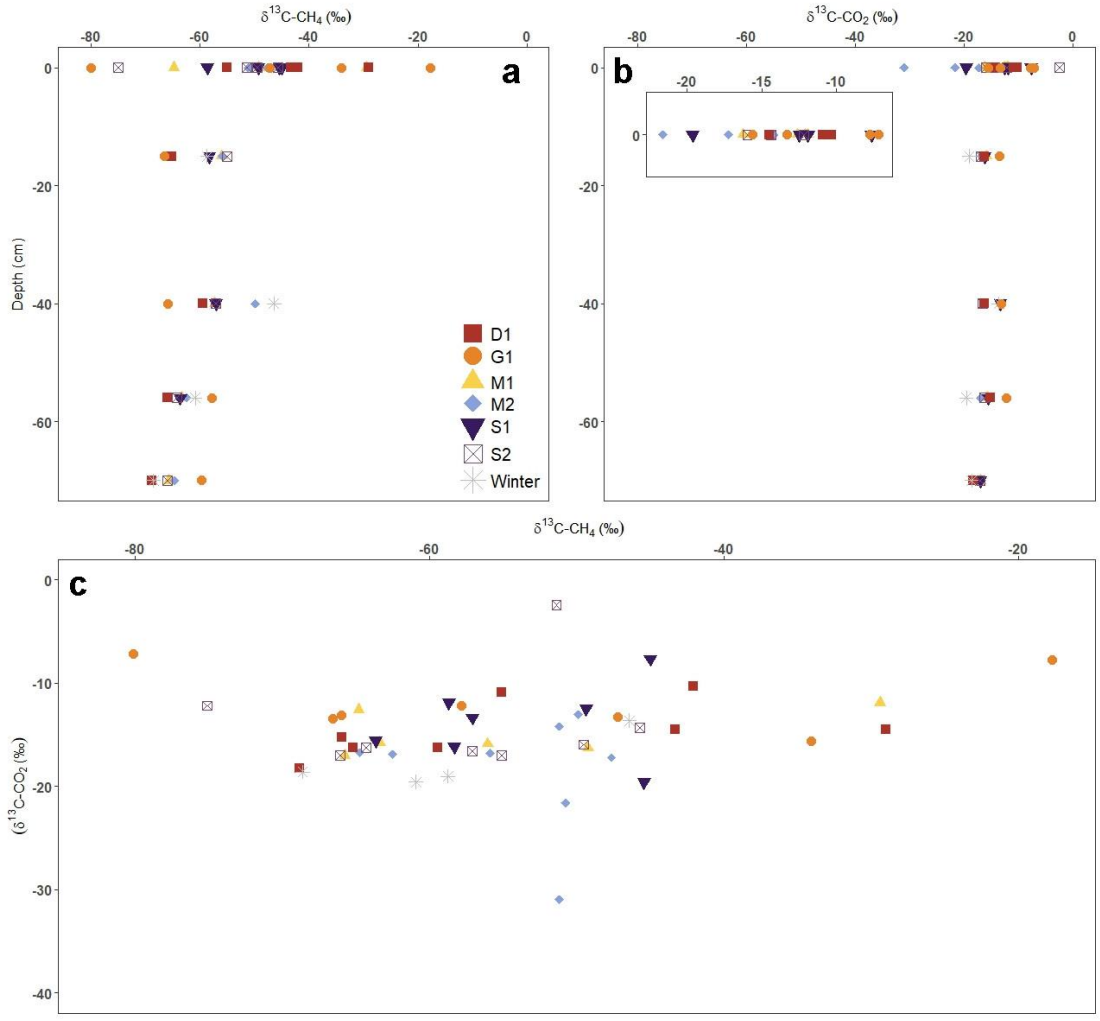

Figure 5.3: Plots showing (a) δ^{13}C-CH_4 and (b) δ^{13}C-CO_2 of the depth profiles and the soil surface fluxes, as well as (c) the relationship between δ^{13}C-CH_4 and δ^{13}C-CO_2. Data at 0 cm in plots (a) and (b) represent soil surface fluxes to the atmosphere. Plot (b) has a zoomed-out subpanel to better resolved the δ^{13}C-CO_2 of the soil flux.

The depth profiles of $\Delta^{14}C$-CH_4 show that most of the CH_4 within the soil is modern or recently produced CH_4 (Fig. 5.4a), particularly during S2 where CH_4 had values between +52.7‰ to +66.0‰. However, we did find older CH_4 gas within the depth profile with $\Delta^{14}C$ up to -517.3‰. Similarly, $\Delta^{14}C$-CO_2 depth profiles showed that CO_2 gas within the soil is modern or recently produced, with some older CO_2 up to -156.1‰ (Fig. 5.4b). Soil CO_2 fluxes had modern or recently produced CO_2, but were generally slightly older than the CO_2 within the soil profile (Fig, 5.4b). The oldest CO_2 flux had a value of -160.8‰. During greenup and maturity, CO_2 was slightly older than during senescence when CO_2 was consistently modern or recently produced. We found no significant relationship between the age of CH_4 and the age of CO_2 at corresponding depths and time points (Fig. 5.4c). The $\Delta^{14}C$ of the bulk soil ranged from +218.2‰ to -110.6‰, with a profile that appears similar to an atmospheric bomb curve.

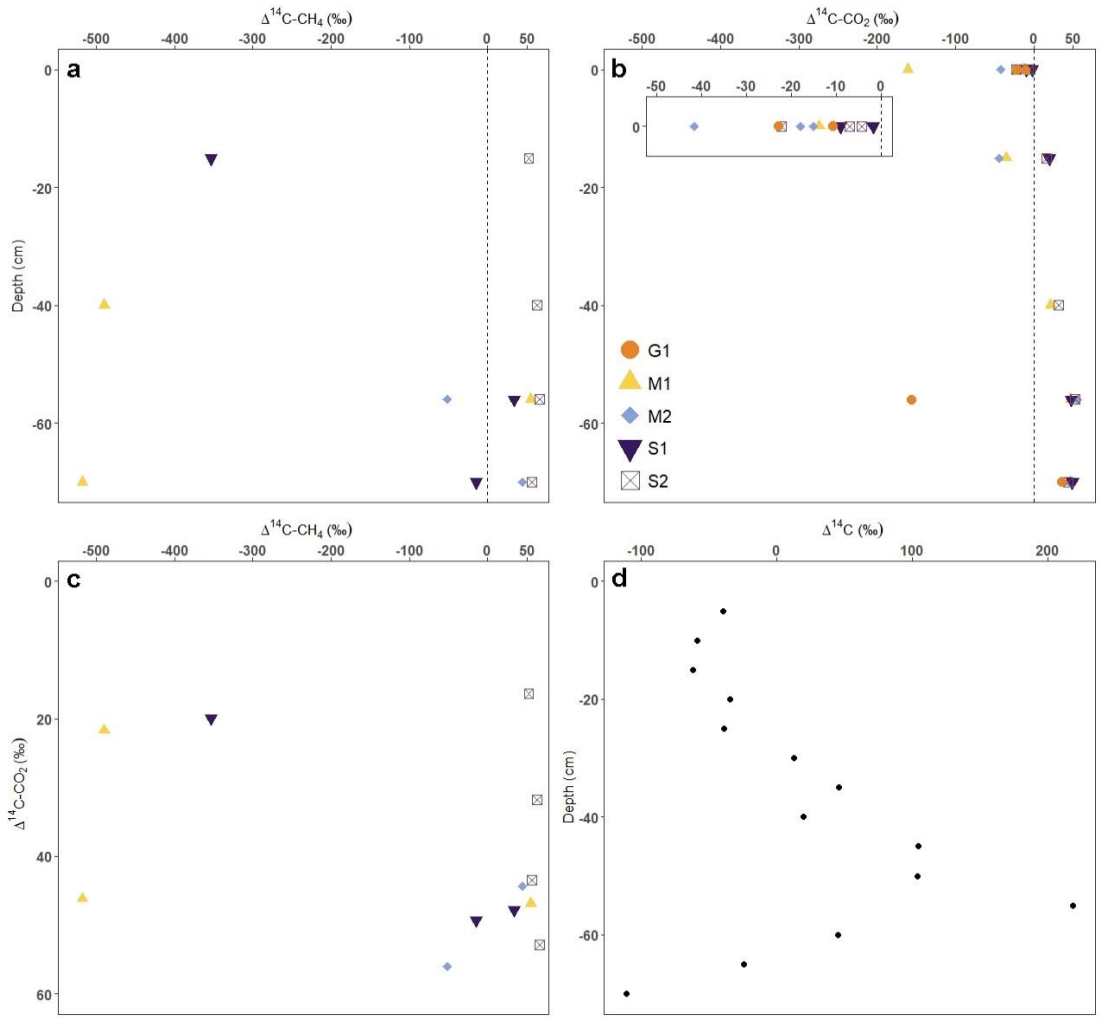

Figure 5.4: Radiocarbon depth profiles of (a) CH_4 and (b) CO_2. Panel (b) also shows the $\Delta^{14}C$-CO_2 of surface soil CO_2 fluxes to the atmosphere which are plotted at 0 cm. Panel (c) shows the relationship between $\Delta^{14}C$-CH_4 and $\Delta^{14}C$-CO_2. Panel (d) shows the age-depth profile of bulk soil $\Delta^{14}C$.

5.3.3 Pore water chemistry

DOC concentrations in the surface waters ranged from 0.40 mM to 1.06 mM with the highest concentrations within the tidal creek during low tide (Fig. 5.5a). Pore water DOC concentrations were higher than the surface waters, ranging from 1.28 mM

to 3.09 mM. Generally, DOC concentrations at -15.5 cm were similar, except for M1. The highest concentrations occurred earlier in the growing season (G1, M1), while the lowest were during D1 and S1. Similar to DOC, surface water DIC concentrations were lower than the pore water, ranging from 1.99 mM to 5.33 mM (Fig. 5.5b). Pore water DIC ranged from 11.5 mM to 29.1 mM. There is a seasonal progression in the DIC concentrations, with the lowest values found during S1, increasing in S2, and peaking during D1. Then the concentrations declined through greenup (G1) and maturity (M1, M2) before reaching their lowest concentrations in early senescence (S1).

$SUVA_{254}$, an indicator of how processed the carbon is via bulk aromaticity, is lower in the surface waters compared to the soil pore waters (Fig. 5.5c). Surface water $SUVA_{254}$ ranges from 2.40 to 3.91, while soil pore water had a broader range from 3.68 to 19.15. The highest values occurred during D1 and M2, while the lowest were during G1 and M1. FI values indicate whether the carbon is more terrestrially derived versus microbially derived. FI values in the surface waters ranged from 1.17 to 1.28, while the pore water was between 1.22 to 1.32 (Fig. 5.5d). These values indicate that the carbon in the surface and pore waters are terrestrially derived.

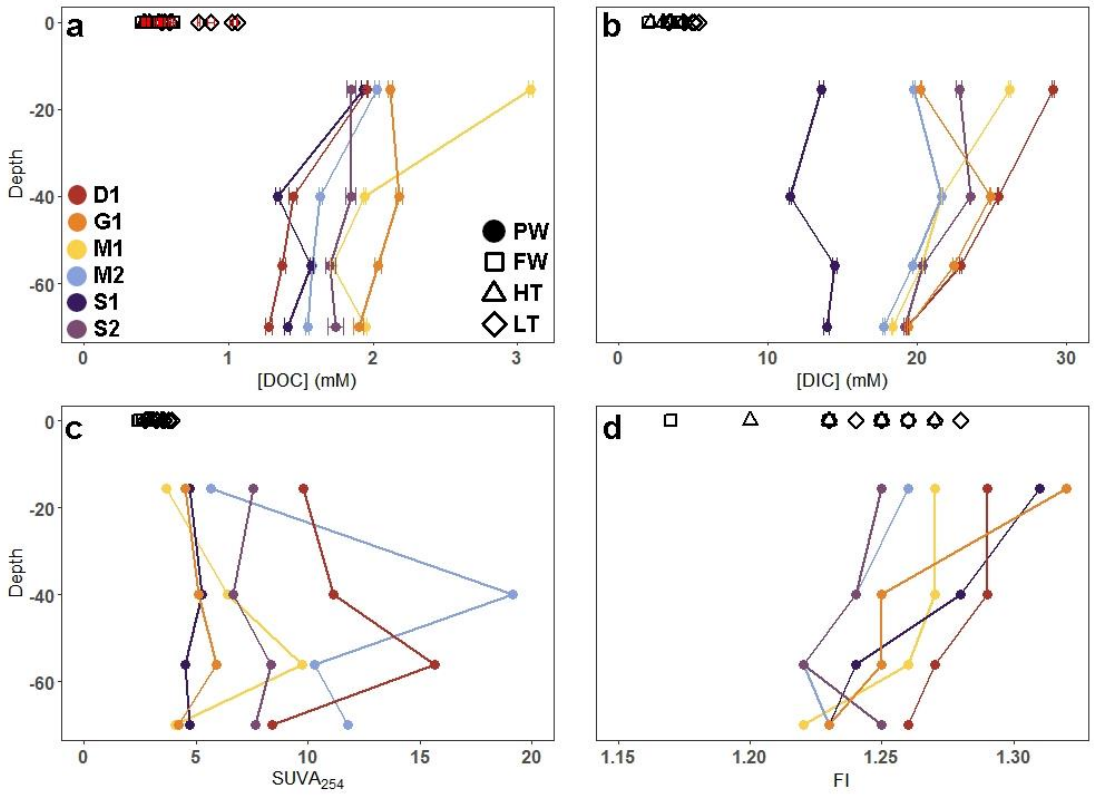

Figure 5.5: Depth profiles and surface water concentrations of (a) DOC, (b) DIC, (c) $SUVA_{254}$, and (d) FI during each of the six campaigns. PW = soil pore water, FW = freshwater at St. Jones River, HT = creek surface water at high tide, LT = creek surface water at low tide.

5.3.4 Microbial community composition

Taxa associated with aerobic and anaerobic methanotrophs were found in the soil profile, with taxa associated with aerobic methanotrophy more prevalent near the soil surface (0-25 cm; Fig. 5.6a). Taxa associated with anaerobic pathways were found deeper in the soil profile, increasing to 0.74% at 40 cm below the surface before declining with depth. As for methanogens, we found taxa associated with two methanogenesis pathways: hydrogenotrophic and methylotrophic (Fig. 5.6a). Taxa associated with hydrogenotrophic methanogenesis were more prevalent in the soil

profile than those associated with methylotrophic methanogenesis. The percentage of taxa associated with hydrogenotrophic methanogenesis increased with depth to 0.77% at 40 cm, before steadily declining to 0.28% at 70 cm below the soil surface. Taxa associated with methylotrophic methanogenesis were found between 20 and 70 cm below the surface, with the highest percentage (0.17%) at 65 cm.

We also assessed the percentage of taxa associated with sulfate reduction, which were found in higher percentages than the methanogens and the methanotrophs (Fig. 5.6b). Taxa associated with sulfate reduction were more abundant closer to the soil surface with a peak of 11% at 10 cm. Their abundance dropped from 20 to 70 cm when compared to the near surface abundances.

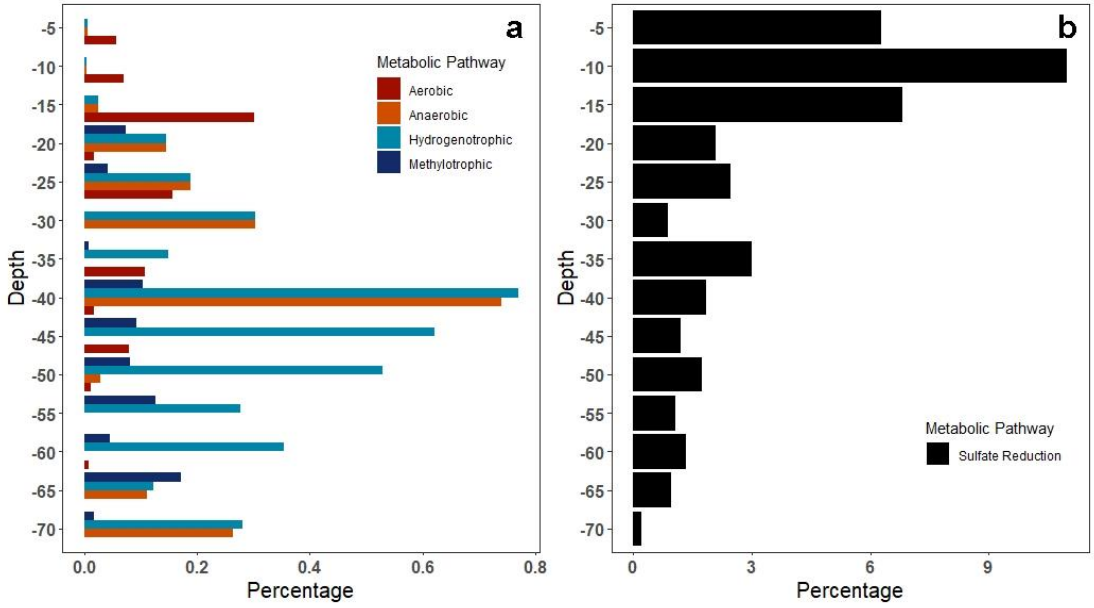

Figure 5.6: Percentage of taxa by depth associated with metabolic pathways. Panel (a) shows methanogenic and anaerobic methanotrophic pathways, while panel (b) shows taxa associated with sulfate reduction.

5.4 Discussion

5.4.1 CH_4 production in the soil

High concentrations of CH_4 were found alongside sulfide within the soil. Previous measurements of CH_4 concentrations at the site ranged from 0 to >892 μM, which was the analytical range of the instrument used (Seyfferth et al., 2020). We have confirmed that CH_4 concentrations are higher, up to 6 mM, exceeding those found in a *S. alterniflora* invaded marsh (up to 140 μmol L^{-1}; Xiang et al., 2015) and in a mixed *Spartina* marsh (up to 500 μM; Bartlett et al., 1987). Our data is comparable to those found in sediments where there is a sulfate-methane transition zone, such as in the open water near a *Phragmites* marsh (up to 1.7 mM; La et al., 2022) and in CH_4 charged sediments in the Gulf of Mexico (0.18 μM to 20 mM; Coffin et al., 2008). The coexistence of high CH_4 concentrations alongside sulfate reduction, as well as the significant positive relationship between CH_4 concentration and S^{2-} (Fig. D.3), indicates the presence of a methanogenesis pathway that does not compete with sulfate reduction (i.e., methylotrophic methanogenesis).

Two lines of evidence, via natural abundance stable isotopes and microbial community composition, point to two key methanogenesis pathways within the soil: methylotrophic and hydrogenotrophic. Depth profiles of $\delta^{13}C$-CH_4 ranged from -68.8 to -46.4‰, which falls within isotopic values associated with hydrogenotrophic (-110 to -60‰; Whiticar, 1999) and acetoclastic methanogenesis (-70 to -50‰; Whiticar, 1999). The range of $\delta^{13}C$-CH_4 values from methylotrophic methanogenesis within natural settings is uncertain, but laboratory cultures have found enrichment factors similar to those for hydrogenotrophic methanogenesis (Krzycki et al., 1987; Londry et

al., 2008; Penger et al., 2012; Summons et al., 1998). Therefore, isotopic data alone suggests that there is a mixture of methanogenesis pathways within the soil.

When coupled with 16s rRNA sequencing, we were able to identify the presence of taxa associated with methylotrophic and hydrogenotrophic methanogenesis. While taxa were found throughout the soil profile, they generally increased with depth, particularly below 15 cm when the percentage of taxa associated with sulfate reduction started to decline. The presence of taxa associated with hydrogenotrophic methanogenesis has been found in coastal wetlands (Sánchez-Carrillo et al., 2021; Xiang et al., 2015; Yuan et al., 2019). However, there have been fewer studies that have assessed the presence of methylotrophic methanogens within their soils since they were thought to be less important than other forms of methanogenesis (Söllinger and Urich, 2019). The presence of taxa associated with methylotrophic methanogens confirmed a hypothesis from a prior study done at the site that postulated that methylotrophic methanogenesis contributed to high CH_4 production within the soil (Seyfferth et al., 2020).

While the importance of methylotrophic methanogens to global CH_4 cycling is still being determined (Söllinger and Urich, 2019), they play an important role at our site due to the presence of *S. alterniflora*. *S. alterniflora* contributes substrates (i.e., TMA; Wang and Lee, 1995, 1994) and precursors to substrates (i.e., dimethylsulfoniopropionate which can be used to produce DMS; (Kiene and Visscher, 1987; Larher et al., 1977) which can used by methylotrophic methanogens. Methanol, another non-competitive substrate, forms through plant lignin and pectin degradation (Donnelly and Dagley, 1980; Schink and Zeikus, 1980). Methylotrophic methanogens do not compete with sulfate reducers for substrate, unlike hydrogenotrophic and

acetoclastic methanogens which compete for H_2 and acetate (Whiticar, 1999). This pathway enables high CH_4 production alongside high sulfate reduction. Several studies have shown that *S. alterniflora* invasion resulted in higher levels of CH_4 production (Xiang et al., 2015; Yuan et al., 2016; Zeleke et al., 2013). Higher production levels have been attributed to an increase in TMA, a non-competitive substrate, which contributed to shifts in the dominant methanogen community from either *Methanosaetaceae* (includes acetoclastic methanogens) or *Methanococcales* (includes hydrogenotrophic methanogens) to *Methanosarcinaceae* which includes methylotrophic methanogens (Yuan et al., 2014, 2016, 2019). Our findings from a native *S. alterniflora* marsh, along with those from marshes that experienced *S. alterniflora* invasion, underscores the importance of reevaluating the contribution tidal salt marshes may have to CH_4 budgets, particularly for marshes vegetated by species that contribute non-competitive substrates for methanogenesis.

While the 16s rRNA identified the presence of taxa associated with methylotrophic and hydrogenotrophic methanogenesis, taxa associated with acetoclastic methanogens were not detected in the soil. One possible reason may be lack of acetate available for acetoclastic methanogenesis due to competition with sulfate reduction, thereby reducing the abundance of acetoclastic methanogens to below the detection limit. This finding necessitates a closer look at the $\delta^{13}C\text{-}CH_4$ depth profiles, particularly at 40 cm where the $\delta^{13}C\text{-}CH_4$ is isotopically heavier than would be expected if the CH_4 was produced via hydrogenotrophic and/or methylotrophic methanogenesis. Concurrent with isotopic enrichment at 40 cm is a peak in the abundance of taxa associated with anaerobic methanotrophs (ANME). ANME have been found in *S. alterniflora* marshes (Zeleke et al., 2013), as well as in estuarine and

marine sediments (Kevorkian et al., 2021; Wallenius et al., 2021; Zhuang et al., 2016). Studies have highlighted that sulfate-driven anaerobic oxidation of methane (S-AOM) likely contributes to some portion of CH_4 oxidation (MO) in coastal wetlands (La et al., 2022; Segarra et al., 2013; Wang et al., 2019). While our isotopic and 16s rRNA data suggest that anaerobic CH_4 oxidation (AOM) occurs at the site, particularly at 40 cm, more information regarding substrate availability and microbial activity is needed to identify the role ANMEs play in salt marsh soils.

5.4.2 CH_4 and CO_2 ages

Within the soil profile, most $\Delta^{14}C$-CH_4 was > modern, particularly during S2, when all four depths were > modern. The shift from older $\Delta^{14}C$-CH_4 earlier in the growing season to entirely > modern in late senescence corresponds to when both soil and ecosystem CH_4 fluxes are at their highest and most variable at the site (Capooci and Vargas, 2022b; Vázquez-Lule and Vargas, 2021). *S. alterniflora* die-off during this period contributes increased amounts of labile organic matter and substrate to soil microbes, particularly for methylotrophic methanogens. Research has shown that DMS concentrations in *S. alterniflora* marsh pore waters peaked during the fall (Tong et al., 2018). Furthermore, in another *S. alterniflora* marsh, TMA concentrations were 8 times higher in the fall than in the summer, corresponding to a nearly 6-fold increase in CH_4 production potential at the site (Yuan et al., 2016). While we did not measure seasonal changes of TMA and DMS concentrations in the pore water, the increase in soil and ecosystem CH_4 fluxes, as well as the presence of taxa associated with methylotrophic methanogenesis in *S. alterniflora*-dominated marshes provides strong evidence for increased CH_4 production via methylotrophic methanogens.

Similarly to $\Delta^{14}C\text{-}CH_4$, $\Delta^{14}C\text{-}CO_2$ also followed a general seasonal pattern, becoming slightly more enriched during senescence particularly at 15 cm. The enriched values during senescence at 15.5 cm is likely due to the input of new labile organic matter (OM), which increased the proportion of CO_2 produced from new OM versus older OM in the soil. *S. alterniflora* has been shown to break-down in three phases (Hicks et al., 1991; Lee et al., 1980; Valiela et al., 1985; White and Howes, 1994). The first two phases of breakdown can contribute to increases in sugars and DOC in the fall (Pakulski, 1986), as well as higher concentrations of biodegradable DOC from senescent material (Shelton et al., 2021; Wang et al., 2014). While soil CO_2 fluxes and concentrations start to decline during senescence, the input of new labile materials contributed young CO_2 to the soil, resulting in an increasingly modern $\Delta^{14}C\text{-}CO_2$. Conversely, the oldest $\Delta^{14}C\text{-}CO_2$ values were generally seen during maturity, suggesting that microbes are accessing older pools of carbon, likely due to, in part, high production rates depleting the easily accessible labile carbon from the previous senescence. Our findings show that $\Delta^{14}C\text{-}CO_2$ exhibits a seasonality indicative of the role plant phenology plays in providing substrates for the soil microbial community.

While the depleted $\Delta^{14}C$ values of CO_2 could be attributed to seasonal dynamics of the availability of older vs. newer carbon in the soil, there are three older than expected $\Delta^{14}C\text{-}CH_4$ values (-517.3‰ and -489.6‰ during M1, -353.3‰ during S1). These values are older than the surrounding OM which ranges from -110.6 to +218.2‰. Since subsurface gas sampling was from a passive gas sampler that remained in place throughout the campaigns, the old CH_4 or the substrate used to produce it likely originated from elsewhere within the marsh. Sampling was done in an area of the marsh where the soil pore waters exchange with creek waters only

during extreme high tides, such as after storm events and during spring high tides (Guimond et al., 2020; Seyfferth et al., 2020). As a result, the soils become strongly anaerobic, with redox values as low as -200 mV (Seyfferth et al., 2020). Sample collection for $\Delta^{14}C$ during M1 and S1 occurred two days after a storm event and a new moon, respectively, resulting in the input of "new" water into the soil. The mixing of tidal or rainwater with the stagnant pore waters could briefly establish connectivity between less connected pore spaces where old labile C is physically protected (Strong et al., 2004) to more connected pore spaces that have been replenished with microbial substrates (Cook et al., 2007). Furthermore, tidal flushing due to spring high tide in S1 could reset redox conditions such that they were less strongly reducing (Cook et al., 2007), therefore providing conditions for old physically protected carbon to get processed, contributing to pockets of old CH_4 within the soil profile. The appearance of older CH_4 after spring tide and a rain event highlights the importance of better understanding how interactions between tidal flushing and pore space connectivity play a role in marsh C cycling, particularly in less hydrologically connected portions.

5.4.3 Fate of CH_4

CH_4 produced within the soil profile can take many paths: diffusion into the atmosphere, long-term storage within the soil, and lateral export into the tidal creek. Furthermore, CH_4 can be oxidized into CO_2 which can then be emitted into the atmosphere or incorporated into the DIC pool. We acknowledge that plant-mediated transport and ebullition can play significant roles in CH_4 fate, but they will not be discussed in context of this study. We did not measure plant mediated CH_4 flux and ebullition infrequently happens at SS as indicated by 79% of CH_4 fluxes measured during the campaigns having an $R^2 \geq 0.90$ and 95% having an $R^2 \geq 0.50$. Furthermore,

we will not be discussing the possibility of long-term storage as a possible fate of CH_4 since $\Delta^{14}C$ data showed that most CH_4 in the marsh is modern and the pool turned over quickly. Therefore, this discussion will focus on three fates: diffusion into the atmosphere (i.e., fluxes), MO, and lateral transport to the tidal creek.

Throughout the campaigns, CH_4 fluxes were generally low, but had high variability particularly during senescence, indicating that the importance of diffusion from the soil to the atmosphere varies throughout the year. A synthesis of CH_4 fluxes from coastal vegetated ecosystems found that salt marshes emitted between -92.6 to 94,129.7 μmol CH_4 m^{-2} day^{-1} with a median flux of 222.4 μmol CH_4 m^{-2} day^{-1} (Al-Haj and Fulweiler, 2020). Daily mean fluxes during the campaigns ranged from 1.88 ± 1.1 μmol CH_4 m^{-2} day^{-1} during G1 to 7.28 ± 59.1 μmol CH_4 m^{-2} day^{-1} during S2, which is lower than the median CH_4 flux from salt marshes. While we found that CH_4 emissions increase with increased CH_4 in the soil, there are several factors that limit the role CH_4 fluxes play in CH_4 transport. One, CH_4 diffusion through water-filled pore spaces is ~10,000x slower than through air-filled pore spaces. Since tidal influence at SS is limited to the first few centimeters of the soil, CH_4 produced in the saturated zone would need to diffuse through water-filled pore spaces to reach the atmosphere. Furthermore, CH_4 fluxes were likely also reduced due to aerobic CH_4 oxidation (MOx) at the anoxic-oxic interface. The percentage of CH_4 that gets oxidized in wetland and marine systems varies widely. Within marine sediments upwards of 90% of CH_4 gets oxidized (Knittel and Boetius, 2009; Reeburgh, 2007), while in wetland ecosystems reported values are lower, including 52 to 79% in a freshwater swamp (Megonigal and Schlesinger, 2002), 71 to 96% in a coastal wetland (La et al., 2022), and 16 to 34% in a freshwater tidal marsh (Van Der Nat and

Middelburg, 1998). These values from the literature suggest that MO likely plays a crucial role in mediating CH_4 emissions from wetland soils. Thus, the combined effects of slow diffusion rates within water-filled pore spaces and MOx near the soil surface likely contributed to low CH_4 fluxes from the soil surface, despite high CH_4 production within the soil profile.

While we did not calculate the percentage of CH_4 oxidized in our study, CH_4 fluxes from the soil show evidence of MO, with $\delta^{13}C\text{-}CH_4$ values up to -17.7‰. During the process of MO, ^{12}C is preferentially oxidized, resulting in the residual CH_4 becoming more enriched (Barker and Fritz, 1981; Coleman et al., 1981; Silverman and Oyama, 1968). When comparing the mean $\delta^{13}C\text{-}CH_4$ at -15.5 cm to the mean $\delta^{13}C\text{-}CH_4$ of CH_4 flux from the soil surface (-59.4‰ ± 4.6‰ vs. -48.4‰ ± 13.7‰), we find that, on average, CH_4 fluxes are 11.3‰ ± 15.7‰ isotopically enriched compared to CH_4 at -15.5 cm. This isotopic difference is comparable to those found between sedimentary CH_4 and CH_4 fluxes from a swamp forest (Happell et al., 1994). When plotting the $\delta^{13}C\text{-}CH_4$ versus $\delta D\text{-}CH_4$ for data collected in July 2021 (Fig. D.4, Appendix D.2), there is a trend towards MO (Whiticar, 1999). Furthermore, we found the presence of taxa associated with MOx in the top 15 cm of the soil, indicating that some proportion of CH_4 produced within the soil profile gets aerobically oxidized at the anoxic-oxic interface. Aerobic methanotrophs have been found near the soil surface in several coastal brackish marshes (McDonald et al., 2005; Moussard et al., 2009; Steinle et al., 2017) and have been shown to have the highest oxidation potential at the anoxic-oxic interface due the presence of O_2 within the oxic zone and the diffusion of CH_4 from the anoxic zone (Amaral and Knowles, 1994; Buchholz et al., 1995; King, 1994, 1990; Segers, 1998). While we did not quantify the rate of MOx,

our isotopic and microbial community composition data suggested that MOx plays a significant role in the CH_4 fate at our site.

The most enriched $\delta^{13}C\text{-}CH_4$ fluxes occurred during D1 and G1 indicating that the proportion of MO is higher during the winter and the early growing season. The MO signal in these fluxes is likely due to the presence of taxa associated with MOx near the soil surface. Aerobic methanotrophs are less sensitive to temperature than methanogenesis (Q_{10} of 1.9 versus 4.1; Segers, 1998). They are also able to oxidize CH_4 in temperatures ranging from -1°C to 30˚C (King and Adamsen, 1992). Subsequently, the rate of CH_4 production decreases more drastically than the rate of MO in soils, thereby shifting the balance of the two processes more towards oxidation in cooler months. As a result, $\delta^{13}C\text{-}CH_4$ fluxes more clearly demonstrate the presence of MO during D1 and G1 than at other times of the year when high levels of CH_4 production can obscure the presence of MO. At high CH_4 concentrations the isotopic shift due to MO is harder to detect (Whiticar and Faber, 1986), particularly since the fractionation factor associated with MOx ranges from 1.003 to 1.021 (Happell et al., 1994; Preuss et al., 2013) compared to 1.055 to 1.090 for hydrogenotrophic methanogenesis (Whiticar and Faber, 1986). Therefore, using natural abundance isotopes to discern the occurrence of MO within the soils becomes difficult and necessitates more targeted approaches such as inhibition experiments, tracer experiments, and microbial activity to elucidate the role MO plays in CH_4 fate.

While the $\delta^{13}C\text{-}CH_4$ flux data showed that MO attenuates CH_4 emissions from the soil to the atmosphere, discerning the importance of MO using the $\delta^{13}C\text{-}CO_2$ is more difficult since most of the data resemble soil CO_2 and DIC isotopic values (Appendix D.3, Fig. D.5). CO_2 produced from MO is isotopically depleted due to

microbial preference for ^{12}C (Barker and Fritz, 1981; Coleman et al., 1981; Silverman and Oyama, 1968), contributing isotopically light CO_2 into the soil CO_2 and DIC pool. However, due to the size of the CO_2 and the DIC pool (of which CO_2 is a part of), as well as inputs of DIC from the tidal creek and continual production of CO_2 from OM, the isotopic signal from MO gets obscured (Whiticar and Faber, 1986). DIC and $\delta^{13}C$-DIC data collected from the site in 2018 show an excess of isotopically light DIC during some periods of the year (Fig. D.6). While excess DIC can come from a variety of sources (e.g., OM production, plant and microbial respiration, tidal exchange), the high CH_4 concentrations, low CH_4 fluxes, and isotopically enriched $\delta^{13}C$-CH_4 suggest that MO likely contributes to the DIC pool. MO has been shown to contribute to the DIC pool in coastal wetland sediments (La et al., 2022), as well as in marine sediments (Chen et al., 2010; Haese et al., 2003; Yoshinaga et al., 2014). A study by La et al., (2022) found that S-AOM contributed to between 2.55 to 8.58% to the pore water DIC pool, consuming 71 to 96% of the CH_4 in the process, illustrating that large amounts of MO minimally impacts the DIC pool.

The variability in the concentrations and quality of DOC within the pore water, the young age of CH_4 and CO_2 within the sediments, as well as high CH_4 concentrations and fluxes from the nearby tidal creek (Trifunovic et al., 2020) suggests a third fate for CH_4: lateral exchange with the tidal creek. While the FI data from the tidal creek, the nearby tidal river, and the pore water indicates that the DOC pool is more terrestrially derived (i.e., ~1.2 versus ~1.8 for microbially-derived (Cory and McKnight, 2005; McKnight et al., 2001), the higher variability in $SUVA_{254}$ appears to reflect the hydrology of SS. Generally, $SUVA_{254}$ values at -15.5 cm are most similar to that of the tidal creek. Previous research at SS showed that the first 10

cm is most likely to be influenced by diurnal tidal cycles and therefore is more hydrologically connected to the tidal creek (Guimond et al., 2020). While our near-surface pore water collection was at -15.5 cm, water from tidal exchange at the surface can percolate downwards and contribute to $SUVA_{254}$ values more aligned with those in the tidal creek. Higher $SUVA_{254}$ values were found deeper in the profile at depths that experience tidal exchange during spring-neap cycles, enabling more processing of DOC. Thus, the $SUVA_{254}$ data show a dynamic and diverse DOC pool within the pore waters that is likely linked to tidal creek at diurnal (near-surface) and spring-neap tidal (at depth) cycles.

The second and third pieces of evidence for lateral movement of CH_4, either via CH_4 or as part of the DIC pool, is the young age of the CH_4 and CO_2 within the soil and high CH_4 fluxes and concentrations from the tidal creek (Trifunovic et al., 2020). With few exceptions, the CH_4 and CO_2 within the soil is > modern which suggest high turnover times. One potential mechanism for high turnover is tidal pumping, which is the exchange of pore water in the sediments with the surface water from the creek via tides (Gleeson et al., 2013; Li et al., 2009; Robinson et al., 2007; Santos et al., 2012). Tidal pumping imports substrates into the pore waters and exports biogeochemical reaction products to the tidal creek (Bouillon et al., 2007; Gleeson et al., 2013; Maher et al., 2013; Santos et al., 2021). At SS, tidal pumping occurs on spring-neap tidal cycles enabling the build-up of reaction products such as CH_4 and DIC. Studies have shown that DIC export via tidal pumping occurs in coastal systems (e.g., Borges and Abril, 2012; Call et al., 2015; Tamborski et al., 2021). However, there is less data on lateral transport of CH_4, with evidence from a tidal freshwater marsh, a mangrove forest, and a mixed mangrove/salt marsh system (Call et al., 2015;

Kelley et al., 1995; Santos et al., 2019). Lateral transport of CH_4 likely occurs at our site as well. CH_4 concentrations upwards of 6000 μmol/mol have been found within the tidal creek (Trifunovic et al., 2020). Furthermore, CH_4 and CO_2 fluxes from the tidal creek have similar $\delta^{13}C\text{-}CH_4$ (-59.51‰ to -41.1‰; Appendix D.4; Table D.1), $\delta^{13}C\text{-}CO_2$ (-23.90 to -11.88‰; Table D.1), and $\Delta^{14}C\text{-}CO_2$ (-12.4‰ to 18.4‰; Table D.1) to those found at SS. Combined, our data suggest that lateral transport of CH_4 plays a role in CH_4 fate at SS. However, there is a need for research that focuses on lateral transport to better quantify the role it plays in CH_4 dynamics.

5.4.4 Future directions

Through a combination of concentration, flux, isotopic, pore water and organic carbon chemistry, and microbial community composition data, we identified that CH_4 dynamics within a tidal salt marsh are biogeochemically heterogeneous, with two pathways for CH_4 production and several potential fates for CH_4 that likely occur simultaneously and vary in importance over tidal and seasonal cycles. While this study is a step towards a better understanding of CH_4 dynamics in a tidal salt marsh, there is still much more work to be done. Thus, we suggest two areas of future research.

One, investigating the role of methylotrophic methanogenesis in producing CH_4 in tidal salt marshes. Future work should focus on expanding our understanding of methanogenic pathways, including research on rates of microbial activity coupled with depth profiles of relevant substrates (e.g., H_2, acetate, TMA) to better understand which microbial pathways are important, as well as how they vary seasonally.

Two, a better understanding of the role MO and lateral CH_4 transport play in CH_4 dynamics. Future work for MO should focus on calculating the activities of ANME coupled to the redox of various redox active elements (i.e., sulfate, manganese,

iron, nitrate, nitrite) both in laboratory experiments and *in situ*. For lateral transport of CH_4, studies should continue to use ^{222}Rn mass balances to better understand the quantity of CH_4 that gets exported into the tidal creek. These studies should be done in different hydrologically connected zones within the marsh to assess the roles they play in the overall CH_4 balance. Additionally, *in situ* labelling experiments should be conducted over tidal cycles and seasonally to quantify where CH_4 goes once it is produced within the soil.

Acknowledgements

This research was supported by the National Science Foundation (#1652594). MC acknowledges support from an NSF Graduate Research Fellowship (#1247394) and from the DOE SCGSR. We thank the onsite support from Kari St. Laurent and the Delaware National Estuarine Research Reserve (DNERR), as well as from Victor and Evelyn Capooci for field assistance during the first campaign.

We thank Alina Ebling for running pore water samples and to the staff at Lawrence Livermore National Laboratory for training and assistance in preparing and running samples for radiocarbon analyses.

REFERENCES

Al-Haj, A.N., Fulweiler, R.W., 2020. A synthesis of methane emissions from shallow vegetated coastal ecosystems. Glob. Chang. Biol. 26, 2988–3005. https://doi.org/10.1111/gcb.15046

Amaral, J.A., Knowles, R., 1994. Methane metabolism in a temperate swamp. Appl. Environ. Microbiol. 60, 3945–3951. https://doi.org/10.1128/aem.60.11.3945-3951.1994

Barker, J.F., Fritz, P., 1981. Carbon isotope fractionation during microbial methane oxidation. Nature 293, 289–291. https://doi.org/10.1038/293289a0

Bartlett, K.B., Bartlett, D.S., Harriss, R.C., Sebacher, D.I., 1987. Methane emissions along a salt marsh salinity gradient. Biogeochemistry 4, 183–202. https://doi.org/10.1007/BF02187365

Borges, A. V., Abril, G., 2012. Carbon dioxide and methane dynamics in estuaries, Treatise on Estuarine and Coastal Science. Elsevier Inc. https://doi.org/10.1016/B978-0-12-374711-2.00504-0

Bouillon, S., Middelburg, J.J., Dehairs, F., Borges, A. V, Abril, G., Flindt, M.R., Ulomi, S., Kristensen, E., 2007. Importance of intertidal intertidal sediment processes and porewater exchange on the water column biogeochemistry in a pristine mangrove creek (Ras Dege, Tanzania). Biogeosciences 4, 311–322. https://doi.org/10.5194/bg-4-311-2007

Buchholz, L.A., Klump, J.V., Collins, M.L.P., Brantner, C.A., Remsen, C.C., 1995. Activity of methanotrophic bacteria in Green Bay sediments. FEMS Microbiol. Ecol. 16, 1–8. https://doi.org/10.1016/0168-6496(94)00063-3

Call, M., Maher, D.T., Santos, I.R., Ruiz-Halpern, S., Mangion, P., Sanders, C.J., Erler, D. V, Oakes, J.M., Rosentreter, J., Murray, R., Eyre, B.D., 2015. Spatial and temporal variability of carbon dioxide and methane fluxes over semi-diurnal and spring-neap-spring timescales in a mangrove creek. Geochim. Cosmochim. Acta 150, 211–225. https://doi.org/10.1016/j.gca.2014.11.023

Capooci, M., Barba, J., Seyfferth, A.L., Vargas, R., 2019. Experimental influence of storm-surge salinity on soil greenhouse gas emissions from a tidal salt marsh. Sci. Total Environ. 686, 1164–1172. https://doi.org/10.1016/j.scitotenv.2019.06.032

Capooci, M., Vargas, R., 2022a. Diel and seasonal patterns of soil CO_2 efflux in a temperate tidal marsh. Sci. Total Environ. 802. https://doi.org/10.1016/j.scitotenv.2021.149715

Capooci, M., Vargas, R., 2022b. Trace gas fluxes from tidal salt marsh soils: Implications for carbon-sulfur biogeochemistry. Biogeosciences Discuss [preprint].

Chen, Y., Ussler, W., Haflidason, H., Lepland, A., Rise, L., Hovland, M., Hjelstuen, B.O., 2010. Sources of methane inferred from pore-water $\delta^{13}C$ of dissolved inorganic carbon in Pockmark G11, offshore Mid-Norway. Chem. Geol. 275, 127–138. https://doi.org/10.1016/j.chemgeo.2010.04.013

Chin, Y.P., Alken, G., O'Loughlin, E., 1994. Molecular weight, polydispersity, and spectroscopic properties of aquatic humic substances. Environ. Sci. Technol. 28, 1853–1858. https://doi.org/10.1021/es00060a015

Coffin, R., Hamdan, L., Plummer, R., Smith, J., Gardner, J., Hagen, R., Wood, W., 2008. Analysis of methane and sulfate flux in methane-charged sediments from the Mississippi Canyon, Gulf of Mexico. Mar. Pet. Geol. 25, 977–987. https://doi.org/10.1016/j.marpetgeo.2008.01.014

Coleman, D.D., Risatti, J.B., Schoell, M., 1981. Fractionation of carbon and hydrogen isotopes by methane-oxidizing bacteria. Geochim. Cosmochim. Acta 45, 1033–1037. https://doi.org/10.1016/0016-7037(81)90129-0

Cook, P.L.M., Wenzhöfer, F., Glud, R.N., Janssen, F., Huettel, M., 2007. Benthic solute exchange and carbon mineralization in two shallow subtidal sandy sediments: Effect of advective pore-water exchange. Limnol. Oceanogr. 52, 1943–1963. https://doi.org/10.4319/lo.2007.52.5.1943

Cory, R.M., McKnight, D.M., 2005. Fluorescence spectroscopy reveals ubiquitous presence of oxidized and reduced quinones in dissolved organic matter. Environ. Sci. Technol. 39, 8142–8149. https://doi.org/10.1021/es0506962

DNREC, 1999. Delaware National Esturaine Research Reserve Estuarine Profile.

Donnelly, M.I., Dagley, S., 1980. Production of methanol from aromatic acids by Pseudomonas putida. J. Bacteriol. 142, 916–924.

Filippa, G., Cremonese, E., Migliavacca, M., Galvagno, M., Folker, M., Richardson, A.D., Tomelleri, E., 2020. phenopix: Process Digital Images of a Vegetation Cover. R Packag. version 2.4.2.

Gleeson, J., Santos, I.R., Maher, D.T., Golsby-Smith, L., 2013. Groundwater-surface water exchange in a mangrove tidal creek: Evidence from natural geochemical tracers and implications for nutrient budgets. Mar. Chem. 156, 27–37. https://doi.org/10.1016/j.marchem.2013.02.001

Guimond, J.A., Seyfferth, A.L., Moffett, K.B., Michael, H.A., 2020. A physical-biogeochemical mechanism for negative feedback between marsh crabs and carbon storage. Environ. Res. Lett 15, 9. https://doi.org/10.1088/1748-9326/ab60e2

Haese, R.R., Meile, C., Van Cappellen, P., De Lange, G.J., 2003. Carbon geochemistry of cold seeps: Methane fluxes and transformation in sediments from Kazan mud volcano, eastern Mediterranean Sea. Earth Planet. Sci. Lett. 212, 361–375. https://doi.org/10.1016/S0012-821X(03)00226-7

Happell, J.D., Chanton, J.P., Showers, W.S., 1994. The influence of methane oxidation on the stable isotopic composition of methane emitted from Florida swamp forests. Geochim. Cosmochim. Acta 58, 4377–4388. https://doi.org/10.1016/0016-7037(94)90341-7

Hicks, R.E., Lee, C., Marinucci, A.C., 1991. Loss and recycling of amino acids and protein from smooth cordgrass (*Spartina alterniflora*) litter. Estuaries 14, 430–439. https://doi.org/10.2307/1352267

Hill, A.C., Vázquez-Lule, A., Vargas, R., 2021. Linking vegetation spectral reflectance with ecosystem carbon phenology in a temperate salt marsh. Agric. For. Meteorol. 307, 108481. https://doi.org/10.1016/j.agrformet.2021.108481

Jacinthe, P.A., Groffman, P.M., 2001. Silicone rubber sampler to measure dissolved gases in saturated soils and waters. Soil Biol. Biochem. 33, 907–912. https://doi.org/10.1016/S0038-0717(00)00236-4

Kelley, C.A., Martens, C.S., Ussler, W., 1995. Methane dynamics across a tidally flooded riverbank margin. Limnol. Oceanogr. 40, 1112–1129. https://doi.org/10.4319/lo.1995.40.6.1112

Kevorkian, R.T., Callahan, S., Winstead, R., Lloyd, K.G., 2021. ANME-1 archaea may drive methane accumulation and removal in estuarine sediments. Environ. Microbiol. Rep. 13, 185–194. https://doi.org/10.1111/1758-2229.12926

Kiene, R.P., Visscher, P.T., 1987. Production and fate of methylated sulfur compounds from methionine and dimethylsulfoniopropionate in anoxic salt marsh sediments. Appl. Environ. Microbiol. 53, 2426–2434.

King, G.M., 1994. Associations of methanotrophs with the roots and rhizomes of aquatic vegetation. Appl. Environ. Microbiol. 60, 3220–3227. https://doi.org/10.1128/aem.60.9.3220-3227.1994

King, G.M., 1990. Dynamics and controls of methane oxidation in a Danish wetland sediment. FEMS Microbiol. Ecol. 74, 309–323. https://doi.org/10.1111/J.1574-6941.1990.TB01698.X

King, G.M., Adamsen, A.P.S., 1992. Effects of temperature on methane consumption in a forest soil and in pure cultures of the methanotroph *Methylomonas rubra*. Appl. Environ. Microbiol. 58, 2758–2763. https://doi.org/10.1128/AEM.58.9.2758-2763.1992

King, G.M., Wiebe, W.J., 1980. Regulation of sulfate concentrations and methanogenesis in salt marsh soils. Estuar. Coast. Mar. Sci. 10, 215–223. https://doi.org/10.1016/S0302-3524(80)80059-4

Kittler, F., Heimann, M., Kolle, O., Zimov, N., Zimov, S., Göckede, M., 2017. Long-term drainage reduces CO_2 uptake and CH_4 emissions in a Siberian permafrost ecosystem. Global Biogeochem. Cycles 31, 1704–1717. https://doi.org/10.1002/2017GB005774

Knittel, K., Boetius, A., 2009. Anaerobic oxidation of methane: Progress with an unknown process. Annu. Rev. Microbiol. 63, 311–334. https://doi.org/10.1146/annurev.micro.61.080706.093130

Krzycki, J.A., Kenealy, W.R., DeNiro, M.J., Zeikus, J.G., 1987. Stable carbon isotope fractionation by *Methanosarcina barkeri* during methanogenesis from acetate, methanol, or carbon dioxide-hydrogen. Appl. Environ. Microbiol. 53, 2597–2599. https://doi.org/10.1128/aem.53.10.2597-2599.1987

La, W., Han, X., Liu, C.Q., Ding, H., Liu, M., Sun, F., Li, S., Lang, Y., 2022. Sulfate concentrations affect sulfate reduction pathways and methane consumption in coastal wetlands. Water Res. 217, 118441. https://doi.org/10.1016/j.watres.2022.118441

Larher, F., Hamelin, J., Stewart, G.R., 1977. L'acide diméthylsulfonium-3 propanoïque de *Spartina anglica*. Phytochemistry 16, 2019–2020. https://doi.org/10.1016/0031-9422(77)80117-9

Lee, C., Howarth, R.W., Howes, B.L., 1980. Sterols in decomposing *Spartina alterniflora* and the use of ergosterol in estimating the contribution of fungi to detrital nitrogen. Limnol. Oceanogr. 25, 290–303. https://doi.org/10.4319/lo.1980.25.2.0290

Legendre, P., 2018. lmodel2: Model II Regression. R Packag. version 1.7-3.

Li, X., Hu, B.X., Burnett, W.C., Santos, I.R., Chanton, J.P., 2009. Submarine ground water discharge driven by tidal pumping in a heterogeneous aquifer. Ground Water 47, 558–568. https://doi.org/10.1111/j.1745-6584.2009.00563.x

Londry, K.L., Dawson, K.G., Grover, H.D., Summons, R.E., Bradley, A.S., 2008. Stable carbon isotope fractionation between substrates and products of *Methanosarcina barkeri*. Org. Geochem. 39, 608–621. https://doi.org/10.1016/j.orggeochem.2008.03.002

Maher, D.T., Santos, I.R., Golsby-Smith, L., Gleeson, J., Eyre, B.D., 2013. Groundwater-derived dissolved inorganic and organic carbon exports from a mangrove tidal creek: The missing mangrove carbon sink? Limnol. Oceanogr. 58, 475–488. https://doi.org/10.4319/lo.2013.58.2.0475

McDonald, I.R., Smith, K., Lidstrom, M.E., 2005. Methanotrophic populations in estuarine sediment from Newport Bay, California. FEMS Microbiol. Lett. 250, 287–293. https://doi.org/10.1016/j.femsle.2005.07.016

McKnight, D.M., Boyer, E.W., Westerhoff, P.K., Doran, P.T., Kulbe, T., Andersen, D.T., 2001. Spectrofluorometric characterization of dissolved organic matter for indication of precursor organic material and aromaticity. Limnol. Oceanogr. 46, 38–48. https://doi.org/10.4319/lo.2001.46.1.0038

McNicol, G., Knox, S.H., Guilderson, T.P., Baldocchi, D.D., Silver, W.L., 2020. Where old meets new: An ecosystem study of methanogenesis in a reflooded agricultural peatland. Glob. Chang. Biol. 26, 772–785. https://doi.org/10.1111/gcb.14916

Megonigal, J.P., Schlesinger, W.H., 2002. Methane-limited methanotrophy in tidal freshwater swamps. https://doi.org/10.1029/2001GB001594

Mer, J. Le, Roger, P., 2001. Production, oxidation, emission and consumption of methane by soils: A review. Eur. J. Soil Biol. 37, 25–50.

Moussard, H., Stralis-Pavese, N., Bodrossy, L., Neufeld, J.D., Colin Murrell, J., 2009. Identification of active methylotrophic bacteria inhabiting surface sediment of a marine estuary. Environ. Microbiol. Rep. 1, 424–433. https://doi.org/10.1111/j.1758-2229.2009.00063.x

Nellemann, C., Corcoran, E., Duarte, C.M., Valdés, L., De Young, C., Fonseca, L., Grimsditch, G., 2009. Blue carbon: A rapid response assessment, United Nations Environment Programme, GRID-Arendal.

Northrup, K., Capooci, M., Seyfferth, A.L., 2018. Effects of extreme events on arsenic cycling in salt marshes. J. Geophys. Res. Biogeosciences 123, 1086–1100. https://doi.org/10.1002/2017JG004259

Oremland, R.S., Marsh, L.M., Polcin, S., 1982. Methane production and simultaneous sulphate reduction in anoxic, salt marsh sediments. Nature 296, 143–145.

Oreska, M.P.J., McGlathery, K.J., Aoki, L.R., Berger, A.C., Berg, P., Mullins, L., 2020. The greenhouse gas offset potential from seagrass restoration. Sci. Rep. 10, 1–15. https://doi.org/10.1038/s41598-020-64094-1

Pakulski, J.D., 1986. The release of reducing sugars and dissolved organic carbon from *Spartina alterniflora* Loisel in a Georgia salt marsh. Estuar. Coast. Shelf Sci. 22, 385–394. https://doi.org/10.1016/0272-7714(86)90063-6

Pataki, D.E., Ehleringer, J.R., Flanagan, L.B., Yakir, D., Bowling, D.R., Still, C.J., Buchmann, N., Kaplan, J.O., Berry, J.A., Pataki, C.:, 2003. The application and interpretation of Keeling plots in terrestrial carbon cycle research. Glob. Biogeochem. Cycles 17, 1022. https://doi.org/10.1029/2001GB001850

Penger, J., Conrad, R., Blaser, M., 2012. Stable carbon isotope fractionation by methylotrophic methanogenic archaea. Appl. Environ. Microbiol. 78, 7596–7602. https://doi.org/10.1128/AEM.01773-12/FORMAT/EPUB

Peterson, P.M., Romaschenko, K., Arrieta, Y.H., Saarela, J.M., 2014. A molecular phylogeny and new subgeneric classification of *Sporobolus* (Poaceae: Chloridoideae: Sporobolinae). Taxon 63, 1212–1243. https://doi.org/10.12705/636.19

Petrakis, S., Barba, J., Bond-Lamberty, B., Vargas, R., 2017a. Using greenhouse gas fluxes to define soil functional types. Plant Soil. https://doi.org/10.1007/s11104-017-3506-4

Petrakis, S., Seyfferth, A., Kan, J., Inamdar, S., Vargas, R., 2017b. Influence of experimental extreme water pulses on greenhouse gas emissions from soils. Biogeochemistry 133, 147–164. https://doi.org/10.1007/s10533-017-0320-2

Petrenko, V. V., Smith, A.M., Brailsford, G., Riedel, K., Hua, Q., Lowe, D., Severinghaus, J.P., Levchenko, V., Bromley, T., Moss, R., Mühle, J., Brook, E.J., 2008. A new method for analyzing ^{14}C of methane in ancient air extracted from glacial ice. Radiocarbon 50, 53–73. https://doi.org/10.1017/S0033822200043368

Poffenbarger, H.J., Needelman, A., Megonigal, J.P., 2011. Salinity influence on methane emissions from tidal marshes. Wetlands 31, 831–842. https://doi.org/10.1007/s13157-011-0197-0

Ponnamperuma, F.N., 1972. The chemistry of submerged soils. Adv. Agron. 24, 29–96.

Preuss, I., Knoblauch, C., Gebert, J., Pfeiffer, E.M., 2013. Improved quantification of microbial CH_4 oxidation efficiency in arctic wetland soils using carbon isotope fractionation. Biogeosciences 10, 2539–2552. https://doi.org/10.5194/bg-10-2539-2013

Quast, C., Pruesse, E., Yilmaz, P., Gerken, J., Schweer, T., Yarza, P., Peplies, J., Glöckner, F.O., 2013. The SILVA ribosomal RNA gene database project: Improved data processing and web-based tools. Nucleic Acids Res. 41, D590–D596. https://doi.org/10.1093/NAR/GKS1219

Reeburgh, W.S., 2007. Oceanic methane biogeochemistry. Chem. Rev. 107, 486–513. https://doi.org/10.1021/cr050362v

Robinson, C., Li, L., Prommer, H., 2007. Tide-induced recirculation across the aquifer-ocean interface. Water Resour. Res. 43. https://doi.org/10.1029/2006WR005679

Rosentreter, J.A., Maher, D.T., Erler, D. V., Murray, R.H., Eyre, B.D., 2018. Methane emissions partially offset “blue carbon” burial in mangroves. Sci. Adv. 4, eaao4985. https://doi.org/10.1126/SCIADV.AAO4985

Sánchez-Carrillo, S., Garatuza-Payan, J., Sánchez-Andrés, R., Cervantes, F.J., Bartolomé, M.C., Merino-Ibarra, M., Thalasso, F., 2021. Methane production and oxidation in mangrove soils assessed by stable isotope mass balances. Water 13. https://doi.org/10.3390/w13131867

Santos, I.R., Burdige, D.J., Jennerjahn, T.C., Bouillon, S., Cabral, A., Serrano, O., Wernberg, T., Filbee-Dexter, K., Guimond, J.A., Tamborski, J.J., 2021. The renaissance of Odum's outwelling hypothesis in "Blue Carbon" science. Estuar. Coast. Shelf Sci. 255, 107361. https://doi.org/10.1016/j.ecss.2021.107361

Santos, I.R., Eyre, B.D., Huettel, M., 2012. The driving forces of porewater and groundwater flow in permeable coastal sediments: A review. Estuar. Coast. Shelf Sci. 98, 1–15. https://doi.org/10.1016/j.ecss.2011.10.024

Santos, I.R., Maher, D.T., Larkin, R., Webb, J.R., Sanders, C.J., 2019. Carbon outwelling and outgassing vs. burial in an estuarine tidal creek surrounded by mangrove and saltmarsh wetlands. Limnol. Oceanogr. 64, 996–1013. https://doi.org/10.1002/lno.11090

Saunois, M., Stavert, A.R., Poulter, B., Bousquet, P., Canadell, J.G., Jackson, R.B., Raymond, P.A., Dlugokencky, E.J., Houweling, S., Patra, P.K., Ciais, P., Arora, V.K., Bastviken, D., Bergamaschi, P., Blake, D.R., Brailsford, G., Bruhwiler, L., Carlson, K.M., Carrol, M., Castaldi, S., Chandra, N., Crevoisier, C., Crill, P.M., Covey, K., Curry, C.L., Etiope, G., Frankenberg, C., Gedney, N., Hegglin, M.I., Höglund-Isaksson, L., Hugelius, G., Ishizawa, M., Ito, A., Janssens-Maenhout, G., Jensen, K.M., Joos, F., Kleinen, T., Krummel, P.B., Langenfelds, R.L., Laruelle, G.G., Liu, L., Machida, T., Maksyutov, S., McDonald, K.C., McNorton, J., Miller, P.A., Melton, J.R., Morino, I., Müller, J., Murguia-Flores, F., Naik, V., Niwa, Y., Noce, S., O'Doherty, S., Parker, R.J., Peng, C., Peng, S., Peters, G.P., Prigent, C., Prinn, R.G., Ramonet, M., Regnier, P., Riley, W.J., Rosentreter, J.A., Segers, A., Simpson, I.J., Shi, H., Smith, S.J., Steele, L.P., Thornton, B.F., Tian, H., Tohjima, Y., Tubiello, F.N., Tsuruta, A., Viovy, N., Voulgarakis, A., Weber, T.S., van Weele, M., van der Werf, G.R., Weiss, R.F., Worthy, D., Wunch, D., Yin, Y., Yoshida, Y., Zhang, W., Zhang, Z., Zhao, Y., Zheng, B., Zhu, Qing, Zhu, Qiuan, Zhuang, Q., 2020. The Global methane budget 2000 – 2017. Earth Syst. Sci. Data 12, 1561–1623. https://doi.org/10.5194/essd-12-1561-2020

Schink, B., Zeikus, J.G., 1980. Microbial methanol formation: A major end product of pectin metabolism. Curr. Microbiol. 4, 387–389. https://doi.org/10.1007/BF02605383

Schloss, P.D., Westcott, S.L., Ryabin, T., Hall, J.R., Hartmann, M., Hollister, E.B., Lesniewski, R.A., Oakley, B.B., Parks, D.H., Robinson, C.J., Sahl, J.W., Stres, B., Thallinger, G.G., Van Horn, D.J., Weber, C.F., 2009. Introducing mothur: Open-source, platform-independent, community-supported software for describing and comparing microbial communities. Appl. Environ. Microbiol. 75, 7537–7541. https://doi.org/10.1128/AEM.01541-09

Segarra, K.E.A., Samarkin, V., King, E., Meile, C., Joye, S.B., 2013. Seasonal variations of methane fluxes from an unvegetated tidal freshwater mudflat (Hammersmith Creek, GA). Biogeochemistry 115, 349–361. https://doi.org/10.1007/s10533-013-9840-6

Segers, R., 1998. Methane production and methane consumption: A review of processes underlying wetland methane fluxes. Biogeochemistry 41, 23–51.

Seyednasrollah, B., Young, A.M., Hufkens, K., Milliman, T., Friedl, M.A., Frolking, S., Richardson, A.D., Abraha, M., Allen, D.W., Apple, M., Arain, M.A., Baker, J., Baker, J.M., Baldocchi, D., Bernacchi, C.J., Bhattacharjee, J., Blanken, P., Bosch, D.D., Boughton, R., Boughton, E.H., Zona, D., 2019. PhenoCam dataset v2.0: Vegetation phenology from digital camera imagery. Oak Ridge, Tennessee. https://doi.org/https://doi.org/10.3334/ORNLDAAC/1674

Seyfferth, A.L., Bothfeld, F., Vargas, R., Stuckey, J.W., Wang, J., Kearns, K., Michael, H.A., Guimond, J., Yu, X., Sparks, D.L., 2020. Spatial and temporal heterogeneity of geochemical controls on carbon cycling in a tidal salt marsh. Geochim. Cosmochim. Acta 282, 1–18. https://doi.org/10.1016/j.gca.2020.05.013

Sharp, J.H., 2002. Analytical Methods for Total DOM Pools, in: Biogeochemistry of Marine Dissolved Organic Matter. Elsevier Science, pp. 35–58.

Shelton, S., Neale, P., Pinsonneault, A., Tzortziou, M., 2021. Biodegradation and photodegradation of vegetation-derived dissolved organic matter in tidal marsh ecosystems. Estuaries and Coasts. https://doi.org/10.1007/s12237-021-00982-7

Silverman, M.P., Oyama, V.I., 1968. Automatic apparatus for sampling and preparing gases for mass spectral analysis in studies of carbon isotope fractionation during methane metabolism. Anal. Chem. 40, 1833–1837.

Söllinger, A., Urich, T., 2019. Methylotrophic methanogens everywhere — physiology and ecology of novel players in global methane cycling. Biochem. Soc. Trans. 47, 1895–1907. https://doi.org/10.1042/BST20180565

Steinle, L., Maltby, J., Treude, T., Kock, A., Bange, H.W., Engbersen, N., Zopfi, J., Lehmann, M.F., Niemann, H., 2017. Effects of low oxygen concentrations on aerobic methane oxidation in seasonally hypoxic coastal waters. Biogeosciences 14, 1631–1645. https://doi.org/10.5194/bg-14-1631-2017

Strong, D.T., De Wever, H., Merckx, R., Recous, S., 2004. Spatial location of carbon decomposition in the soil pore system. Eur. J. Soil Sci. 55, 739–750. https://doi.org/10.1111/j.1365-2389.2004.00639.x

Stuiver, M., Polach, H.A., 1977. Discussion: Reporting of ^{14}C data. Radiocarbon 19, 355–363.

Summons, R.E., Franzmann, P.D., Nichols, P.D., 1998. Carbon isotopic fractionation associated with methylotrophic methanogenesis. Org. Geochem. 28, 465–475. https://doi.org/10.1016/S0146-6380(98)00011-4

Taillardat, P., Thompson, B.S., Garneau, M., Trottier, K., Friess, D.A., 2020. Climate change mitigation potential of wetlands and the cost-effectiveness of their restoration. Interface Focus 10. https://doi.org/10.1098/rsfs.2019.0129

Tamborski, J.J., Eagle, M., Kurylyk, B.L., Kroeger, K.D., Wang, Z.A., Henderson, P., Charette, M.A., 2021. Pore water exchange-driven inorganic carbon export from intertidal salt marshes. Limnol. Oceanogr. 66, 1774–1792. https://doi.org/10.1002/LNO.11721

Tong, C., Morris, J.T., Huang, J., Xu, H., Wan, S., 2018. Changes in pore-water chemistry and methane emission following the invasion of *Spartina alterniflora* into an oliogohaline marsh. Limnol. Oceanogr. 63, 384–396. https://doi.org/10.1002/lno.10637

Trifunovic, B., Vázquez-Lule, A., Capooci, M., Seyfferth, A.L., Moffat, C., Vargas, R., 2020. Carbon dioxide and methane emissions from temperate salt marsh tidal creek. J. Geophys. Res. Biogeosciences 125. https://doi.org/10.1029/2019JG005558

Valiela, I., Teal, J.M., Allen, S.D., Van Etten, R., Goehringer, D., Volkmann, S., 1985. Decomposition in salt marsh ecosystems: The phases and major factors affecting disappearance of above-ground organic matter. J. Exp. Mar. Bio. Ecol. 89, 29–54. https://doi.org/10.1016/0022-0981(85)90080-2

Van Der Nat, F.-J.W.A., Middelburg, J.J., 1998. Seasonal variation in methane oxidation by the rhizosphere of *Phragmites australis* and *Scirpus lacustris*. Aquat. Bot. 61, 95–110. https://doi.org/10.1016/S0304-3770(98)00072-2

Vázquez-Lule, A., Vargas, R., 2021. Biophysical drivers of net ecosystem and methane exchange across phenological phases in a tidal salt marsh. Agric. For. Meteorol. 300. https://doi.org/10.1016/j.agrformet.2020.108309

Vogel, J.S., Southon, J.R., Nelson, D.E., Brown, T.A., 1984. Performance of catalytically condensed carbon for use in accelerator mass spectrometry. Nucl. Instruments Methods Phys. Res. Sect. B 289–293. https://doi.org/10.1016/0168-583X(84)90529-9

Wallenius, A.J., Dalcin Martins, P., Slomp, C.P., Jetten, M.S.M., 2021. Anthropogenic and environmental constraints on the microbial methane cycle in coastal sediments. Front. Microbiol. 12. https://doi.org/10.3389/fmicb.2021.631621

Wang, Jiaqi, Hua, M., Cai, C., Hu, J., Wang, Junren, Yang, H., Ma, F., Qian, H., Zheng, P., Hua, B., 2019. Spatial-temporal pattern of sulfate-dependent anaerobic methane oxidation in an intertidal zone of the east China sea. Appl. Environ. Microbiol. 85. https://doi.org/10.1128/AEM.02638-18

Wang, X., Chen, R.F., Cable, J.E., Cherrier, J., 2014. Leaching and microbial degradation of dissolved organic matter from salt marsh plants and seagrasses. Aquat. Sci. 76, 595–609. https://doi.org/10.1007/s00027-014-0357-4

Wang, X.C., Lee, C., 1995. Decomposition of aliphatic amines and amino acids in anoxic salt marsh sediment. Geochim. Cosmochim. Acta 59, 1787–1797. https://doi.org/10.1016/0016-7037(95)00082-B

Wang, X.C., Lee, C., 1994. Sources and distribution of aliphatic amines in salt marsh sediment. Org. Geochem. 22, 1005–1021. https://doi.org/10.1016/0146-6380(94)90034-5

Ward, N., Megonigal, P.J., Bond-Lamberty, B., Bailey, V., Butman, D., Canuel, E., Diefenderfer, H., Ganju, N.K., Goñi, M.A., Graham, E.B., Hopkinson, C.S., Khangaonkar, T., Langley, J.A., McDowell, N.G., Myers-Pigg, A.N., Neumann, R.B., Osburn, C.L., Price, R.M., Rowland, J., Sengupta, A., Simard, M., Thornton, P.E., Tzortziou, M., Vargas, R., Weisenhorn, P.B., Windham-Myers, L., 2020. Representing the function and sensitivity of coastal interfaces in Earth system models. Nat. Commun. 11. https://doi.org/10.1038/s41467-020-16236-2

Weishaar, J.L., Aiken, G.R., Bergamaschi, B.A., Fram, M.S., Fujii, R., Mopper, K., 2003. Evaluation of specific ultraviolet absorbance as an indicator of the chemical composition and reactivity of dissolved organic carbon. Environ. Sci. Technol. 37, 4702–4708. https://doi.org/10.1021/es030360x

White, D.S., Howes, B.L., 1994. Long-term ^{15}N-nitrogen retention in the vegetated sediments of a New England salt marsh. Limnol. Oceanogr. 39, 1878–1892. https://doi.org/10.4319/lo.1994.39.8.1878

Whiticar, M.J., 1999. Carbon and hydrogen isotope systematics of bacterial formation and oxidation of methane. Chem. Geol. 161, 291–314. https://doi.org/10.1016/S0009-2541(99)00092-3

Whiticar, M.J., Faber, E., 1986. Methane oxidation in sediment and water column environments - Isotope evidence. Org. Geochem. 10, 759–768. https://doi.org/10.1016/S0146-6380(86)80013-4

Xiang, J., Liu, D., Ding, W., Yuan, J., Lin, Y., 2015. Invasion chronosequence of *Spartina alterniflora* on methane emission and organic carbon sequestration in a coastal salt marsh. Atmos. Environ. 112, 72–80. https://doi.org/10.1016/j.atmosenv.2015.04.035

Xiao, K.Q., Beulig, F., Røy, H., Jørgensen, B.B., Risgaard-Petersen, N., 2018. Methylotrophic methanogenesis fuels cryptic methane cycling in marine surface sediment. Limnol. Oceanogr. 63, 1519–1527. https://doi.org/10.1002/lno.10788

Yoshinaga, M.Y., Holler, T., Goldhammer, T., Wegener, G., Pohlman, J.W., Brunner, B., Kuypers, M.M.M., Hinrichs, K.U., Elvert, M., 2014. Carbon isotope equilibration during sulphate-limited anaerobic oxidation of methane. Nat. Geosci. 7, 190–194. https://doi.org/10.1038/ngeo2069

Yuan, J., Ding, W., Liu, D., Kang, H., Xiang, J., Lin, Y., 2016. Shifts in methanogen community structure and function across a coastal marsh transect: Effects of exotic *Spartina alterniflora* invasion. Sci. Rep. 6. https://doi.org/10.1038/srep18777

Yuan, J., Ding, W., Liu, D., Xiang, J., Lin, Y., 2014. Methane production potential and methanogenic archaea community dynamics along the *Spartina alterniflora* invasion chronosequence in a coastal salt marsh. Appl. Microbiol. Biotechnol. 98, 1817–1829. https://doi.org/10.1007/s00253-013-5104-6

Yuan, J., Liu, D., Ji, Y., Xiang, J., Lin, Y., Wu, M., Ding, W., 2019. *Spartina alterniflora* invasion drastically increases methane production potential by shifting methanogenesis from hydrogenotrophic to methylotrophic pathway in a coastal marsh. J. Ecol. 107, 2436–2450. https://doi.org/10.1111/1365-2745.13164

Zeleke, J., Sheng, Q., Wang, J.G., Huang, M.Y., Xia, F., Wu, J.H., Quan, Z.X., 2013. Effects of *Spartina alterniflora* invasion on the communities of methanogens and sulfate-reducing bacteria in estuarine marsh sediments. Front. Microbiol. 4. https://doi.org/10.3389/fmicb.2013.00243

Zhuang, G.-C., Elling, F.J., Nigro, L.M., Samarkin, V., Joye, S.B., Teske, A., Hinrichs, K.-U., Ltd, E., 2016. Multiple evidence for methylotrophic methanogenesis as the dominant methanogenic pathway in hypersaline sediments from the Orca Basin, Gulf of Mexico. Geochim. Cosmochim. Acta 187, 1–20. https://doi.org/10.1016/j.gca.2016.05.005

Zhuang, G.-C., Heuer, V.B., Lazar, C.S., Goldhammer, T., Wendt, J., Samarkin, V.A., Elvert, M., Teske, A.P., Joye, S.B., Hinrichs, K.-U., 2018. Relative importance of methylotrophic methanogenesis in sediments of the Western Mediterranean Sea. Geochim. Cosmochim. Acta 224, 171–186. https://doi.org/10.1016/j.gca.2017.12.024

Chapter 6

CONCLUSION

This research seeks to understand how trace gas fluxes in salt marsh soils change over time (i.e., patterns), as well as how biophysical factors and biogeochemical pathways (i.e., processes) influence them. Over the course of four studies, common themes emerged with respect to patterns and processes, as well as the measurement techniques used to collect the data.

6.1 A note about trace gas patterns

Over annual and seasonal cycles, patterns emerged for CO_2, CH_4, and N_2O fluxes from tidal salt marsh soils. There were no discernable seasonal patterns for CS_2 and DMS. CO_2 fluxes positively correlated with temperature. This finding algins with observations in temperate terrestrial ecosystems and provides support for the use of temperature dependence functions in models. However, different areas of the marsh may have different temperature sensitivities and models will need to account for that. Similarly, CH_4 fluxes have been found to have a temperature dependence, albeit generally weaker than that of CO_2. More importantly, though, is the finding that CH_4 peaks during plant senescence. This highlights the role *S. alterniflora* die-off and the subsequent release of organic matter and microbial substrates plays in soil biogeochemical processes, as well as the importance of measuring fluxes beyond the summer months. While N_2O fluxes at St. Jones are very low, they loosely follow along with plant phenological stages, shifting from source to sink and vice versa depending

on the interaction between plant growth and nutrient availability and reinforcing the need to better understand the role plants play in salt marsh soil biogeochemistry and trace gas production.

Zooming into diel cycles, three patterns emerged. One, there were no consistent diel patterns for CO_2 fluxes. This contrasted with the idea that CO_2 fluxes peak around the same time of day that temperature does, as seen in temperate, terrestrial ecosystems. Therefore, modelling diel CO_2 fluxes based on a temperature dependence function will not accurately capture CO_2 dynamics in salt marsh soils. The lack of diel patterns is likely due to the continuously changing interactions between temperature (24-hour cycle) and tides (24 hours 50 minutes). Two, CH_4, N_2O, and CS_2 fluxes were highly variable. This observation is important for CH_4, which was highly variable under controlled lab conditions, as well as in the field. Methane's high variability significantly contributes to the differences in the calculation of GWP between the control and treatment scenarios in Chapter 2, as well as in the calculation of SGWP between continuous and discrete scenarios in Chapter 4. Therefore, it is necessary to evaluate how CH_4 fluxes change during storm surges, as well with the use of different measurement techniques since GWP and SGWP calculations can affect how scientists and policymakers view tidal salt marshes as a natural climate solution. Third, DMS fluxes appeared to occur only during mid-day at St. Jones. While the mechanisms as to why that happened are uncertain, it reinforces the need for measurements to be done outside of the traditional daytime, low tide window.

6.2 A note about processes that govern trace gas fluxes

To better understand the processes that govern trace gas emission from tidal salt marsh soils, different approaches were taken depending on whether the research

was conducted in the lab or in the field. In the lab, the flow-through mesocosm set-up coupled with high-frequency GHG measurements and pore water chemical analyses contributed to a better understanding of how salinity changes shifted biogeochemical processes and therefore GHG emissions. Under changing salinity conditions, the biogeochemical processes that produce GHGs continuously evolved, with electron acceptors playing different roles throughout the simulated storm surge. The experiment underscored the importance of the sulfur cycle in contributing to CO_2 and CH_4 fluxes and highlighted that the production of GHGs in salt marsh soils is biogeochemically complex. Furthermore, after salinity returned to normal, CH_4 and N_2O emissions went back to baseline within 15 days, highlighting the resilience of the salt marsh and its biogeochemical processes to storm surges.

In the field, research into processes focused on both biophysical and biogeochemical factors. Due to a large amount of available biophysical data collected by the St. Jones staff through the site's participation in the National Estuarine Research Reserve's System-wide Monitoring Program, there were opportunities to investigate the role temperature, tides, PAR, and NDVI play in trace gas fluxes. The key biophysical takeaway is that temperature plays an important role in CO_2 and CH_4 emissions on seasonal scales, but not on diel scales, likely due to the influence of tides. Other biophysical factors, such as water level, salinity, PAR, and NDVI also play a role in explaining the variability in CO_2 fluxes, but to a lesser extent. As for biogeochemical processes, a focused investigation on CH_4 dynamics in the marsh revealed that the processes that produce (hydrogenotrophic and methylotrophic methanogenesis), consume (aerobic and anaerobic CH_4 oxidation), and transport CH_4 (diffusion into the atmosphere, lateral transport to the tidal creek) are

biogeochemically heterogenous and vary in importance from season to season. These findings underscore the need for targeted approaches to better understand CH_4 dynamics in tidal salt marshes.

6.3 A note about the importance of tides and site hydrology

Interspersed throughout the dissertation chapters are discussions about the role of tides and site hydrology in salt marsh carbon biogeochemistry. The marsh does not get flooded frequently, which contributes to the lack of differences in CO_2 fluxes at high and low tides since there generally is no overlying water to impede gas diffusion. However, the two study sites, TS and SS, are hydrologically different due to location and site topography, which has implications for trace gas emissions. The TS site, located near the tidal creek, experiences the diurnal tidal cycle, resulting in frequent changes in redox and a high turnover of substrates and reactants at. This likely translates into less build-up of CO_2 in the upper soil profile and limits CH_4 production to deeper in the soil, below oxic-anoxic zone driven by the tides. On the other hand, the SS site is less hydrologically connected to the tidal creek, exchanging water only during extremely high tides (e.g., spring high tide, storm events), with slight diurnal tidal variations limited to very close to the soil surface. As a result, the soils are strongly reducing and contribute to favorable CH_4 production throughout the soil profile. Furthermore, CO_2 and CH_4 can build-up over spring-neap tidal cycles due to lack of exchange. These differences between the two sites highlights the importance of understanding the role tides and site topography can play in carbon biogeochemistry throughout a tidal salt marsh.

6.4 A note about trace gas measurement techniques

Both continuous, automated and manual measurement techniques were used throughout this research. As continuous, automated systems become more prevalent in measuring trace gases from tidal salt marsh soils, it is important to assess whether researchers obtain similar information from the two techniques. Here are four key takeaways. One, with regards to CO_2, manual and automated measurements capture similar patterns, means, distributions, and temperature dependencies regardless of whether data is collected continuously or manually during daytime low tide. Therefore, carbon budgets and models using discrete CO_2 data likely are accurately representing CO_2 flux from tidal salt marsh soils. Two, continuous measurements of trace gases allow for more robust analyses of biophysical drivers, as seen in Chapter Three where temperature was the only significant explanatory variable for manual measurements, but temperature, as well as water level, salinity, PAR, and NDVI were significant explanatory variables for continuous measurements. Therefore, in order to better inform models about the biophysical factors that explain the variability in CO_2 fluxes, more studies using continuous measurement data are needed. Three, continuous measurements are needed to capture temporal variability, particularly for CH_4, while four, manual measurements are needed to assess spatial variability, particularly to identify hot spots within the marsh. Moving forward, both continuous and manual measurements will need to be utilized to better inform our understanding of trace gas spatiotemporal dynamics.

6.5 A note about future directions for trace gas research in tidal salt marshes

While the findings from this research helped fill knowledge gaps surrounding the patterns and processes that govern trace gas emissions from tidal salt marsh soils,

there remains open questions about the role of trace gases in marshes. Here are four future directions that will aid in better understanding trace gas emissions from salt marsh soils that can ultimately help inform carbon budgets, Earth system models, and the overall source/sink potential of marshes.

- More long-term, high frequency data of trace gases
    - Due to lack of measurements, the range of CH_4 and N_2O emissions from tidal salt marshes has not been well-constrained. More measurements are needed to assess the temporal and spatial variability of CH_4 and N_2O so accurate budgets can be calculated, as well as to understand why CH_4 fluxes are driven by pulse emissions.

    - Not much is known about trace gas behavior in the non-summer months due to difficulties measuring in the winter, as well as the assumption that fluxes remain low due to low ecological activity. However, there is evidence to suggest that marshes may be a carbon source during senescence and dormancy, as seen with CH_4 emissions peaking during senescence. More information is needed to accurately assess how fluxes during senescence and dormancy affect assessments of a marsh's potential to store carbon.

    - In order to untangle the lack of consistent diel patterns for CO_2, CH_4, N_2O, and CS_2, high-frequency data of emissions coupled with water quality, and meteorological data is needed. Understanding the drivers of diel fluxes is important to inform models, particularly since diel patterns have non-linear responses to temperature and water level.

- Connecting the carbon and sulfur cycles, particularly with regards to CH_4
    - CH_4 fluxes from tidal salt marsh soils are not low, despite two types of methanogenesis (acetoclastic and hydrogenotrophic) being outcompeted by sulfate reduction. There is a need to assess the role of a third methanogenesis pathway, methylotrophic methanogenesis, in producing CH_4 in tidal salt marsh soils. This includes conducting assessments of the soil microbial community, as well as their activities.

    - The process by which methylotrophic methanogenesis produces CH_4 can involve the use of sulfur-based substrates such as dimethylsulfide and methanethiol, which directly links the carbon and sulfur cycles together. More information is need about the availability of these substrates within the soils, as well as when they are available. In

particular, the relationship between *S. alterniflora*, CH_4 flux, and the substrate availability for methylotrophic methanogenesis during senescence needs to be investigated.

- CS_2 fluxes were an order of magnitude higher at St. Jones than what has been reported in the literature. However, the reason for this discrepancy is uncertain due to the lack of CS_2 flux data from marshes, as well as uncertainity around how CS_2 is produced.

- Untangling the importance of different processes and fates of CH_4
  - In addition to better understanding CH_4 production as suggested above, more research needs to be done regarding the role of both aerobic and anaerobic CH_4 oxidation in attenuating CH_4 emissions from salt marsh soils. Research into the activities of aerobic and anaerobic CH_4 oxidizers, as well as their importance throughout the soil profile are needed.

  - Quantifying the roles of diffusion into the atmosphere, CH_4 oxidation, and lateral transport to better inform CH_4 budgets. With *in situ* isotope labelling experiments, researchers can start to untangle CH_4 pathways within the soil. Furthermore, these experiments should occur in different marsh hydrological zones, as well as throughout the growing season to incorporate changes in substrate availability.

- Better understanding of whether salt marshes are a source or sink of N_2O
  - St. Jones tidal salt marsh soils were at times small sources of N_2O, as well as small sinks. More long-term data on N_2O fluxes is needed to assess whether marshes are a source or a sink, as well as the mechanisms behind it. In particular, more research is needed in marshes that receive high nitrogen inputs due to anthropogenic activities. There is evidence that increased nitrogen inputs may result in N_2O emissions. Since N_2O is a potent greenhouse gas, marshes that are overall sources may offset their carbon storage potential.

Appendix A

SUPPLEMENTARY MATERIALS - EXPERIMENTAL INFLUENCE OF STORM-SURGE SALINITY ON SOIL GREENHOUSE GAS EMISSIONS FROM A TIDAL SALT MARSH

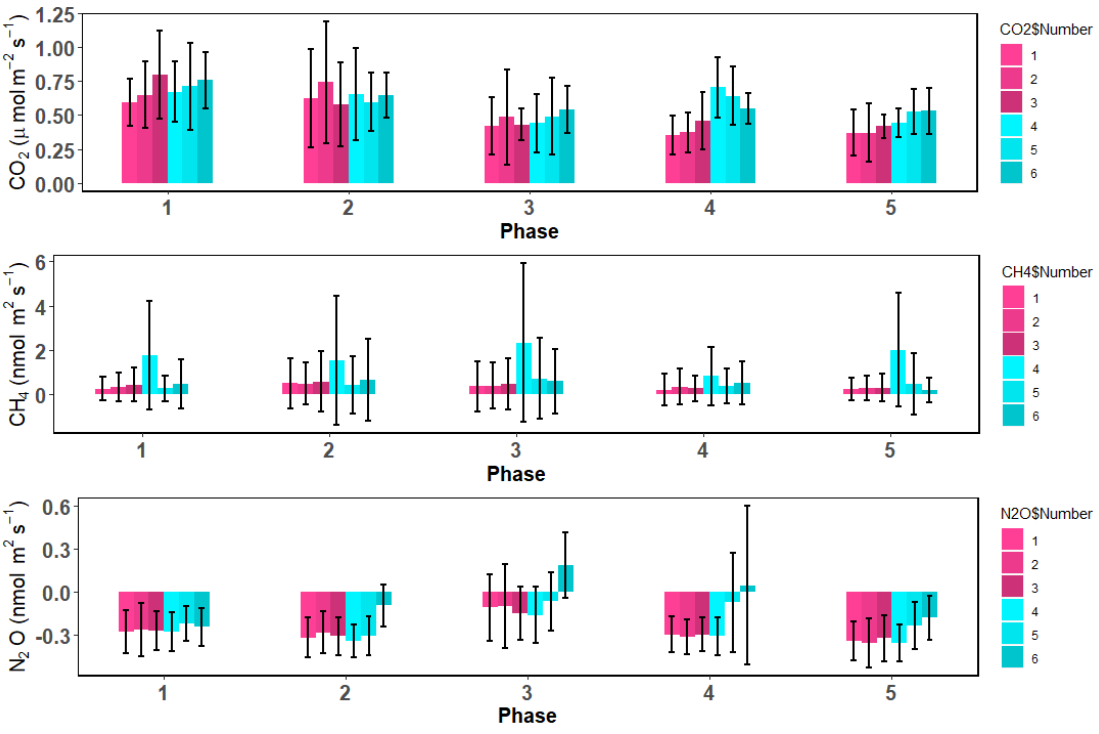

Figure A.1: Means by phases for each of the mesocosms. Control mesocosms are in pink (#1-3) and treatment mesocosms are in blue (#4-6).

Table A.1: Mean, minimum, and maximum of the calculated daily averages during each phase for the control and treatment mesocosms.

		Control					**Treatment**				
		I	II	III	IV	V	I	II	III	IV	V
Redox (mV)	Mean ± SD	177.9 ± 30.7	156.4 ± 19.4	163.6 ± 33.3	141.5 ± 4.9	172.4 ± 27.4	157.3 ± 30.6	139.6 ± 21.0	152.8 ± 42.8	141.1 ±22.5	159.5 ± 39.0
	Min	132.7	134.2	106.2	135.3	149.9	116.2	116.7	104.2	120.2	130.4
	Max	210.9	191.7	205.0	146.0	225.5	197.8	178.8	230.9	163.7	239.9
pH	Mean ± SD	6.78 ± 0.1	6.90 ± 0.2	6.78 ± 0.1	6.82 ± 0.1	6.83 ± 0.1	6.65 ± 0.1	6.72 ± 0.1	6.84 ± 0.1	6.88 ± 0.1	6.83 ± 0.1
	Min	6.65	6.67	6.69	6.75	6.68	6.50	6.56	6.68	6.79	6.75
	Max	6.92	7.12	6.89	6.88	7.00	6.83	6.84	6.97	6.92	6.96
Fe^{2+} (mg/L)	Mean ± SD	1.97 ± 1.5	7.64 ± 4.6	7.94 ± 3.2	11.8 ± 1.3	14.5 ± 4.9	4.74 ± 2.6	11.87 ± 3.2	9.04 ± 3.9	15.19 ± 2.1	21.90 ± 6.67
	Min	0.41	4.86	4.60	10.57	6.80	1.80	6.43	4.76	12.70	9.63
	Max	4.59	16.87	13.90	13.28	21.57	8.43	15.72	14.68	17.19	28.41
SO_4^{2-} (mg/L)	Mean ± SD	242.5 ± 48.9	279.7 ± 24.6	306.9 ± 23.4	257.6 ± 127.3	316.6 ± 18.9	240.2 ± 54.5	253.2 ± 40.7	206.9 ± 5.0	240.4 ± 21.8	260.0 ± 68.2
	Min	172.9	230.7	223.8	0.29	273.3	156.5	196.0	0.40	212.4	0.35
	Max	331.1	316.8	327.4	327.9	343.9	323.8	319.9	234.0	270.9	304.8
S^{2-} (mg/L)	Mean ± SD	0.20 ± 0.09	0.25 ± 0.07	0.24 ± 0.03	0.24 ± 0.04	0.23 ± 0.04	0.20 ± 0.06	0.27 ± 0.07	0.26 ± 0.04	0.26 ± 0.07	0.24 ± 0.05
	Min	0.01	0.17	0.21	0.19	0.14	0.09	0.21	0.21	0.20	0.14
	Max	0.26	0.38	0.28	0.30	0.27	0.25	0.42	0.32	0.36	0.28
TN_b (mg/L)	Mean ± SD	4.41 ± 1.0	3.98 ± 0.36	4.62 ± 2.0	3.33 ± 0.2	3.87 ± 0.12	4.28 ± 0.69	4.38 ± 0.33	4.63 ± 1.65	3.72 ± 0.17	4.05 ± 0.24
	Min	3.62	3.50	2.82	3.15	3.75	3.61	3.82	3.70	3.53	3.80
	Max	5.77	4.37	8.89	3.49	4.08	5.61	4.75	8.35	3.88	4.42

Appendix B

SUPPLEMENTARY MATERIALS – DIEL AND SEASONAL PATTERNS OF SOIL CO_2 EFFLUX IN A TEMPERATE TIDAL MARSH

Table B.1: Summary of the linear model results for each site.

Model	Variable	Coefficient	Lower CI	Upper CI	t-value	p-value	R^2
Continuous SS	Intercept	-0.390	-0.501	-0.278	-6.86	<0.001	0.52
$\log(CO_2) \sim$ ATemp	ATemp	0.064	0.058	0.070	20.60	<0.001	
Manual SS	Intercept	-2.259	-2.849	-1.668	-7.98	<0.001	0.73
$\log(CO_2) \sim$ ATemp	ATemp	0.110	0.078	0.141	7.29	<0.001	
Continuous TS	Intercept	-2.852	-3.002	-2.702	-37.42	<0.001	0.52
$\log(CO_2) \sim$ ATemp	ATemp	0.095	0.086	0.103	21.49	<0.001	
Manual TS	Intercept	-2.675	-3.310	-2.040	-8.68	<0.001	0.65
$\log(CO_2) \sim$ ATemp	ATemp	0.109	0.076	0.142	6.84	<0.001	

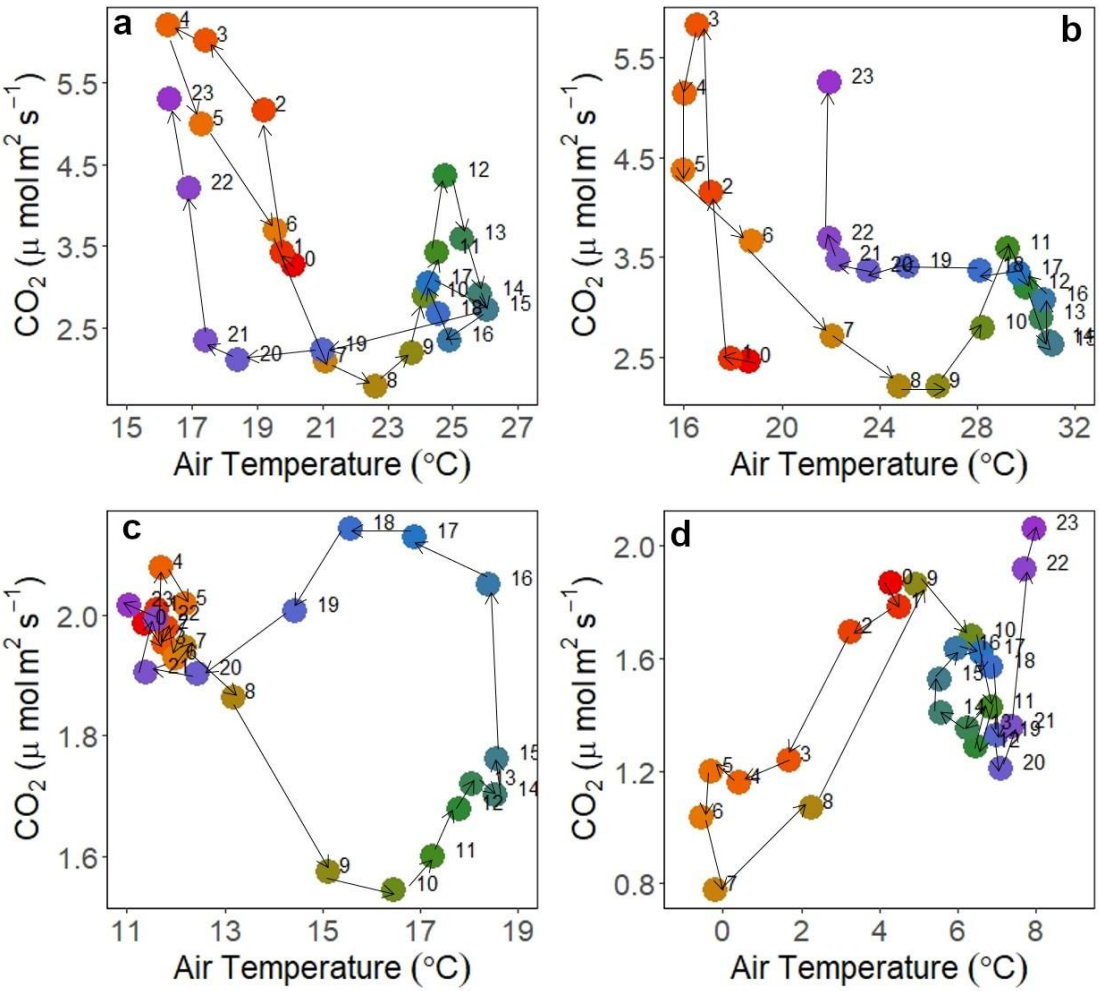

Figure B.1: Hysteresis graphs of CO_2 flux versus air temperature using hourly data at SS during the spring tide on DOY (a) 166, (b) 195, (c) 290, and (d) 335 in 2018.

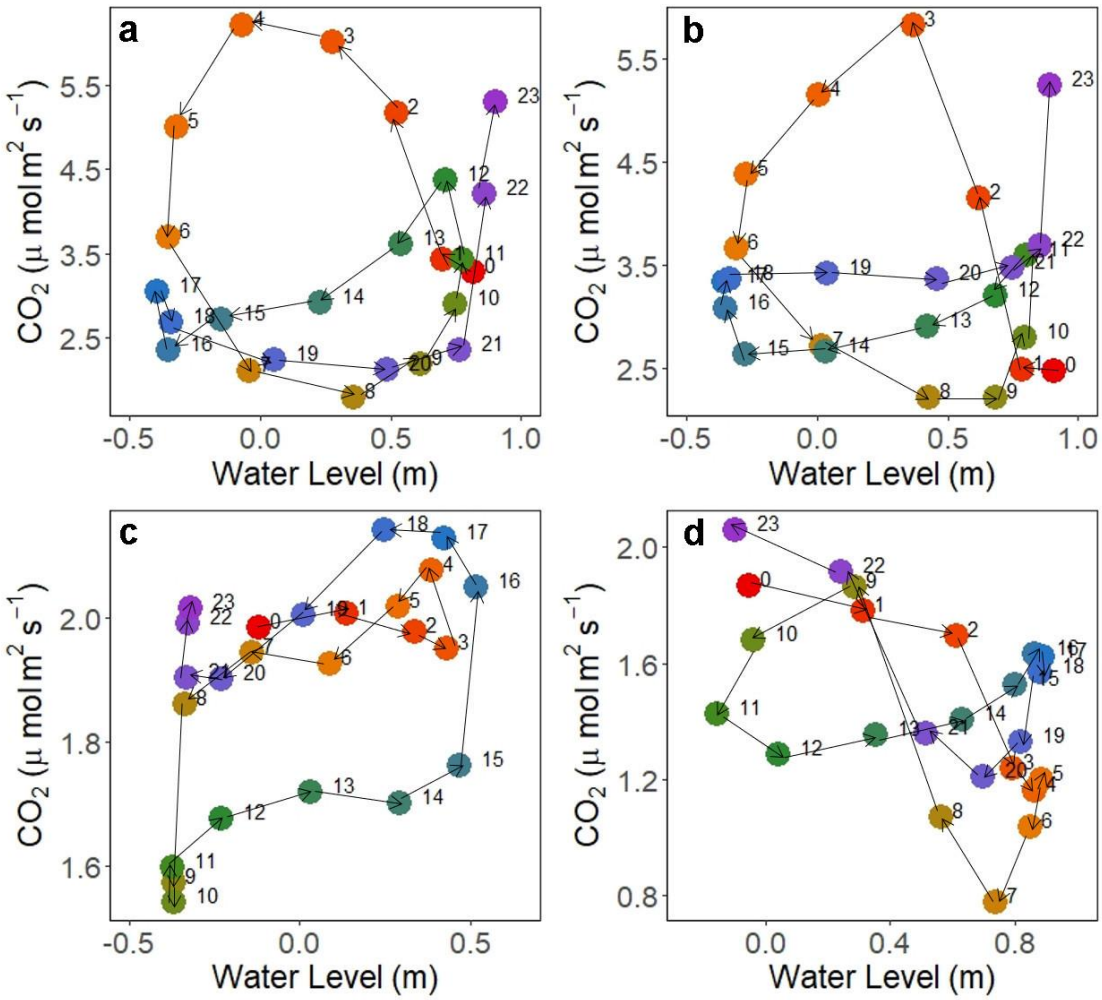

Figure B.2: Hysteresis graphs of CO_2 flux versus water level using hourly data at SS during the spring tide on DOY (a) 166, (b) 195, (c) 290, and (d) 335 in 2018.

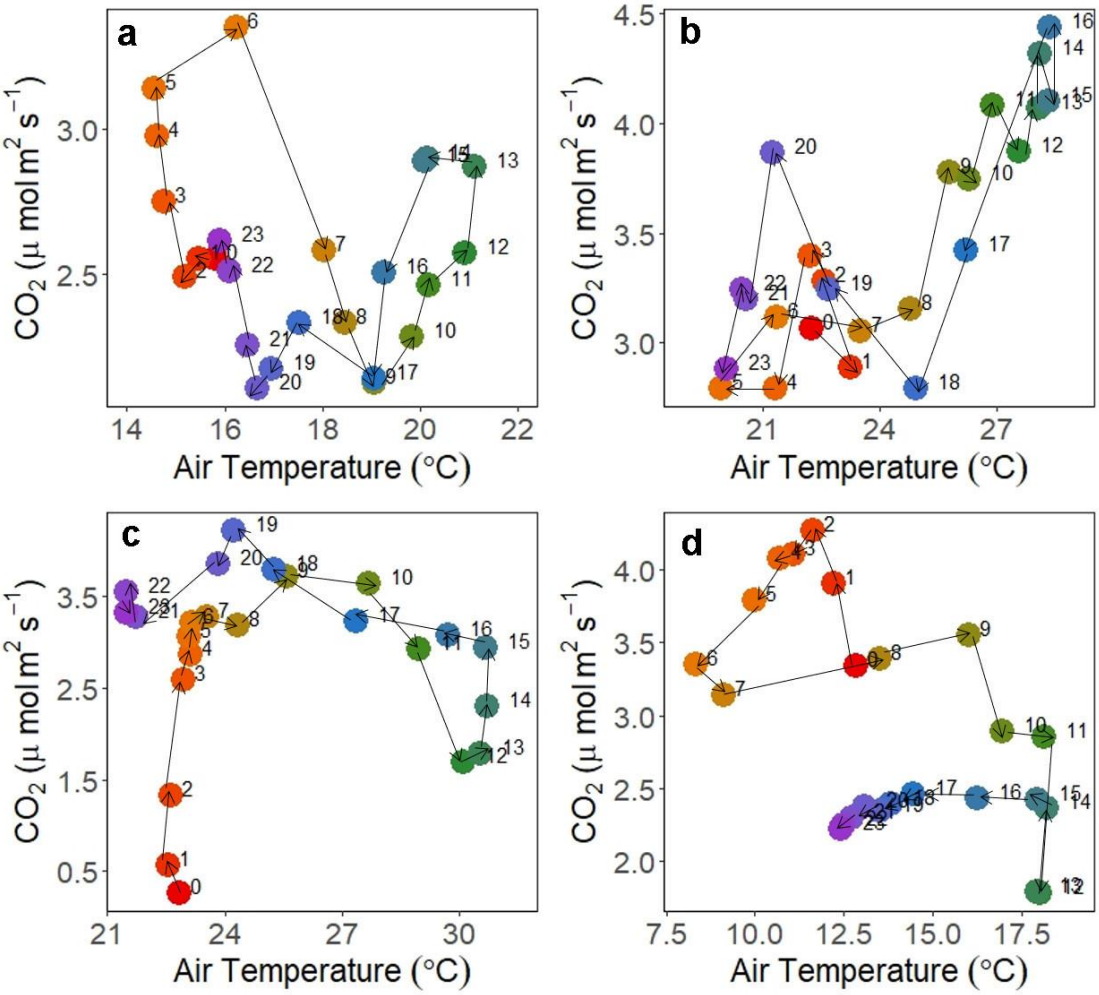

Figure B.3: Hysteresis graphs of CO_2 flux versus air temperature using hourly data at SS during the neap tide on DOY (a) 157, (b) 200, (c) 269, and (d) 311 in 2018.

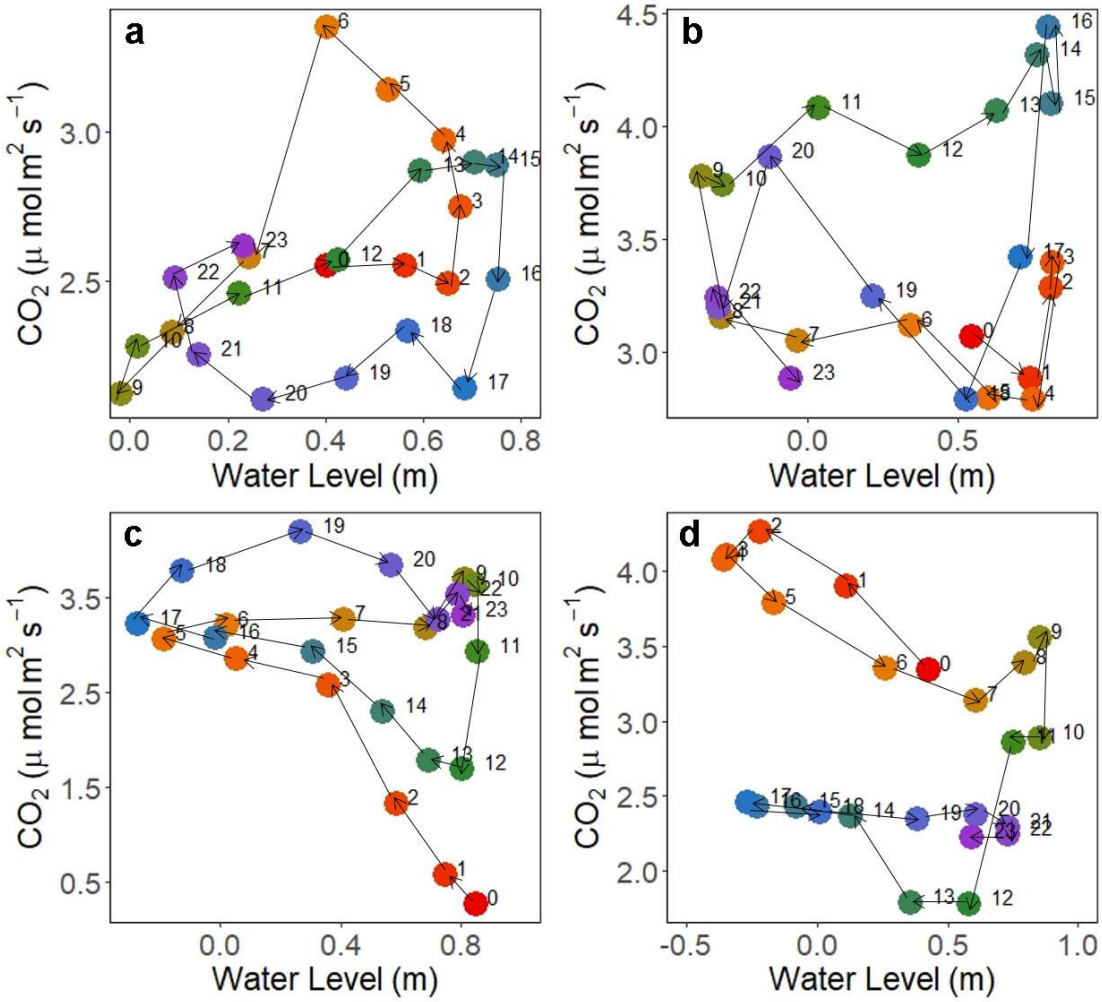

Figure B.4: Hysteresis graphs of CO_2 flux versus water level using hourly data at SS during neap tide on DOY (a) 157, (b) 200, (c) 269, and (d) 311 in 2018.

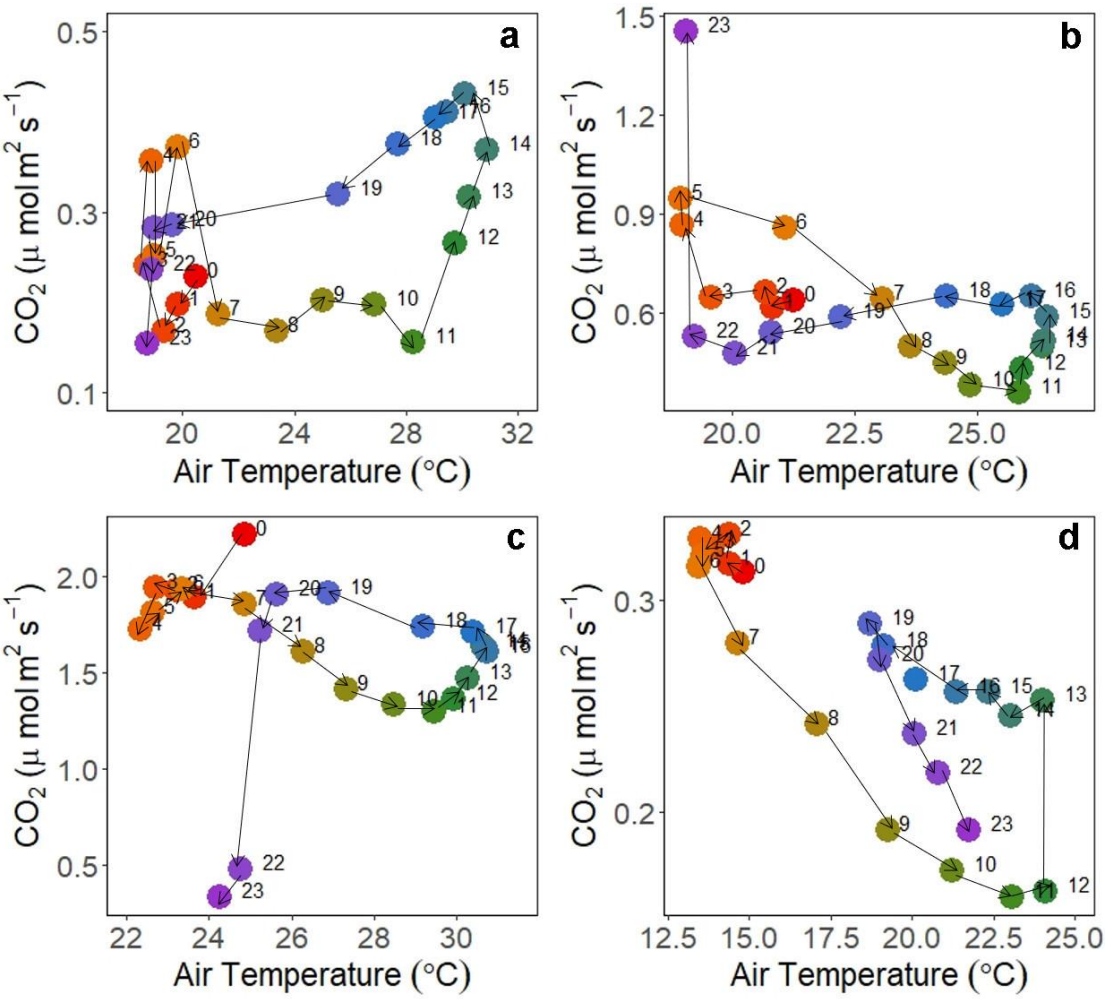

Figure B.5: Hysteresis graphs of CO_2 flux versus air temperature using hourly data at TS during the spring tide on DOY (a) 136, (b) 194, (c) 221, and (d) 305 in 2018.

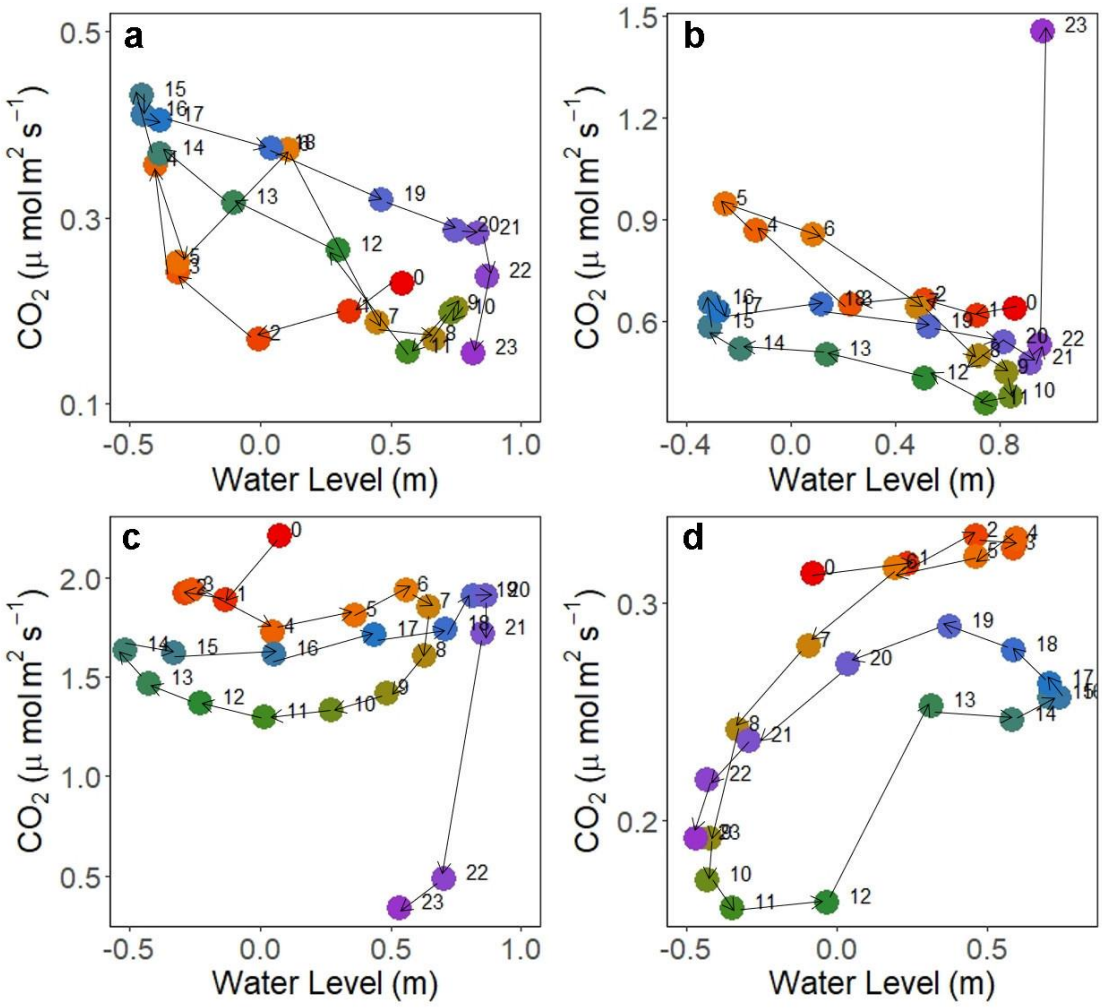

Figure B.6: Hysteresis graphs of CO_2 flux versus water level using hourly data at TS during the spring tide on DOY (a) 136, (b) 194, (c) 221, and (d) 305 in 2018.

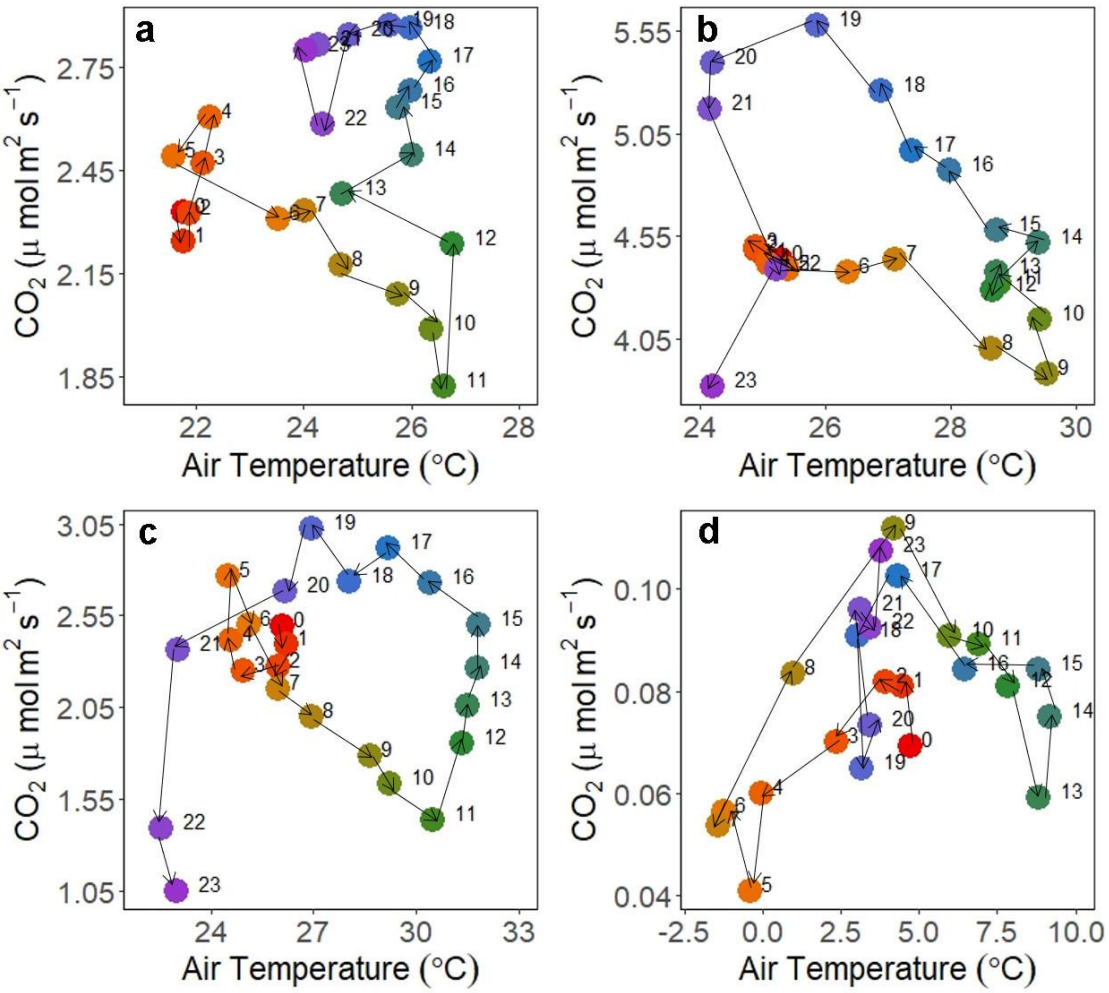

Figure B.7: Hysteresis graphs of CO_2 flux versus air temperature using hourly data at TS during the neap tide on DOY (a) 171, (b) 187, (c) 230, and (d) 357 in 2018.

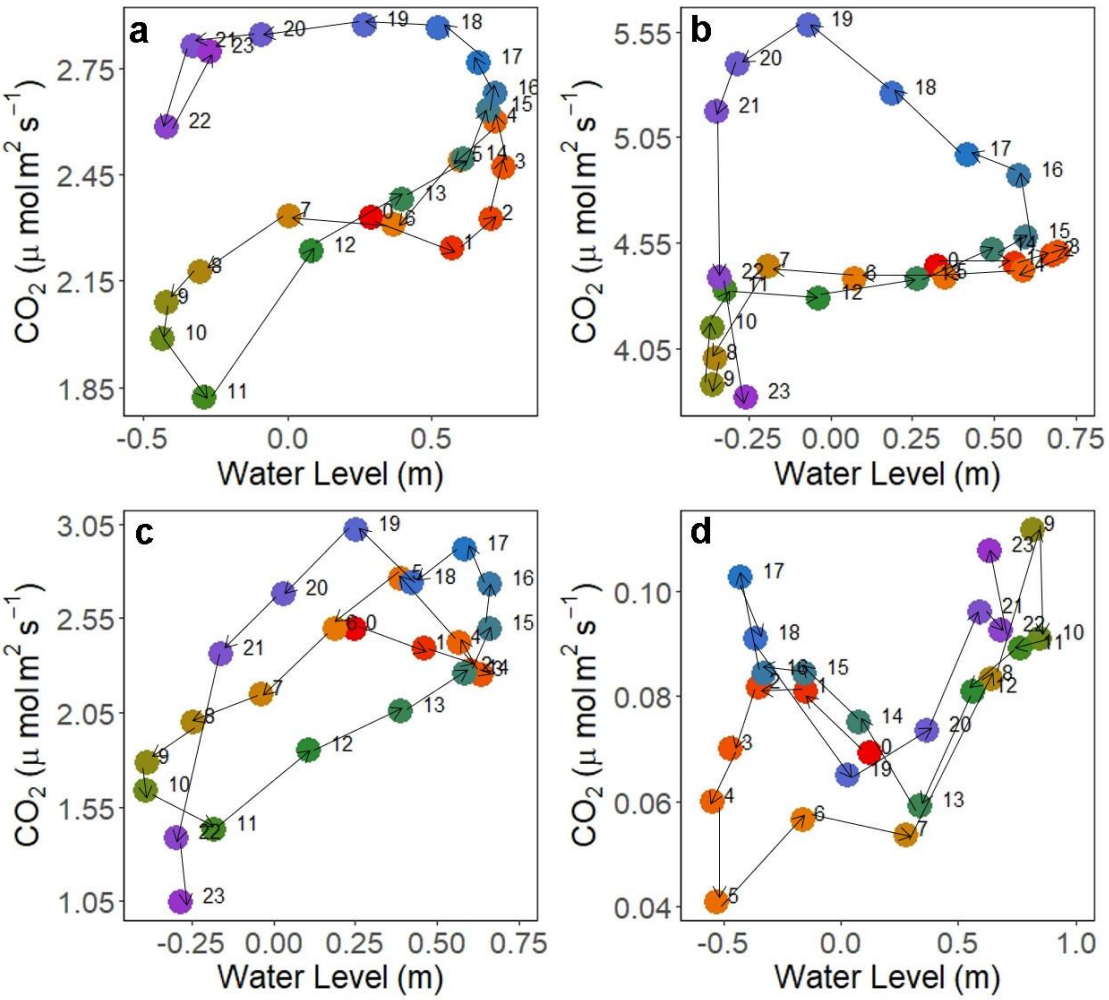

Figure B.8: Hysteresis graphs of CO_2 flux versus water level using hourly data at TS during the neap tide on DOY (a) 171, (b) 187, (c) 230, and (d) 357 in 2018.

Appendix C

SUPPLEMENTARY MATERIALS – TRACE GAS FLUXES FROM TIDAL SALT MARSH SOILS: IMPLICATIONS FOR CARBON-SULFUR BIOGEOCHEMISTRY

Table C.1: Overview of CS_2 and DMS fluxes from various *Spartina alterniflora* marshes.

Site	Time Frame/ Location	CS_2 (nmol m^{-2} s^{-1})	DMS (nmol m^{-2} s^{-1})	References
Wallops Island, VA	August/September Annual	0.006 0.68	NA 1.85	Carroll et al., 1986; Adams et al., 1981
North Carolina (Cedar Island Wildlife Refuge, Cox's Landing)	Summer *Spartina* Mud Flat Single Plant	 0.48 < 0.02 0.10	 1.75 < 0.04 NA	Aneja et al., 1981, 1979a, 1979b; Lamb et al., 1987; Goldan et al., 1987; Adams et al., 1981b
St. Marks National Wildlife Refuge, FL	January *Spartina* (W) Sand May *Spartina* (WD) October *Spartina* (WD) Sand Annual	 < 0.0009 < 0.0009–0.004 < 0.0009–0.003 < 0.0009–0.08 < 0.0009–0.04 0.52	 0.09–1.63 0.004–0.01 0.002–4.82 0.14–1.27 <0.001–0.15 1.22	De Mello et al., 1987; Cooper et al., 1987; Adams et al., 1981b
Chapman's Marsh, NH	August	NA	1.1–1.67 Max: 5.3	Morrison and Hines, 1990
Long Island, NY	Fall	NA	Max: 3.80	Hill et al., 1978
Louisiana	Annual	0.002–0.02	0.01–1.25	DeLaune et al., 2002

Canary Marsh, DE	August Intertidal Infrequently Flooded Unknown	 0.006 0.06 0.07	 0.04 0.90 0.48	Adams et al., 1981a, 1981b
Great Sippewissett Marsh, MA	Annual	0.08	2.84	Steudler and Peterson, 1985, 1984

Notes:

- For locations with multiple studies, the highest mean or widest range is reported here
- For two locations, the maximum flux was reported in addition to the other data (Chapman's Marsh and Long Island)

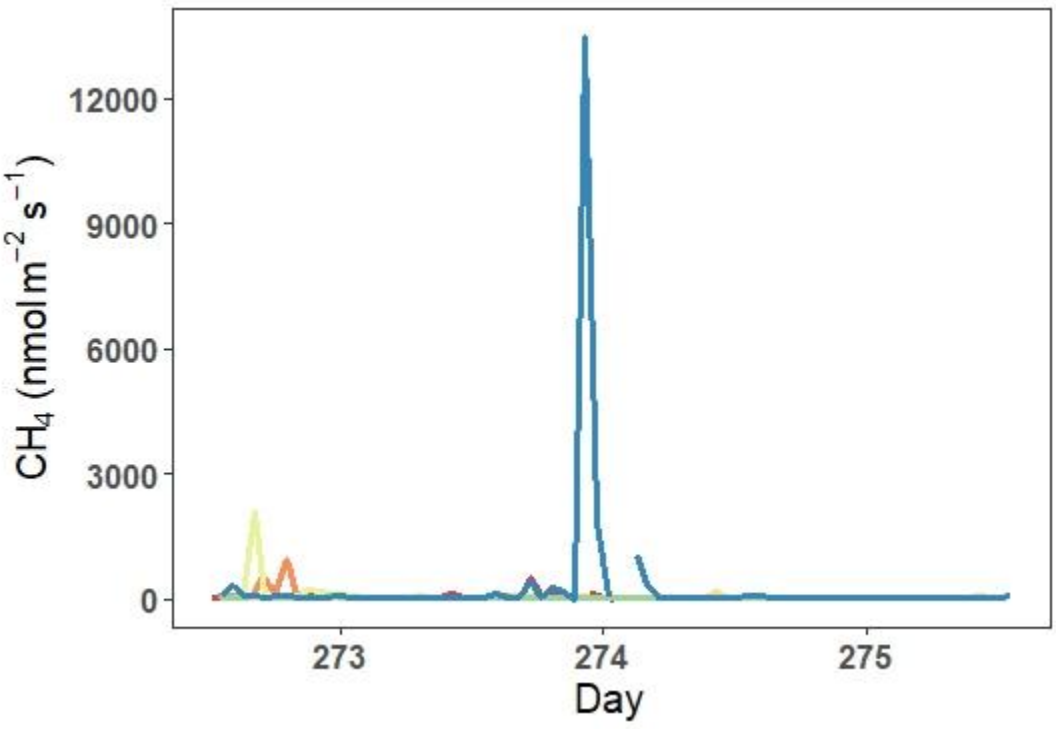

Figure C.1: Full range of CH_4 fluxes from each chamber during S2. Each color designates a different chamber.

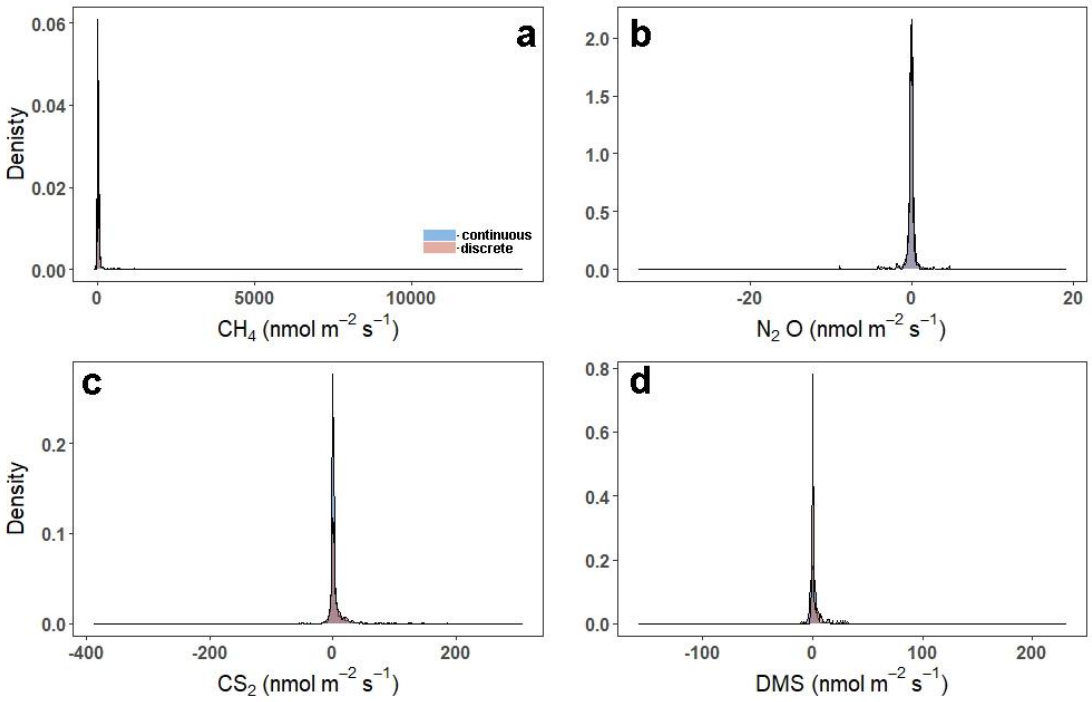

Figure C.2: Density plots comparing the distribution of fluxes throughout all campaigns (continuous) to those measured during daytime low tide (discrete) for (a) CH_4, (b) N_2O, (c) CS_2, and (d) DMS. Note: the scales on the x- and y-axes are different. This figure shows the full distributions of the density plots shown in Figure 4.4.

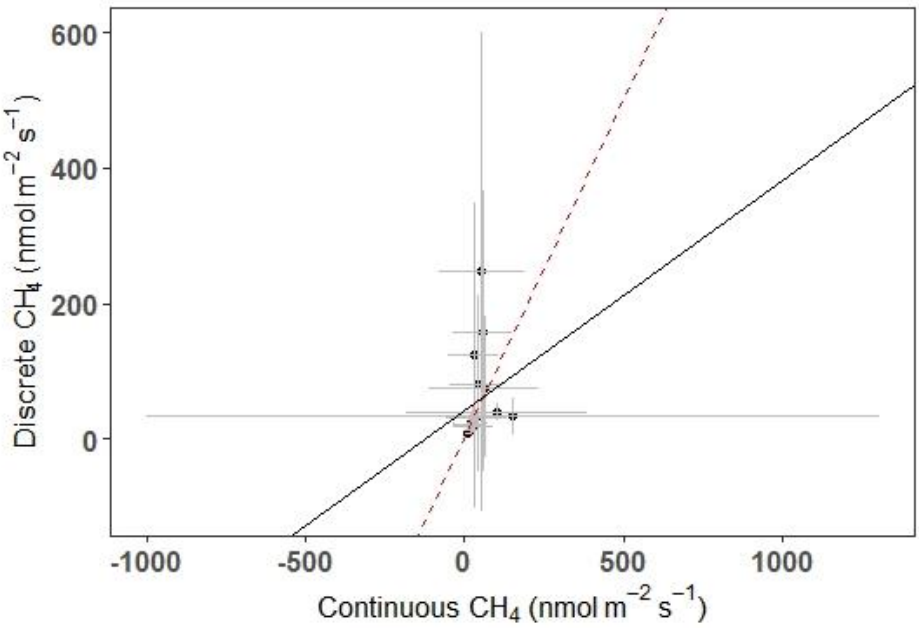

Figure C.3: Plot comparing the daily average of continuous to discrete measurements for CH_4. Red dashed line is the 1:1 line, while the black solid line is the trend line. This figure shows the full error bars for Figure 4.5b.

REFERENCES

Adams, D.F., Farwell, S.O., Pack, M.R., Robinson, E., 1981a. Biogenic sulfur gas emissions from soils in eastern and southeastern United States. J. Air Pollut. Control Assoc. 31, 1083–1089. https://doi.org/10.1080/00022470.1981.10465330

Adams, D.F., Farwell, S.O., Robinson, E., Pack, M.R., Bamesberger, W.L., 1981b. Biogenic sulfur source strengths. Environ. Sci. Technol. 15, 1493–1498. https://doi.org/10.1021/es00094a012

Aneja, V.P., Overton, J.H., Aneja, A.P., 1981. Emission survey of biogenic sulfur flux from terrestrial surfaces. J. Air Pollut. Control Assoc. 31, 256–258. https://doi.org/10.1080/00022470.1981.10465218

Aneja, V.P., Overton, J.H., Cupitt, L.T., Durham, J.L., Wilson, W.E., 1979a. Direct measurements of emission rates of some atmospheric biogenic sulfur compounds. Tellus 31, 174–178. https://doi.org/10.1111/j.2153-3490.1979.tb00895.x

Aneja, V.P., Overton, J.H., Cupitt, L.T., Durham, J.L., Wilson, W.E., 1979b. Carbon disulphide and carbonyl sulphide from biogenic sources and their contributions to the global sulphur cycle. Nature 282, 493–496. https://doi.org/10.1038/282493a0

Carroll, M.A., Heidt, L.E., Cicerone, R.J., Prinn, R.G., 1986. OCS, H_2S, and CS_2 fluxes from a salt water marsh. J. Atmos. Chem. 4, 375–395. https://doi.org/10.1007/BF00053811

Cooper, D.J., De Mello, W.Z., Cooper, W.J., Zika, R.G., Saltzman, E.S., Prospero, J.M., Savoie, D.L., 1987. Short-term variability in biogenic sulphur emissions from a Florida *Spartina alterniflora* marsh. Atmos. Environ. 21, 7–12.

De Mello, W.Z., Cooper, D.J., Cooper, W.J., Saltzman, E.S., Zika, R.G., Savoie, D.L., Prospero, J.M., 1987. Spatial and diel variability in the emissions of some biogenic sulfur compounds from a Florida *Spartina alterniflora* coastal zone. Atmos. Environ. 21, 987–990. https://doi.org/10.1016/0004-6981(87)90095-3

DeLaune, R.D., Devai, I., Lindau, C.W., 2002. Flux of reduced sulfur gases along a salinity gradient in Louisiana coastal marshes. Estuar. Coast. Shelf Sci. 54, 1003–1011. https://doi.org/10.1006/ecss.2001.0871

Goldan, P.D., Kuster, W.C., Albritton, D.L., Fehsenfeld, F.C., 1987. The measurement of natural sulfur emissions from soils and vegetation: Three sites in the Eastern United States revisited. J. Atmos. Chem. 5, 439–467. https://doi.org/10.1007/BF00113905

Hill, F.B., Aneja, V.P., Felder, R.M., 1978. A technique for measurement of biogenic sulfur emission fluxes. J. Environ. Sci. Heal. Part A Environ. Sci. Eng. 13, 199–225. https://doi.org/10.1080/10934527809374804

Lamb, B., Westberg, H., Allwine, G., Bamesberger, L., Guenther, A., 1987. Measurement of biogenic sulfur emissions from soils and vegetation: application of dynamic enclosure methods with Natusch filter and GC/FPD analysis. J. Atmos. Chem. 5, 417–437. https://doi.org/10.1007/BF00113904

Morrison, M.C., Hines, M.E., 1990. The variability of biogenic sulfur flux from a temperate salt marsh on short time and space scales. Atmos. Environ. Part A. Gen. Top. 24A, 1771–1779. https://doi.org/10.1016/0960-1686(90)90509-L

Steudler, P.A., Peterson, B.J., 1985. Annual cycle of gaseous sulfur emissions from a New England *Spartina alterniflora* marsh. Atmos. Environ. 19, 1411–1416. https://doi.org/10.1016/0004-6981(85)90278-1

Steudler, P.A., Peterson, B.J., 1984. Contribution of gaseous sulphur from salt marshes to the global sulphur cycle. Nature 311, 455-457. https://doi.org/10.1038/311455a0

Appendix D

SUPPLEMENTARY MATERIAL – METHANE DYNAMICS IN TIDAL SALT MARSH SOILS: A MULTI-DISPLINARY APPROACH TO UNDERSTANDING PRODUCTION AND FATE

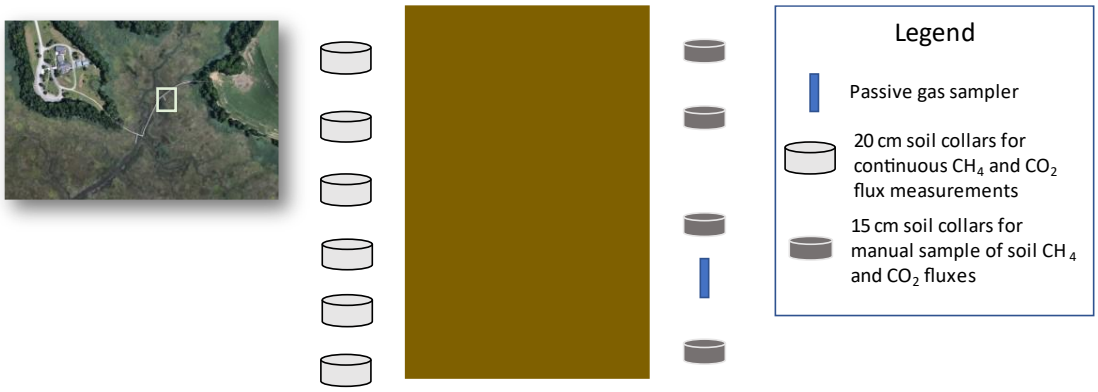

Figure D.1: (L) Aerial view of St. Jones Reserve with a box denoting the SS site. (R) General schematic of the location of chambers and the passive gas sampler relative to each other and the boardwalk.

D.1 Conversion of CH_4 and CO_2 concentrations from ppmv to mM

Gas measured in ppmv is equivalent to μmol mol^{-1} due to Dalton's Law of Partial Pressures. The first step towards converting the gas concentrations to mM is to convert it to mg L^{-1} using the molecular weight of the gas (CO_2 = 41.01 g mol^{-1}, CH_4 = 16.04 g mol^{-1}) and using standard pressure and a temperature of 20°C to convert moles of gas into liters (1 mol gas = 24 L at 20°C). See example below for CO_2.

$$\frac{X\ \mu mol\ CO_2}{mol}\ x\ \frac{44.01\ \mu g\ CO_2}{1\ \mu mol\ CO_2}\ x\ \frac{1\ mg\ CO_2}{1000\ \mu g\ CO_2}\ x\ \frac{1\ mol}{24\ L} = X\ \frac{mg\ CO_2}{L}$$

Once, the gas concentration has been converted to mg L^{-1}, the next step is to convert it to mM (e.g., mmol L^{-1}) using the molecular weight of the gas.

$$\frac{X\ mg\ CO_2}{L}\ x\ \frac{1\ mmol\ CO_2}{44.01\ mg\ CO_2} = X\ mM\ CO_2$$

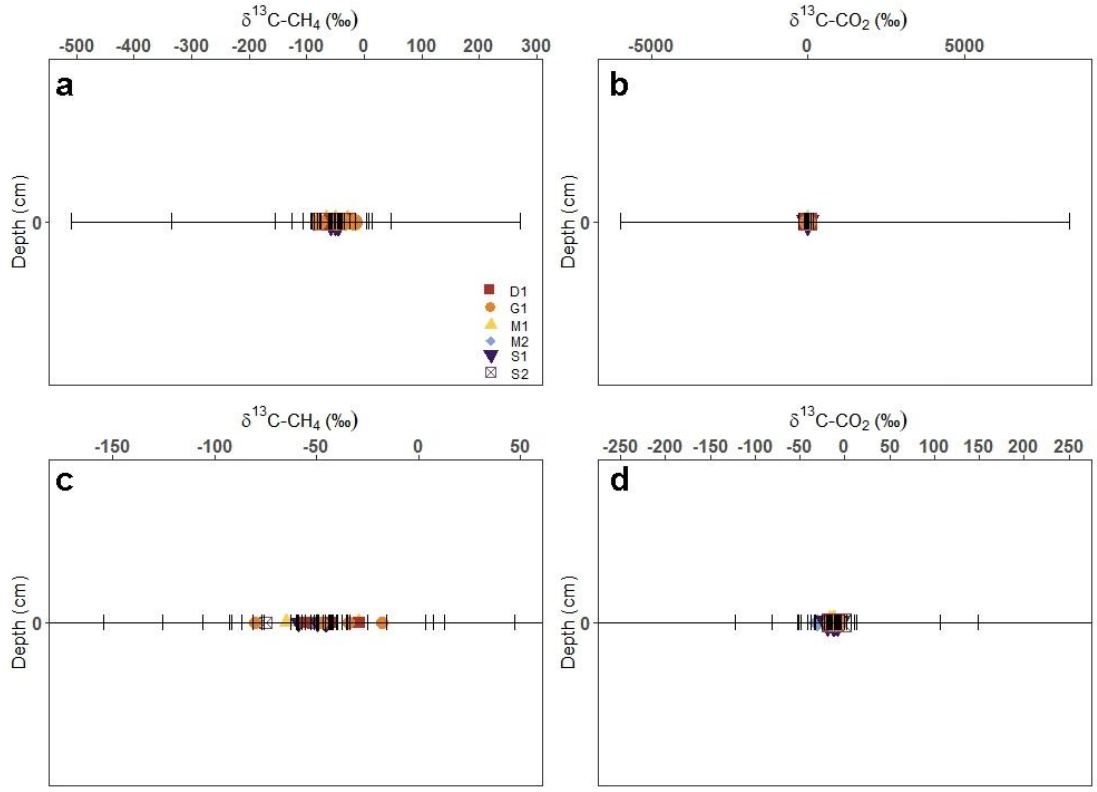

Figure D.2: Confidence intervals (95%) associated with each soil efflux $\delta^{13}C\text{-}CH_4$ (a, c) and $\delta^{13}C\text{-}CO_2$ (b, d) keeling plot. Confidence intervals were calculated using a bootstrap method. Panels c and d are zoomed-in versions of a and b respectively, to better see the variability in 95% confidence intervals.

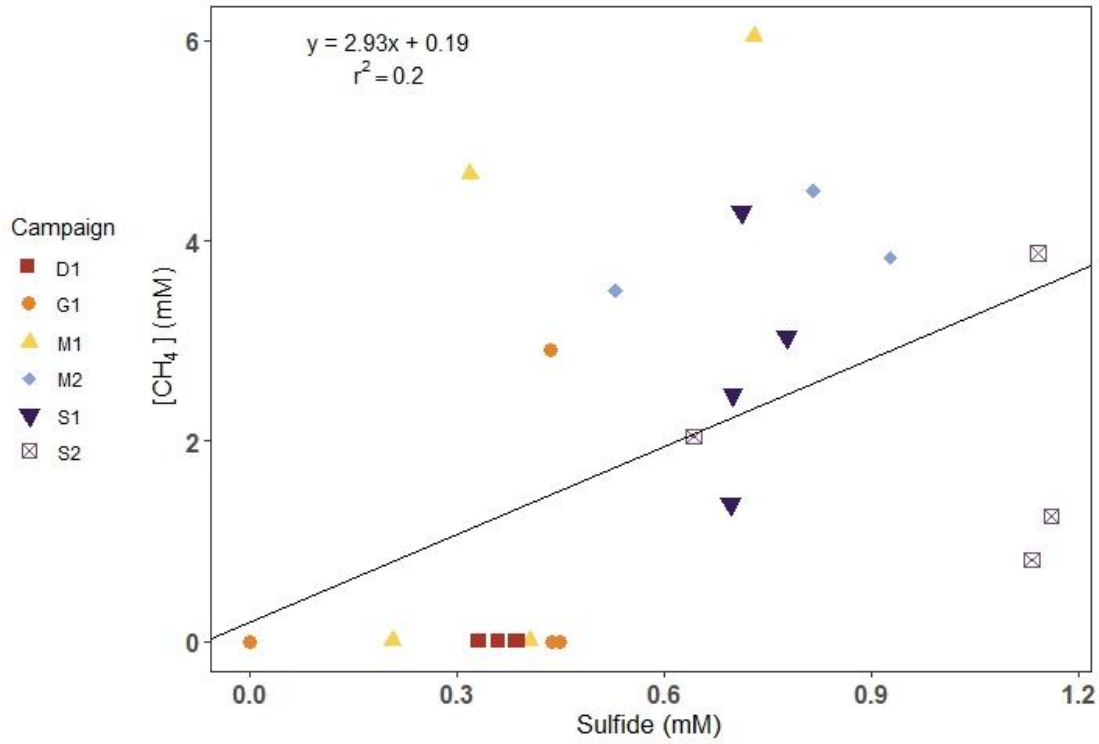

Figure D.3: Relationship between pore water sulfide concentrations and soil CH_4 concentrations for all campaigns and all depths.

D.2 Materials and methods – $\delta D\text{-}CH_4$ and $\delta^{13}C\text{-}CH_4$

On July 16, 2021, gas samples were collected to measure $\delta^{13}C\text{-}CH_4$ and $\delta D\text{-}CH_4$. Gas samples from the depth profile and soil efflux were collected as described in Section 5.2.4. Water flux samples from the tidal creek at low tide were collected using a floating chamber (20 cm) coupled with an Ultraportable Greenhouse Gas Analyzer (UGGA; Los Gatos Research, San Jose, CA) in a closed loop. An in-line sampling port and a gas-tight syringe was used to take samples at 0, 5, 10, and 15 minutes after the chamber was lowered onto the surface of the tidal creek. Gas samples were injected into N_2-filled exetainers and the process was repeated two more times for a total of three sampling events at low tide.

Samples were sent to the University of California-Davis Stable Isotope Facility. $\delta\ ^{13}C\text{-}CH_4$ and $\delta\ D\text{-}CH_4$ were analyzed using a ThermoScientific Delta V Plus isotope ratio mass spectrometer (IRMS).

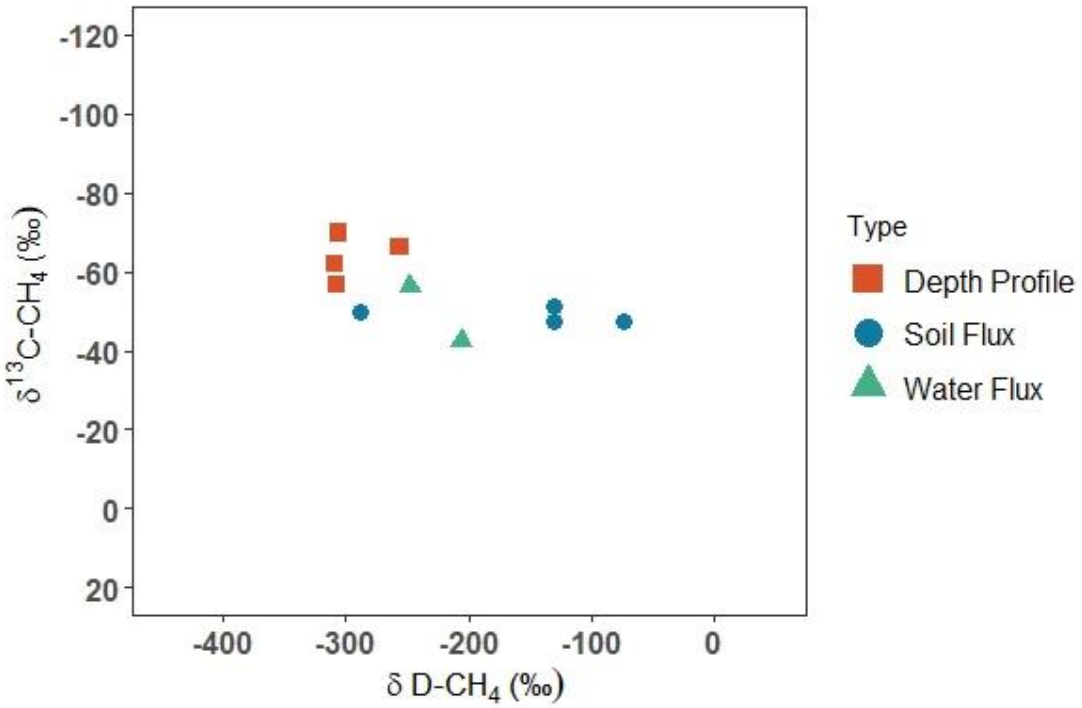

Figure D.4: Combination plot of δ^{13}C-CH_4 and δD-CH_4 from gas samples collected on July 16, 2021.

D.3 Materials and methods – δ^{13}C-DIC

On March 14, July 11, and October 9, 2018, soil pore water was collected for [DIC] and δ^{13}C-DIC analyses at low and high tide. Surface water samples from the tidal creek (high, low, and mid tide), the St. Jones River, and in the Delaware Bay next to the mouth of the Murderkill River were collected, as well as groundwater samples from adjacent to the tidal salt marsh.

Pore water samples were collected using a PushPoint (M.H.E Products) connected to a peristaltic pump via tubing with a needle at the outlet. Samples were pumped from -15.5, -40, -56, and -70 cm below the soil surface, through a 0.2 μm syringe filter into He-filled 12 mL exetainers. Samples were refrigerated upside down in water before being sent to the Isotope Facility at the University of Connecticut. Samples were run on a Thermo Delta V Plus IRMS.

Mixing curves for isotopic data were calculated according to Fry (2002) and Guardiani et al. (2021).

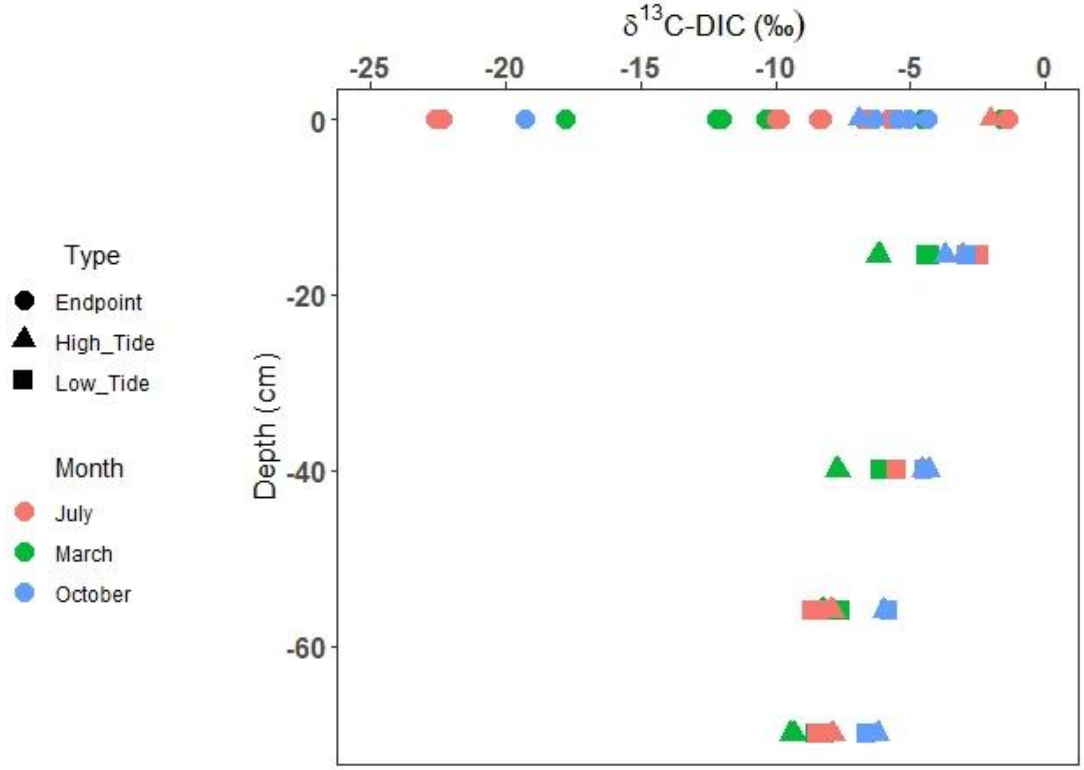

Figure D.5: Depth profile of δ^{13}C-DIC from pore water at high and low tide ("High_Tide", "Low_Tide"), as well as δ^{13}C-DIC from a variety of endmembers (located at 0 cm). Endmembers (i.e., "Endpoint) includes surface water from the tidal creek (high, mid, and low tide), St. Jones River, and Delaware Bay at the outlet of the Murderkill River, as well as groundwater near the site. Data was collected in 2018.

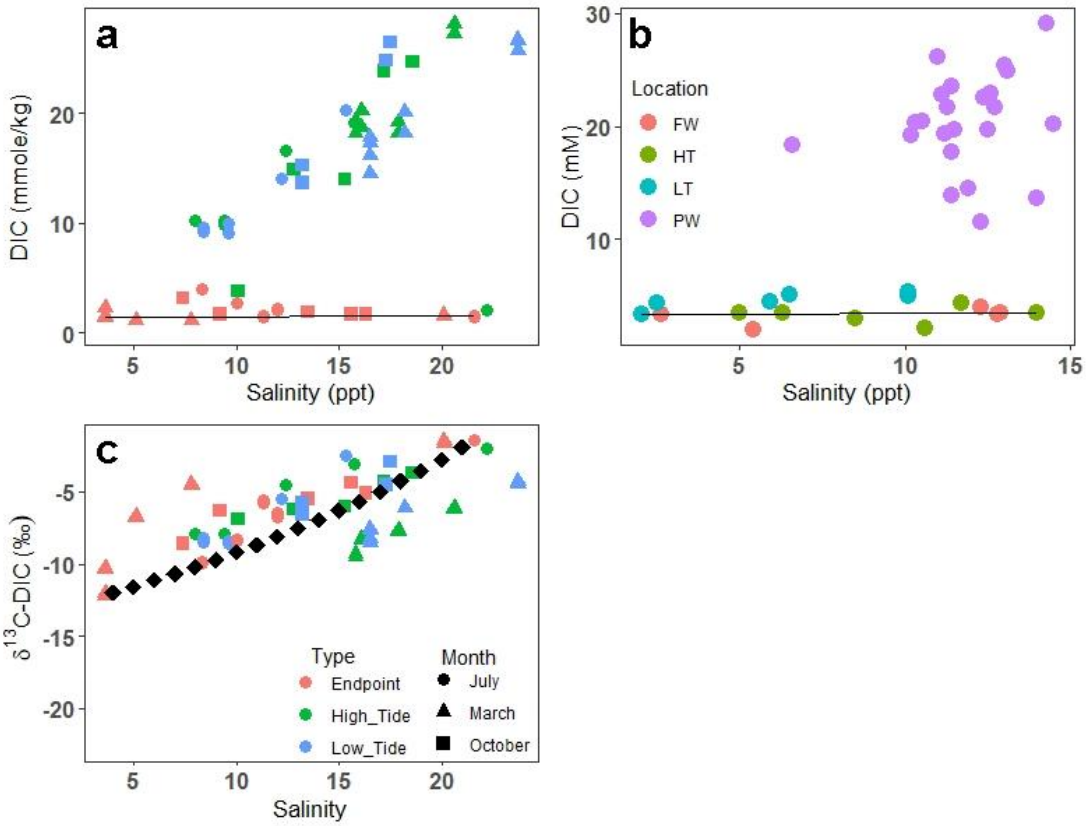

Figure D.6: DIC mixing plots for data collected during (a) 2018 and (b) 2020-2021 field campaigns, as well as (c) δ^{13}C-DIC mixing plots for 2018. Black diamonds in panel (c) denote the mixing curve. Note: x and y-axes are different.

D.4 Materials and methods – $\delta^{13}C\text{-}CH_4$, $\delta^{13}C\text{-}CO_2$, and $\Delta^{14}C\text{-}CO_2$ from the tidal creek

Water flux samples from the tidal creek for $\delta^{13}C$ analyses were collected using a floating chamber (20 cm) coupled with the UGGA in a closed loop. An in-line sampling port and a gas-tight syringe was used to take samples at 0, 5, 10, and 15 minutes after the chamber was lowered onto the surface of the tidal creek. Gas samples were injected into N_2-filled exetainers. The sampling was done at both low and high tide.

For $\Delta^{14}C$ samples from the tidal creek at low tide, a chamber outfitted with a fan, soda lime trap, and two ball valves was connected to the UGGA in order to purge the headspace of CO_2. Then the ball valves were closed and the UGGA was disconnected to allow for CO_2 to accumulate in the headspace. Once enough CO_2 accumulated, the headspace was extracted via a flow controller and a water trap into a 1 L stainless steel flask.

Stable isotope samples were sent to the University of California-Davis Stable Isotope Facility. $\delta^{13}C\text{-}CH_4$ and $\delta^{13}C\text{-}CO_2$ were analyzed using a ThermoScientific Delta V Plus isotope ratio mass spectrometer (IRMS). Radiocarbon samples were sent to the Center for Accelerator Mass Spectrometry at Lawrence Livermore National Laboratory for graphitization and were run on the Van de Graaff FN accelerator mass spectrometer.

Table D.1: $\delta^{13}C\text{-}CH_4$, $\delta^{13}C\text{-}CO_2$, and $\Delta^{14}C\text{-}CO_2$ of gas efflux from the surface of the tidal creek during the six field campaigns. LCI = lower 95% confidence interval, UCI = upper 95% confidence interval.

Campaign	**Tide**	**$\delta^{13}C\text{-}CH_4$ (LCI – UCI)**	**$\delta^{13}C\text{-}CO_2$ (LCI – UCI)**	**$\Delta^{14}C\text{-}CO_2$**
D1	High	-51.0 (-53.5 to -50.2)	-23.9 (-31.1 to -22.5)	NA
	Low	-58.5 (-66.0 to -55.8)	-20.5 (-52.1 to -10.2)	NA
G1	High	-45.7 (-46.6 to -43.5)	-17.5 (-19.9 to -15.6)	NA
	Low	-58.8 (-59.7 to -57.1)	-22.2 (-30.2 to -14.9)	-12.4
M1	High	-57.6 (-58.1 to -57.0)	-11.9 (-14.5 to -9.89)	NA
	Low	-54.2 (-63.8 to -48.4)	-22.9 (-26.4 to -19.0)	+4.9
M2	High	-44.7 (-50.8 to -43.5)	-22.3 (-53.7 to -9.36)	NA
	Low	-56.4 (-57.5 to -56.3)	-19.9 (-24.7 to -18.9)	+12.8
S1	High	-48.1 (-62.6 to -31.9)	-15.0 (-15.7 to -14.3)	NA
	Low	-57.8 (-58.1 to -56.4)	-20.5 (-21.1 to -17.7)	+18.4
S2	High	-41.1 (-46.1 to -33.8)	-16.8 (-21.6 to -14.5)	NA
	Low	-59.5 (-62.3 to -47.6)	-20.9 (-21.1 to -12.8)	+7.3

REFERENCES

Fry, B., 2002. Conservative mixing of stable isotopes across estuarine salinity gradients: A conceptual framework for monitoring watershed influences on downstream fisheries production. Estuaries. 25, 264-271. https://doi.org/10.1007/BF02691313

Guardiani, J., Tobias, C., Smith, R., 2021. Seasonal carbon dynamics in a temperate lagoonal estuary: New River, NC, USA. Estuaries and Coasts. https://doi.org/10.1007/s12237-021-00992-5

Appendix E

REPRINT PERMISSION LETTERS

E.1 Reprint permission from Science of the Total Environment

Reprint permission for:

- 10.1016/j.scitotenv.2019.06.032
- 10.1016/j.scitotenv.2021.149715

Re: Permission Request for Dissertation [220601-000983]

Permissions Helpdesk <permissionshelpdesk@elsevier.com> Thu, Jun 2, 2022 at 2:16 AM

Reply-To: Permissions Helpdesk <permissionshelpdesk@elsevier.com>
To: mcapooci@udel.edu

Dear Margaret Capooci,

Thank you for sharing us the information.

We hereby grant you permission to reprint the material below at no charge in your thesis subject to the following conditions:

1. If any part of the material to be used (for example, figures) has appeared in our publication with credit or acknowledgement to another source, permission must also be sought from that source. If such permission is not obtained then that material may not be included in your publication/copies.

2. Suitable acknowledgment to the source must be made, either as a footnote or in a reference list at the end of your publication, as follows:
"This article was published in Publication title, Vol number, Author(s), Title of article, Page Nos, Copyright Elsevier (or appropriate Society name) (Year)."

3. Your thesis may be submitted to your institution in either print or electronic form.

4. Reproduction of this material is confined to the purpose for which permission is hereby given

5. This permission is granted for non-exclusive world English rights only. For other languages please reapply separately for each one required. Permission excludes use in an electronic form other than submission. Should you have a

specific electronic project in mind please reapply for permission.

6. Should your thesis be published commercially, please reapply for permission.

This includes permission for the Library and Archives of Canada to supply single copies, on demand, of the complete thesis. Should your thesis be published commercially, please reapply for permission- Canada
This includes permission for UMI to supply single copies, on demand, of the complete thesis. Should your thesis be published commercially, please reapply for permission- ROW

7. Posting of the full article online is not permitted. You may post an abstract with a link to the Elsevier website www.elsevier.com, or to the article on ScienceDirect if it is available on that platform.

8. Article can used be in the University library if it is embedded in the thesis and not used commercially.

If you have any additional questions, feel free to contact us.

Kind regards,

Thomas Rexson Yesudoss
Copyrights Coordinator
ELSEVIER | HCM - Health Content Management

E.2 Reprint permission from Biogeosciences

As noted on Biogeosciences website:

https://www.biogeosciences.net/policies/licence_and_copyright.html

Copyright

- Authors retain the copyright of their manuscript and its final journal article. Regarding copyright transfers please see below.
- Authors grant Copernicus Publications an irrevocable non-exclusive licence to publish the article or versions of the manuscript, if preprints are foreseen, electronically and in print format and to identify itself as the original publisher.
- Authors grant Copernicus Publications commercial rights to produce hardcopy volumes of the journal for sale to libraries and individuals.
- Authors grant any third party the right to use the article or versions of the manuscript, if preprints are foreseen, freely as long as its original authors and citation details are identified.
- The article and corresponding preprints are distributed under the Creative Commons Attribution 4.0 License. Unless otherwise stated, associated material is distributed under the same licence:

Creative Commons Attributions 4.0 License
You are free to:

Share — copy and redistribute the material in any medium or format

Adapt — remix, transform, and build upon the material for any purpose, even commercially.

Under the following conditions:

Attribution — You must give appropriate credit, provide a link to the licence, and indicate if changes were made. You may do so in any

reasonable manner, but not in any way that suggests the licenser endorses you or your use.
No additional restrictions — You may not apply legal terms or technological measures that legally restrict others from doing anything the licence permits.

Notices

- The licenser cannot revoke these freedoms as long as you follow the licence terms.
- You do not have to comply with the licence for elements of the material in the public domain or where your use is permitted by an applicable exception or limitation.
- No warranties are given. The licence may not give you all of the permissions necessary for your intended use. For example, other rights such as publicity, privacy, or moral rights may limit how you use the material.
- The CC BY License, of which 4.0 is the recent version, was developed to facilitate open access – namely, free immediate access to, and unrestricted reuse of, original works of all types.
- Under this liberal licence, authors agree to make posted materials legally available for reuse, without permission or fees, for virtually any purpose. Anyone may copy, distribute, or reuse these works, as long as the author and original source are properly cited. Thus, CC BY facilitates the dissemination, transfer, and growth of scientific knowledge.
- Please read the full legal code of this licence.